MECHANISTIC STUDY OF PRECIPITATION SQUEEZE TREATMENTS USING PHOSPHONATE AND PHOSPHATE ESTER SCALE INHIBITORS

by

Alsu Valiakhmetova

Submitted for the degree of Doctor of Philosophy

Heriot-Watt University

Institute of Petroleum Engineering

School of Energy, Geoscience, Infrastructure and Society

Edinburgh, Scotland, UK

December 2019

ABSTRACT

One of the challenges associated with water injection during oil and gas production is mineral scale formation within the production systems. Scale deposited on downhole equipment, tubulars and perforations can lead to production decline and eventually cause well abandonment. Proactive approach of preventing scale precipitation applying scale inhibitor "squeeze" treatments is recognised to be the one of the most economically and technically favourable option for scale management in most oilfields.

One of the factors determining the success of the squeeze treatment is good retention of the scale inhibitor within the formation rock, which leads to an extended squeeze lifetime. The two main retention mechanisms are *adsorption* and *precipitation*. Field cases have shown that implementing precipitation squeezes may result in an extended squeeze lifetime, compared to pure adsorption treatments, with some additional benefits for production. Thus, the current thesis is on the topic of precipitation squeeze treatments.

In the first part of this research, we examine the factors that govern the retention and subsequent release of phosphonate scale inhibitors in precipitation squeezes: viz. equilibrium solubility and the dissolution rate. The equilibrium solubility diagrams of 3 common phosphonate SI/Ca/Mg precipitates were obtained as a function of both temperature and brine Mg/Ca molar ratio, in static solubility tests. Subsequently, the flow rate effect and dissolution rates were measured in non-equilibrium sand pack flooding tests. In addition, we define other parameters that must be considered in the dissolution model, in order to accurately predict scale inhibitor returns in precipitation treatments.

Conclusions derived from the study allowed a qualitative dissolution model to be developed by Flow Assurance and Scale Team (Heriot-Watt University) that describes phosphonate SIs release in precipitation treatments. All the data obtained in this work can be directly used to calculate the dissolution rates under different flow rates and numerically model the dissolution behaviour of the phosphonate SI/Ca complexes. Once the data and model are incorporated into the squeeze design software, more accurate predictions of the inhibitor return in precipitation squeeze operations can be obtained.

The second part of the thesis presents a comprehensive study on the precipitation behaviour and performance of phosphate esters, again in the context of precipitation squeeze treatments. It is shown, that this class of scale inhibitors can effectively mitigate

scale formation at lower temperatures which represent the most severe thermodynamic conditions for sulphate scale inhibition. FTIR and NMR analytical techniques have been applied to explain the inhibition efficiency data versus temperature variation, showing the structural changes in the phosphate ester solutions over the temperature range 20-95^{o}C. Finally, the mechanism of phosphate ester performance is discussed and compared to those of conventional phosphonate scale inhibitors.

The results obtained in this part of thesis are of practical significance for the effective design of lower temperature phosphate esters squeeze treatments, as this chemistry represents (i) a more environmentally friendly alternative to phosphonate scale inhibitors, and (ii) a chemical that is significantly easier to detect within produced brine (by ICP) than many polymers currently used by the industry.

To my grandfathers,

Gusman Valiakhmetov and Mukatdis Shakirov.

ACKNOWLEDGEMENTS

I would like to express my gratitude to the people who contributed generously to the work presented in this thesis and supported me through this fascinating journey towards becoming a Doctor of Philosophy.

The first mention goes to the management of Flow Assurance and Scale Team: Prof. Ken Sorbie, Prof. Eric Mackay, Dr. Lorraine Boak, and Mike Singleton. These people within a moment have changed the direction not only of my professional but also personal life, by offering me an opportunity to come to Scotland and conduct this PhD study in Heriot-Watt University. Thank you for the opportunity to become a part of the international "scale" family, for sponsoring this PhD, for your constant feedback, and for trust to present the research on various international conferences and contests.

Both my supervisors, Prof. Ken Sorbie and Dr. Lorraine Boak, have been great mentors and contributed immensely to my personal and professional development. You encouraged me to be not only a researcher, but an *explorer*; your taught me some life wisdom and thus, shaped not only my thesis, but also my personality. Thank you for the personal approach and giving me freedom to conduct the work in a creative and independent way. Lorraine, you have also been a great English grammar advisor and proof-reader of the thesis and all the papers I have published. Thank you, now every time when I use *an* article, I remember you!

All the experimental studies conducted in this work would not be completed without a support of the FAST laboratories personnel. I would like to thank Katherine McIver, Dr. Lorraine Boak and Wendy McEwan for giving me general laboratory and ICP-OES trainings in the beginning of my studies, for running my samples on ICP-OES; Dr. Alexander Graham, Alan Beteta, Ivan Davis and Robin Shields for assistance with running sandpack flooding tests and fruitful discussion of the test results; Khosro Jarahian for helping me with the ESEM-EDX analysis; Thomas McGravie and Tom Clark for the technical support. I also thank Dr. Oscar Vazquez for his help on SQUEEZE training and general discussions on squeeze treatments design.

My experience in FAST group would not be that enjoyable without one very special person - Heather O'Hara. You are the best administrative assistant I have ever had a chance to work with!

My sincere words of gratefulness go to Dr. Myles Jordan for his guidance and insightful comments on the research conducted on phosphate ester chemistry that covers Chapters 6 and 7 of the thesis, our discussions were very valuable and inspiring.

My deep appreciation goes to Prof. Mike Christie. Thank you for being a great mentor, for your inspiring guidance on how to "resonate" when presenting the research to the audience. I must mention, I am fascinated by your "superpower" of guiding people without putting any pressure on them! I do appreciate your constant encouragement and support during preparation to the regional and international stages of the SPE student paper contests. All the prizes I have got on those contests are because of your "superpower", mentioned above.

I would like to acknowledge all my friends and peers who made my student life in Heriot-watt University full of fun moments: Mohamed Arab, Khosro Jarrahian, Giulia Ness, Duarte Silva, Odilla Vilhena, Hydra Rodrigues, Xu Wang, Suzanny Carvalho. A very special thank you goes to my dear friend Silvio Pasquarella for encouraging me to consider moving to Edinburgh to do this PhD study and for accompanying me through this journey. Anna Novozilova, Darima Donitova, Natasha Markova, Alina Bekmukhametova, Natasha Zakharova, Anna Ishkova and Oleg Ishkov – thank you all for your constant 24/7 support over these years.

Finally, I would like to thank my parents and my big family for supporting me in a strong desire to pursue my goals and dreams. My dear cousin Regina Shakirova, since you are the only family member who has had an experience of studying and living abroad, your emotional support was very valuable during all these times. I would like to express my gratitude to all the members of my family, my grandparents, uncles and aunts, cousins - even over five thousand kilometres, I could feel your love, support and blessings.

Thank you all.

ACADEMIC REGISTRY

Research Thesis Submission

Name*:*	Alsu Valiakhmetova		
School:	School of Energy, Geoscience, Infrastructure and Society		
Version: *(i.e. First, Resubmission, Final)*		Degree Sought:	PhD, Petroleum Engineering

Declaration

In accordance with the appropriate regulations I hereby submit my thesis and I declare that:

1. The thesis embodies the results of my own work and has been composed by myself
2. Where appropriate, I have made acknowledgement of the work of others
3. Where the thesis contains published outputs under Regulation 6 (9.1.2) these are accompanied by a critical review which accurately describes my contribution to the research and, for multi-author outputs, a signed declaration indicating the contribution of each author (complete Inclusion of Published Works Form – see below)
4. The thesis is the correct version for submission and is the same version as any electronic versions submitted*.
5. My thesis for the award referred to, deposited in the Heriot-Watt University Library, should be made available for loan or photocopying and be available via the Institutional Repository, subject to such conditions as the Librarian may require
6. I understand that as a student of the University I am required to abide by the Regulations of the University and to conform to its discipline.
7. Inclusion of published outputs under Regulation 6 (9.1.2) shall not constitute plagiarism.
8. I confirm that the thesis has been verified against plagiarism via an approved plagiarism detection application e.g. Turnitin.

* *Please note that it is the responsibility of the candidate to ensure that the correct version of the thesis is submitted.*

Signature of Candidate*:*		Date:	

Submission

Submitted By *(name in capitals):*	
Signature of Individual Submitting:	
Date Submitted:	

For Completion in the Student Service Centre (SSC)

Received in the SSC by *(name in capitals):*			
Method of Submission (Handed in to SSC; posted through internal/external mail):			
*E-thesis Submitted (**mandatory for final theses**)*			
Signature:		Date:	

LIST OF CONTENTS

1. Introduction 1
1.1. Oilfield Scale Problem 1
1.2. Scale Management Strategies 2
1.3. Problem Statement 4
1.4. Research Outline 5

2. Literature Review 7
2.1. Scale Inhibition Mechanism 7
2.2. Oilfield Scale Inhibitors 10
2.3. Weak Polyacid Theory 11
2.4. Polymeric Scale Inhibitors 12
2.5. Phosphonate Scale Inhibitors 14
2.6. Inhibitor Retention Mechanisms 15
2.7. Scale Inhibitor Retention Modelling 18
2.8. Phosphonate Inhibitor Complexation 19
2.8.1. Rice University Brine Chemistry Consortium 19
2.8.2. Michigan University 22
2.8.3. Heriot-Watt University 26

3. Equilibrium Solubility and Inhibition Efficiency of Phosphonate_ Calcium_ Magnesium Precipitates 32
3.1. Introduction 32
3.2. Experimental details 34
3.2.1. Materials 34
3.2.2. Precipitation Tests 35
3.2.3. Solubility Test 37
3.2.4. Static Barium Sulphate Inhibition Efficiency Tests 39
3.2.5. Precipitation and Re-Dissolution Experiments 41
3.3. Results and Discussion 41
3.3.1. Stoichiometry of OMTHP_Ca, DETPMP_Ca, and HEDP_Ca Complexes 41
3.3.2. Solubility of the SI_Ca_Mg Complexes 44
3.4. Inhibition Efficiency of Precipitated Phosphonate SI 57
3.5. Summary and Conclusions 60

4. Non-Equilibrium Dissolution of Phosphonate_Calcium_Magnesium Complexes in Bottle Tests 63
4.1. Introduction 63
4.2. Experimental details 66
4.2.1. Materials 66
4.2.2. Dissolution Test versus Brine Replacement 66
4.2.3. Environmental Scanning Electron Microscopy - Energy Dispersive X-Ray 68
4.2.4. X-Ray Crystallography ..... **Error! Bookmark not defined.**
4.3. Results and discussion 70
4.3.1. Dissolution Study versus Brine Replacement: in Ca^{2+} and Mg^{2+} Brines 70
4.3.2. Modelling the DETPMP/Ca Dissolution in Tests 1-3 77
4.3.3. ESEM/EDX Analysis of DETPMP_Ca Precipitates 81
4.3.4. XRD for DETPMP/Ca Precipitates 84
4.4. Summary and Conclusions 86

5. Non-Equilibrium Dissolution of the Phosphonate_Calcium Precipitates in Porous Media 87
5.1. Introduction 87
5.2. Experimental Details 89
5.2.1. Materials 89
5.2.2. Experimental Apparatus 89
5.2.3. General Sand Pack Flooding Procedure 90
5.2.4. Pack Characterization Data 93
5.2.5. Flooding Regimes 93
5.3. Results and Discussion 95
5.3.1. Non-Equilibrium Flooding Experiments: Sand Pack 1 95
5.3.2. Sand Pack 2 100
5.3.3. Sand Pack 2b 105
5.3.4. Precipitate Pack 3 110
5.3.5. XRD data for Silica Sand and DETPMP/Ca Precipitate 113
5.3.6. Morphology of Silica Sand and DETPMP/Ca Precipitate Substrate by ESEM/EDX 115
5.4. Summary and Conclusions 117

6. Precipitation Behaviour of Phosphate Ester Scale Inhibitors 120

6.1. Introduction 120
6.2. Experimental Details 123
6.2.1. Materials 123
6.2.2. Precipitation and Re-Dissolution Experiments 124
6.2.3. Static Barium Sulphate Inhibition Efficiency Test 125
6.3. Results and Discussion 126
6.3.1. PE_1_Ca Precipitation Behaviour: Stoichiometry 126
6.3.2. PAPE_Ca Complex Stoichiometry at different pH and T 134
6.3.3. Precipitation pH Effect on Inhibition Efficiency of the Phosphate Ester_Ca Complexes 138
6.3.4. Temperature Effect on the Inhibition Efficiency of Phosphate Ester_Ca Precipitates 144
6.4. Summary and Conclusions 152

7. Inhibition Efficiency of Phosphate Esters in Precipitation Squeeze Processes 154
7.1. Introduction 154
7.2. Experimental Details 155
7.2.1. Materials 155
7.2.2. Static Barium Sulphate Inhibition Efficiency Test 156
7.2.3. FTIR Spectroscopy 157
7.2.4. NMR Spectroscopy 157
7.3. Results and Discussion 158
7.3.1. Phosphate Ester Inhibition Efficiency versus Temperature: Comparison with Phosphonate and Polymer 158
7.3.2. NMR analysis 167
7.3.3. FTIR Analysis 174
7.4. Summary and Conclusions 176

8. Conclusions and Recommendations 177

References 186

LIST OF PUBLICATIONS

Valiakhmetova A., Sorbie K. S., Jordan M.M., and Boak L. S. *Phosphate Ester Scale Inhibitors Performance and Thermal Stability for Application at Low Temperature Conditions* (in progress).

Valiakhmetova A., Sorbie K. S., and Boak L. S. *Dissolution Behaviour of Phosphonate Scale Inhibitor_Calcium Complex in Precipitation Squeeze Treatments* (in progress).

Valiakhmetova A., Sorbie K. S., Boak L. S., and Shaw S. S. *Solubility and Inhibition Efficiency of Phosphonate Scale Inhibitor_Calcium_Magnesium Complexes for Application in a Precipitation-Squeeze Treatment.* Paper SPE-178977-PA, SPE Production & Operations, 2017.

Valiakhmetova A., Sorbie K. S., Jordan M.M., and Boak L. S. *Novel Studies on Precipitated Phosphate Ester Scale Inhibitors for Precipitation Squeeze Application.* Paper SPE-184511-MS, SPE International Conference on Oilfield Chemistry, Montgomery, Texas, USA, 2017.

Valiakhmetova A., Sorbie K. S., Boak L. S., and Shaw S. S. *Solubility and Inhibition Efficiency of Phosphonate Scale Inhibitor_Calcium_Magnesium Complexes for Application in Precipitation Squeeze Treatment.* Paper SPE-178977-MS, SPE International Conference & Exhibition on Formation Damage Control, Lafayette, Louisiana, USA, 2016.

NOMENCLATURE

DTPA	Diethylenetriaminepentaacetic Acid
EDTA	Ethylenediaminetetraacetic Acid
MIC	Minimum Inhibitor Concentration
[SI]	Scale Inhibitor Concentration
SI	Scale Inhibitor
DETPMP	Diethylene-Triamine-Pentakis (Methylene Phosphonic Acid) - Penta Phosphonate
DETPMP/Ca	Diethylene-Triamine-Pentakis (Methylene Phosphonic Acid) and Calcium Complex
DETPMP/Ca/Mg	Diethylene-Triamine-Pentakis (Methylene Phosphonic Acid) and Calcium, and Magnesium Complex
VS-Co	Vinylsulphonate Acrylic Acid Co-Polymer
OMTHP	Octamethylene-Tetraamine-Hexakis (Methylene Phosphonic Acid) – Hexa Phosphonate
NSSW	North Sea Sea Water
NFFW	Nelson Forties Formation Water
SI_M_n	Scale Inhibitor and Divalent Cation Complex
N Or n -	Stoichiometric Coefficient
M	Divalent Cation
PV	Pore Volume
Γ (C)	Adsorption Isotherm
Π (C)	Solubility Function
Γ/Π	Coupled Adsorption /Precipitation Process
Cs	Equilibrium Solubility
IE	Inhibition Efficiency
SR	Saturation Ratio
PE_Ca	Phosphate Ester Scale Inhibitor and Calcium Complex
T	Temperature, ^oC
HEDP	1-Hydroxyethane 1,1-Diphosphonic Acid
ICP-OES	Inductively Coupled Plasma Atomic Emission Spectroscopy
ESEM-EDX	Environmental Scanning Electron Microscopy - Energy Dispersive X-Ray

XRD	X-Ray Powder Diffraction
DW	Distilled Water
RT	Room Temperature
PAPE	Polyhydric Alcohol Phosphate Ester
PE_1	Phosphate Ester - Scale Inhibitor 1

CHAPTER 1. INTRODUCTION

1.1. Oilfield Scale Problem

Oilfield scale is an inorganic crystalline deposit with a relatively low aqueous phase solubility that can form in oil and gas production systems and considered as one of the major flow assurance issues (Vetter 1976, Kan and Tomson 2012, Olajire 2015). Scale precipitation in a near-wellbore formation area can plug the pores, causing decline in rock permeability and leading to formation damage. Scale also adheres on the metal surface of production tubulars and top side equipment. This can cause number of technical issues, such as malfunction of heat transfer in separators, corrosion developing under scale deposits, valve blockage and even unscheduled equipment shutdowns (Bonnett, Fieler et al. 1991). Moreover, scale deposited on pipelines and tubulars reduces the diameter of the production tubing, that in turn causes production decline and, eventually, well abandonment. One of the most severe shutdowns of production system caused by water scaling was reported in (Crabtree, Eslinger et al. 1999) for the BP (formerly British Petroleum) operated Miller field, where well production fell from 30,000 bbl/day to 0 bbl/day within 24 hours. The reason was barium sulphate scale precipitating in production tubulars. This case, as well as the examples mentioned above, clearly demonstrate the severity of the technical and economic consequences associated with scale precipitation during production, thereby requiring the scale management strategy to be defined during the early conceptual phase of a field development plan.

The most common mineral scales detected in oilfields are calcium carbonate (Vetter and Farone 1987, Dyer and Graham 2002), calcium sulphate, barium sulphate and strontium sulphate (Shen and Crosby 1983, Bader 2006). Sulphate scale precipitation is primarily caused by the chemical incompatibility between formation brine and sea water, injected for maintaining downhole pressure (Yuan and Todd 1989, Crabtree, Eslinger et al. 1999, Sorbie and Mackay 2000). The chemical reaction can be described by the following equation:

$$Ba^{2+}\ (Sr^{2+},\ Ca^{2+}) + SO_4^{2-} \rightarrow BaSO_{4\,(s)}\ (SrSO_{4\,(s)},\ CaSO_{4\,(s)}) \qquad (1.1)$$

Carbonate scales precipitate when the thermodynamic equilibrium in the carbonate system, that includes dissolved bicarbonate, carbonate, carbon dioxide, H^+, OH^-, is shifted, mainly due to pressure drop below the CO_2 bubble point pressure:

$$Ca + 2HCO_3^- \rightarrow CO_{2\,(g)} + H_2O + CaCO_{3\,(s)} \quad (1.2)$$

Precipitation of one type of mineral scale may result in the co-precipitation of other minerals (Todd, Yuan et al. 1994, Hennessy and Graham 2002), hence scale deposits found in production systems are a mix of different inorganic salts.

1.2. Scale Management Strategies

It can be challenging to remove the scale deposits once they have built up, especially in the offshore production environment, where scale remediation comes at a higher cost. Mechanical scale removal methods are the most effective ones (Johnson, Eslinger et al. 1998), but the application can be limited by the cost, down time in production (Jordan, Sjuraether et al. 2001), and by location of the scale deposits that is not accessible by mechanical tools (Crabtree, Eslinger et al. 1999). As an alternative to the mechanical clean-up, scale can be removed by chemical dissolvers that generally come at lower cost but have to be selected according to the type of scale. Removal acids, such as hydrochloric acid, are widely used for dissolving carbonate scales, whereas strong chelating agents, for example DTPA and EDTA, can effectively deal with sulphate scales (Putnis, Putnis et al. 1995, Almubarak, Ng et al. 2017).

Alternatively, another scale management strategy widely adopted by the industry is *preventing* scale formation rather than dealing with the consequences of its uncontrolled precipitation (Bonnett, Fieler et al. 1991, Poynton, Kelly et al. 2004, Al Salami and A. Kader 2010). Even if scale was built up uncontrolled and removed mechanically or chemically, these removal operations are generally followed by scale *prevention* treatments (Hernandes, Melo et al. 2008). The most common prevention measures described in literature include:

- **Sulphate reduction**, where seawater is de-sulphated prior to injection into the reservoir, using nanofilters (Bader 2006, Baraka-Lokmane, Lesage et al. 2018). This method can reduce the concentration of SO_4^{2-} ions down to 10mg/L, thereby significantly reducing the sulphate scale risks.
- **Continuous scale inhibitor injection** into the production well, upstream the separator or manifolds is the preferred option when scaling occurs within a well or in specific units of the top side facilities, but not in the near wellbore area (Graham, Dyer et al. 1998, Kelland 2014).

- **Squeeze treatments** - scale prevention via *scale inhibitor squeeze treatments* is applied when scaling occurs within the near-wellbore formation. The method ensures protection of both the formation area and production tubing with equipment. Therefore, this is recognised to be the one of most economically and technically favourable option for scale management in offshore and subsea fields (Poynton, Kelly et al. 2004, Hernandes, Melo et al. 2008, Jordan and Mackay 2016).

Since the current research is in the context of squeeze treatments, the focus of this review will be on this method. Scale inhibitor squeeze treatments comprise of pre-flush brine followed by injecting a chemical - scale inhibitor, usually in a "bullhead" injection, into the near wellbore area of a producing well. Generally, the scale inhibitor is dissolved in a sea water or available produced brine, however, there are other "unconventional" placement methods described in the literature, for example, by injecting nanoparticles coated with scale inhibitors to extend the release time of the chemical (Shen, Zhang et al. 2008). The scale inhibitor "bullhead" injection is followed by an over-flush brine, which displaces the SI deeper into the formation, further away from the wellbore area. After a shut-in period to allow the chemical to adequately "retain" within the formation rock, usually 6-24 hours, the well is put back on to production. After that, the inhibitor is released into the produced brine that passes through the treated areas of formation rock, ensuring protection from scale deposition within the entire near-wellbore area, production tubing, and top side facilities. Once the chemical is depleted from the formation rock and has reached the minimum inhibitor concentration (MIC) below which it cannot prevent (or sufficiently delay) scale formation, the treatment needs to be repeated. In the industry, squeeze treatment lifetimes can vary significantly from 1 week to 18 months, depending on the well and production characteristics, however the average is 6 to 12 months. A better metric for a squeeze life is the number of "treated barrels" of water produced, i.e. the number of barrels of water containing scale inhibitor concentration, [SI] $\geq$ MIC.

A schematic scale inhibitor return profile, Figure 1.1, shows the concentration of scale inhibitor in the produced brine fluids after the well is brought back onto production. Ideally, squeeze treatments should provide a long return period of scale inhibitor. Squeeze lifetime is measured as the volume of produced brine that contains dissolved scale inhibitor at the concentration greater than MIC which protects the well. The main factor determining the successfulness of the squeeze operation and longer squeeze lifetimes is

good retention of scale inhibitor within the formation rock. The scale inhibitor concentration in the squeeze pill, squeeze brine composition and pH have a significant impact on the retention of the scale inhibitor and are *under control* of the operators performing the squeeze design and treatment.

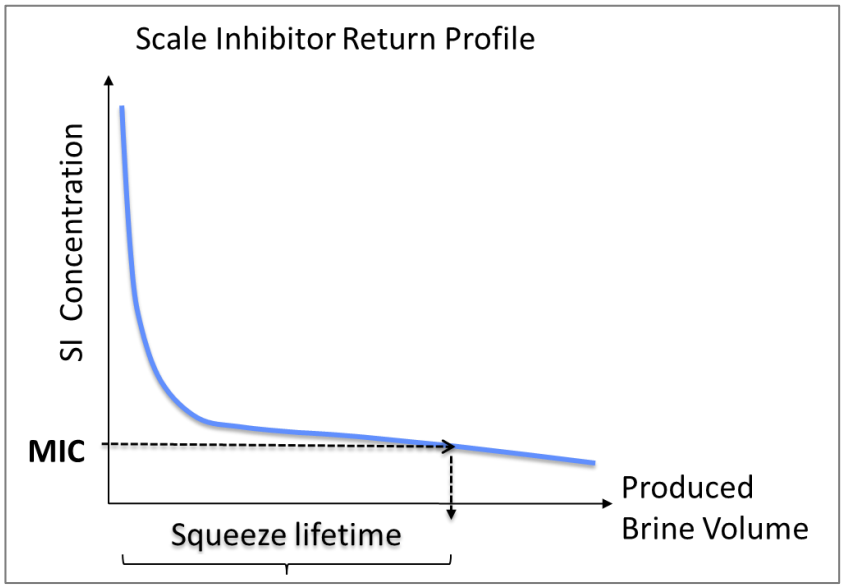

Figure 1.1 Typical scale inhibitor return profile

The main scale inhibitor retention mechanisms within the formation rock are *adsorption* and/or *precipitation* (Sorbie and Gdanski 2005, Sorbie 2010, Todd, Savin et al. 2012). Adsorption is a primary mechanism, present in all squeeze treatments performed in oilfields. Inhibitor release into a bulk brine after the adsorption treatments is governed by the adsorption isotherm. Generally, the "pure" adsorption treatments result in a shorter squeeze lifetime, compared to coupled adsorption/precipitation treatments, which allow a greater amount of inhibitor to be retained within the formation matrix. This would provide longer squeeze lifetimes with a desirable "long tail" on the return profile which is a positive factor from an economic point of view.

1.3. Problem Statement

Although precipitation squeezes have been applied extensively within the industry, there is still no clear understanding of the precipitation/dissolution processes that occur in these treatments. As described in Sorbie, Jiang et al. 1993, the inhibitor/calcium precipitates solubility (~10^{-4} M) is too high compared to the return inhibitor concentrations seen in the oilfields and in core flooding experiments (~10^{-5}-10^{-6} M). This may either show that

the precipitation and dissolution are not the controlling return mechanism or that a more complicated precipitation process is occurring that requires further exploration and fundamental understanding.

On the other hand, the fact that the full picture of the precipitation model is missing affects the way field squeeze treatments are currently designed. For example, in-house software SQUEEZE (Heriot-Watt University) that is widely used within the industry to design and optimize squeeze treatment operations relies on a quite simplified precipitation model (Sorbie 2012), does not consider the chemical properties of the scale inhibitors, which, in turn, may have a significant impact on the prediction of the inhibitor return in oilfields.

Therefore, this thesis is focused on defining a *qualitative* model that describes phosphonate scale inhibitor retention and release processes, as well as the effect of the precipitation reaction on the activity of the released inhibitor species, during these precipitation squeeze treatments. This will enable better fundamental understanding of all these processes occurring between a brine and precipitate over a squeeze lifetime. It is intended, that this work contributes to the development of a full precipitation model by supplementing and proving the existing simplified mathematical model with experimental data. Once the data and the qualitative model is implemented into the SQUEEZE code, this should allow more accurate predictions of the inhibitor return in produced brine and inhibitor's fate after the squeeze operations to be obtained.

1.4. Research Outline

Chapter 1 introduces the basic oilfield scale problem and covers the main scale management strategies applied within the industry. It defines the problem that is going to be addressed in the dissertation and provides the general outline of the experimental work conducted.

In *Chapter 2*, a critical review on the knowledge available in the literature for scale inhibitor applications in oil and gas fields is undertaken. Since the current study is contexted around precipitation squeeze treatments, a review of the published studies on the scale inhibitor precipitation and dissolution processes and factors affecting the release of the inhibitor from the porous media will be covered.

Chapter 3 expands the fundamental understanding of phosphonate scale inhibitor precipitation *thermodynamics* in terms of solubility and the inhibition efficiency of the precipitated complexes. The studies performed are:

- The effect of brine chemistry and temperature on the release (re-dissolution) of the precipitated inhibitor into the bulk solution;
- The effect of the precipitation process on the final inhibition performance of the re-dissolved inhibitor species.

Chapter 4 focuses on the dissolution *kinetics* of phosphonate DETPMP/Ca/Mg precipitates and factors that govern their dissolution into the *bulk* solution, prior to moving to dynamic flooding experiments in porous media. The factors that govern the precipitate dissolution are determined both experimentally and via numerical studies.

Chapter 5 explores the non-equilibrium dissolution behaviour of the DETPMP/Ca precipitate in porous medium. The dissolution behaviour observed in the study is in agreement with the bulk observations. However, our results do not correlate with the "classic" dissolution model that is currently used for the phosphonate SI precipitation model. A new qualitative model describing the dissolution of phosphonate/calcium complexes in precipitation squeeze treatments is presented.

Chapter 6 focuses on the precipitation behaviour of phosphate ester scale inhibitors - another class of scale inhibitor applied in oilfields that has been found to be a promising inhibitor for application at low temperatures. It is shown, that the phosphate ester precipitation process is quite different from that of the phosphonate inhibitors trends established and observed earlier in the study.

Chapter 7 expands the previous study on the phosphate ester chemistry by comparing its inhibition efficiency to the efficiencies of the "classic" inhibitors used in the industry: sulphonated co-polymer VS-Co and phosphonate DETPMP over a wide range of temperatures. Recommendations are given on the application conditions at which the phosphate ester scale inhibitors perform at their best.

Chapter 8 summarizes the main conclusions obtained in the study and shows how these findings address the problem outlined as the objective of the dissertation. Some suggestions for future work are also presented.

CHAPTER 2. LITERATURE REVIEW

In this Chapter, a critical review of the knowledge available on scale inhibitors applications in oil and gas fields is presented. The review covers different aspects of scale inhibitor applications, including the inhibitor chemistry, scale inhibition mechanisms, inhibitor retention and release mechanisms within the formation matrix. Finally, since the current study discusses precipitation squeeze treatments, a review of published work on the precipitation and dissolution processes of the scale inhibitor/divalent cations complexes is provided. Thereby, the Chapter will show how the studies conducted in this dissertation link to the previous work on scale inhibitor retention and release mechanisms.

2.1. Scale Inhibition Mechanism

Scale inhibitors applied in the oil and gas industry are water-soluble chemical compounds that are able to either prevent or retard mineral scale formation at threshold sub-stoichiometric concentrations (Sorbie and Laing 2004). Scale inhibition may operate mechanistically during any phase of the scaling process.

The main factor determining crystallization onset (i.e. scale formation) is supersaturation. Supersaturation refers to the increased concentration of the scale-forming ions currently dissolved in the solution above the amount that would be present at equilibrium. Thus, precipitation is a "reaction" of the system to bring the saturated solution to equilibrium. In oilfields, a supersaturated state occurs when incompatible waters, such as formation and sea water brines, containing high amounts of scale-forming ions are mixed in the production flow systems, or when the thermodynamic conditions, i.e. temperature and pressure, are changing, for example, while produced fluids move along a production well towards top side facilities (Vetter and Farone 1987, Zhang, Shaw et al. 2001, Mackay, Jordan et al. 2003, Ramstad, Tydal et al. 2005).

Crystallization is a complex multistep process, which generally occurs through the following steps (Al-Roomi and Hussain 2016):

- *Aggregation.* When scale-forming anions and cations come together and form a cluster of micro-nuclei, or embryo-crystals.

- *Nucleation.* Some of those micro-nuclei grow further into nuclei. Nucleation may occur on a surface, which is known as heterogeneous nucleation, or in the bulk solution, as homogeneous nucleation. Generally, scale formation occurring in oil and gas production systems is a combination of both types of nucleation (Al-Roomi and Hussain 2016).
- *Crystal growth.* Nuclei, after achieving a certain size, start agglomerating and grow into a crystalline structure.
- *Agglomeration.* The crystals continue to grow into a larger scale deposit through adsorption of scale-forming ions from the solution.

It has been reported, that adsorption of scale inhibitor species on the surfaces of nuclei or crystals, blocks the active growth sites of sulphate and carbonate crystals (Raistrick 1949, Otani 1960, Breen, Diel et al. 1990, Benton, Collins et al. 1993). This causes a thermodynamic instability of the crystals and also increases the energy barrier for further crystal growth (Benton, Collins et al. 1993). In addition to adsorption, it is suggested that polymeric scale inhibitor molecules can chelate scale-forming ions, reducing the saturation ratio (Sarig and Raphael 1972).

Scale inhibitors predominantly operate during one of the crystallization stages. They can prevent or retard the crystallization process mechanistically through either nucleation inhibition, or crystal growth retardation (Graham, Boak et al. 2003). Most inhibitors operate through *both* crystal growth retardation and nucleation inhibition mechanisms, even though usually one mechanism predominates, depending on the chemistry of the scale inhibitor (Sorbie and Laing 2004).

Recent work shows that divalent cations, present in the formation or sea water brines where scale inhibitor is deployed, have a significant impact on the scale inhibition mechanism, thereby giving more detailed insight on the scale inhibition mechanism (Boak, Graham et al. 1999, Graham, Boak et al. 2003, Shaw, Sorbie et al. 2012, Shaw, Sorbie et al. 2012). Calcium cations (Ca^{2+}) have a positive effect on the inhibition efficiency of the scale inhibitors, increasing the concentration of Ca^{2+} significantly improves their performance. Magnesium cations (Mg^{2+}) are found to “poison” the scale inhibitors which results in performance decline when Mg concentration in the solution is increasing.

This is because phosphonate scale inhibitors can form complexes with both Mg^{2+} and Ca^{2+} cations via chelating mechanisms. These complexes, rather than "free" scale inhibitor ions, are involved in the scale inhibition mechanism. Because the scale inhibitor/Ca complex has an appropriate size, that can be incorporated into the barium sulphate crystal lattice and retards its further growth. This means these complexes have a significant role in barium sulphate scale inhibition (Shaw, Sorbie et al. 2012). The scale inhibitor/Mg complexes however have a smaller size that is not compatible with the crystal lattice size of barium sulphate, thus it does not affect the crystal growth. As the scale inhibitor chelated with Mg^{2+} is not involved into the inhibition process, therefore Mg^{2+} are believed to "poison" the inhibitor. Schematics shown in Figure 2.1 describe how the scale inhibitor/calcium complex, denoted as Ca-SI, can influence the crystal growth behaviour.

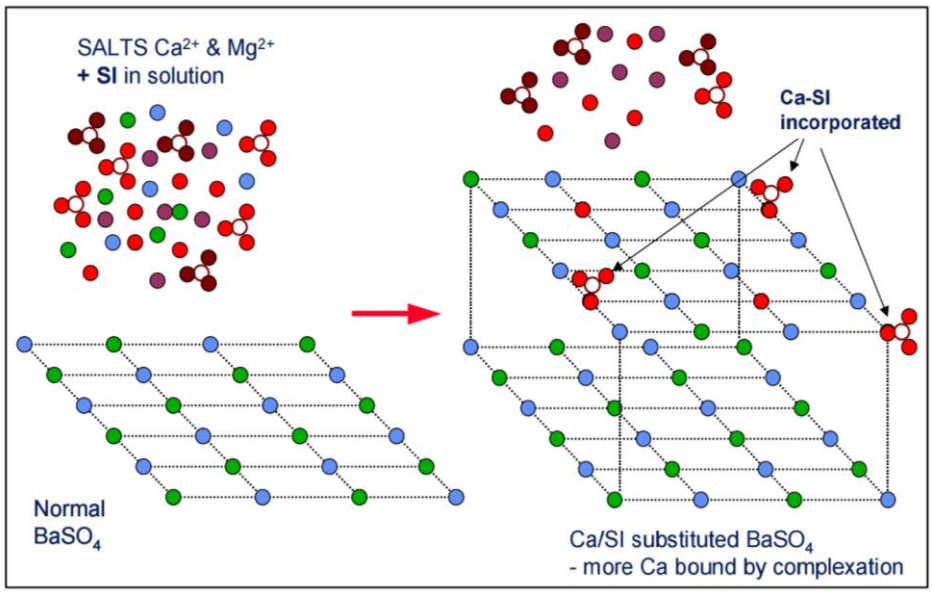

Figure 2.1 SI/Ca^{2+} complex incorporation into the barite lattice (Sorbie and Laing 2004)

Consequently, the minimum inhibition concentration (MIC) also depends on the Mg^{2+}/Ca^{2+} molar ratio in brine. It was found for phosphonate scale inhibitors DETPMP, OMTHP, HMDP and HMTPMP, that MICs generally decrease when the Mg/Ca ratio decreases in the system (Shaw, Sorbie et al. 2012). In field applications, this is going to have a significant effect, since the Mg/Ca ratio in produced brine changes over the production period. During the initial stages of production, the produced brine composition is mainly linked to the formation water composition, where the Mg/Ca ratio is close to 0. However, once the injected sea water breaks through, the produced brine composition

changes, and the Mg/Ca ratio starts increasing. Therefore, the Mg/Ca ratio in the produced brine needs to be monitored continuously to allow the control of scale precipitation.

Low molecular weight (below 10,000 Da) polymeric scale inhibitors PPCA and PVS show no sensitivity to the presence of Mg^{2+} ions, in respect to their performance against barium sulphate scale, but this was found only in low salinity systems (Boak, Graham et al. 1999). In other inhibition efficiency studies (Shaw, Sorbie et al. 2012), conducted at higher salinity and higher saturation ratios for 9 polymeric scale inhibitor species, Mg was found to be detrimental to the performance of all inhibitors.

The highest inhibition efficiencies for polymeric inhibitors were recorded when the Ca^{2+} concentration in the brine stayed within 1000-2000 mg/L. At higher concentrations, incompatibility between inhibitor and Ca^{2+} leads to precipitation of the inhibitor decreasing the amount of dissolved SI available in brine and hence a lower inhibition efficiency performance.

In addition to alkaline earth metals, like Ca^{2+} and Mg^{2+}, other divalent cations also can affect the inhibition efficiency of scale inhibitors. For example, a trace level of zinc ions Zn^{2+} is found to enhance the inhibition efficiency of phosphonate inhibitors BHPMP and DTPMP, but shows no effect on the efficiency of polymeric PPCA (Kan, Fu et al. 2009). The complexation occurs between Zn and the amine group, that only the phosphonate inhibitors molecules contain. Generally, Zn ions are not naturally available in produced brines at high concentration, thus, it may be added into the injected scale inhibitor pill prior to injection.

2.2. Oilfield Scale Inhibitors

The most common classes of scale inhibitors applied in the industry and reported in recent literature are organic phosphonates, phosphate esters and organic polymers (Lawless, Bourne et al. 1993). In most cases, scale inhibitors are applied individually, even although they can be designed or expected to have combined scale and corrosion inhibition properties (Lawless, Bourne et al. 1993, Fan, Bain et al. 2002, Wylde, Turner et al. 2017). General recommendations on the selection process for scale inhibitors for barium sulphate inhibition are available (Shaw, Sorbie et al. 2012), where the classification of phosphonate and polymer inhibitors, based on their sensitivity to the saturation ratio of brine salinity and Mg/Ca ratio, has been developed.

Shaw and Sorbie (2015) show the synergetic effect of using blends of phosphonate and polymeric SIs. The MICs of blends are found to be significantly lower than that of the individual compounds (tested at the total blend concentration). This is due to the different inhibition mechanism each component of the blend predominantly performs through. Phosphonates operate mainly as crystal growth retardants, whereas polymers are excellent nucleation inhibitors. Therefore, having both compounds in the injected scale inhibitor pill targets both processes simultaneously, reducing consumption of the chemicals. However, there is no evidence on using the scale inhibitor blends in oilfield applications in the literature.

2.3. Weak Polyacid Theory

Most of the scale inhibitors applied in oilfields are weak polyacids, that can be denoted as H_nA (Todd, Savin et al. 2012, Shaw and Sorbie 2014). The degree of dissociation of scale inhibitors is determined by dissociation constant *pK* and this is a function of solution pH. Figure 2.2 illustrates the speciation of phosphonate scale inhibitor DETPMP, denoted as $H_{10}A$, over a wide pH range, which occurs according to the following chemical equations 2.1 – 2.10.

$$H_{10}A \leftrightarrow H_9A^- + H^+ \qquad K_1 = [H^+] \cdot [H_9A^-] / [H_{10}A] \tag{2.1}$$

$$H_9A^- \leftrightarrow H_8A^{2-} + H^+ \qquad K_2 = [H^+] \cdot [H_8A^{2-}] / [H_9A^-] \tag{2.2}$$

$$H_8A^{2-} \leftrightarrow H_7A^{3-} + H^+ \qquad K_3 = [H^+] \cdot [H_7A^{3-}] / [H_8A^{2-}] \tag{2.3}$$

$$H_7A^{3-} \leftrightarrow H_6A^{4-} + H^+ \qquad K_4 = [H^+] \cdot [H_6A^{4-}] / [H_7A^{3-}] \tag{2.4}$$

$$H_6A^{4-} \leftrightarrow H_7A^{5-} + H^+ \qquad K_5 = [H^+] \cdot [H_5A^{5-}] / [H_6A^{4-}] \tag{2.5}$$

$$H_5A^{5-} \leftrightarrow H_7A^{6-} + H^+ \qquad K_6 = [H^+] \cdot [H_4A^{6-}] / [H_5A^{5-}] \tag{2.6}$$

$$H_4A^{6-} \leftrightarrow H_7A^{7-} + H^+ \qquad K_7 = [H^+] \cdot [H_3A^{7-}] / [H_4A^{6-}] \tag{2.7}$$

$$H_3A^{7-} \leftrightarrow H_7A^{8-} + H^+ \qquad K_8 = [H^+] \cdot [H_2A^{8-}] / [H_3A^{7-}] \tag{2.8}$$

$$H_2A^{8-} \leftrightarrow H_7A^{9-} + H^+ \qquad K_9 = [H^+] \cdot [H_1A^{9-}] / [H_2A^{8-}] \tag{2.9}$$

$$HA^{9-} \leftrightarrow A^{10-} + H^+ \qquad K_{10} = [H^+] \cdot [A^{10-}] / [HA^{9-}] \tag{2.10}$$

The phosphonate species become more dissociated, or deprotonated, when pH increases (Figure 2.2). Also, dissociation constant K, decreases when moving to the next

dissociation step: for DETPMP the *p*K (logarithmic scale) varies from $pK_3 = 2.8$, to $pK_7 = 7.17$, and $pK_{10} = 12$.

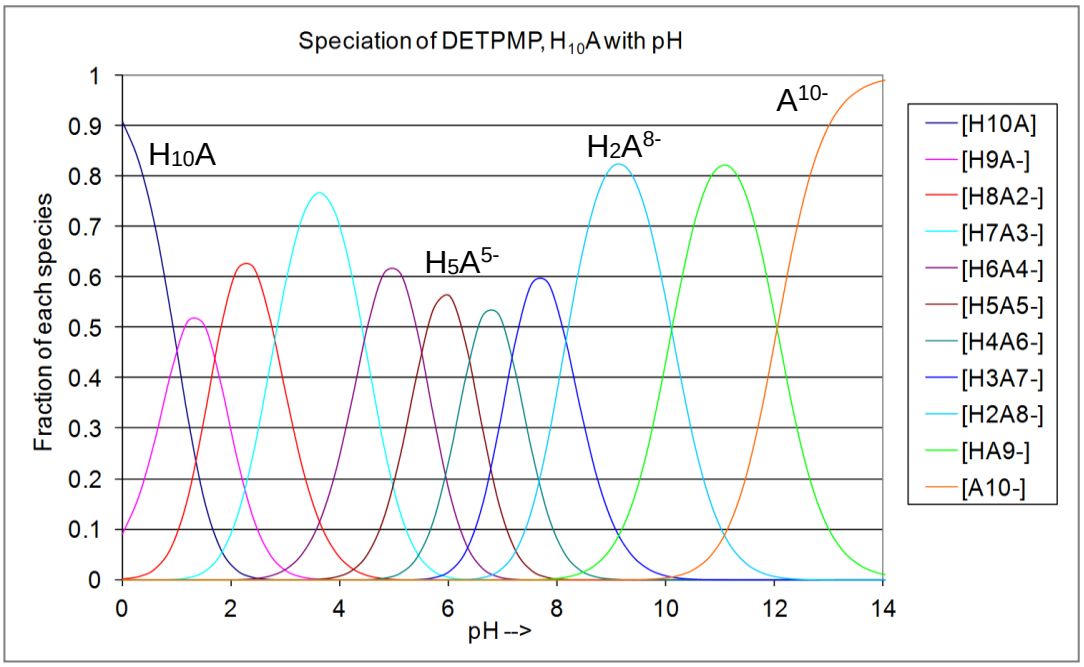

Figure 2.2 DETPMP speciation over pH range

The degree of dissociation of a scale inhibitor defines its *inhibition efficiency*, which improves as pH increases. Each functional group within the inhibitor molecule has a different dissociation versus pH and different inhibition efficiency at a given pH. Polymeric inhibitor PPCA, that contains both phosphonate and carboxylic groups in the molecule, gives almost no dissociation at pH 2, therefore poor performance at low pH, and nearly complete dissociation and maximum performance at pH 7.22. In contrast, strongly acidic functional groups, such as sulphonic acid, $-SO_3H$, will be completely dissociated to $-SO^{3-}$ even at low pH values. Thereby, incorporation of vinyl sulphonic acid groupings into the backbone of polyacrylate inhibitors has been shown to enhance barium sulphate inhibitor efficiency at the lower pH values. This is beneficial for fields that produce low pH fluids.

2.4. Polymeric Scale Inhibitors

Generally, polymeric SIs used in oilfields are relatively low molecular weight species (up to 10,000 Da). The most commonly used polymeric species are shown below in Figure 2.3: PPCA (phosphino polycarboxylic acid), PVS (poly-vinyl sulphonate), and VS-Co

(vinyl sulphonate acrylic acid copolymer) (Jordan, Sorbie et al. 1997, Poynton, Kelly et al. 2004, Shaw, Sorbie et al. 2012, Farooqui and Sorbie 2016).

Polymeric scale inhibitors PVS and VS-Co perform quite well even at lower pH values, since PVS generally occurs in a highly dissociated state even in a lower pH due to the high dissolution constant of the sulphonate groups. Polymeric scale inhibitors represent a wide group of chemicals, thus, not all polymers perform through identical mechanisms. In contrast to PVS and VS-Co, PPCA is more effective at higher pH. PPCA contains both carboxylic and phosphonate groups, means it does not act as a classic polymer but shows similar trends to phosphonate scale inhibitors (Shaw, Sorbie et al. 2012).

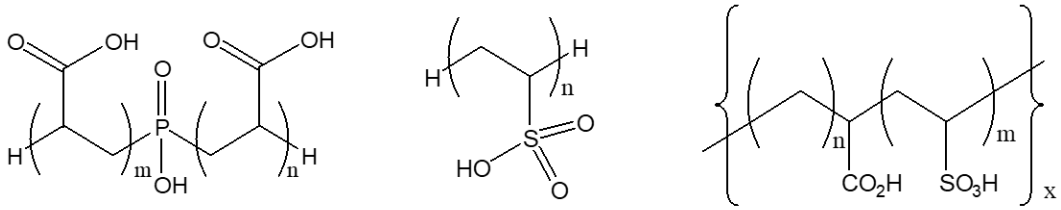

Phosphino polycarboxylic acid **PPCA**

Sulphonated polyacrylic acid co-polymer **VS-Co**

Polyvinyl sulphonate **PVS**

Figure 2.3 Common types of polymeric scale inhibitors used in the oil and gas industry

In a standard static inhibition efficiency test, polymers perform significantly better at the short term 2-hour test, compared to the longer term 22-hour test. Polymers also perform better than phosphonate scale inhibitors in dynamic tube blocking test (TBR), where scale inhibitors are assessed under dynamic flow conditions. This is due to the fact, that polymeric SIs predominantly inhibit nuclei that form at the initial stages of scaling process. Thus, polymers performance is highest in a short-term test, before crystal growth onset occurs. PVS is a classic example of a polymeric inhibitor with weak metal binding properties, thus, it has very limited crystal growth inhibition properties, but works predominantly through the nucleation inhibition mechanism.

PPCA can work equally well through both nucleation inhibition and crystal growth retardation, even though it is gradually consumed with time into the lattice of growing crystals (Graham, Boak et al. 2003). Phosphonate groups within the PPCA polymeric species can bind Ca^{2+} cations (Xiao, Kan et al. 2001) which perform crystal growth retardation.

2.5. Phosphonate Scale Inhibitors

The chemical structures of some phosphonate species used in oilfields are shown in Figure 2.4. Phosphonates are recognised as one of the most important groups of oilfield scale inhibitors, particularly against sulphate and carbonate scales and offer several advantages such as (Browning and Fogler 1995):

- Phosphonates are able to inhibit scale at threshold concentrations (parts per million) and show excellent performance even at those lower concentrations.
- Phosphonates have a good thermal stability over a wide temperature range and pH, thus they can inhibit scale in different reservoirs and at various conditions.
- Phosphonates inhibit different types of scale, making them flexible from well to well.
- Phosphonates can be easily detected in the produced brine by the fast, routine and well-established Inductively Coupled Plasma technique (by detection of phosphorus).

The chemical properties of phosphonate scale inhibitors can be fully described by the weak acid dissociation theory presented earlier in section 2.3.

Phosphonate species can bind divalent cations, such as Ca^{2+}, Mg^{2+}, Ba^{2+}, Sr^{2+} etc., forming complexes denoted as SI_M_n, where *n* is the molar ration of cations to scale inhibitor, or stoichiometry. Stoichiometry is a function of pH: with increasing pH, the number of divalent cations bound to the SI molecule also increases. As mentioned earlier, the SI/Ca complexes are involved in the scale inhibition through a crystal growth retardation mechanism (Boak, Graham et al. 1999, Graham, Boak et al. 2003, Shaw, Sorbie et al. 2012, Shaw, Sorbie et al. 2012).

There is a relationship between the structure of metal/phosphonate SI complexes and SI performance that was shown by Shaw, Welton et al. (2012). The best performance is going to be shown by the phosphonate species that can form the most stable 5- and 6-membered complexes, i.e. hexa-phosphonate OMTHP, and penta-phosphonates DETPMP and HMTPMP.

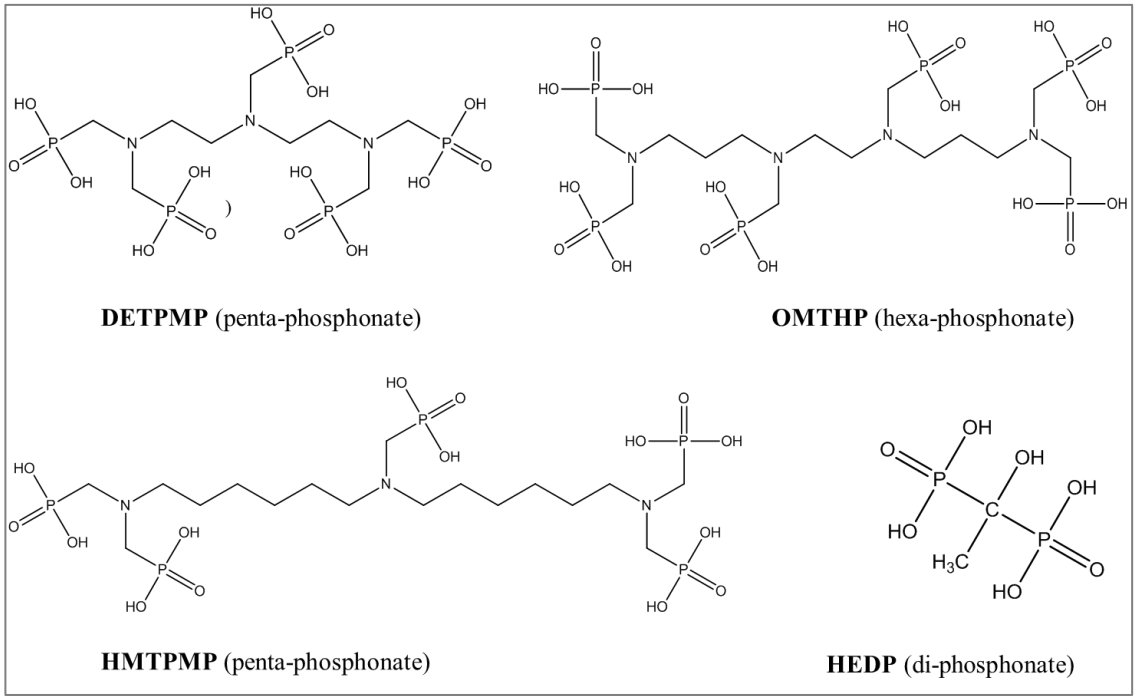

Figure 2.4 Common organophosphonate scale inhibitors

2.6. Inhibitor Retention Mechanisms

Squeeze treatments were first introduced in the 1950s in corrosion inhibitor applications (Poetker and Stone 1956). Later, this technique was also implemented for scale inhibitor deployment.

The two main mechanisms of scale inhibitor retention occurring in formation rock are adsorption and precipitation although both can be described by one coupled adsorption/precipitation model (Sorbie 2010, Vazquez, Sorbie et al. 2010). There is no clear-cut line between these two types of squeezes, both mechanisms can occur together depending on the chemistry of the scale inhibitor and on the formation brine parameters such as divalent cations concentration, pH and temperature. The primary factors, determining inhibitor retention in squeeze treatments are scale inhibitor concentration and pill pH, rock mineralogy and temperature. Mineralogy, in the case of carbonate rocks, will affect the nature of the cations that are going to be released (dissolved) into the bulk solution during the injection of the acidic inhibitor pill, thereby changing the apparent brine composition. This resulting brine composition will then determine the nature of the precipitated scale inhibitor/metal complexes, and therefore, the solubility and subsequent concentration of the inhibitor in the return brine.

Both adsorption and precipitation can occur in the reservoir, regardless of the formation minerology. However, precipitation reactions occurring in sandstone and carbonate reservoirs is based on different interactions. An acidic inhibitor pill injected into a carbonate formation causes rock dissolution, thereby releasing ions, mainly Ca^{2+} and Mg^{2+}, which in turn interact with the scale inhibitor ions yielding SI/divalent cation precipitates with a lower solubility (i.e. rock/inhibitor interaction). The conditions under which the reactions occur determines the chemical characteristics of the SI/metal solid complexes, for example its solubility (Kan, Fu et al. 2004, Jarrahian, Sorbie et al. 2018). For sandstone formations, due to its mineralogy, usually negligible amounts of cations are released from the rock into solution. If precipitation occurs in sandstone reservoir, it is due to interaction between the scale inhibitor and cations in the injected "squeeze" brine (i.e. brine/inhibitor interaction).

Mineralogy can significantly affect scale inhibitor adsorption onto the rock surface. Adsorption occurs via Van-der-Waals interactions between the inhibitor and formation (Sorbie, Jiang et al. 1993). Generally, adsorption depends on temperature, pH, rock minerology, brine composition and ionic strength, and very significantly on the chemistry of the scale inhibitor that is used (Zhang, Mackay et al. 2000). Adsorption of phosphonate scale inhibitors onto the negatively charged silica sand surface is higher at lower pH, since the species are less dissociated and less negatively charged or even neutral (Kan, Yan et al. 1991, Sorbie, Jiang et al. 1993). However, when divalent cations (like Ca^{2+}) are present in the system, the adsorption of inhibitor may be lower at pH 4, than at both pH 2 and pH 6. This is caused by a relative weakening of both the hydrogen bonding, when moving from pH 2 to pH 4, and calcium binding mechanisms, which is higher at pH 6, therefore the entire inhibitor/calcium complex can adsorb on the negatively charged silica through Ca^{2+} (Sorbie, Jiang et al. 1993). Adsorption of phosphonate scale inhibitors can be enhanced by increasing the contact time and surface area between the scale inhibitor solution and sandstone core (Kan, Yan et al. 1991). Calcite formation rock generally carries a positive charge; therefore, the adsorption of phosphonate inhibitors is greater at the higher pH.

The adsorption isotherm usually denoted $\Gamma(C)$, is a function that describes the relationship between the concentration of the scale inhibitor on the rock surface and in the bulk solution, that is in a contact with the rock. The adsorption isotherm is an input parameter to the squeeze design simulator, which is used to predict the return profile of the scale

inhibitor after the treatment, which is generally derived from the experimental core flood data. The adsorption isotherm has two simple analytical forms, that are commonly used in the field and are referred to as the Freundlich and Langmuir adsorption isotherms. A Freundlich isotherm is described by the equation:

$$\Gamma(C) = kC^{n} \tag{2.11}$$

The Langmuir isotherm is given by:

$$\Gamma(C) = \frac{a*\Gamma max*C}{1+aC} \tag{2.12}$$

Where Γ (C) –mass of adsorbed inhibitor (in mg) per g of rock; a, k, n – coefficients that depend upon adsorbent and inhibitor conditions; C – concentration of the inhibitor in solution; Γmax – maximum amount of adsorbed material in the current conditions.

Precipitation, or "phase separation" scale inhibitor treatments are usually carried out to extend the squeeze lifetime (Browning and Fogler 1995). Precipitation squeeze treatments are based on a chemical reaction between a scale inhibitor and divalent cations where the mixed complexes SI_M_n of lower solubility are formed (equation 2.13), where SI is partially deprotonated phosphoric acid, M – divalent cation, SI_M_n – metal/inhibitor complex, and n is a stoichiometric coefficient:

$$SI + nM^{2+} \leftrightarrow SI\_M_n \tag{2.13}$$

The key parameters for precipitation treatments leading to a controlled SI release within the porous medium are (i) the SI (complex) solubility *Cs* and (ii) the kinetic dissolution rate *r* (Browning and Fogler 1995, Sorbie 2012). Hence, in terms of precipitation squeeze treatments, SI solubility and kinetic dissolution rate parameters control the level of SI concentration released and the overall treatment lifetime in the precipitation squeezes. Solubility depends on several factors, such as the nature of SI and the divalent cation (mainly Ca^{2+} and Mg^{2+}, but also Ba^{2+}, Sr^{2+} and Fe^{2+}), the brine composition and pH, the precipitation temperature (T), the rock mineralogy etc.

Injecting different divalent cations such as Ca, Mg, Fe, and Zn within the inhibitor pill can give another degree of freedom for controlling the precipitation and hence the return of the inhibitor after the squeeze treatment (Tomson, Kan et al. 2008, Kan, Fu et al. 2009).

Authors suggest that Fe, Zn and Ca ions can extend the return of phosphonate SIs DTPMP and BHPMP. This is due to the SI/Fe and SI/Zn complexes generally having a lower solubility. For example, an Fe^{2+} complex with NTMP scale inhibitor $Fe_{2.5}$HNTMP has a solubility product of ~10^{-33}, which is considerably lower than the solubility products of NTMP/Ca^{2+} precipitates, ~10^{-19} (Friedfeld, He et al. 1998) or ~10^{-22} (Tomson, Kan et al. 2004). If the inhibitor needs to be produced at higher concentrations, Mg^{2+} can be added to increase the return level of the inhibitor. These ions can improve the retention of the chemistry if added at a molar ratio of 0.1:1 to the scale inhibitor.

Sometimes, formation damage concerns from applying precipitation treatments may arise. Browning and Fogler (1995) have observed significant formation damage resulting from calcium-HEDP precipitation in a core flooding experiment. However, the damage incurred during the precipitation reaction was restored, probably by re-dissolution of the precipitated complex, during the first 10% of the treatment lifetime. In such cases, this effect would be more of a clean-up issue, rather than being more permanent formation damage.

2.7. Scale Inhibitor Retention Modelling

There are different but related modelling approaches to describe scale inhibitor retention within formation rock during squeeze treatment. The main three "schools of thought" describe the scale inhibitor retention as follows:

1. Researchers from *Heriot-Watt University (Flow Assurance and scale Team)* determine the SI retention through generalised adsorption isotherm, Γ (C); precipitation is determined by a solubility function, Π (C), and a dissolution rate constant. Both processes are described through one coupled adsorption/precipitation model (Kan, Yan et al. 1991, Sorbie, Yuan et al. 1991, Sorbie, Wat et al. 1992, Sorbie and Gdanski 2005).

2. Researchers from *Halliburton* developed individual adsorption models that match the specific formation mineralogy (Gdanski and Funkhouser 2005, Gdanski 2008). The authors focus only on the adsorption treatments, trying to avoid any precipitate formation during the squeeze operation, as it raises formation damage concerns.

3. *Rice University (Brine Chemistry Consortium)* describes the SI retention by adsorption mechanism at low SI concentrations (up to 1%) and by precipitation mechanism at higher concentrations which is based on the solubility of the various SI/Ca precipitates (Kan, Fu et al. 2004, Tomson, Kan et al. 2004, Tomson, Kan et al. 2008). This approach mainly describes scale inhibitor retention in carbonate-rich fields and it is based on the following two reactions. The first reaction is calcite dissolution due to the low pH value of the inhibitor pill. Subsequently, the dissolution rate decreases due to the surface poisoning effect by the SI coating the surface. The second reaction is precipitation of SI/Ca solids.

Joint research by the Heriot-Watt University and Halliburton groups (Sorbie and Gdanski 2005) compared the above approaches, giving suggestions on which approach should be applied in order to obtain better field data prediction for different scenarios. More recent work has shown that the SI squeeze can be described either by a pure adsorption process, governed by $\Gamma(C)$ or as a coupled adsorption /precipitation process, denoted Γ/Π (Sorbie, 2010; Vazquez et al, 2010; several works by Shaw and Sorbie; Jarrahian et al, 2018). Which mechanism, and associated mathematical description, applies in a particular situation depends on a range of conditions as discussed above.

2.8. Phosphonate Inhibitor Complexation

Since the current research covers precipitation squeeze treatments, the following section of the literature review is focused on highlighting the knowledge generated by numerous worldwide research groups on the precipitation and dissolution processes of the scale inhibitor/divalent cation complexes. The main research schools working on the fundamentals of scale inhibitor precipitation and dissolution processes with the focus on their application in squeeze treatments are Brine Chemistry Consortium of Rice University, Michigan University, and the Flow Assurance and Scale Team at Heriot-Watt University.

2.8.1. *Rice University Brine Chemistry Consortium*

As mentioned earlier, this group's approach in modelling the scale inhibitor return profile is that the return of a scale inhibitor is governed by an adsorption isotherm at the lower

inhibitor concentrations, whereas precipitation/dissolution mechanisms operate at higher inhibitor concentrations (Kan, Fu et al. 2004). However, the main focus of the research within the Consortium is on the fundamentals of the scale inhibitor precipitation process and on developing the precipitation model, since the inhibitor concentration injected during the squeeze treatments is usually quite high (over 1%).

A number of papers from the group describe the stoichiometry of phosphonate /Ca precipitates, along with the factors defining the stoichiometry. It is shown, that the stoichiometry is mainly a function of solution pH, but also of temperature, ionic strength (Kan, Fu et al. 2005). In (Kan, Fu et al. 2004, Tomson, Kan et al. 2004, Kan, Fu et al. 2009). It was found that the reaction conditions determine not only the stoichiometry of the phosphonate precipitates that form, but also their structure. Both *amorphous* and *crystalline* calcium/phosphonate scale inhibitor precipitates were observed forming during the precipitation reactions; the initial structure will depend mainly on solution pH.

This phase structure will define the chemical and physical properties of the precipitate, affecting its solubility and therefore the return concentrations of the inhibitor after the squeeze treatment. Authors report two crystalline Ca/NTMP and one amorphous Ca/NTMP precipitates that were forming in (Kan, Fu et al. 2004). Using the speciation model, the solubility products of these calcium/NTMP precipitates, but also of other inhibitors complexes with divalent cations (DTPMP, BHPMP and polymer PPCA) were calculated as a function of ionic strength and temperature. It was the crystalline phase of the calcium/NTMP precipitate that had the lowest solubility product, with a logarithmic constant equal to $pK_{sp} = 24.2$, whereas the amorphous phases had considerably higher solubilities of $pK_{sp} = 22.6$ and $pK_{sp} = 21.3$, respectively.

In the same study (Kan, Fu et al. 2004, Kan, Fu et al. 2009), the authors show for three phosphonate (NTMP, DTPMP and BHPMP) and the polymeric PPCA inhibitor, that the inhibitor/calcium precipitates that form initially (straight after the inhibitor is mixed with calcium) are *amorphous* solids with higher solubility. However, the amorphous phase is stable only until fresh solution starts flowing over the precipitates. The flow initiates the crystalline phase development, although the transition is not found to be affected by increasing flow rates, but rather by the cumulative brine volume. Since the crystalline phase is much less soluble than the amorphous one (around 2 orders of magnitude for

Ca/NTMP and 1 order for Ca/DTPMP complexes), this leads to the precipitate's solubility variation (Kan, Fu et al. 2004).

In another study, the authors define three distinguish phases, or regions, in the inhibitor return profile for the precipitation squeeze treatments (Tomson, Kan et al. 2008):

- *Phase 1:* return of the chemical that has not been retained within the rock (short phase, ~ first 3 pore volumes).
- *Phase 2:* dissolution from the highly soluble *amorphous* phase.
- *Phase 3:* dissolution from the *crystalline* phase with lower solubility.

In their latest work (Zhang, Shen et al. 2016), the existence of an additional "middle" phase of the $Ca_{2.5}$DETPMP precipitate is reported, which is, basically, the transitional state between the amorphous and crystalline phases. This middle phase has a typcal crystalline structure with sharp edges and more regular shape, observed via XRD and SEM images, however its solubility is higher than that of the "pure" crystalline phase.

Another study was dedicated to the interaction between calcite rock and a scale inhibitors (Kan, Fu et al. 2004). Results show, that the scale inhibitor retention and return in carbonate rocks are predominantly controlled by the scale inhibitor concentration and pills' pH (or acidity). Once the acidic inhibitor pill is injected, the rock dissolution reaction occurs with Ca^{2+} and CO_3^{2-} being released into the bulk solution, this results in a new equilibrium pH having to be established in the system. In addition, the inhibitor/calcium precipitation itself causes pH variation. Both reactions occuring in the calcite/scale inhibitor system determine the final established pH and therefore, will define the inhibitor retention.

At higher phosphonate concentrations, the calcite surface becomes covered with multiple layers of adsorbed scale inhibitor ions (up to 20 molecular layers) which is known as the calcite surface "poisoning" effect. As a consequence, the rock cannot be further dissolved and retention occurs due to mixed calcium/phosphonate SI solid phase precipitation. However, since there are less CO_3^{2-} anions dissolved in the bulk solution, its pH is more acidic, which makes the inhibitor/calcium complexes more soluble, therefore, the amount of precipitation and retention in general are limited by the surface poisoning effect (Kan, Fu et al. 2004).

To enhance the retention of scale inhibitors and extent the squeeze lifetime, there are studies dedicated to the interaction of scale inhibitors with transition metals, such as Fe^{2+}, Zn^{2+}, Co^{2+}, Ni^{2+}, Cu^{2+} (Tomson, Kan et al. 2008, Kan, Fu et al. 2009). The most common divalent cations found in formation or sea water brines are Ca^{2+}, Mg^{2+}, Ba^{2+}, and Sr^{2+}. The complexation of those ions with scale inhibitors is the primary mechanism in precipitation squeeze treatments. However, scale inhibitors can bind not only the alkaline earth cations, mentioned above, but also transition metals, such as Fe^{2+}, Zn^{2+}, Co^{2+}, Ni^{2+}, Cu^{2+} cations. The binding constant of transition metals to ligands, for example to the phosphonate group of a scale inhibitor, is higher than alkaline earth metals. The metal/ligand complex stabilities increase in the order: $Ca^{2+} < Mn^{2+} < Fe^{2+} < Co^{2+} < Ni^{2+} < Cu^{2+} \approx Zn^{2+}$ (Kan, Fu et al. 2009). With increasing the complex stability, the solubility of the complexes should decrease, thus, a longer return lifetime is expected. The experimental study on the effect of including these metal additives in a scale inhibitor pill shows that Zn improved the BHPMP inhibitor retention from 29% to 90%, and PPCA retention from 38 to 83%. The normalised squeeze lifetime was found to increase by a factor of 6 for polymeric PPCA, and by a factor of 66 for the phosphonate BHPMP, all due to the inclusion of Zn in the inhibitor pill (Kan, Fu et al. 2009).

2.8.2. *Michigan University*

The studies on the stoichiometry and morphology of various phosphonate scale inhibitor precipitates have been conducted at Michigan University (Browning and Fogler 1995, Browning and Fogler 1995, Browning and Fogler 1996, Browning and Fogler 1996, Browning and Fogler 1996a, Pairat, Sumeath et al. 1997, Tantayakom, Fogler et al. 2004, Tantayakom, Fogler et al. 2005, Tantayakom, Fogler et al. 2005). The conclusions from these studies confirm the ones of Rice University Brine Chemistry Consortium.

Both solution pH and the molar ratio of Ca/HEDP and Ca/AMTP available in a brine are found to affect the chemical-physical properties of the forming precipitates (Browning and Fogler 1995, Browning and Fogler 1996, Browning and Fogler 1996a). By varying these parameters, the distinct inhibitor/calcium precipitates with different stoichiometry (i.e. calcium to inhibitor molar ratio) can form (Pairat, Sumeath et al. 1997). For example, below pH 3.9 all the resulting Ca/HEDP precipitates were found to be 1:1 precipitates, whereas above pH 4.7 - 2:1 precipitates. With increasing solution pH, the molar ratio of calcium to scale inhibitor in the precipitate increases, as the degree of dissociation of a

scale inhibitor increases, which leads to a greater amount of the precipitate forming, which is of interest from an application point of view (Tantayakom, Fogler et al. 2004, Tantayakom, Fogler et al. 2005).

The stoichiometry is found to determine the phase structure and morphology of the precipitates (Browning and Fogler 1996). When the stoichiometry decreases, the precipitate state transfers from amorphous to crystalline (Figure 2.5). Pairat, Sumeath et al. (1997) show, that a Ca/ATMP solid with stoichiometry 1:1 has a crystalline sheet-like structure, whereas both the 2:1 Ca/ATMP and 3:1 Ca/ATMP precipitates were characterised as amorphous spherical-shaped materials.

The chemical nature of the phosphonate scale inhibitor may also have an impact on the precipitate's morphology. As in the example mentioned above for the tri-phosphonate ATMP/Ca precipitate, the stoichiometry will affect the morphology of the particles. However, in the case of penta-phosphate DETPMP, no significant morphological difference was observed for precipitates with different stoichiometry. The DETPMP particles do not appear as a single particle, but rather as agglomerates (Tantayakom, Fogler et al. 2005), therefore, when comparing the dissolution rates of both ATMP/Ca and DETPMP/Ca precipitates, the DETPMP complex is found to dissolve slower. Thus, DETPMP has a potential application in precipitation treatments as it may give longer squeeze lifetimes.

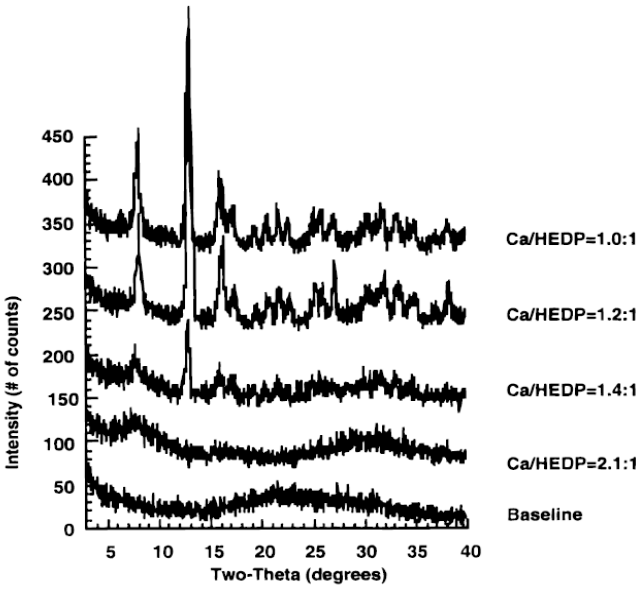

Figure 2.5 X-ray diffraction patterns of the calcium-HEDP precipitates versus the precipitate stoichiometry (Browning and Fogler 1996)

Their flooding test results show the crystalline 1:1 precipitate dissolves faster than the amorphous 2:1 precipitate (Browning and Fogler 1996), which is in agreement with the mathematical model developed for the 2:1 Ca/HEDP precipitate dissolution process in porous media. Pairat, Sumeath et al. 1997 have shown that the longest lifetime during the flooding tests was obtained for the Ca/ATMP precipitate with the higher stoichiometry 3:1, whereas the 1:1 precipitate showed the shortest lifetime. Thus, the authors suggest using the *amorphous* 3:1 calcium-ATMP precipitate for squeeze treatments, since this was released from the porous medium more slowly, giving a longer lifetime.

Browning and Fogler 1996 go on to a model for a scale inhibitor/Ca (HEDP/Ca) return curve that features 5 specific regions (Figure 2.6). For the precipitation reaction occurring *in situ* in a micromodel flooding rig. Time-lapse photographs taken during each regime are also shown in Figure 2.7 (Browning and Fogler 1996). The five regions are:

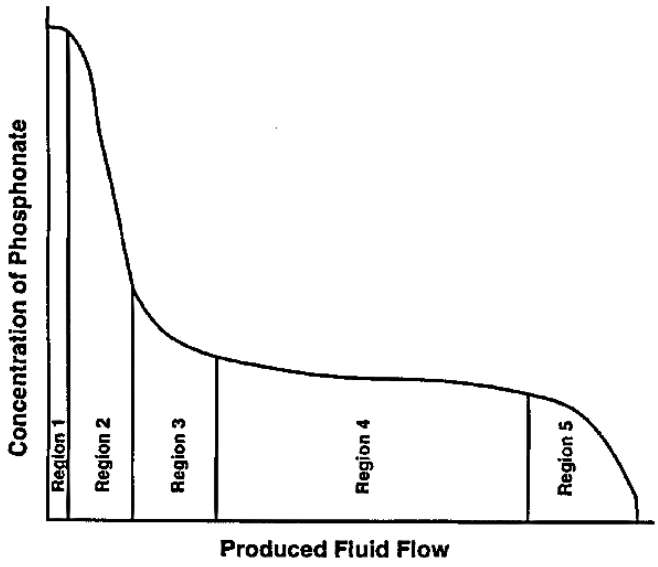

Figure 2.6 Scale inhibitor return resulting from the 1:1 HEDP/Ca precipitate dissolution (Browning and Fogler 1996)

1. First 1-2 pore volumes of the return brine contain saturated HEDP solution with loose fibrous particles of the HEDP/Ca precipitate that has not retained in the media.
2. Inhibitor return in the next region is governed by the dissolution of the fibrous particles that are not trapped within the pore throats, as these are in greater contact with the flooded fluid, compared to the trapped particles. The dissolution

is strongly affected by the hydrodynamics of flow around the fibres, i.e. by the flow rates.

3. Joint dissolution of both un-trapped particles and particles located in pore throats. In this regime, the dissolution rate is still governed by hydrodynamics.
4. Once the "free" bulk particles have dissolved, dissolution is *not* governed by the fluid rates, but rather controlled by diffusion from the fibrous surface to the pore throat entrance.
5. Migration of the precipitate from the pore throats is shown to determine dissolution at the last stages.

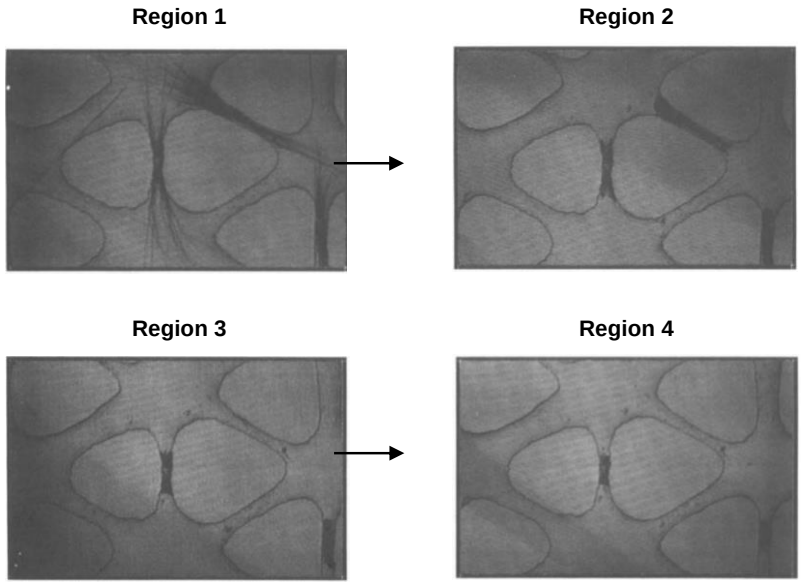

Figure 2.7 Release regimes of 1:1 HEDP/Ca precipitate (Browning and Fogler 1996)

An ideal squeeze treatment scenario is where precipitation does not occur immediately but some period of time after the scale inhibitor was pumped into a producer. This allows the SI pill to move through the near-wellbore area without precipitating and avoids formation damage. This can be achieved using an inhibitor pill of low inhibitor concentration and low pH, as well as being in the presence of monovalent (Li, Na, and K) and divalent (Sr, Ba and Mg) cations (Tantayakom, Fogler et al. 2005). The order of precipitation retardation for these cations is as follows: Li < Na < K< Sr < Ba < Mg. Retardation occurs due to the listed cations adsorbing onto the SI/Ca nuclei leading to an increase in the surface free energy of the SI/Ca complex, which delays precipitation.

Phosphonate scale inhibitor precipitation experiments were conducted in the presence of Mg and Ca ions, where dissolution rates and the morphology of the Ca/ATMP, Mg/ATMP, and Ca/Mg/ATMP precipitates were examined (Tantayakom, Fogler et al. 2004). It was found, that both dissolution rates of the phosphonate precipitates and their morphology primarily depend on the *total* number of cations bound to the scale inhibitor molecule, rather than on the individual Mg:SI and Ca:SI ratios. The dissolution rates decreased with increasing the total molar ratio of divalent cations to ATMP in the precipitate, which was also shown in their earlier work for HEDP di-phosphonate inhibitor (Browning and Fogler 1995).

In addition, it was found that the presence of Mg in the inhibitor pill can have both positive and negative impacts with respect to field applications (Tantayakom, Fogler et al. 2004). Mg ions can delay precipitation, allowing the inhibitor pill to pass the near-wellbore area as a single phase. However, the amount of the SI/Ca precipitate that is going to form is decreased due to the presence of Mg in the system, which results in shorter squeeze lifetimes (Tantayakom, Fogler et al. 2005).

2.8.3. *Heriot-Watt University*

Extensive studies on phosphonate complexation and precipitation processes have been performed by the Flow Assurance and Scale Team (FAST) at Heriot-Watt University.

Firstly, the stoichiometry *n* of the scale inhibitor/calcium complexes, denoted as SI_Ca_n, of 9 common phosphonate species was established experimentally (Shaw and Sorbie 2014). It was shown, that the number of calcium ions a scale inhibitor can bind at some specific conditions is a function of solution pH. The pH controls the speciation and dissociation degree of the scale inhibitor, which, in turn, determines the number of available binding sites within the phosphonate molecule. With increasing pH, the scale inhibitor molecule becomes more dissociated, therefore, the number of binding sites available within the molecule increases.

Another factor affecting the stoichiometry *n* is the chemical nature of the scale inhibitor. The more phosphoric and carboxylic functional groups the inhibitor molecule contains, the higher the Ca/SI ratio in the precipitate is likely to be. The presence of nitrogen atoms in the scale inhibitor structure increases the chelating capacity of the inhibitor, thus, the stoichiometry values are higher (Shaw and Sorbie 2014).

For the phosphonate scale inhibitors, the maximum theoretical number of binding sites is equal to the number of phosphonate groups within the molecule. An example of the tri-phosphonate NTP/Ca complex structure at higher pH (i.e. a higher degree of dissociation) is illustrated in Figure 2.8. The chelating capacity of calcium cations by inhibitor is believed to occur via the oxygen atoms of two phosphonate groups, as well as via the oxygen of the phosphonate group and the nitrogen (Shaw and Sorbie 2014, Shaw and Sorbie 2015).

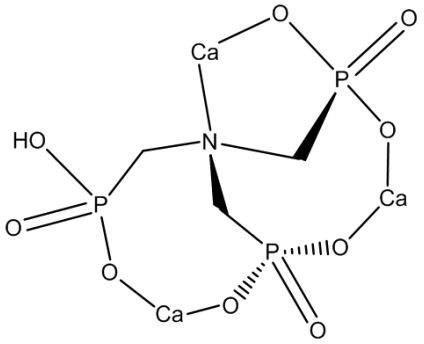

Figure 2.8 Ca/NTP complex at molar ratio Ca/SI = 3:1 (Shaw and Sorbie 2014)

If there is more than one type of divalent cations available in the brine, then scale inhibitors can form mixed metal complexes. The stoichiometry of bi- and tri-metal complexes, denoted as SI_Ca_{n1}_M_{n2} and SI_Ca_{n1}_M_{n2}_M_{n3} (where M is one of the divalent cations: Mg, Ba, Sr) have also been established experimentally within the FAST group. At a fixed pH, the total number (n_1+ n_2) or (n_1+n_2+n_3) of all the cations (*n* total), bound to one phosphonate molecule, is always constant. Thus, the available metal-binding sites on the SI is constant at the fixed pH. As pH increases, the total *n*, i.e. (n_1+n_2), in the SI_Ca_{n1}_Mg_{n2} complex increases up to a theoretical maximum, which is shown to be the number of phosphonate groups within the inhibitor molecule. As an example, for tri-phosphonate NTP, the maximum *n* is found to be ~3, for penta-phosphonate DETPMP – 5.

If there is more than one metal cation present in the brine, then competition for the binding site will occur between the different cations and will depend on the relative binding constants of the metals and their solution concentrations. Experimentally, it was found that the magnitude of the DETPMP/M^{2+} binding constant increases in the order: Ba^{2+} < Sr^{2+} < Mg^{2+} < Ca^{2+}, therefore the equilibrium solubility of the phosphonate complexes formed by these cations is expected to decrease when moving from Ba to Ca. Tests have

also demonstrated that the phosphonate complexes SI/Mg, SI/Sr and SI/Ba are much more soluble than SI/Ca precipitates.

The stoichiometry data collected, was used to develop a model that predicts the formation of phosphonate precipitates. This model is based on the following set of equilibrium (2.14 – 2.16) and mass balance (2.17-2.19) equations, where, to simplify the description, the phosphate group is denoted as "P":

$$\underset{x_1}{Ca^{2+}} + \underset{\bar{x}_2}{P} \rightleftharpoons \underset{x_3}{P\_Ca} \qquad K_{b1} = \frac{x_3}{x_1 . \bar{x}_2} \tag{2.14}$$

$$\underset{x_4}{Mg^{2+}} + \underset{\bar{x}_2}{P} \rightleftharpoons \underset{x_5}{P\_Mg} \qquad K_{b2} = \frac{x_5}{x_4 . \bar{x}_2} \tag{2.15}$$

$$\underset{\bar{x}_6 = x_3 + x_5}{SI\_Ca_{N1}\_Mg_{N2(aq)}} \rightleftharpoons \underset{x_7}{SI\_Ca_{N1}\_Mg_{N2(s)}} \qquad \text{Solubility} = \bar{x}_6 \tag{2.16}$$

$$Ca: \quad x_{10} = x_1 + x_3 + \frac{x_3 . x_7}{\bar{x}_6} = x_1 + x_3 \left(1 + \frac{x_7}{\bar{x}_6} \right) \tag{2.17}$$

$$Mg: \quad x_{40} = x_4 + x_5 + \frac{x_5 . x_7}{\bar{x}_6} = x_4 + x_5 \left(1 + \frac{x_7}{\bar{x}_6} \right) \tag{2.18}$$

$$"P": \quad \bar{x}_{20} = \bar{x}_2 + \bar{\bar{x}}_6 + x_7 \tag{2.19}$$

The only variables in the model are the Ca^{2+} and Mg^{2+} binding constants to the "P" (phosphonate) group. These are denoted as K_{b1} and K_{b2}, respectively. It is shown, as long as these binding constants are sufficiently high (>10^{10}), then it is just the *ratio* of these constants that determines the stoichiometry of $SI\_Ca_{n1}\_Mg_{n2}$.

Another finding is, that a fraction of "non-SI" phosphorus-containing impurities of phosphonate scale inhibitor stock products should be taken into account when modelling the precipitation behaviour, up to 19% for the DETPMP inhibitor (Shaw and Sorbie 2014).

In all cases, Ca^{2+} ions bind to the phosphonate groups *more strongly* than Mg^{2+} ones. Using a single pair of binding constants for Ca and Mg to the available phosphonate groups, $K_{b1} = 3.5 \cdot 10^{10}$ and $K_{b2} = 1.0 \cdot 10^{10}$, gave a good match for all 9 phosphonates tested in the work (Shaw and Sorbie 2015). Both the modelled and experimental data for the DETPMP scale inhibitor were in good agreement and are shown in Figure 2.9. This model can be easily generalised to any arbitrary number of cations case. For example, the set of equilibrium equations for a three cation complex is quite similar to that for the two cation model:

$$\underset{\bar{x}_2}{"P"} + \underset{x_1}{Ca^{2+}} \rightleftharpoons \underset{x_3}{P\_Ca} \quad ; \quad K_{b1} = \frac{x_3}{\bar{x}_2 . x_1} \tag{2.20}$$

$$\underset{\bar{x}_2}{"P"} + \underset{x_4}{Mg^{2+}} \rightleftharpoons \underset{x_5}{P\_Mg} \quad ; \quad K_{b2} = \frac{x_5}{\bar{x}_2 . x_4} \tag{2.21}$$

$$\underset{\bar{x}_2}{"P"} + \underset{x_8}{Ba^{2+}} \rightleftharpoons \underset{x_9}{P\_\mathrm{Ba}} \quad ; \quad K_{b3} = \frac{x_9}{\bar{x}_2 . x_8} \tag{2.22}$$

And the mass balances are as follows:

$$\text{MB } "P": \quad \bar{x}_{20} = \bar{x}_2 + x_3 + x_5 + x_7 \tag{2.23}$$

$$\text{MB "Ca"}: \quad x_{10} = x_1 + x_3 \tag{2.24}$$

$$\text{MB } "Mg": \quad x_{40} = x_4 + x_5 \tag{2.25}$$

$$\text{MB } "Ba": \quad x_{80} = x_8 + x_9 \tag{2.26}$$

The three cation case model results for the DETPMP/Ca/Mg/Ba complex is shown in Figure 2.9.

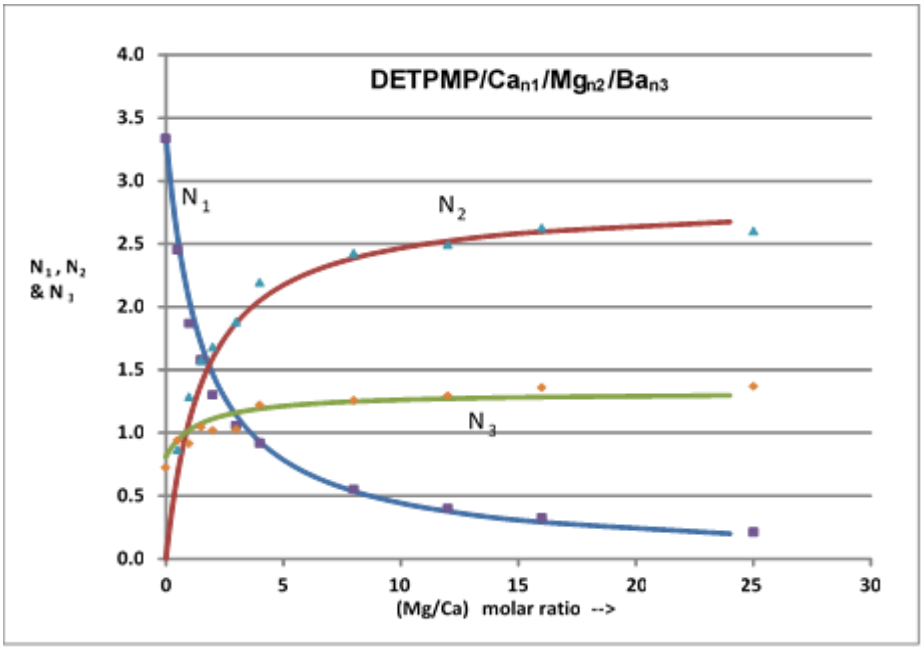

Figure 2.9 DETPMP/Ca$_{n1}$/Mg$_{n2}$/Ba$_{n3}$ modelling results

Thus, the structure and stoichiometry of mono-cation SI_Ca$_n$, di-cation SI_Ca$_{n1}$_Mg$_{n2}$ and SI_Ca$_{n1}$_Sr$_{n2}$, and three-cation complexes SI_Ca$_{n1}$_Mg$_{n2}$_Ba$_{n3}$ of 9 common phosphonate species have been established experimentally and their precipitation behaviour modelled.

Stoichiometry is just one part of the precipitation model. As noted earlier, for a full description of the precipitation squeeze process, the equilibrium solubility of the precipitated complex as well as the kinetic dissolution rate must be measured. According to the precipitation squeeze model developed within the group, these are the parameters controlling the level of scale inhibitor released and hence, the overall treatment lifetime of a precipitation squeeze (Sorbie 2012).

The current thesis is a logical continuation of the earlier research and will focus on defining these two parameters for phosphonate scale inhibitors as well as highlighting the key factors affecting the phosphonate scale inhibitors re-dissolution from the precipitated phase, such as solution pH and composition, temperature. The results of these studies are presented in Chapters 3 – 5 below.

This review highlights that the most common scale inhibitors applied in oilfields are organic phosphorus compounds, either phosphonates or phosphorus containing polymers. There is also a group of phosphate ester inhibitors, yet to be extensively explored, and

these will also be studied in this thesis. The objective of these phosphate ester studies, described in detail in Chapters 6 and 7, is to evaluate their precipitation behaviour and examine the inhibition efficiency of the phosphate ester precipitated complexes. This work will establish whether these new phosphate ester products can be applied in precipitation squeeze applications.

CHAPTER 3. EQUILIBRIUM SOLUBILITY AND INHIBITION EFFICIENCY OF PHOSPHONATE_CALCIUM_MAGNESIUM PRECIPITATES

The current studies expand our fundamental understanding of phosphonate scale inhibitors (SI) precipitation behaviour in terms of their solubility (*Cs*) and the inhibition efficiency of their precipitated complexes.

3.1. Introduction

Precipitation squeeze treatments are based on a chemical reaction between a scale inhibitor and divalent cations where mixed complexes $SI\_M^{2+}{}_n$ of lower solubility are formed (M = divalent cation). During production, the precipitate re-dissolves into the produced brine that flows over the SI retained on the rock to some concentration and this mobile phase SI protects the production well from uncontrolled scale precipitation.

According to current precipitation models described in the literature, two parameters control the level of SI released into the brine and the overall squeeze treatment lifetime: scale inhibitor equilibrium solubility (*Cs*) and kinetic dissolution rate (Browning and Fogler 1995, Sorbie 2012). The solubility *Cs*, ideally, should be within a narrow concentration range that is above some minimum inhibition concentration (MIC), but does not exceed the MIC value significantly. This ensures scale prevention and provides longer squeeze lifetimes, without producing the chemical at higher concentrations than is required. On the other hand, if the solubility of the precipitated complex is too low, then even at full solubility Cs, the [SI] would be <MIC.

The solubility of the $SI\_M^{2+}{}_n$ complex depends on a number of factors, such as the nature of the SI and the divalent cations (mainly calcium and magnesium, but also barium, strontium, iron, etc.), the brine composition and pH, the precipitation temperature (T) etc. Theoretically, any change in parameters and conditions during precipitate dissolution *should* lead to an equilibrium shift and hence, to a solubility variation of the precipitated SI_M_n complex. This, in turn, *may* also impact the scale inhibitor retention and even affect its inhibition efficiency. These hypotheses will be investigated in the current chapter.

Magnesium (Mg^{2+}) and calcium (Ca^{2+}) ions are the most common divalent cations naturally occurring in production fluids, but both the ions are also present in the minerals of carbonate rock formations. SI_Ca_n and SI_Mg_n complexes are the most common SI precipitates that form during precipitation squeezes. The concentration of Mg and Ca ions, as well as their molar ratio Mg/Ca, in a produced brine may vary widely. During the early stages of a wells lifetime, the initial produced brine composition is, in fact, the same as that of the near-well formation water at that time; thus, the Mg/Ca ratio in the produced brine is expected to be close to that of this produced formation water. As an example, the Mg/Ca molar ratio of Nelson Forties formation water is ~0.2. However, during production when the sea water injected into the reservoir to maintain pressure breaks through, the Mg/Ca ratio increases, theoretically up to ~5.3 equivalent to 100% North Sea sea water composition. Another example is when the brine used during a squeeze treatment to deploy the SI pill and where the SI precipitate was formed, is replaced by the flowback formation brine, once the well is brought back on to production. This brine composition variation *might* be one of the factors affecting the release of the scale inhibitor into the brine from the precipitated phase. Therefore, the focus of the current chapter is on studying the correlation between *the brine chemistry* and the *equilibrium concentration Cs, i.e. solubility,* of the scale inhibitor in that brine.

Prior to performing these solubility studies, the stoichiometry *n* of the SI_M_n complex was determined as the first step towards describing the precipitation behaviour of phosphonate scale inhibitors. During previous work, the structure and stoichiometry of mono-cation SI_Ca_n (Shaw and Sorbie 2014) and di-cation $SI\_Can_1\_Mgn_2$ complexes (Shaw and Sorbie 2015) of 9 common phosphonate species were established experimentally, and the precipitation behaviour was also modelled. In this work, those studies will be complemented by the modification of the previous experimental methodology. This alternative method used to define the stoichiometry n of the SI_Ca_n precipitates was found to give more precise data. Subsequently, we extend these stoichiometry studies by measuring the *solubility* of various precipitated scale inhibitor/divalent metal ion complexes as a function of temperature and Mg/Ca ratio in a brine.

The specific objectives of the work described in this Chapter are:

I. to measure the *stoichiometry n* of various SI_Ca_n complexes;

II. to measure the *solubility* of the SI precipitated with Ca and Mg, i.e. *Cs* of the SI_Ca_{n1}_Mg_{n2} species, while varying the Mg/Ca molar ratio from all Ca to all Mg;

III. to determine the effect of temperature, Mg/Ca molar ratio and SI nature on the precipitate solubility under static bottle test conditions;

IV. to establish the *effect of the precipitation process* on the inhibition efficiency ~~*activity*~~ of precipitated and then re-dissolved phosphonate;

V. to explore the effect of co-precipitated divalent cations (Ca and Mg) on the final inhibition efficiency ~~*activity*~~ of the SI species, re-dissolved from those SI/Ca or SI/Ca/Mg precipitates.

The results obtained in this work contribute to our fundamental understanding of how the brine chemistry where the SI precipitate is deployed affects (i) the release (re-dissolution) of the precipitated SI into the bulk solution and (ii) the inhibition efficiency of the precipitated and then re-dissolved SI species. Both of these properties are of great importance for the effective design and modelling of precipitation squeeze treatments.

3.2. Experimental details

3.2.1. *Materials*

The structures of all the phosphonate species studied in this work are shown in Table 3.1. Three common and commercially available phosphonate scale inhibitors supplied by Italmatch (OMTHP, DETPMP, and HEDP) were used to conduct precipitation tests in brines prepared with the salts, $MgCl_2 \cdot 6H_2O$ and $CaCl_2 \cdot 6H_2O$ (both from Sigma Aldrich and used as received). The scale inhibitor concentrations quoted in the work are all as ***active*** concentrations.

Table 3.1 Chemical structures of the tested SIs

Scale Inhibitor Abbreviation	Chemical Structure
OMTHP (hexa-phosphonate)	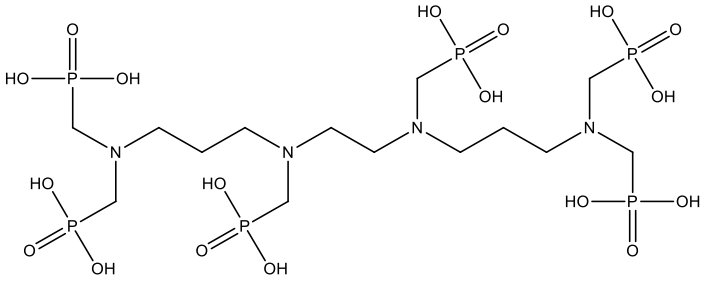
DETPMP (penta-phosphonate)	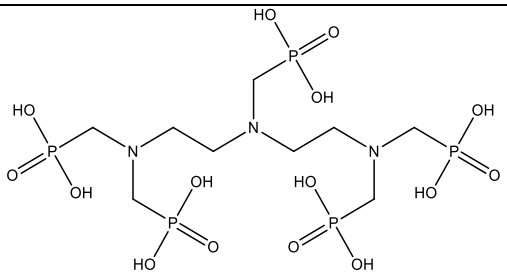
HEDP (di-phosphonate)	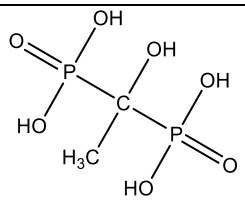

3.2.2. *Precipitation Tests*

Precipitation experiments were conducted in order to find the molar ratio of Ca^{2+} to SI, or stoichiometry *n* in the SI_Ca_n^{2+} precipitates. The phosphonate SIs studied in this context are HEDP (di-phosphonate), DETPMP (penta-phosphonate) and OMTHP (hexa-phosphonate). These tests were conducted at different pH values (pH 3.5, 4.0, and 5.5) and at a temperature of, T = 95ºC. It was highlighted in previous work that most precipitation of SI_Ca_n^{2+} complexes was observed at higher temperatures (Shaw and Sorbie 2014, Shaw and Sorbie 2015), due to endothermic nature of the precipitation reaction. As most precipitate was observed to form under these (higher T) conditions, then the lowest solubility of the SI_M_n^{2+} is expected to be found at higher temperatures.

The procedures used in the stoichiometry study are shown schematically in Figure 3.1. Two methods were applied in the study; i.e. by precipitate and by supernatant assay. In order to find the molar ratio Ca^{2+}/SI in the precipitates, samples containing SI in a concentration range 500-3000 ppm active and 2000 ppm Ca were prepared. After mixing

the SI and Ca brines, a sample was taken from the mixed solution in order to obtain the control - maximum concentrations of the SI and Ca in the initial solution. After that, all the test solutions were pH adjusted to the pH value required for the particular test using dilute hydrochloric acid HCl(aq) and/or sodium hydroxide NaOH(aq). The pH was monitored continually and re-adjusted if required, until a stable pH was achieved.

This step was important since, upon initial pH adjustment, the precipitation of the $SI\_M_n^{2+}$ complex occurs and causes a change in the solution pH (by ~0.5-2 pH units). To perform this, the bottles were left to stand for a few hours to allow equilibrium to be reached, then more precise pH adjustment could be done. During the next pH adjustments, each solution was shaken to ensure that there was maximum interphase contact between the solid and liquid phases. This step was then repeated until a required pH was achieved in all the test bottles.

Subsequently, all test bottles were sealed and placed in an oven at 95°C for 12-24 hours to obtain maximum precipitation. After that, the top solutions were sampled, which gave the supernatant samples.

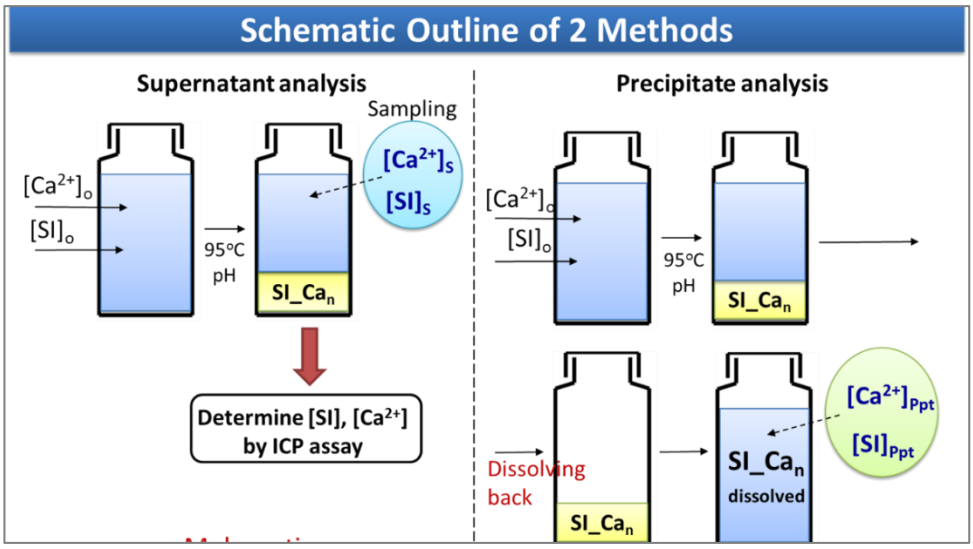

Figure 3.1 Schematic outline of supernatant and precipitate analysis for measuring the stoichiometry of SI_M_n precipitates

The precipitate was then collected using vacuum filtration through a 0.45µm filter paper and placed into a volume of distilled water. Subsequently, all the precipitates were fully dissolved by adding a few drops of 35% wt. HCl. By adding concentrated HCl, the SI associates back into its acid form and hence the SI_Ca complex dissolves. 1 ml of sample

from each bottle was added to 9 ml distilled water and analysed by Inductively Coupled Plasma Method (ICP) for P and Ca content to find the molar ratio Ca:SI in the SI_Ca_n complex by the "precipitate" method.

Supernatant and control samples were also collected and assayed by ICP spectroscopy for [SI] and [Ca^{2+}] and the concentration changes ΔSI and ΔCa^{2+} were determined in order to find the stoichiometry of the complex by the "supernatant" method.

3.2.3. *Solubility Test*

The solubility test procedure consists of precipitation and subsequent dissolution steps. There were *two* series of solubility tests. All the conducted solubility experiments are listed in Table 3.2.

Table 3.2 Series 1 and 2* experiments conditions: molar ratio [Mg^{2+}]/[Ca^{2+}], [Ca^{2+}], [Mg^{2+}], and [Cl^{-}] (ppm and mM/L).

Test №	**Test №***	**Solution molar ratio [Mg^{2+}]/ [Ca^{2+}]**	**[Ca^{2+}] ppm**	**[Mg^{2+}] ppm**	**[Cl^{-}] ppm**	**[Ca^{2+}] mM/L**	**[Mg^{2+}] mM/L**	**Comments**
1	1	0	2000	0	~3,538	49.9	0.0	**All Ca^{2+}**
2		0.5	1333	404	~3,538	33.3	16.6	Ca^{2+} in excess
3	2	1	1000	606	~3,538	25.0	24.9	**Equimolar test**
4		1.5	800	728	~3,538	20.0	30.0	Mg^{2+} in excess
5		2	667	809	~3,538	16.6	33.3	Mg^{2+} in excess
6		3	500	910	~3,538	12.5	37.4	Mg^{2+} in excess
7	3	4	400	970	~3,538	10.0	39.9	Mg^{2+} in excess
8	4	8	222	1078	~3,538	5.5	44.4	Mg^{2+} in excess
9		12	154	1120	~3,538	3.8	46.1	Mg^{2+} in excess
10	5	16	118	1142	~3,538	2.9	47.0	Mg^{2+} in excess
11	6	25	77	1166	~3,538	1.9	48.0	Mg^{2+} in excess
12	7	∞	0	1213	~3,538	0.0	49.9	**All Mg^{2+}**

* - for the experiments conducted with DETPMP and HEDP SIs only.

The first series of the solubility experiments was conducted to find the static solubility of the SI_Ca_Mg complexes where *the brine composition did not change between the precipitation and dissolution steps.* This series was carried out for DETPMP, HEDP and OMTHP inhibitors. The schematic experimental procedure is shown in Figure 3.2. SI was added to the acidified (in order to avoid immediate precipitation) Ca^{2+}/Mg^{2+} solutions prepared by adding appropriate quantities of $CaCl_2 \cdot 6H_2O$ and/or $MgCl_2 \cdot 6H_2O$ to distilled

water. In order to keep the ionic strength constant, since it can affect the apparent solubility of the precipitates, the solution molar ratio of Mg/Ca was varied such that the total number of moles (X) of divalent ions ($X = [Ca^{2+}] + [Mg^{2+}]$) in each test solution was kept constant ($X \approx 49.9$ mM/L). The SI concentration was fixed at 2000 ppm as this was found to be an optimal concentration yielding a sufficient amount of precipitate for all tested SIs.

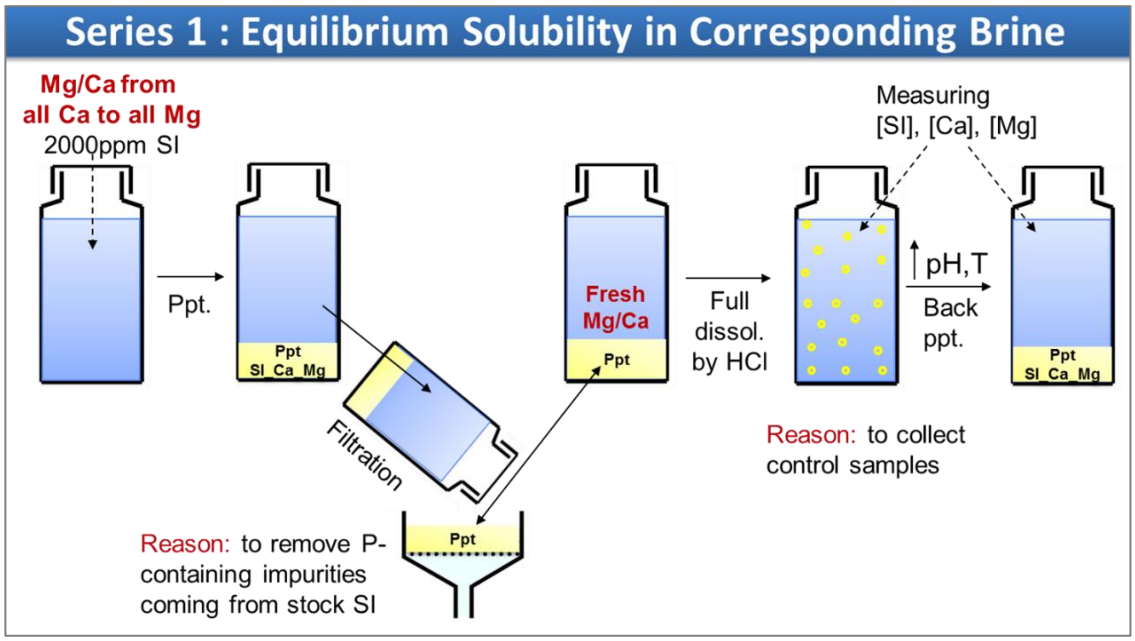

Figure 3.2 Experimental procedure for Series 1 equilibrium solubility test

All test solutions were then pH adjusted to pH 8.5 using dilute HCl(aq) and/or NaOH(aq). The pH was measured continually and re-adjusted if required, until a stable value of pH 8.5 was achieved, as described earlier in Section 3.2.2. The test pH needed to allow maximum SI precipitation but at the same time to avoid the formation of $Mg(OH)_2$ or $Ca(OH)_2$ precipitates, which have a precipitation onset at pH ~10 and pH ~12, respectively.

Subsequently, all samples were placed in an oven at 95°C, as generally the solubility of the phosphonate complexes is expected to decrease with increasing temperature due to exothermic nature of the dissolution reaction. After that, the precipitate was collected using vacuum filtration through a 0.22 μm filter and placed into "fresh" brine of the same Mg/Ca molar ratio, as in the initial precipitation step. The brine replacement is a necessary step since the initial SI solution involves phosphorus-containing impurities of SI stock product, which are going to affect the final phosphorus concentration in the solution once

the precipitate has formed and hence, the solubility data. Finally, all the precipitates were re-dissolved into the "fresh" brine by adding a few drops of 35% HCl. The control samples were taken from these solutions of dissolved precipitate and analysed by ICP for Mg, Ca and SI content in the system. Subsequently, these were precipitated again at pH 8.5. The pH was monitored continually and re-adjusted if required, until a stable pH of 8.5 was achieved. After 24 hours 1 ml of sample from each bottle was added to 9 ml DW and analyzed by ICP for P, Ca, and Mg content to find the solubility of the SI_Ca_Mg complexes at 20^{o}C. After that, the bottles were transferred to an oven at 50^{o}C, 75^{o}C and 95^{o}C where sampling was repeated after 24 hours at each temperature.

In the second series of the solubility experiments, *the precipitate was formed in a brine with one certain composition (molar ratio Mg/Ca = 4) and subsequently was placed into a solution of different Mg/Ca ratios.* This models the more common scenario when the precipitate is formed in the brine used for the squeeze treatment, but after the treatment it dissolves in the produced brine which generally has a different [Mg] and [Ca] content. The final equilibrium conditions (SI, Ca and Mg concentrations) were then measured to determine if the precipitate composition and solubility had changed, i.e. if it had exchanged divalent cations to equilibrate in the new Mg/Ca brine.

To conduct the second series of experiments, the procedure described above for Series 1 was changed only at the initial precipitation step. SI was initially precipitated at the same Mg/Ca composition brine, chosen as Mg/Ca=4. These precipitates were subsequently placed into brine with different Mg/Ca ratio, from all Ca to all Mg. The solubility was found over temperatures ranging from 20^{o}C to 95^{o}C. The rest of the steps are identical to the procedure described above for the first series of solubility tests.

3.2.4. *Static Barium Sulphate Inhibition Efficiency Tests*

Static barium sulphate inhibition efficiency (IE) tests were carried out at 95^{o}C at 2 hours (short-term) and 22 hours (long-term) sampling after the mixing of North Sea Sea Water (NSSW) with Nelson Forties Formation Water (NFFW) at the volume ratio 60:40, respectively. Prior to mixing the brines, SI was dissolved in NSSW to give final concentrations 4, 8, and 20 ppm. Samples of NSSW with SI and samples of NFFW were placed in an oven and waterbath at 95^{o}C for an hour. A sodium acetate/acetic acid buffer was used to buffer all samples at pH 5.5. NSSW and NFFW compositions are given in

Table 3.3.

Table 3.3 NSSW and NFFW compositions

North Sea Sea Water (NSSW)			Nelson Forties Formation Water (NFFW)		
Ion	ppm	Composition	Ion	ppm	Composition
Na^+	10890	NaCl	Na^+	31275	NaCl
Ca^{2+}	428	$CaCl_2{\cdot}6H_2O$	Ca^{2+}	2000	$CaCl_2{\cdot}6H_2O$
Mg^{2+}	1368	$MgCl_2{\cdot}6H_2O$	Mg^{2+}	739	$MgCl_2{\cdot}6H_2O$
K^+	460	KCl	K^+	654	KCl
Ba^{2+}	0	$BaCl_2{\cdot}2H_2O$	Ba^{2+}	269	$BaCl_2{\cdot}2H_2O$
Sr^{2+}	0	$SrCl_2{\cdot}6H_2O$	Sr^{2+}	771	$SrCl_2{\cdot}6H_2O$
SO_4^{2-}	2960	Na_2SO_4	SO_4^{2-}	0	Na_2SO_4
Cl^-	19773	-	Cl^-	55279	-

A solution containing 1000ppm commercial polyvinyl sulphonate scale inhibitor (PVS) and 3000ppm potassium (as KCl) in distilled water, adjusted to pH 8 – 8.5 was used as the samples dilution solution, in order to quench the inhibition reactions in a given sample. Since the standard analytical approach currently used within Flow Assurance and Scale Team (FAST) laboratories for barium is Inductively Coupled Plasma Spectroscopy (ICP), the potassium is only included in this solution to act as an ionisation suppressant for the Atomic Absorption determination of barium. 9ml of this KCl/PVS solution is added to a test tube at room temperature. After the required time interval (2 and 22 hours), 1ml of the particular test supernatant water is removed and immediately added to the 9ml of quenching KCl/PVS solution. The samples are then analysed by ICP for the barium ions and IE was calculated with the following equation:

$$\%Efficiency(t) = \frac{(M_B - M_I)x100}{M_B} = \frac{(C_O - C_B) - (C_O - C_I)x100}{(C_O - C_B)} = \frac{(C_I - C_B)x100}{(C_O - C_B)} \quad (3.1)$$

Where:

M_B = Mass of barium (or other cations) precipitated in supersaturated blank solution.

M_I = Mass of barium (or other cations) precipitated in test solution.

C_O = Concentration of barium (or other cations) originally in solution (i.e. t=0).

C_I = Concentration of barium (or other cations) at sampling.

C_B = Concentration of barium (or other cations) in the blank solution (no inhibitor) at the same conditions and sampling time as C_I above.

(t) = Sampling time.

3.2.5. *Precipitation and Re-Dissolution Experiments*

The main reason for conducting the inhibition efficiency (IE) experiments, described in this Chapter, is to compare the inhibition performance of precipitated SI (when re-dissolved) with the commercial stock product. Therefore, prior to the inhibition efficiency tests, precipitation and re-dissolution experiments were carried out in order to prepare the re-dissolved precipitate stock solution. Similar experiments carried out of polymeric SIs (PPCA) had previously shown that there were significant differences between the IE of the original product and the precipitated SI_Ca complex (Farooqui and Sorbie, 2016).

In order to obtain the precipitated product, SI was added to a solution containing 2000 ppm Ca, 739 ppm Mg (the same concentrations as in NFFW composition used in this study, Mg/Ca=0.6). The solution pH was adjusted to pH 5.5. As described in Section 3.2.2, precipitation of the SI_Ca_Mg complexes leads to pH variation, therefore pH must be re-checked continually until a stable pH of 5.5 is achieved. Subsequently, solutions were placed into a water bath at 95^{o}C and left there overnight. The precipitate was collected using vacuum filtration with 0.22μm filters and was dissolved by adding a few drops of 35% HCl. A 1ml sample was extracted and added to 9ml DW and analyzed by ICP for SI concentration, and then this data was used as the "stock concentration" to prepare the SI test solutions for the IE experiment.

3.3. Results and Discussion

3.3.1. *Stoichiometry of OMTHP_Ca, DETPMP_Ca, and HEDP_Ca Complexes*

As a training exercise, the stoichiometry of the mono-cation SI_Ca_n complexes was established before embarking on the solubility and inhibition efficiency studies of the precipitated SI_Ca_Mg complexes. The methodology described earlier in Shaw and Sorbie 2014, Shaw and Sorbie 2015 was supplemented in the current work by a "precipitate" direct assay. Those studies had shown, when modelling the precipitation behaviour of the phosphonate scale inhibitors by using the supernatant assay data, that allowance must be made for phosphorus-containing non-SI impurities in the SI stock solution. If these impurities are present in the supernatant liquid, then the supernatant assay would give inaccurate results. The direct "precipitate" assay should provide more accurate stoichiometry data for the precipitated complexes.

The molar ratio *n* of Ca^{2+}/SI in the SI_Ca_n precipitates was determined at different pH values and T = 95°C. The phosphonate SIs studied in this context are HEDP (di-phosphonate), DETPMP (penta-phosphonate) and OMTHP (hexa-phosphonate). The initially prepared SI/Ca solution and the generated supernatant and re-dissolved precipitate solutions were sampled and the molar ratio of Ca^{2+} to SI was calculated for both methods and compared.

Figure 3.3 shows the experimental results obtained from assaying both the supernatant and precipitate of the OMTHP_Ca_n complexes at pH3.5 and pH4.0.

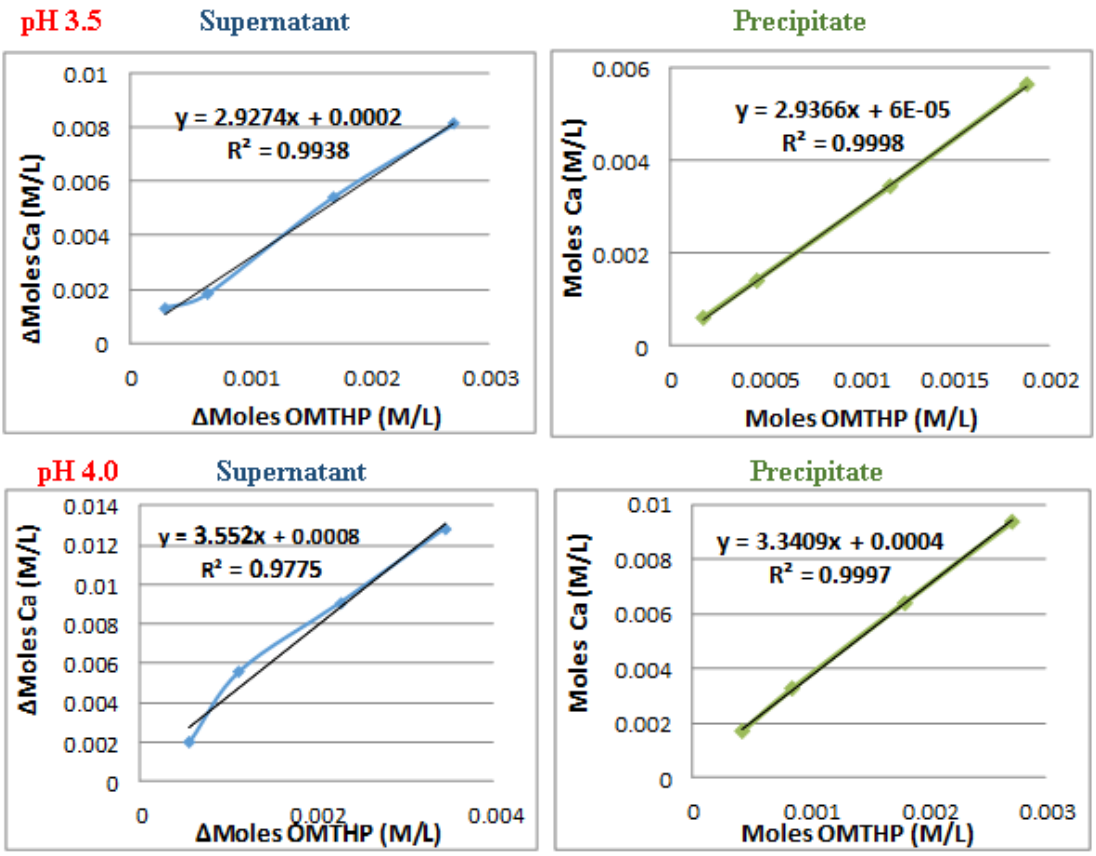

Figure 3.3 ΔCa (M/L) versus ΔOMTHP(M/L) in supernatant and precipitate at pH 3.5 and pH 4, [Ca^{2+}] = 2000ppm, [SI] = 500, 1000, 2000, and 3000ppm.

The stoichiometry *n* of the OMTHP_Ca_n complex was found to be ~ 2.9 and ~ 3.5 at pH3.5 and pH4.0, respectively; i.e the stoichiometry increased with increasing solution pH. This occurred in agreement with the acid dissociation theory, described in the literature review. The degree of dissociation of the phosphonate species, therefore the number of available binding centres, increases with increasing solution pH. Thus, the

molar ratio of bound cations to a phosphonate SI ion was expected to increase, as obtained experimentally.

Figure 3.4 and Figure 3.5 present the corresponding experimental results obtained for both the supernatant and re-dissolved DETPMP_Ca and HEDP_Ca precipitates at pH5.5, 95ºC.

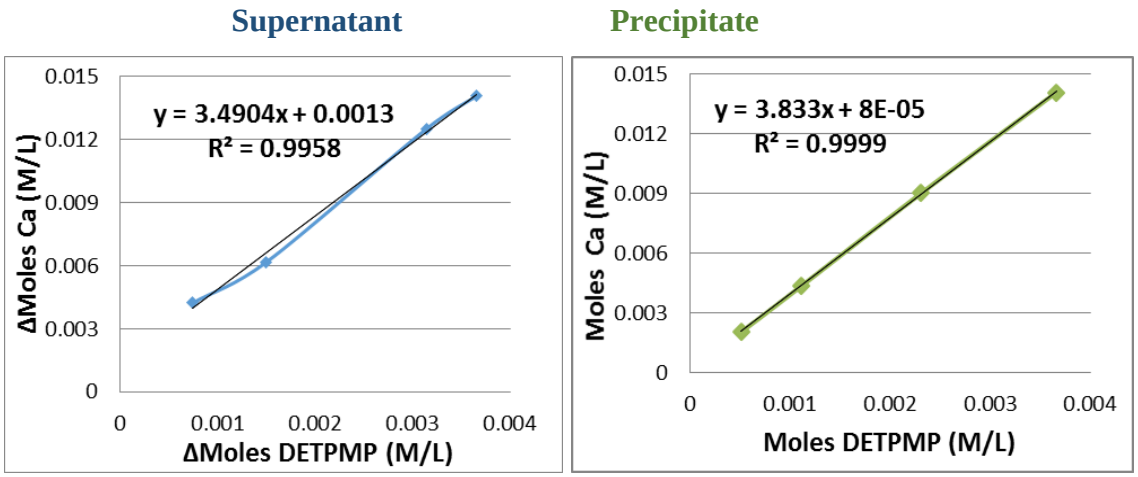

Figure 3.4 ΔCa (M/L) versus ΔDETPMP (M/L) in supernatant and precipitate at pH 5.5, [Ca^{2+}] = 2000ppm, [SI] = 500, 1000, 2000, and 3000ppm.

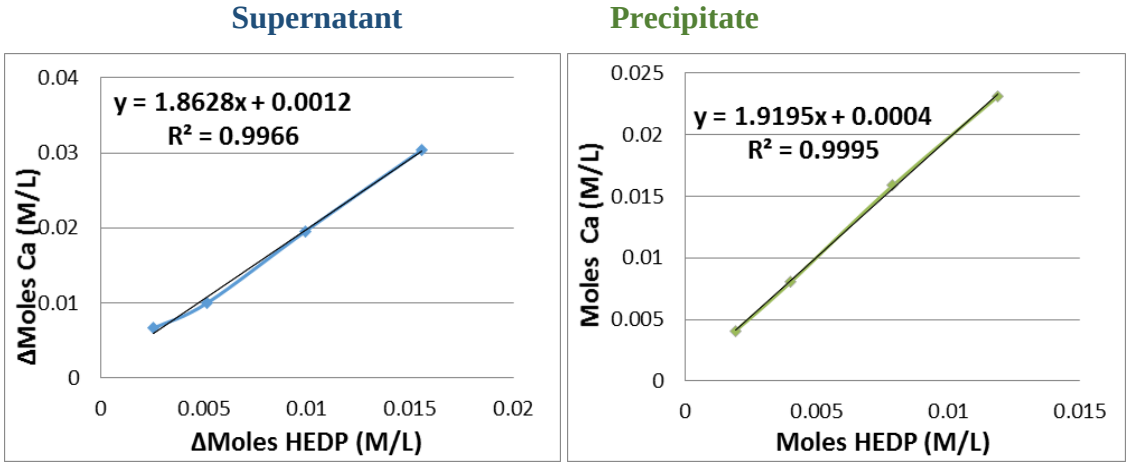

Figure 3.5 ΔCa (M/L) versus ΔHEDP(M/L) in supernatant and precipitate at pH 5.5, [Ca^{2+}] = 2000ppm, [SI] = 500, 1000, 2000, and 3000ppm.

The graphs show ΔCa (M/L) versus ΔOMTHP (M/L) in the supernatant solution, and Ca (M/L) versus OMTHP (M/L) in the re-dissolved precipitate solution, where [Ca^{2+}] = 2000ppm, and [SI] = 500, 1000, 2000, and 3000ppm. Stoichiometry *n* of the DETPMP_Ca_n complex is ~ 4 and *n* for the HEDP_Ca_n complex is ~ 2 at pH 5.5.

It can be seen from the graphs presented above that it was possible to find *directly* the SI and Ca^{2+} concentrations in the precipitate, instead of calculating the ΔSI and ΔCa^{2+} from the supernatant data. For all the experiments conducted, both the supernatant and precipitate methods provide reliable results as they are in good agreement with the previously published results for SI_Ca complexes (Shaw and Sorbie 2014). However, the data obtained from sampling the re-dissolved precipitate solution gives "smoother" profiles of the stoichiometry *n* in the SI_Ca_n complexes, thus providing more accurate and reliable results, compared to the "supernatant" method.

3.3.2. *Solubility of the SI_Ca_Mg Complexes*

Constant Mg/Ca molar ratio:Series 1

The first series of solubility measurement tests was carried out for SI_Ca_Mg complexes precipitated at pH 8.5, T= 95^{o}C for 3 phosphonates species: OMTHP, DETPMP and HEDP. During both the precipitation and dissolution steps, the Mg/Ca molar ratio was varied from all Ca to all Mg, i.e. from Mg/Ca=0 to Mg/Ca=∞ and over a wide temperature range, 20-95^{o}C. Specific solubility measurements were carried out at 4 temperatures: T = 20^{o}C, 50^{o}C, 75^{o}C and 95^{o}C. Figure 3.6 presents the solubility results for OMTHP_Ca_Mg complexes (OMTHP concentration in solution, ppm) at pH8.5 over the temperature range, T = 20 - 95^{o}C.

Both Figure 3.6a and Figure 3.6b present identical data and show clearly that the inclusion of Mg greatly increases the solubility of the phosphonate/metal complexes when the Mg/Ca ratio exceeds 1. Figure 3.6b presents an alternative view of the solubility data illustrating the coupled effects of Mg/Ca molar ratio and temperature on the solubility of the SI/mixed divalents precipitated complexes.

The trend of these results is in good agreement with data published by Tantayakom, Fogler et al. 2005. The solubility of the precipitated OMTHP metal complex is lowest when there is only Ca in the precipitate (Mg/Ca=0 case), with [OMTHP] ~85 ppm released into the bulk. In this case, the temperature effect is less significant as solubility changes only from 85 to 45ppm (4% to 2% of max [SI] contained in the test bottle) over the tested range, 20-95^{o}C. Increasing the Mg content in the solution induces SI release and the solubility increases greatly. Moreover, the temperature effect becomes much more significant; for example, in the sample containing only Mg, the solubility decreases

from ~1600ppm to 300ppm (90% to 17% of SI containing in the test bottle) over the tested temperature range. The same solubility vs. temperature trend has been previously established for inorganic phosphates, i.e. solubility of phosphates generally decreases with increasing temperature mainly due to the exothermic effect of their dissolution process.

a)

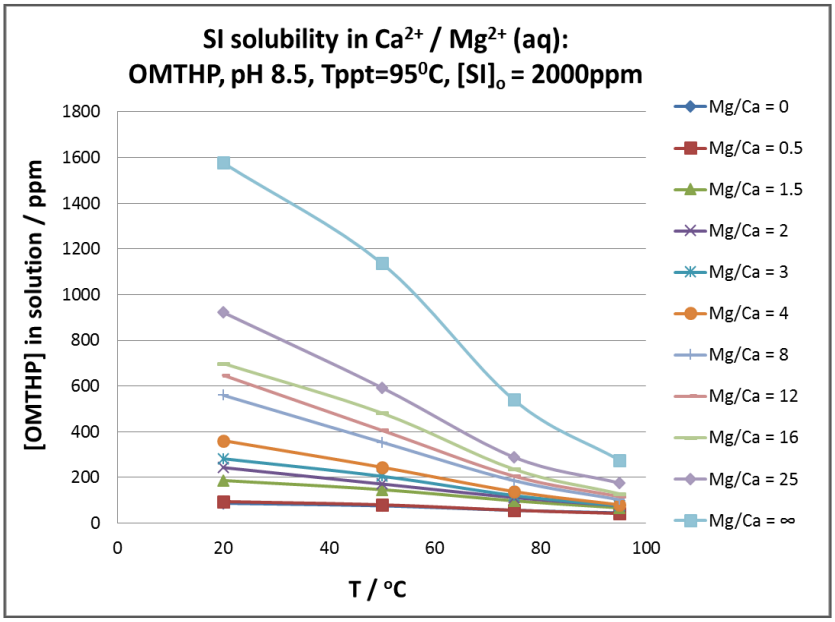

b)

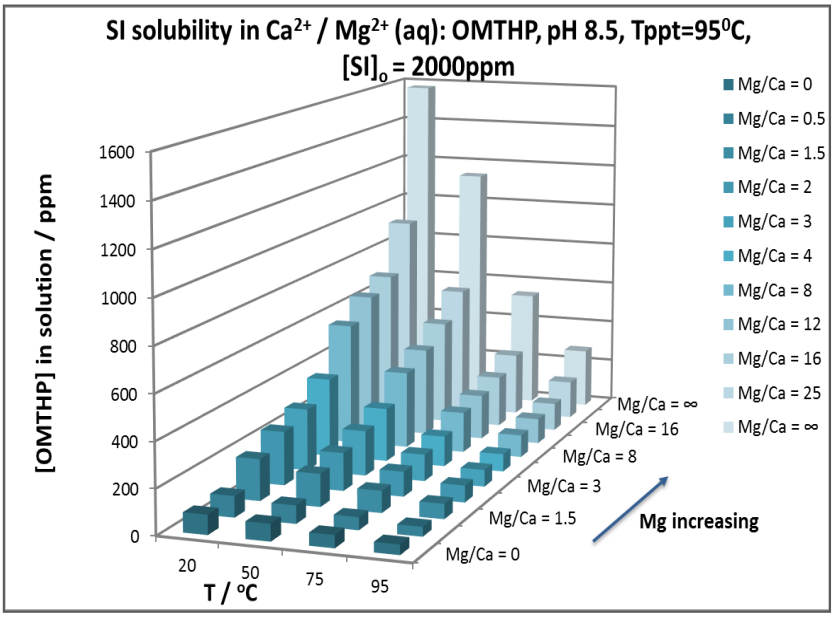

Figure 3.6 OMTHP_Ca_Mg complex solubility vs. Mg/Ca molar ratio and temperature at pH 8.5, Tppt=95°C, [SI]o = 2000ppm: 2D (a) and 3D views (b).

The data shows that SI_Ca_Mg precipitates become more soluble with an increasing proportion of Mg in the brine. Therefore, the phosphonate/Mg complex dissolution

should be a more favourable process from a thermodynamic point of view that requires *lower* energy to break the bonds in the precipitate structure allowing ions to form. Indeed, the negative Gibbs free energy change of the EDTMP (tetra-phosphonate SI)/divalent cation complexes formation evaluated by Sawada, Miyagawa et al. 1993 shows that the negative energy change is lower when the SI/*Mg* complex forms, i.e. $-\Delta G = 47.6$ kJ/mol, whereas for the corresponding Ca complex this value is 53.0 kJ/mol. Therefore, thermodynamically, the phosphonates/Mg complexes are less stable than the corresponding Ca complexes. In addition, in other work (Shaw and Sorbie 2015) it was shown that Ca binds stronger to the SI molecule rather than Mg, which is supported by a lower hydration enthalpy value for Mg^{2+} cations, $\Delta H = -1926$ kJ/mol, than for $Ca^{2+} = -1579$ kJ/mol. Thus, dissolution of the SI_Mg complex should be the preferred path than that of the corresponding SI_Ca complexes, which is indeed what is observed in the current work.

a)

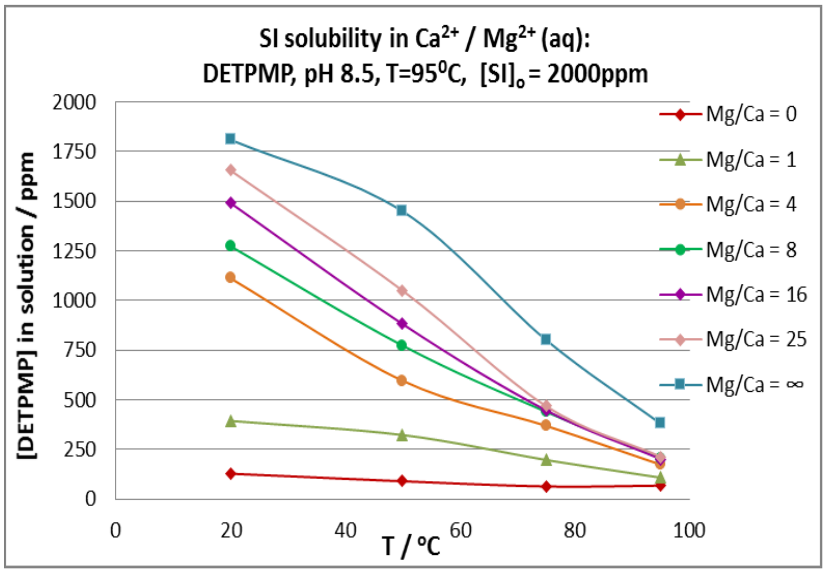

b)

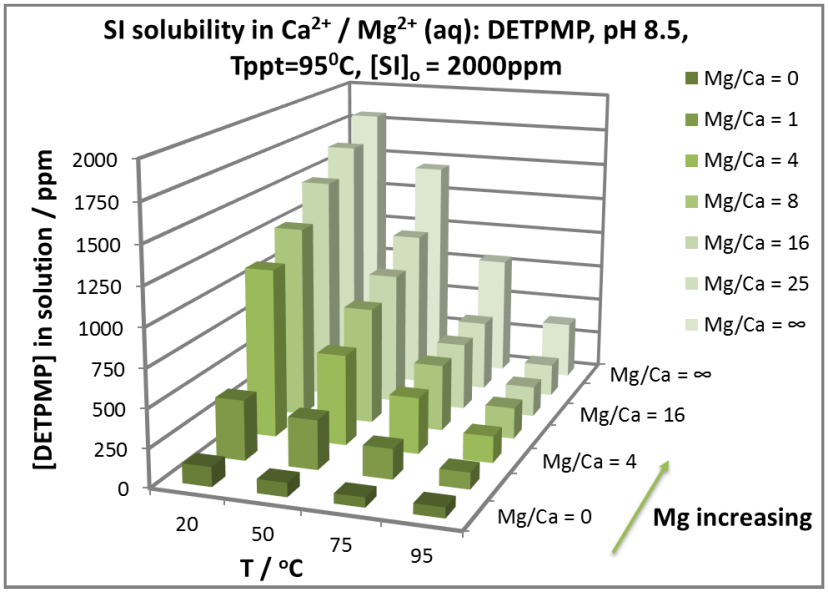

Figure 3.7 DETPMP_Ca_Mg complex solubility vs. Mg/Ca molar ratio and T at pH 8.5, Tppt=95ºC, $[SI]_o$ = 2000ppm: 2D (a) and 3D views (b).

Figure 3.7 and Figure 3.8 present the DETPMP_Ca_Mg and HEDP_Ca_Mg complexes solubility data, respectively, at pH 8.5 over the temperature range, 20 - 95ºC. The trends observed for these solubility plots are very similar to those trends discussed for the OMTHP inhibitor above. Increasing the Mg content in the solution (and in the precipitate) greatly increases the precipitate solubility for both SIs. Moreover, the temperature effect becomes more significant; in the samples containing only Mg, the solubility decreases for DETPMP from ~1650ppm to 400ppm (95% to 22% of precipitated SI) and for HEDP from ~670ppm to 70ppm (35% to 4% of precipitated SI) over the test temperature range, 20-95ºC.

a)

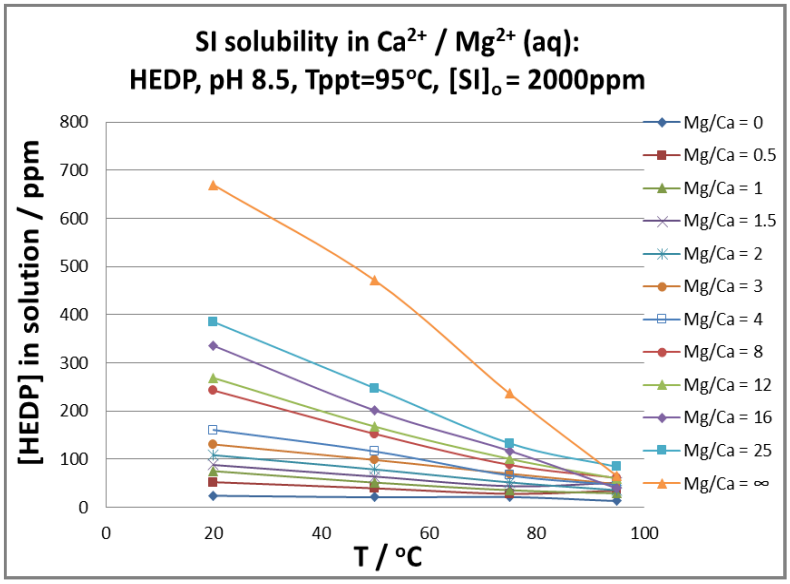

b)

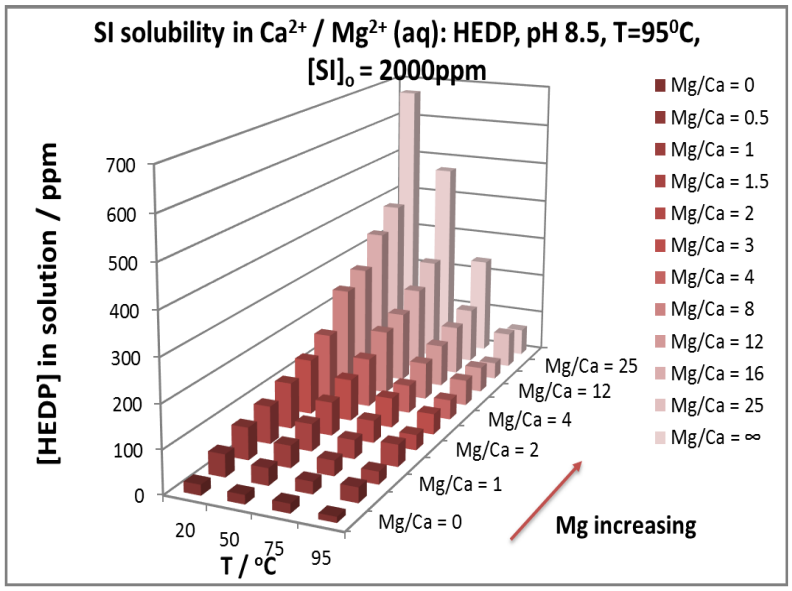

Figure 3.8 HEDP_Ca_Mg complex solubility vs. Mg/Ca molar ratio and T at pH 8.5, Tppt=95°C, $[SI]_o$ = 2000ppm: 2D (a) and 3D views (b).

To demonstrate the repeatability of these experiments and the reliability of the methodology, the OMTHP solubility experiment was repeated using different batches of OMTHP scale inhibitor, and the comparison of the repeats is presented in Figure 3.9. The ICP-OES gives an approximate instrumental error of 10% (up to 200 ppm in this experiment). However, the results of the repeated solubility tests are well within this error.

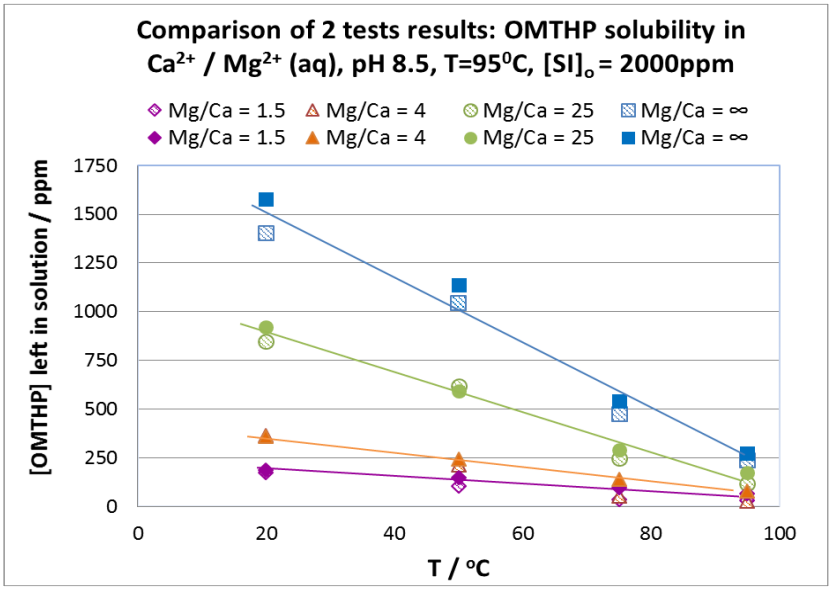

Figure 3.9 Comparison of repeats for OMTHP_Ca_Mg solubility vs. Mg/Ca molar ratio and T at pH 8.5, Tppt=95°C, [SI]o = 2000ppm

According to the experimental data obtained in this work, the solubility of the SI_Ca_Mg complexes increases for the different phosphonate species in the order: HEDP (di-phosphonate) << OMTHP (hexa-phosphonate) ≤ DETPMP (penta-phosphonate). All the metal/phosphonate complexes become more soluble with increasing Mg proportion and less soluble with an increase of brine temperature, in which the precipitate deployed.

Effect of Mg/Ca molar ratio variation: Series 2

In the Series 1 sequence of experiments above, the solubility of the SI_Ca_Mg precipitates was measured in the ***same brine*** where the precipitation reaction occurred. The data generated during those experiments can be used directly to predict the solubilities of the SI precipitates that form during a squeeze treatment, as long as the composition of the squeeze brine is known. However, once the well is brought back onto production, the squeeze brine will be replaced by a produced flowback brine. This brine will generally have a different chemical composition and more specifically, a different Mg/Ca ratio to that of the brine used in the squeeze treatment. Therefore, this final brine will determine the solubility of the precipitate during the squeeze lifetime. In addition, under field application conditions produced brine compositions can also vary quite significantly over the SI squeeze lifetime. Therefore, in the next study, the effect of the brine composition variation on the SI precipitate solubility will be investigated experimentally.

In recent work, the phosphonate precipitate/bulk system has been described by the chemical equilibrium equations 2.20-2.22 shown earlier in Chapter 2 (Shaw and Sorbie 2014, Shaw and Sorbie 2015). It is important to note from these equations, that the SI solubility is in a dynamic equilibrium with various parameters, including the concentrations of divalent cations in the bulk solution and in the precipitated phase. Therefore, any change of brine composition *should* lead to the re-distribution of all parameters within the brine/precipitate system according to the aforementioned equations, including the *solubility*. Essentially, if anything is changed in the system, such as changing the brine, then the system (supernatant brine and precipitate) should re-equilibrate, although this may take some time to occur.

To assess this hypothesis and define the effect of brine composition variation on the SI precipitate solubility, the *Series 2* solubility studies were conducted. The experimental procedure was identical to that used in the previous Series 1 study, except for one modification. All the precipitates were produced in a brine with the same Mg/Ca molar ratio, chosen as Mg/Ca=4. Subsequently, these precipitates were placed into 7 solutions with different Mg/Ca compositions, from all Ca to all Mg, and the solubilitites of those precipitates were measured as a function of temperature.

The solubility data for the DETPMP_Ca_Mg complex, as well as the Mg and Ca concentrations in those Series 2 systems are plotted in Figure 3.10, Figure 3.11, and Figure 3.12. The line for Mg/Ca=4 (Series 2) represents the Series 1 test conditions.

It was found in Series 2 that if the DETPMP/Ca/Mg precipitate formed at Mg/Ca=4 is placed not in its corresponding Mg/Ca=4 solution, but in solutions with *lower* Mg proportion, the solubility of the resulting complex decreases. This can be seen in the Mg/Ca = 1 and Mg/Ca=0 data in Figure 3.10. For these tests, the initially prepared SI precipitate is "richer" in Mg than the brine where it was placed, i.e. n_2 in this DETPMP_Ca_{n1}_Mg_{n2} precipitate is higher than it would be in equilibrium. To equilibrate the system, some additional Mg must come out from the precipitate into the bulk solution, and this is exactly what was observed. In Figure 3.12, in the case of Mg/Ca = 0, quite a high concentration of Mg is measured, ~200ppm; all the Mg is coming out of the precipitate, whilst some Ca should be going into the precipitated phase, as observed in Figure 3.11, where the Mg/Ca = 0 line shows a decline in [Ca] as more Ca is removed from the bulk solution with the increase in temperature.

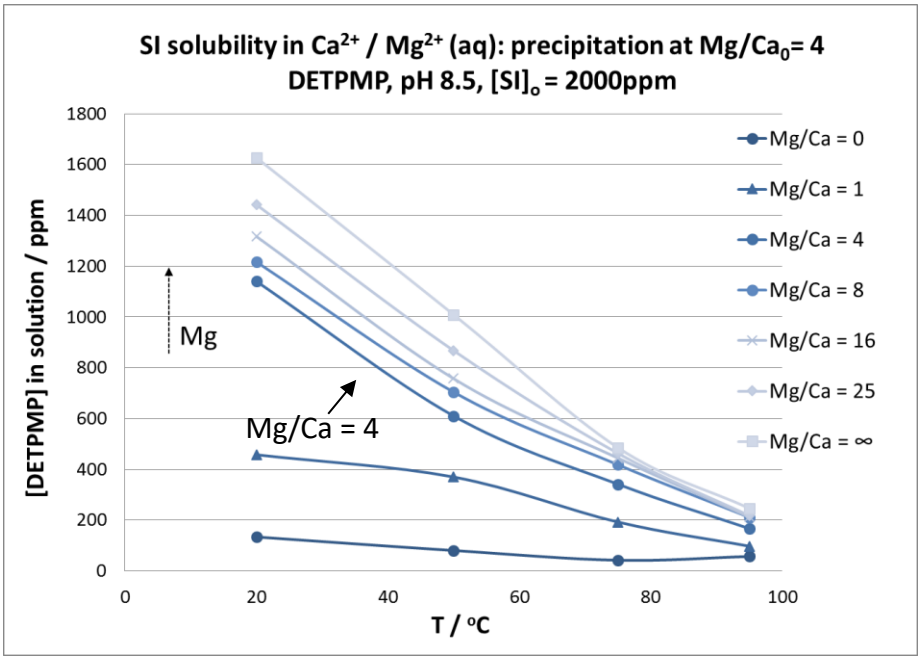

Figure 3.10 Series 2 DETPMP_Ca_Mg complex solubility vs. Mg/Ca molar ratio and T at pH 8.5, $[SI]_o$ = 2000ppm.

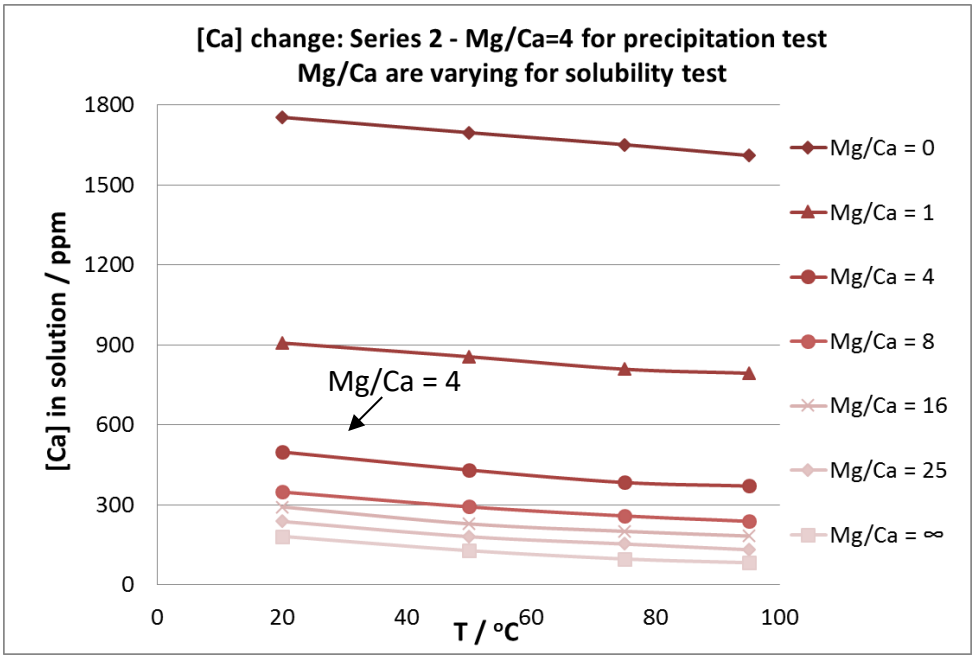

Figure 3.11 $[Ca^{2+}]$ in bulk in Series 2 solubility test versus Mg/Ca molar ratio and T at pH 8.5, $[SI]_o$= 2000ppm.

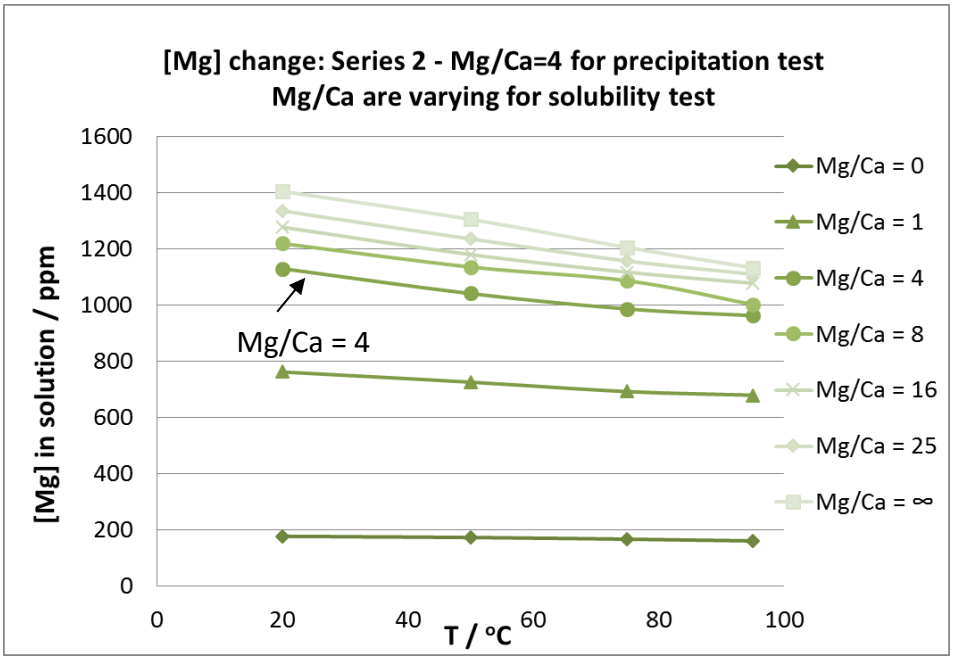

Figure 3.12 $[Mg^{2+}]$ in bulk in Series 2 solubility test versus Mg/Ca molar ratio and T at pH 8.5, $[SI]_o$= 2000ppm.

For example, in Figure 3.13 it is shown that the Mg/DETPMP ratio, i.e. n_2 in these DETPMP_Ca_{n1}_Mg_{n2} precipitates, goes down when the Mg/Ca ratio of the brine is decreasing, whereas the Ca/DETPMP ratio increases, which is shown in Figure 3.14. Thus, changing the Mg/Ca ratio in the *brine*, where the precipitate is deployed, also leads to variation of the stoichiometry and the amount of Ca and Mg contained within the *precipitate*.

For the cases above the Mg/Ca=4 lines, the SI precipitate is also not in equilibrium with the brine. These precipitates are somewhat deficient in Mg than would be the case for the equilibrium precipitates for these particular brines. After placing these precipitates into the brine, the Mg molar ratio in the precipitate increases since some bulk Mg is going into the precipitate, whereas Ca is coming out and its ratio in the precipitate decreases. This is observed in Figure 3.13 and Figure 3.14.

To summarise the Series 2 tests, the final precipitate DETPMP_Ca_{n1}_Mg_{n2} composition was shown to be different to the one that was initially obtained from the Mg/Ca =4 case in all the tested brines. n_1 (Ca molar ratio in the precipitate) decreases as the Mg/Ca molar ratio in the brine increases, whereas n_2 (Mg ratio in the precipitate) increases. These results are in good agreement with previous work performed within the group (Shaw and Sorbie 2015). In that work, it was shown that the ratio n_2/n_1 of the stoichiometric

coefficients *in the precipitate* SI_Ca_{n1}_Mg_{n2} itself changes proportionally to the Mg/Ca ratio variation *in a brine*, which is what has been observed in the current work and the precipitate's solubility variation has been determined.

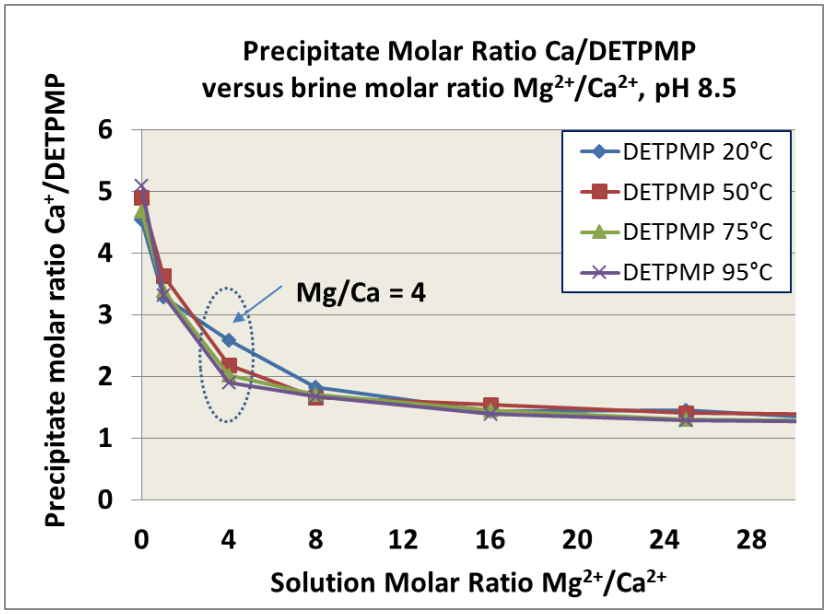

Figure 3.13 Molar ratio of Ca/DETPMP in DETPMP/Ca/Mg precipitates of Series 2 solubility test, pH 8.5, versus varying Mg/Ca ratio in a brine

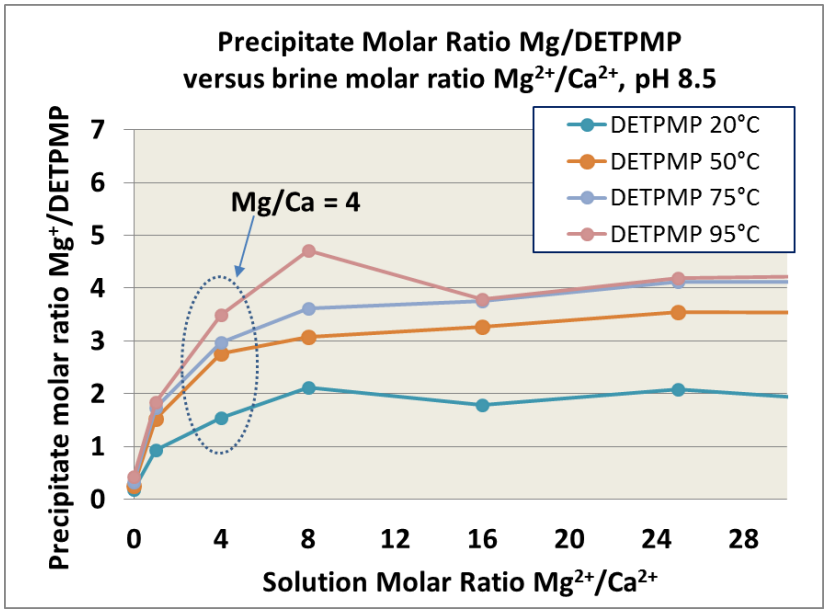

Figure 3.14 Molar ratio of Mg/DETPMP in DETPMP/Ca/Mg precipitates of Series 2 solubility test, pH 8.5, versus varying Mg/Ca ratio in a brine

It can be concluded from the results obtained in the Series 2 study that the solubility of the phosphonate/metal complexes depends on the equilibrium distribution of Mg and Ca

between the bulk solution and the precipitate in the system. Any change of [Mg] and [Ca] in the brine during the dissolution of the precipitate will lead to the re-speciation of the precipitate, thus changing the Ca/SI and Mg/SI ratios in the phosphonate/metal complexes. However, this should be occurring in a predictable manner according to the equilibrium balance 2.20-2.22, mentioned earlier.

Series 1 and Series 2 Studies Comparison

From the Series 2 studies, it is known that the apparent composition of the brine where the precipitate is deployed does affect the solubility of the precipitate. To further investigate the phenomena of phosphonate SI solubility change versus Mg/Ca ratio variation in the brine, the Series 2 (dotted lines) solubility was compared directly with the Series 1 data (solid line) in Figure 3.15. By doing this, the following assumptions are tested:

1. It is the *overall Mg and Ca* content available in the system during both precipitation and dissolution steps as well as their ratio that determines the solubility of the phosphonate_Ca_Mg complex. This was the main conclusion obtained from the Series 2 studies described above.
2. *Only the final brine composition* determines the phosphonate/metal complexes solubility - if this is true, then the results for both cases should be identical, as the final Mg/Ca composition in Series 1 corresponds to the final conditions of Series 2.

However, the results shown in Figure 3.15 are quite different for Series 1 and Series 2, as anticipated in the discussion of the equilibrium equations above. To explain these results further, bulk solutions of both test samples were analysed for [Mg] and [Ca] and these are presented by solid lines for Series 1 and dotted lines for Series 2 in Figure 3.16 and Figure 3.17.

The Series 1 and Series 2 results for the Mg/Ca=4 line, i.e. complex solubility and the final [Mg^{2+}] and [Ca^{2+}], correspond well, as they represent the *same* experimental conditions. Series 1 solubility values are slightly higher than Series 2 for only one case, Mg/Ca=1 brine. This was due to the Mg proportion in the brine during the precipitation step being greater in Series 2, therefore this precipitate is “richer” in Mg than the Series 1 precipitate. Thus, the overall [Mg] (Figure 3.12) in solution is higher in Series 2 case,

making this precipitate more soluble than the Series 1 case. Therefore, the solubility is determined by the overall Mg and Ca in the system, rather than only by the final brine composition.

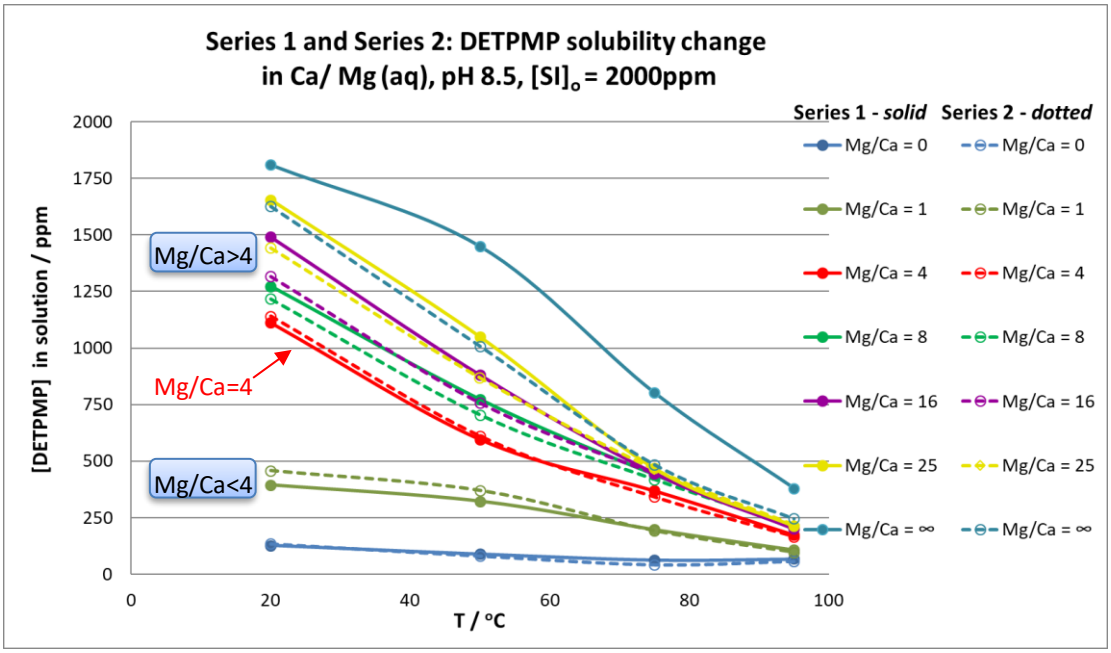

Figure 3.15 Series 1 (solid line) and Series 2 (dotted line) data for the DETPMP_Ca_Mg complex solubility vs. Mg/Ca molar ratio and T at pH 8.5.

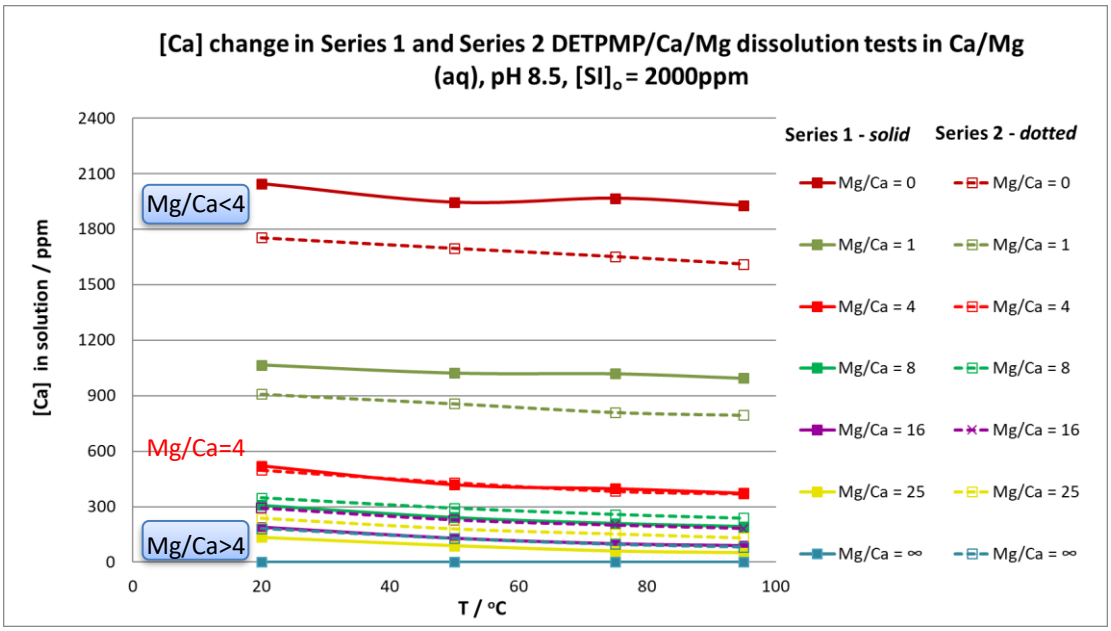

Figure 3.16 Comparison of [Ca^{2+}] in the bulk of Series 1 (solid line) and Series 2 (dotted line) solubility tests versus Mg/Ca molar ratio and T at pH 8.5.

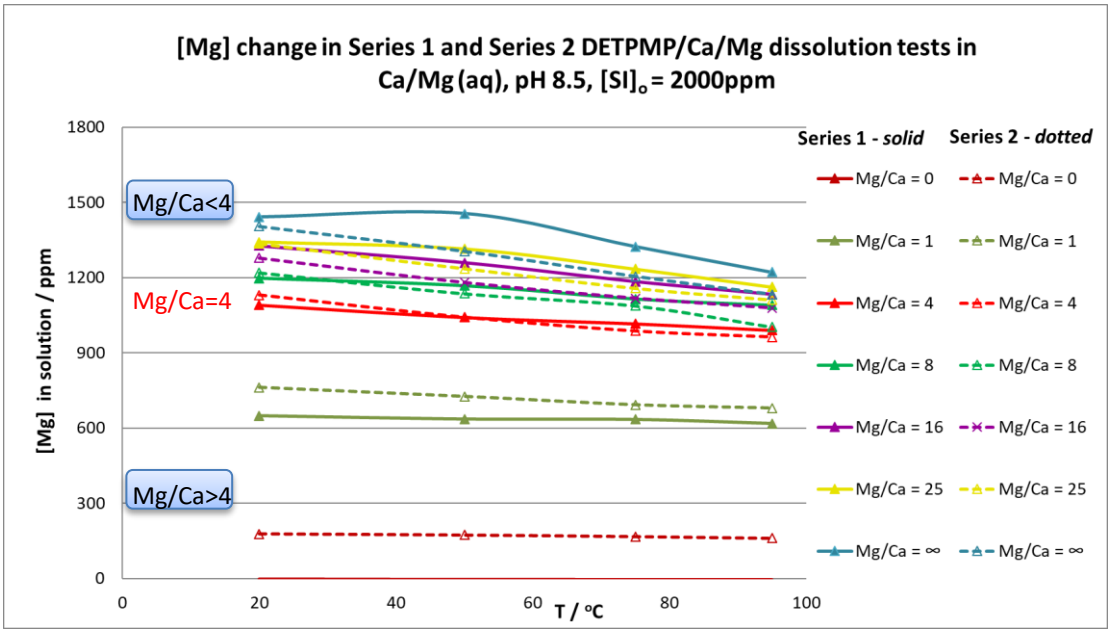

Figure 3.17 Comparison of [Mg^{2+}] in the bulk of Series 1 (solid line) and Series 2 (dotted line) solubility tests versus Mg/Ca molar ratio and T, pH 8.5.

In summary it is shown, that increasing the Mg proportion in the bulk solution and in the precipitate makes the phosphonate/Ca/Mg complex much more soluble, which is in agreement with the thermodynamics behind the complexes dissolution. It is shown that any change of Mg/Ca molar ratio in the brine during the phosphonate SI precipitate dissolution leads to a re-distribution of Ca, Mg and SI concentrations between a precipitate and bulk solution. Therefore, ~~complex~~ solubility of the complexes is determined by the total Mg/Ca molar ratio in the system rather than by the initial or final precipitation conditions; i.e. we observe a full re-speciation of the SI complex and divalent ions in accord with the equilibrium equations presented above.

Under field conditions, these results show that both the "squeeze" brine and produced brine will affect the solubility of the precipitate and this is going to vary during the squeeze lifetime. However, the equilibrium solubility values obtained in the Series 1 study can be directly used to predict the equilibrium solubility *Cs* of the precipitates that form during the shut-in periods of squeeze treatments. The further re-speciation occurring when the "squeeze" brine is replaced by a flowback brine can also be modelled based on the Series 2 data presented in this Chapter.

3.4. Inhibition Efficiency of Precipitated Phosphonate SI

It has been established for PPCA, the polymeric SI, that the precipitated SI has a much higher inhibition efficiency (IE) for preventing barite scale than the stock SI solution ((Farooqui and Sorbie 2016). For polymeric SIs, this has been shown to be due to the fact that the precipitate is rich in higher molecular weight components of the polymer and these tend to give the higher IE. Phosphonate SI stock solutions are expected to have mostly a single molecule composition, therefore precipitation effect on the inhibition efficiency of precipitated and re-dissolved species should not be significant. In order to check this hypothesis, the IE against barium sulphate of the precipitated phosphonate SI/divalent complexes was evaluated and compared to the SI stock solution. The key reason is to establish if the precipitated phosphonate SI complex in a precipitation process shows the same IE as the stock phosphonate SI solution before precipitation. In order to establish any effect due to the specific cations involved in the precipitate, the SIs (OMTHP, DETPMP, and HEDP) being tested were precipitated with only Ca in one series of experiments, and with both Ca and Mg in another.

The inhibition efficiency results for the precipitated and then re-dissolved SI complexes obtained at pH 5.5, T=95°C for the OMTHP_Ca and OMTHP_Ca_Mg complexes are shown in Figure 3.18 and Figure 3.19, respectively. These inhibition efficiency results are compared with the inhibition efficiency of the stock OMTHP solution. Both the OMTHP_Ca and OMTHP_Ca_Mg precipitates have slightly (~5-10%) higher performance than the stock solution which might be within experimental error or due to some impurities in the stock SI product.

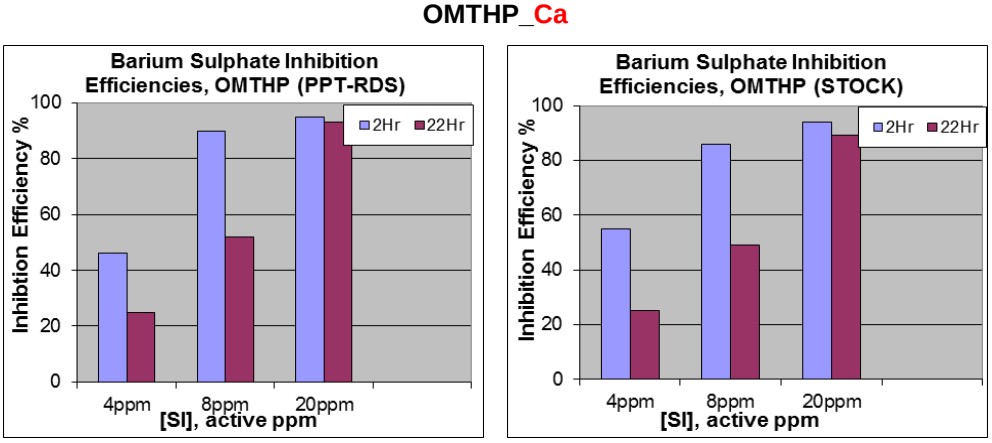

Figure 3.18 Barium sulphate inhibition efficiencies of OMTHP_Ca precipitate (left) and OMTHP stock (right) at pH5.5, 95°C.

OMTHP_Ca_Mg

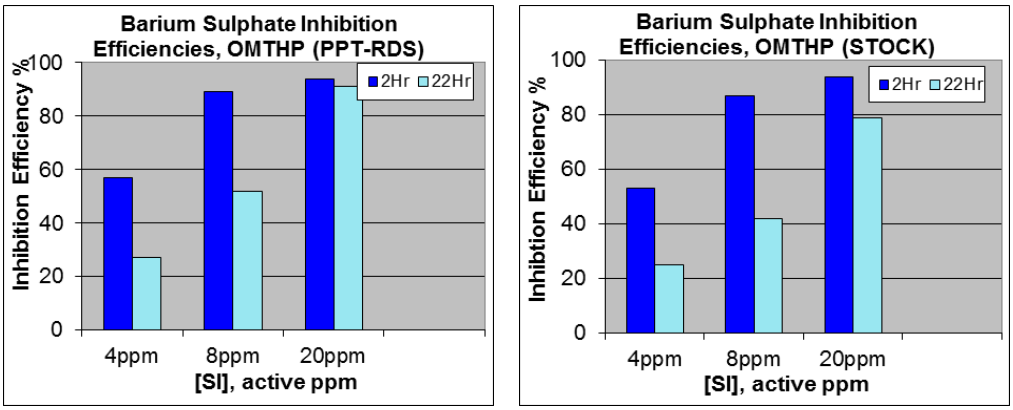

Figure 3.19 Barium sulphate inhibition efficiencies of OMTHP_Ca_Mg precipitate (left) and OMTHP stock (right) at pH5.5, 95ºC.

DETPMP_Ca

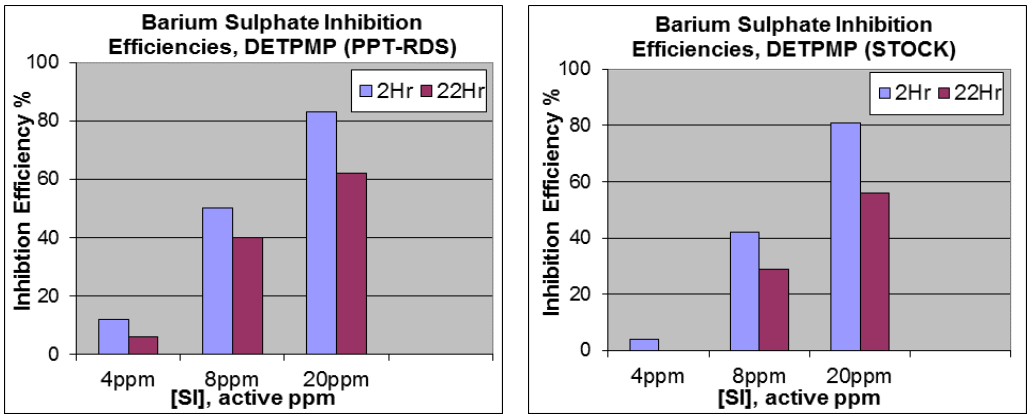

Figure 3.20 Barium sulphate inhibition efficiencies of DETPMP_Ca precipitate (left) and DETPMP stock (right) at pH5.5, 95ºC

DETPMP_Ca_Mg

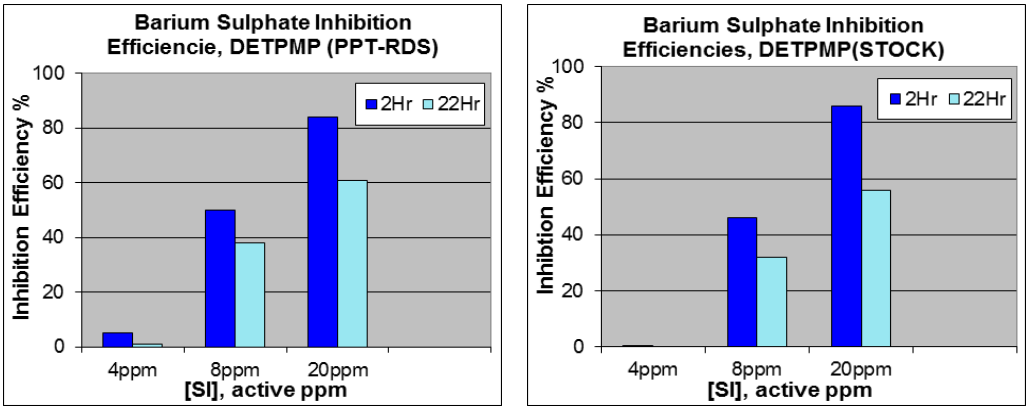

Figure 3.21 Barium sulphate inhibition efficiencies of DETPMP_Ca_Mg precipitate (left) and DETPMP stock (right) at pH5.5, 95ºC.

Figure 3.20 and Figure 3.21 present the inhibition efficiency results for the precipitated and re-dissolved SI complexes of DETPMP_Ca and DETPMP_Ca_Mg, at pH5.5 and T=95ºC, where they are compared with the inhibition efficiency of the stock DETPMP. Both the DETPMP_Ca and DETPMP_Ca_Mg precipitates again have a slightly higher inhibition efficiency than the stock solution of about ~5-10%, which may be within experimental error or due to some impurities in the stock SI product.

Figure 3.22 and Figure 3.23 present the inhibition efficiency test results for the precipitated and re-dissolved SI complexes of HEDP_Ca and HEDP_Ca_Mg, precipitated at pH 5.5 and T=95ºC, where they are compared with the stock HEDP. Both the HEDP_Ca and HEDP_Ca_Mg precipitates have approximately the same low inhibition efficiency as the stock solution.

HEDP_Ca

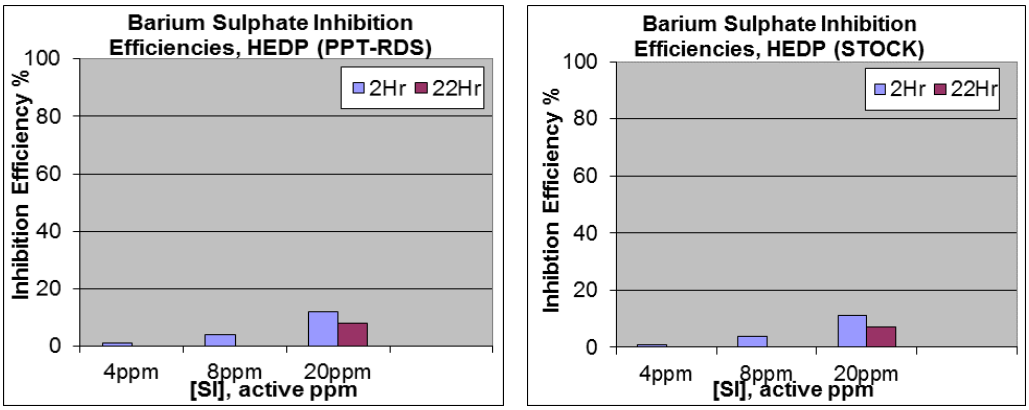

Figure 3.22 Barium sulphate inhibition efficiencies of HEDP_Ca precipitate (left) and HEDP stock (right) at pH5.5, 95ºC

HEDP_Ca_Mg

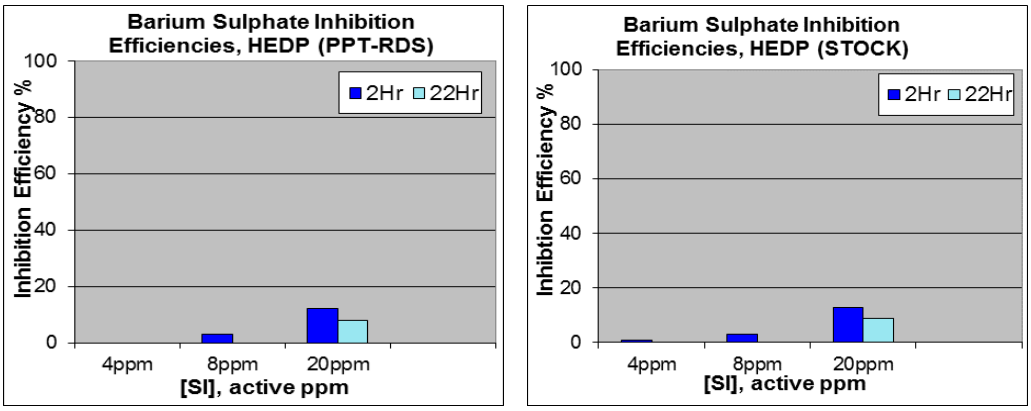

Figure 3.23 Barium sulphate inhibition efficiencies of HEDP_Ca_Mg precipitate (left) and HEDP stock (right) at pH5.5, 95ºC

Overall, the precipitation process itself does not significantly affect the final inhibition efficiency of the phosphonate SIs. Generally, the inhibition efficiency of the precipitated and re-dissolved phosphonates are approximately the same as that of the stock SI solution, although possibly with a slightly improved efficiency of 5-10% occurring for the precipitated OMTHP and DETPMP over their stocks. This marginally improved IE for the precipitated samples *may* be due to small amounts of phosphorus-containing impurity in the SI stock. However, unlike the case for the precipitated and stock polymeric SIs, it is clearly not a very important effect for the phosphonates and so practically the IE of the stock and precipitated phosphonate SIs are almost the same for all three phosphonate species studied in this work.

3.5. Summary and Conclusions

Solubility of the phosphonate/divalent complexes SI_Ca_Mg: It has been shown, that all the phosphonate/metal precipitated complexes tested in the study become less soluble with increasing temperature and much more soluble as the proportion of Mg in the brine increases.

The solubility of the SI_Ca_Mg complex increases for the different phosphonate species in the order: HEDP (di-phosphonate) << OMTHP (hexa-phosphonate) ~ DETPMP (penta-phosphonate).

Any change of Mg/Ca molar ratio in a brine during SI re-dissolution causes a re-distribution of Ca, Mg and SI concentrations between the precipitate and bulk solution,

leading to the solubility variation. Therefore, the stoichiometries n_1 and n_2 of the SI_Ca_{n1}_Mg_{n2} precipitated complexes is also going to vary. This probably occurs in accord with the equilibrium equations proposed to describe the complex formation of these species (denoted with the stoichiometry, SI_Ca_{n1}_Mg_{n2}) in previous work (Shaw and Sorbie 2014, Shaw and Sorbie 2015).

Inhibition efficiency of the precipitated phosphonates: The precipitation process itself does not significantly affect the final inhibition efficiency of the phosphonate SIs. Generally, the inhibition efficiency of precipitated and re-dissolved phosphonate complexes, such as SI_Ca and SI_Ca_Mg, are approximately the same as that of the stock SI solution for all three phosphonate species studied in this work.

Field significance: This work demonstrates that the solubility of these SI_Ca_{n1}_Mg_{n2} complexes, i.e. [SI] released into the bulk solution, varies as the brine composition changes. In a field precipitation squeeze application, the brine used in the main SI treatment will determine the stoichiometry and solubility of the complex which is formed (mainly as the SI slug propagates out into the hotter region some distance from the well). However, the situation changes when this brine is replaced by the flowback (produced) formation brine when the well is brought back on to production after the squeeze treatment. It is this flowback brine which will determine the subsequent solubility of the precipitated complex by re-speciation, although it is noted there will also be a *kinetic* component in the dynamic return system since the re-speciation will probably not be instantaneous. The application brine is within our control, but the return brine composition is a "given" (which can be measured). However, the results described in this Chapter do suggest how this can be used positively, or at least accounted for, in a specific precipitation squeeze process. When the higher retention via precipitation mechanism is required, it is suggested to keep the Mg/Ca ratio at this low level during squeeze treatments (ideally, remove all Mg from the squeezed brine). The solubility of various phosphonate/metal complexes measured in the current part of the study can be directly used as input data to model precipitation squeeze treatments.

It has been shown, that all the tested SI_Ca_Mg precipitates have quite high solubility over a wide range of Mg/Ca molar ratios from all Mg to all Ca and over a temperature range, 20 - 95^{o}C. Thus, even for the lowest solubility case, it is still higher than the SIs MIC values; MIC is below 50 ppm for all the tested phosphonate SIs (Shaw, Sorbie et al.

2012). In the 95ºC tests, which are closer to the reservoir conditions, the solubility generally does not exceed 200ppm. Therefore, the solubility *Cs* stays within a concentration range that is above MIC but does not exceed it significantly, giving potential promise for effective scale prevention and longer squeeze lifetimes during precipitation treatments.

Therefore, the solubility data obtained in this study for 3 common phosphonate SIs can be used as input data for the precipitation/dissolution model. This will allow to obtain an accurate prediction for the solubility of the SI/Ca/Mg precipitates forming during squeeze treatments, and if necessary to control the solubility of the precipitates by controlling the Mg/Ca ratio in the "squeezed" brine.

CHAPTER 4. NON-EQUILIBRIUM DISSOLUTION OF PHOSPHONATE_CALCIUM_MAGNESIUM COMPLEXES IN BOTTLE TESTS

In the previous Chapter, the thermodynamics of phosphonate/Ca/Mg precipitates dissolution has been defined. The equilibrium solubility of phosphonate/metal complexes was measured as a function of pH, Mg/Ca molar ratio and temperature. It was shown that any change of Mg/Ca molar ratio in a brine during the dissolution process led to a re-distribution of all the Ca, Mg and SI concentrations between the precipitate and the bulk solution, leading to a variation in the solubility. The current Chapter focuses on the dissolution *kinetics* of those phosphonate/Ca/Mg precipitates and aims to define the factors that govern dissolution in the bulk tests, prior to moving to dynamic flooding experiments in porous media.

4.1. Introduction

In the precipitation treatment model, developed within the FAST group, the scale inhibitor (SI) precipitate's *solubility Cs* and *dissolution rate r* are believed to be the key parameters for precipitation squeeze treatments. These parameters control the level of SI concentration released and the overall treatment lifetime in precipitation squeezes, according to Noyes-Whitney equation (4.1):

$$\frac{dC}{dt} = r \cdot (Cs - C)$$

Where:

dC/dt – Solute dissolution rate ($g \cdot s^{-1}$)

r – Dissolution rate constant, s^{-1}, which related to the surface area of the solute particle A, m^2; thickness of the concentration gradient d, m; and diffusion coefficient D, $m \cdot s^{-1}$:

$$k = \frac{A \cdot D}{d}$$

Cs – Saturation concentration, i.e. solubility (g or moles/L)

C – Concentration in the bulk solvent/solution (g or moles/L)

The solubility of the phosphonate/divalent cations precipitates, presented in Chapter 3 for the Series 1 and Series 2 studies, represent the inhibitor concentration at full

thermodynamic *equilibrium* conditions. However, under oilfield conditions, most of the processes do not occur at full equilibrium. Potentially, the precipitation reaction itself may reach equilibrium during the shut-in period of the squeeze treatment. However, once the well is brought back on to production, the equilibrium will shift due to flow effects and brine composition changing from the squeeze brine to the production brine, as described above.

Also, it was noticed that the higher SI solubility concentrations, measured at equilibrium in the previous Chapter, are never recorded at the end of the squeeze treatments, although the dissolution mechanism should govern the release of the SI at that stage of the treatment lifetime. An example was described by (Sorbie et al., 1993), that the phosphonate SI/calcium precipitates solubility (~10^{-4} M) was too high compared to the inhibitor return concentrations (~10^{-5}-10^{-6} M) observed under both the field conditions and in coreflood experiments. This means, that dissolution process has not been fully understood and therefore, required some further exploration.

However, before describing our studies in a flooding system, dissolution of the SI/Ca precipitates will first be explored in bulk solutions, while replacing the supernatant brine repetitively in a series of bottle tests. By monitoring the SI concentration in the bulk solution, we can observe the brine replacement effect on the SI return concentration but avoiding the flow rate effect which will be used in dynamic sand pack flooding experiments. The effect of the size of the precipitate particles, brine replacement and brine composition variation on the apparent SI solubility will be explored. This needed to be established in the bulk before moving to non-equilibrium dissolution studies in porous media, since the understanding of these effects on dissolution will help to (i) define the experimental design for the sand pack studies and (ii) to interpret the release behaviour of the precipitated inhibitor into the brine during those experiments. The results will be supplemented by numerical modelling studies that explain the observed solubility data.

Finally, the structural and morphological transitions occurring during the dissolution tests will be monitored. The phase transition effect has been described earlier in the literature (Browning and Fogler 1995, Browning and Fogler 1996, Zhang, Shen et al. 2016). According to those studies, initial highly soluble amorphous phosphonates/calcium precipitates may develop into crystalline structure of a lower solubility, as the volume of brine passing over the precipitate during flooding tests increases, which is also accompanied by a decrease of calcium in the SI/Ca precipitate and the precipitate's

apparent solubility. The difference between amorphous and crystalline structures is shown in Figure 4.1. In a crystalline phase (Figure 4.1a), atoms are arranged neatly in a long-range order, whereas amorphous material (Figure 4.1b) is packed randomly without distinguishable order in the structure. To monitor the structural changes in the phosphonate precipitates during the dissolution tests, X-Ray Crystallography (XRD) was applied to the different precipitate size fractions prior to and after conducting the dissolution experiments. Environmental Scanning Electron Microscopy - Energy Dispersive X-Ray (ESEM-EDX) patterns were also recorded for the same precipitates in order to observe the materials' surface texture.

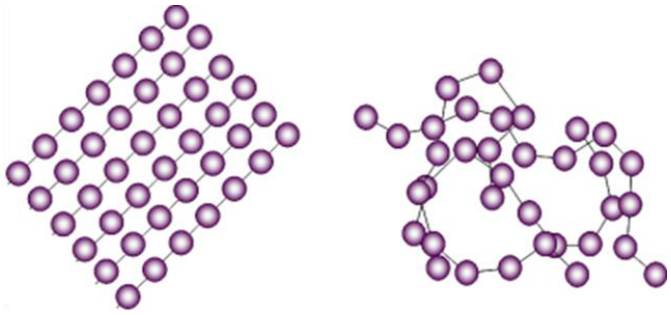

a **b**

Figure 4.1 Two possible arrangements of the elements in a solid: a – crystalline, b – amorphous

Thus, the following experimental studies will be presented in the current Chapter:

I. Dissolution of the DETPMP/Ca precipitates in Ca^{2+} and Mg^{2+} brines while replacing the supernatant as a "fresh" brine;

II. Numerical studies on the DETPMP/Ca precipitates dissolution in Ca^{2+} brine versus brine replacement;

III. ESEM/ EDX and XRD patterns for the precipitates obtained before and after the dissolution test.

The aim of conducting these studies in the bulk is to extend our understanding of the phosphonate SI re-dissolution process and evaluate bulk dissolution kinetics and associated factors that will have an impact on the apparent solubility of phosphonate SI precipitates, prior to moving to the non-equilibrium studies in porous media.

4.2. Experimental details

4.2.1. *Materials*

The commercially available phosphonate scale inhibitor DETPMP supplied by Italmatch was used to conduct the precipitation tests. All concentrations presented in the report are active concentrations. The structure of DETPMP was shown earlier in Table 3.1. The test brines were made up with the salts, $MgCl_2 \cdot 6H_2O$ and $CaCl_2 \cdot 6H_2O$ (both from Sigma Aldrich, used as received).

4.2.2. *Dissolution Test versus Brine Replacement*

To obtain the precipitated SI/cation complex product for this study and the following sand pack flooding tests (CHAPTER 4), SI was added to a 5L solution containing 5000 ppm Ca with the final [SI] = 10,000ppm. The solution was pH adjusted to pH 8.5 in order to achieve maximum precipitation of the SI/Ca complex. Subsequently, the solution was placed in a waterbath at 95^{o}C and left for 24 hours. The precipitate was collected using vacuum filtration with 0.45µm filters and left to dry at room temperature. Once the precipitate was dry, it was crushed and sized through different sieves and 3 fractions of precipitate material with different size distributions as listed below were collected:

- < 100 µm,
- 100-250 µm,
- > 250 µm.

Finally, a specific amount of the DETPMP/Ca precipitate obtained was added to 100ml DW and dissolved using a few drops of 35% HCl (aq). A 1ml sample from the dissolved precipitate test solution bottles was added to 9ml of DW and analysed by ICP-OES for [P] and [Ca] content to determine the stoichiometry n of the DETPMP_Ca_n complex.

The DETPMP/Ca precipitate dissolution test versus brine replacement was conducted in *four* steps (Tests 1-4), as denoted in Table 4.1. When moving to the next series, the precipitate was separated (by filtration) from the previous brine and each time placed into a "fresh" brine. This allowed the changing of the apparent solubility to be observed as the precipitate was placed into a fresh brine, as well as how the brine composition variation would affect the solubility, as Ca^{2+} brine was replaced by Mg^{2+} brine. In Chapter 3, it was observed that replacing the brine composition, i.e. changing Mg/Ca ratio in the brine,

should lead to the precipitate's solubility variation. In the current Chapter, we aim to monitor the kinetics of this process, evaluating how rapidly this solubility variation will occur.

The first three dissolution tests were conducted in 2000ppm Ca^{2+} brine, whereas in the last test, Test 4, the solubility was measured in a 1213ppm Mg^{2+} solution (molar concentration of divalents kept constant at 50mM/L in order to maintain the ionic strength constant). All samples were collected at room temperature, 20°C. The Ca^{2+} and Mg^{2+} solutions were prepared with concentrations as given in Table 4.1. The pH value of both brines was then adjusted to pH 6.0 using dilute HCl (aq) and/or NaOH (aq).

Table 4.1 Brine parameters

Test №	$[Ca^{2+}]$ ppm	$[Mg^{2+}]$ ppm	$[Cl^{-}]$ ppm	$[Ca^{2+}]$ mM/L	$[Mg^{2+}]$ mM/L	Comments
1,2,3	2,000	0	~3,538	49.9	0.0	All Ca^{2+}
4	0	1213	~3,538	0.0	49.9	All Mg^{2+}

The test procedure:

1. 0.4g of each DETPMP/Ca precipitate fraction was placed into a 100ml solution of 2000ppm Ca^{2+} brine:
    - Bottle 1 – <100 µm particles,
    - Bottle 2 – 100-250 µm,
    - Bottle 3 – >250 µm.
2. Then, each solution containing precipitate was stirred for ~30minutes, using a magnet stirrer and a stirrer bar.
3. The solutions were then left at room temperature for 1-2 hours to allow the precipitate to settle to the bottom of the test bottles, before the top solution was sampled using a 0.22 µm filter to avoid fine particles being transferred to the samples. A 1ml filtered sample was added to 9ml of distilled water. These were denoted as *filtered samples*.
4. After the filtered samples were collected, the bottles were placed in a centrifuge for 5 minutes, followed by the sampling of 1 ml of the top solution into 9ml distilled water *without* using any filters. These samples were marked as *centrifuged samples*.
5. Steps 2-4 were repeated until the SI concentration in the brine reached a constant value. The pH was continuously measured over the entire study.
6. Once a constant value was achieved for the solubility, all the test solutions

containing the DETPMP/Ca precipitate were collected using vacuum filtration through a 0.45 µm filter and placed into a "fresh" 100ml of 2000ppm Ca^{2+} brine. This was the start of Test 2.

7. Steps 2-4 described for Test 1 were performed again for Tests 2 and 3.
8. In the last test, Test 4, the Ca^{2+} brine was replaced by Mg^{2+} brine and the procedure was repeated as described above.
9. All the collected samples were analysed by ICP-OES for [P] and [Ca] or [Mg] content in order to determine the solubility of the DETPMP_Ca precipitate.

The schematic procedure is shown in Figure 4.2.

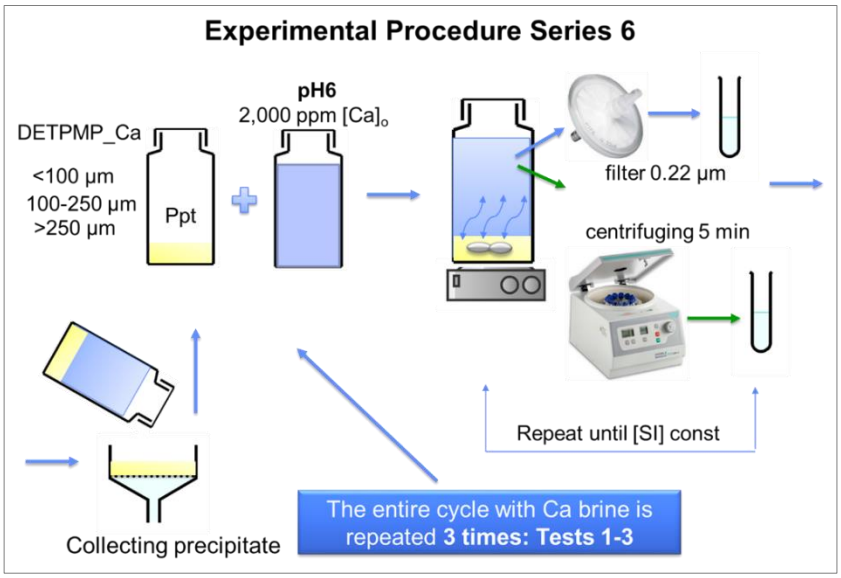

Figure 4.2 Solubility versus brine replacement, Tests 1-3

The remaining precipitates were collected after all the dissolution tests, using vacuum filtration through a 0.22 µm filter and along with the initial DETPMP/Ca precipitates, were analysed by ESEM-EDX and XRD techniques to detect any structural changes that occurred during the dissolution tests.

4.2.3. *Environmental Scanning Electron Microscopy - Energy Dispersive X-Ray*

A Philips XL30 Environmental Scanning Electron Microscope (ESEM), with an Oxford Instruments cryo-stage, and an energy dispersive x-ray detector (EDX) was used to image and analyse the DETPMP/Ca precipitate grains before and after the dissolution tests, as well as some silica sand and the mixed silica/scale inhibitor substrate after the sand pack experiments. The scanning electron microscope uses an electron beam to scan across the

surface of a sample. As the electrons strike the sample, a variety of signals are generated, and it is the detection of these signals that produces an image or the elemental composition of a sample. A very general summary of the procedure is as follows:

1. Select the required detector;
2. Load samples into chamber;
3. Select mode – high, low, environmental and the corresponding conditions;
4. Ensure chamber is ready for use;
5. Focus the detector;
6. The SEM is now ready to image/analyse the samples;
7. When the process is finished, release the samples from the chamber.

4.2.4. *Powder X-Ray Diffraction*

X-Ray Diffraction was used to obtain structural information of the DETPMP/Ca precipitates at different stages of the experiments, allowing us to detect any structural changes that occurred during dissolution. A Bruker AXS P4 4-circle X-ray Diffractometer (Crystallography Service at Heriot-Watt University) was used in this work. XRD patterns were collected for all the fractions of DETPMP/Ca precipitate before starting the dissolution tests. After finishing the tests, the precipitates were filtered, dried and gently crushed into a powder and again analysed on the XRD diffractometer.

X-ray Diffraction is based on the interference of monochromatic X-rays and the crystalline structure of the samples. These X-rays are generated by a cathode ray tube, filtered to produce monochromatic radiation and directed towards the sample. The interaction of the incident rays with the sample produces interference and a diffracted ray, when conditions satisfy Bragg's Law:

$$n\lambda = 2d \sin \theta \qquad (4.2)$$

Where λ - the wavelength of electromagnetic radiation, d - the lattice spacing, and θ - the diffraction angle in a crystalline sample. These diffracted X-rays are then detected, processed and counted. By scanning the sample through a range of 2θ angles, all possible diffraction directions of the lattice are collected due to the random orientation of the powdered material.

4.3. Results and discussion

4.3.1. *Dissolution Study versus Brine Replacement: in Ca^{2+} and Mg^{2+} Brines*

The DETPMP/Ca precipitate was produced prior to conducting the dissolution studies. This precipitate will also be used for the later sand pack flooding experiments, presented in Chapter 5.

Precipitate Characterization

DETPMP was precipitated in a 2L solution containing 5,000ppm Ca (Figure 4.3a). The produced precipitate was filtered through a 0.45µm filter paper whilst at 95ºC and pH 8.5 (Figure 4.3b). Once the precipitate had dried, it was crushed and sieved. Three distinctive size fractions: <100 µm, 100-250 µm, and >250 µm were collected.

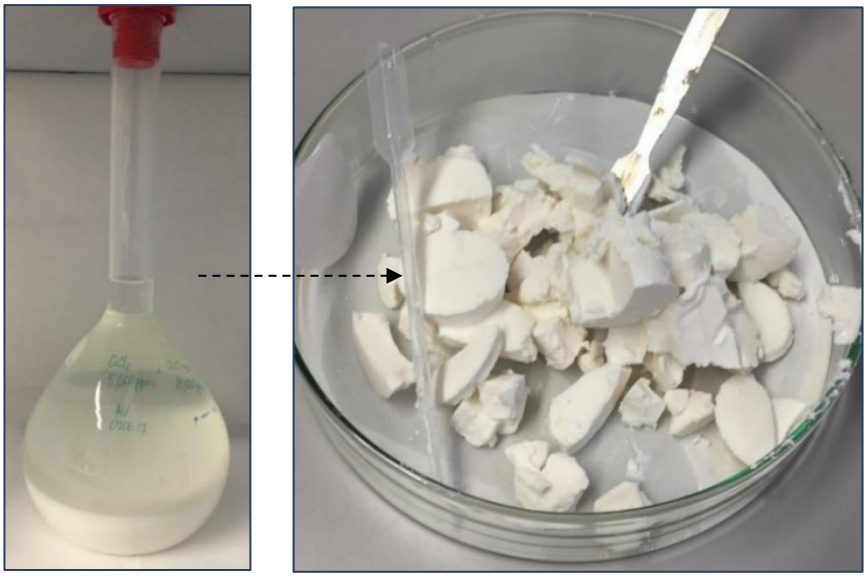

(a) **(b)**

Figure 4.3 DETPMP_Ca precipitate formed at pH 8.5 and T=95ºC: a) in solution before filtration; b) after filtration

To characterise the produced DETPMP_Ca_n precipitate, i.e. to find the stoichiometry n, only the smallest grain size fraction <100µm was used. Two samples of 0.2538g and 0.2658g were taken from this fraction and dissolved in distilled water, by adding a few drops of 35% HCl. After the solids were fully dissolved, samples were taken from the top solutions and analysed by ICP-OES for SI and Ca content. The data obtained from these tests were then used to calculate the stoichiometry n of the DETPMP_Ca_n complexes presented in Table 4.2.

Table 4.2 <100µm DETPMP_Ca Precipitate Characterisation

Moles DETPMP (mole/L)	Moles Calcium (mole/L)	Ca/ DETPMP ratio
0.00228	0.0128	5.59
0.00225	0.0123	5.46

The average stoichiometry of the DETPMP_Ca precipitate found experimentally was n = 5.52. In our earlier experiments in Chapter 3, it was shown that at these conditions the stoichiometry of the corresponding DETPMP_Ca complex was expected to be ~ 4. The higher stoichiometry values, i.e. higher calcium content, obtained for the current precipitate may be caused by surface coating of dissolved calcium left on the precipitate after filtration. When prepared for characterization, this would mean it was present in the test solution during ICP-OES analysis.

DETPMP/Ca Dissolution Study in Bottle Tests

Four tests were conducted with brine replacement. In ***Test 1***, the apparent solubility of the DETPMP/Ca complex fractions, described above, was measured in 100ml of 2000ppm Ca brine. Each measurement was taken after 30 minutes of stirring the test solutions, followed by sampling via 0.22 µm filters that were used to avoid fine particles contaminating the sample.

The results for Test 1 are shown in Figure 4.4. The DETPMP concentration reached a constant value after 43 hours at *~350ppm* for the middle size fraction 100-250µm, and slightly lower values of *335ppm* and *320ppm* for the smaller <100µm and greater >250µm fractions, respectively. Since ICP-OES analytical method allows 10% experimental error, it can be concluded, the solubility for all the fractions reached a similar value.

As an alternative to filtration, the test bottles were also centrifuged for 5-7 min, followed by sampling of the top supernatant solution and analysing the samples for SI and Ca content. Centrifuging should cause the smaller precipitate particles to settle on the bottom of the test bottles, thus removing them from the top solution. The data for the centrifuged samples is shown in Figure 4.5, whereas the comparison of the data obtained from both methods is shown in Figure 4.6. The SI concentration values obtained using both centrifuging and filtration methods are very close and in a good agreement. Both methods can be used in sand pack tests to avoid fine particles contaminating the samples, however, centrifuging may be a cheaper and more convenient option to apply.

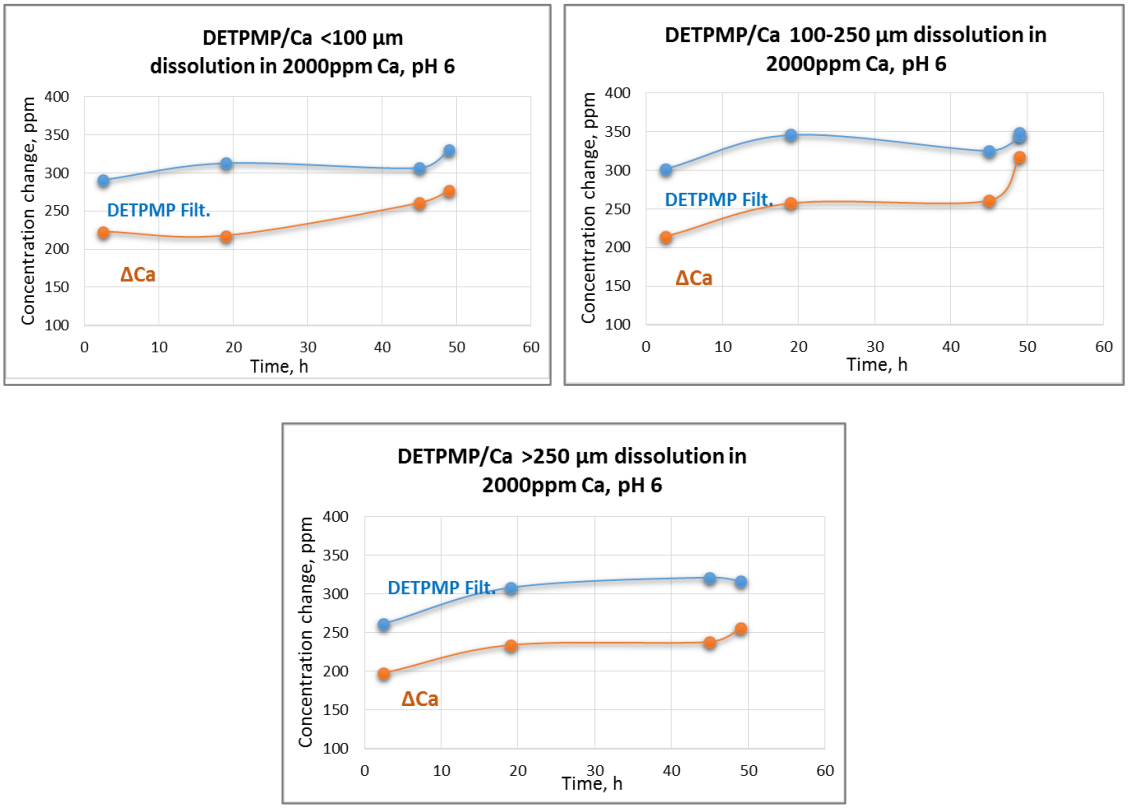

Figure 4.4 Scale inhibitor DETPMP and Ca concentration change in Test 1 during the precipitate dissolution - samples are taken using 0.22 µm filters: Ca 2000ppm, pH6, 20ºC.

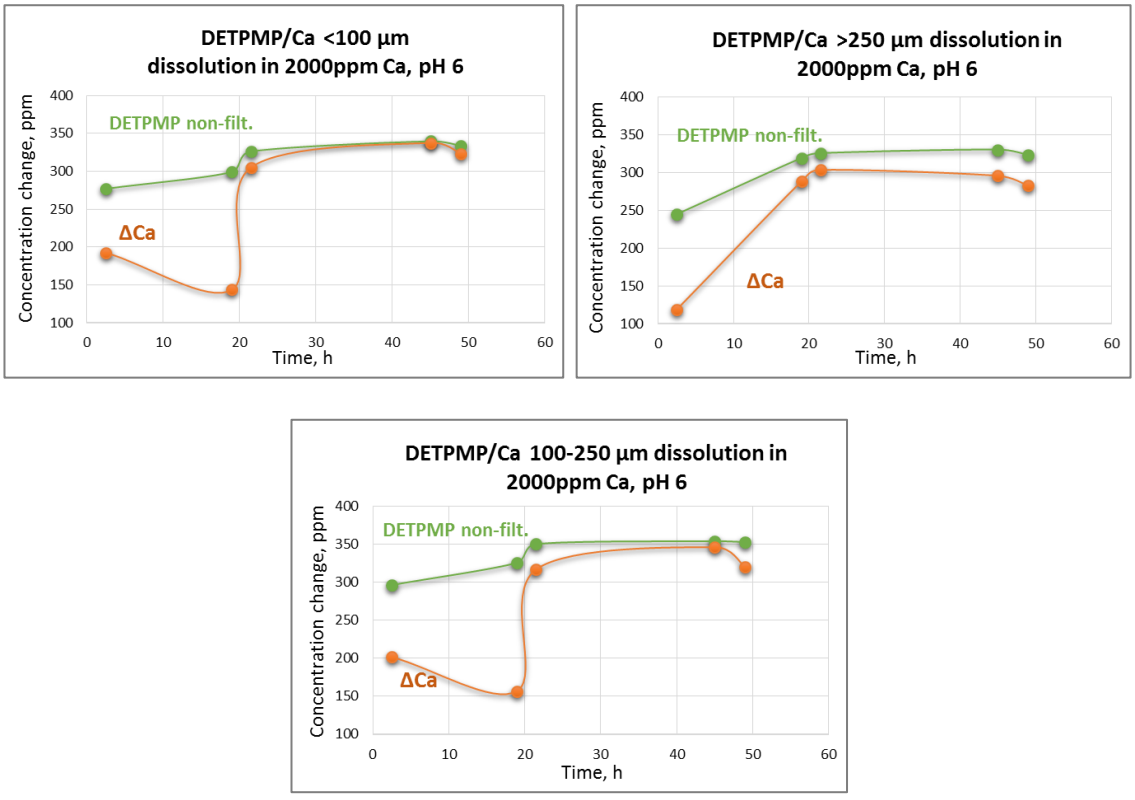

Figure 4.5 DETPMP and Ca concentration change during DETPMP/Ca dissolution in Ca 2000ppm, pH6, 20ºC in Test 1 - centrifuged samples

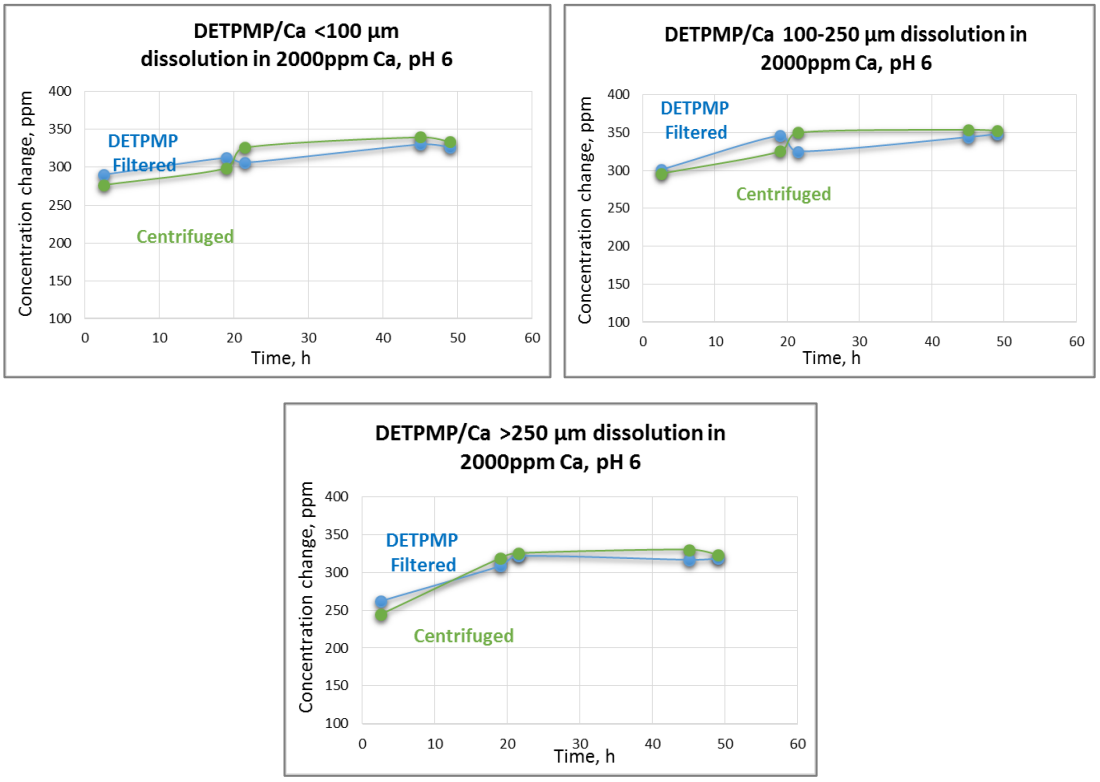

Figure 4.6 DETPMP/Ca precipitate dissolution in Test 1 – comparison of [DETPMP] and [Ca] data obtained from the filtered and centrifuged samples

Subsequently, the DETPMP/Ca precipitates, not dissolved in Test 1, were filtered and placed in "fresh" Ca brine of the same characteristics: 100ml, 2000ppm Ca, pH 6, T = 20°C. The dissolution parameters obtained in these systems – denoted as ***Test 2***, are shown in Figure 4.7. The data for all the size fractions used in the test shows that the constant SI concentration of ~125ppm was reached within the first 44 hours. The Ca concentration change during this dissolution test is less significant; the final ΔCa was recorded at ~50-80ppm, compared to ΔCa ~300ppm in Test 1.

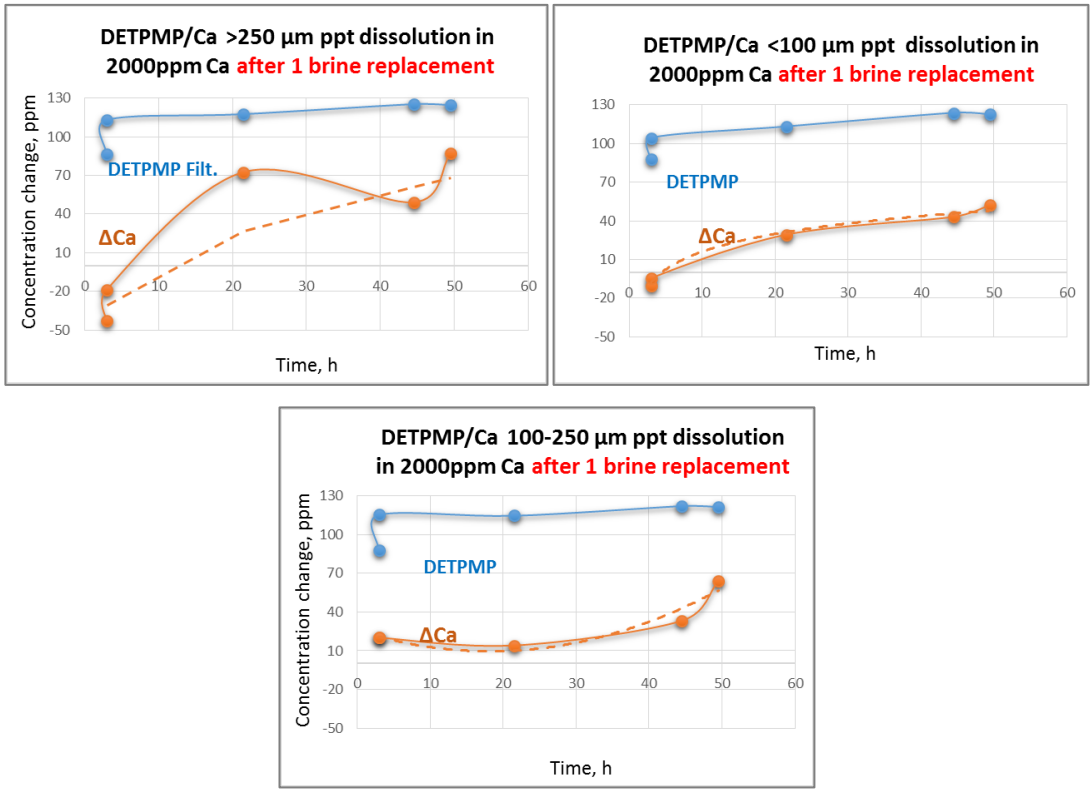

Figure 4.7 DETPMP/Ca precipitate dissolution in Test 2 after 1 brine replacement – samples taken after centrifuging; Ca 2000ppm, pH6, 20°C.

Subsequently, the precipitates were again filtered and placed into another "fresh" Ca brine with the same characteristics: 2000ppm Ca, pH 6, T = 20°C, denoted as ***Test 3*** study. The results of the SI solubility versus time (up to 170 hours) are shown in Figure 4.8. A constant SI concentration ~*90ppm* was reached by the end of the experiment. This value is lower than the solubility measured in Test 1, ~350ppm, and Test 2, ~125ppm. The data obtained for Ca is "noisy", which causes difficulties with analysing the trend, thereby it is not presented here. However, generally the Ca concentration variation during this dissolution Test 3 is quite low, from ~60ppm to ~90ppm, average ΔCa of all the fraction cases was recorded at ~40ppm, which is close to ΔCa observed for the previous Test 2, i.e. 50-80ppm. However, these are not a significant variation compared to the ΔCa ~300ppm in Test 1.

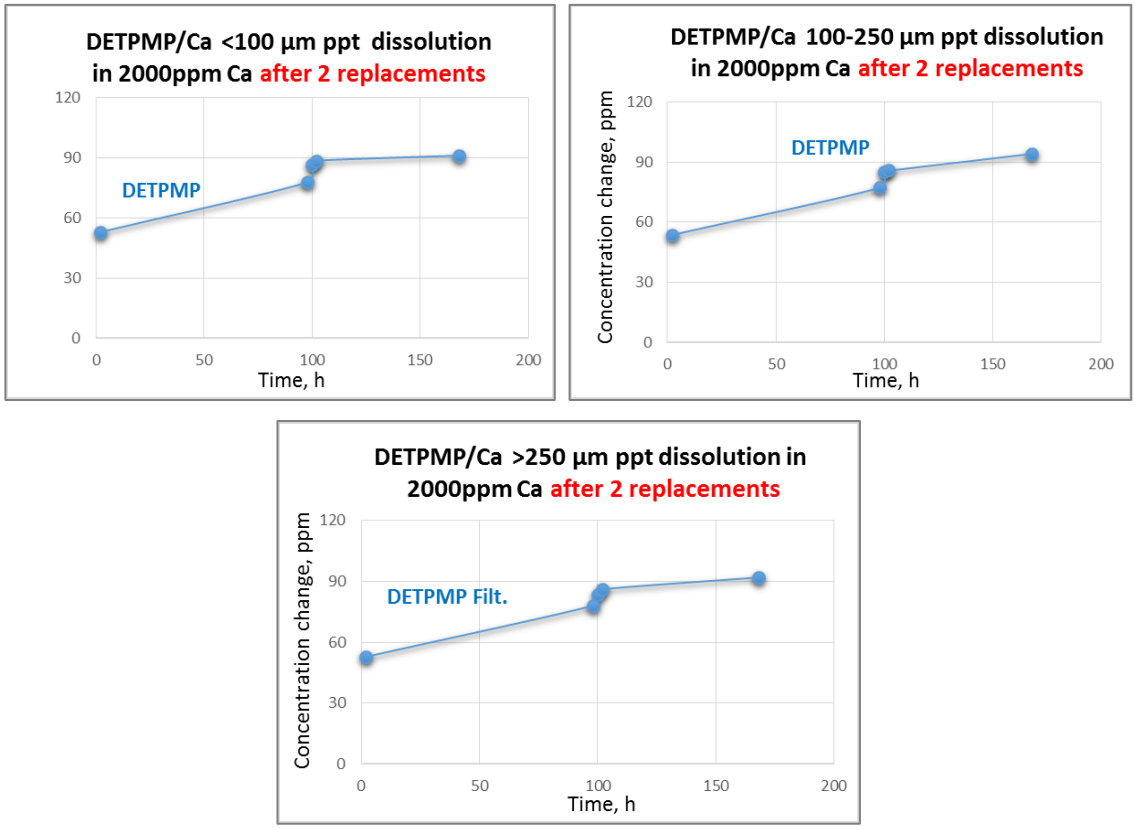

Figure 4.8 DETPMP/Ca precipitate dissolution in Series 3 after 2 brine replacements – samples taken after centrifuging; Ca 2000ppm, pH6, 20ºC.

In the next ***Test 4***, the DETPMP/Ca precipitate from the Test 3 solutions was placed into a "fresh" *Mg* brine. Hence, the Ca 2000ppm brine was replaced by 1213ppm Mg brine (both brines have the same molar concentration of cations, ~50mM), to define the effect of cation exchange in a solvent on the final solubility of the DETPMP/Ca precipitate. The results are plotted in Figure 4.9.

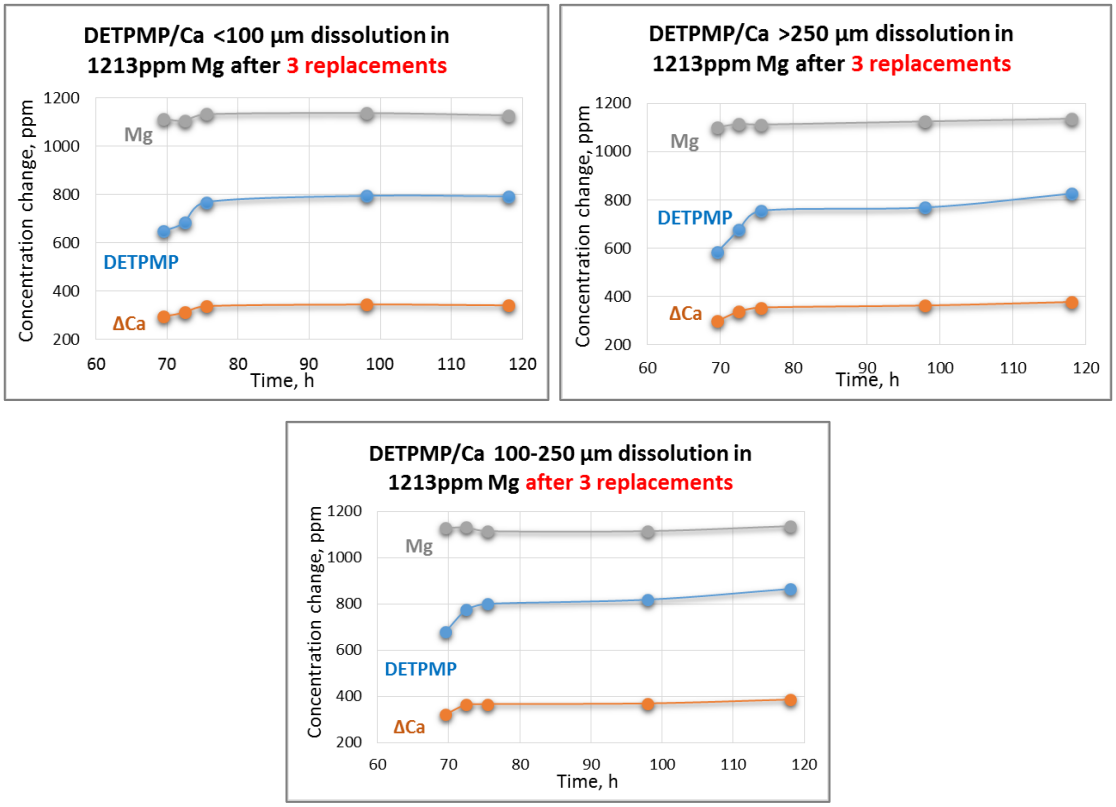

Figure 4.9 DETPMP/Ca precipitate dissolution in Series 4 after 3 brine replacements – samples taken after centrifuging; Mg 1213ppm, pH6, 20°C.

The DETPMP/Ca apparent solubility increases significantly once the precipitate is placed into Mg brine, up to ~800ppm. This is a notable increase, compared to the previous SI concentrations measured in Tests 1-3 in Ca brine: 350ppm, 125ppm and 90ppm, respectively. Thus, introducing Mg cations in the bulk where the phosphonate/Ca precipitate is deployed, makes the SI precipitate more soluble. This observed effect is in agreement with the conclusions made in Chapter 3 on thermodynamics of the phosphonate/metal complexes.

The Mg concentration in the bulk solution is shown to slightly decrease by ~60ppm, due to some Mg cations replacing Ca cations in the precipitated phase, as was also described in Chapter 3. Also, some Ca comes out of the precipitate phase into the bulk solution, therefore Ca measured at equilibrium increased from 0ppm to ~300ppm.

Thus, in this part of the study it was shown:

- During the ***Test 1-3*** studies, the apparent solubility of the DETPMP/Ca precipitate is gradually decreasing as it moves to the next "fresh" Ca 2000ppm brine: from 350ppm to 125ppm, and then to 90ppm. In the cases where only Ca brine was

used, the ΔCa concentration in the bulk, due to complex dissolution, also decreases when moving from Test 1 to the end of Test 3.

- The placement of the precipitate into Mg brine led to a significant increase in apparent SI solubility from 90ppm (Test 3) to 800ppm (Test 4), which is in agreement with the thermodynamic equilibrium solubility studies discussed in Chapter 3.
- The precipitate size does not have a noticeable effect on the dissolution rates of the phosphonate/Ca precipitates, at least at the long-term tests (50, 170 and 110 hours) conducted in this study, since the solubility values measured for all the fractions varied within 10% (probably, the effect of the particle sizes on the dissolution kinetics may be noticeable when the solubility measurements are taken after minutes, not hours as in the current study).

To understand the reasons behind the solubility variation during Tests 1-3, the processes occurring in these systems are described numerically, as shown in the next section. By analysing the calculated data, the reasons causing the solubility variation ~~could~~ can be identified.

4.3.2. *Modelling the DETPMP/Ca Dissolution in Tests 1-3*

To characterise the reactions occurring when the DETPMP/Ca precipitate is left to dissolve in the series of bulk tests (Tests 1-3) numerically, it was assumed that the system was a continuously stirred tank reactor (CSTR). The calculations are based on the following statements:

- Dissolution occurs at steady state giving a uniform composition throughout the entire test bottle (reactor);
- The precipitate that enters into the next series has the same composition as the one that exited the previous series.

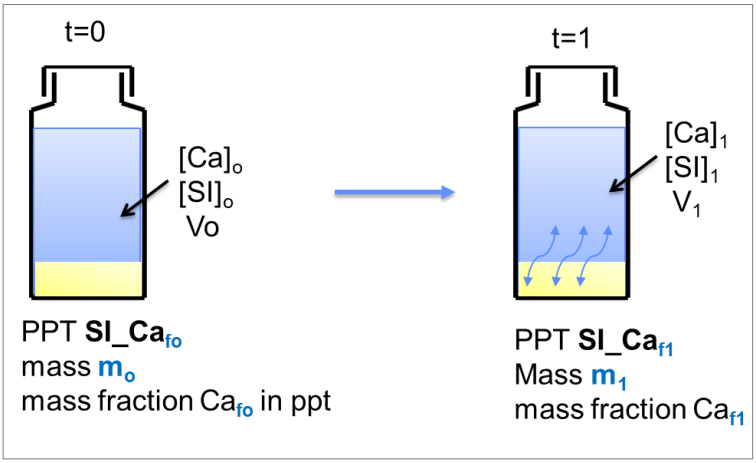

Figure 4.10 Test 1-3 dissolution modelling parameters

The schematic illustrating the parameters used in modelling the dissolution process is presented in Figure 4.10, where:

SI_Ca$_{fo}$ – initially placed precipitate with *fCa$_o$* – mass fraction of Ca;
SI_Ca$_{f1}$ – the final precipitate equilibrated with the brine, which may have different Ca fraction, *fCa$_1$*;
[Ca]$_o$ and *[SI]$_o$* – Initial Ca and SI concentrations in the fresh brine, volume *V$_o$*;
V$_1$ – final brine volume (was varying due to samples removing);
[Ca]$_1$ and *[SI]$_1$* – final equilibrium concentrations of Ca and SI reached;
m$_1$ and *m$_2$* – mass of the DETPMP_Ca precipitate before and after the dissolution test.

To note, the mass fraction was used instead of *n* – molar ratio of Ca to SI, however, the *n* can be expressed through mass fraction via the following equation:

$$n = \frac{n(Ca)}{n\,(SI)} = \frac{f(Cao)\cdot mass\ ppt\cdot M(SI)}{f(SIo)\cdot mass\ ppt\cdot M(Ca)} = \frac{f(Cao)\cdot M(SI)}{(1-fCao)\cdot M(Ca)} \quad (4.3)$$

The calculations were based on the following mass balance equations for Ca and SI:

In (brine) + In (precipitate) = Out (brine) +Out (precipitate)

$$V_o \cdot [Ca]_o + m_o \cdot fCa_o = V_1 \cdot [Ca]_1 + m_1 \cdot fCa_1 \quad (4.4)$$

$$V_o \cdot [SI]_o + m_o \cdot fSI_o = V_1 \cdot [SI]_1 + m_1 \cdot fSI_1 \quad (4.5)$$

Since fCa + fSI = 1, then the last equations can be modified to (4.6), giving a system of 2 equations with 2 unknown parameters: Ca_{f1} and m_1.

$$Vo \cdot [SI]_o + m_o \cdot (1 - Ca_{fo}) = V_1 \cdot [SI]_1 + m_1 \cdot (1 - Ca_{f1}) \quad (4.6)$$

Calculations, summarised in Table 4.3 show, that the stoichiometry *n* of the DETPMP_Ca_n precipitate decreases each time we are moving to the next brine over Tests 1-3. The corresponding pH measurements obtained experimentally for these solutions are presented in Table 4.4.

Table 4.3 DETPMP/Ca stoichiometry variation versus brine replacement

Stoichiomery	Brine replacement	1 fraction <100μm	2 fraction 100-250μm	3 fraction >250μm
n_0	-	5.5375	5.5375	5.5375
n_1	1st brine	3.8954	3.9640	4.1979
n_2	2nd brine	3.7347	3.6864	3.7534
n_3	3rd brine	3.6623	3.4146	3.3400

Table 4.4 pH and apparent solubility variation in Tests 1-3

Test	pH average	Solubility average	Solubility [SI]			pH		
			1 fraction	2 fraction	3 fraction	1 fraction	2 fraction	3 fraction
1st brine	7.58	336.5	334	353	323	7.56	7.60	7.57
2nd brine	7.33	123.0	123	122	125	7.28	7.32	7.39
3rd brine	7.16	92.5	91	94	92	7.18	7.13	7.17

By the end of Test 1, the initial precipitate with stoichiometry n ~5.5 reaches n ~4, followed by the solution pH increasing from 6 to ~7.6. This DETPMP/Ca stoichiometry corresponds with the value measured in previous studies at pH ~7.6 (Shaw and Sorbie 2014), that can be seen in Figure 4.11.

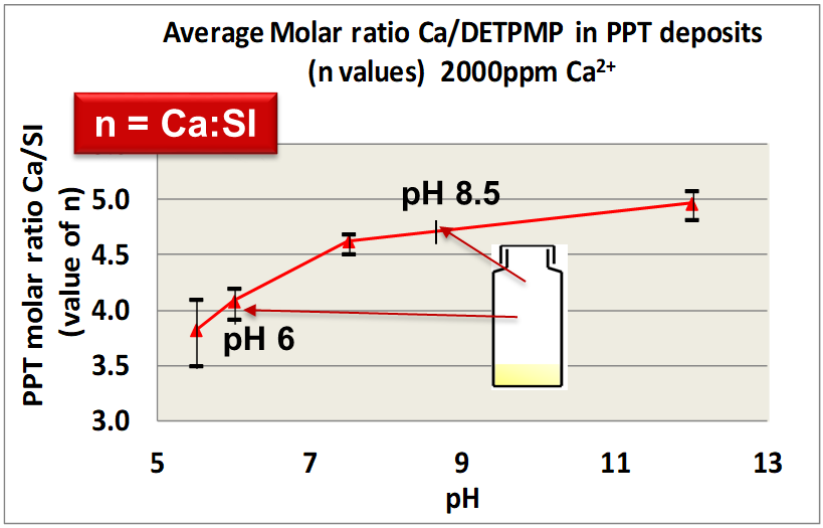

Figure 4.11 Stoichiometry of DETPMP/Ca precipitate versus pH (Shaw and Sorbie 2014)

Placing the precipitate into Ca brine at pH 6 leads to an immediate pH increase to pH 7.6, followed by SI being releasing into the bulk. This is probably due to the DETPMP/Ca complex being obtained from a solution at higher pH 8.5 and then subsequently placed in solution at pH 6. Since the SI releases into the bulk at the speciation appropriate to the apparent bulk pH, i.e. highly dissociated at pH 8.5 DETPMP species become *less dissociated* (or more associated) at the lower pH. This occurs in accordance with the SI dissociation theory, presented earlier in section 2.3. Thus, the SI species being associated with the H^+ ions coming from the water molecules lead to some OH^- releasing into the bulk. As a result, the brine *pH increases*. This re-speciation causes more SI to be released during the initial dissolution step due to the difference in pH between precipitation and dissolution brines.

The stoichiometry of the precipitate decreases as it moves to the next brine, which, in turn, leads to a decrease in both its *apparent* solubility and pH values. In Tests 2-3, pH decreased gradually, from ~7.58 (Test 1) to ~7.33 (Test 2) and to 7.16 (Test 3), however, pH variation was less significant, than on the initial dissolution step. This was followed by the average solubility decreasing from 337ppm to 123pm and 93ppm, respectively. The solubility variations in these following steps were due to continuous re-speciation of the precipitate to the apparent pH. Therefore, the stoichiometry of the precipitate was changing while reaching equilibrium and establishing a new equilibrium pH value. All the processes together are coupled in a schematic in Figure 4.12.

Thereby, by conducting the numerical studies, it was found that the dissolution of the DETPMP_$Ca_{5.5}$ precipitate in Tests 1-3 was followed by a stoichiometry decrease, which lead to the SI apparent solubility and solution pH gradually decreasing.

The phosphonate SI dissolution is governed by the continuous re-speciation of SI and Ca concentrations between the bulk and precipitate, leading to the leftover precipitate's stoichiometry decline. Brine pH does also vary during the dissolution process and the apparent pH in turn is going to affect the speciation of the precipitate. Thus, the apparent solubility of the phosphonate SI should be coupled with the apparent pH and phosphonates speciation and stoichiometry versus pH and solved numerically in the precipitation model.

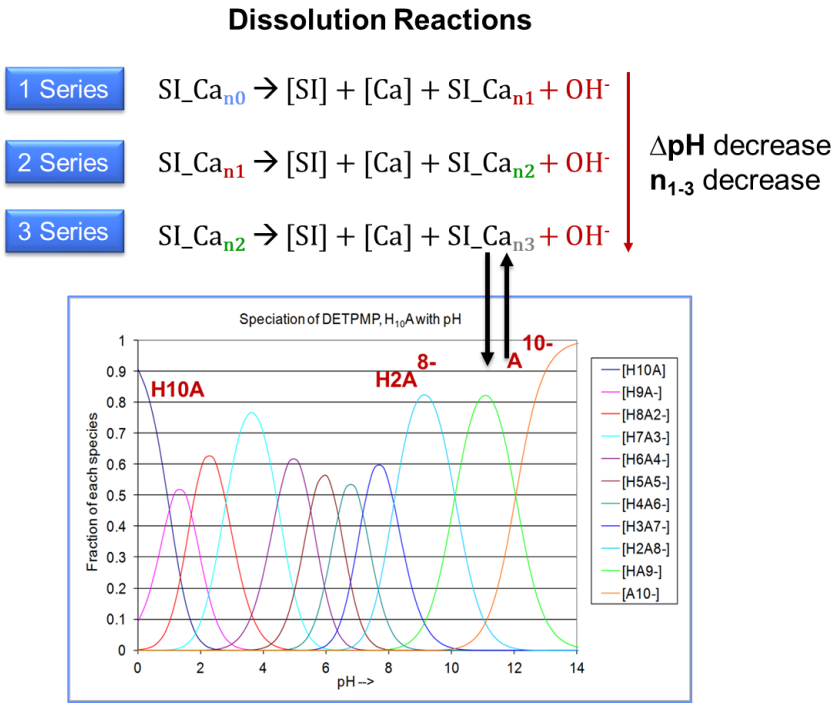

Figure 4.12 Processes occurring in DETPMP/Ca precipitate – Ca brine during precipitate dissolution versus brine replacement

4.3.3. *ESEM/EDX Analysis of DETPMP_Ca Precipitates*

One of the reasons behind the DETPMP/Ca precipitate solubility variation observed during the brine replacement may be a phase transition from an amorphous into a crystalline structure occurring during dissolution. In the literature it has been shown, that the phase of the phosphonate precipitates determines its morphology and *solubility* (Pairat, Sumeath et al. 1997). For example, amorphous calcium organophosphates are shown to have a significantly higher solubility than the same solids with a crystalline phase. To see if any structural changes occurred in the DETPMP/Ca precipitate morphology during the bulk dissolution study, at the end of the study, all the precipitate fractions were collected, dried and analysed by ESEM-EDX. The ESEM images of the <100µm; 100-250µm; and >250µm DETPMP_Ca precipitate fractions collected prior to and after the dissolution tests are shown in Figure 4.13, Figure 4.14, and Figure 4.15, respectively.

Initially, there are many fine grains and particles detected (i) in the bulk of the <100µm DETPMP/Ca fraction and (ii) stuck on the surface amorphous smooth material with some facets and edges developing on the surface, which may indicate the onset of the transition

from amorphous to a crystalline phase. The same conclusion can be derived from the images shown in Figure 4.14 and Figure 4.15 for the 100-250µm and >250µm DETPMP_Ca fractions, respectively.

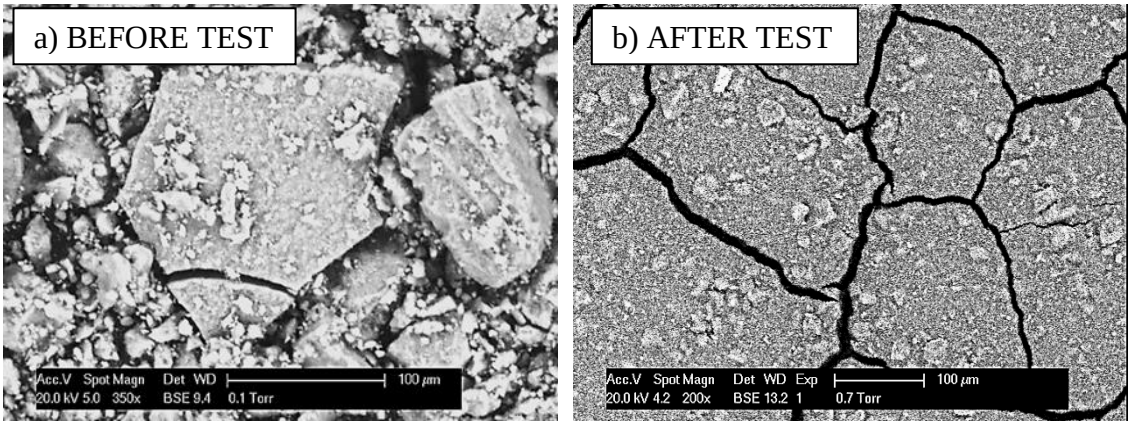

Figure 4.13 ESEM image of <100µm DETPMP_Ca precipitate particles before (a) and after (b) the dissolution experiments

Table 4.5 EDX signals on the <100µm DETPMP_Ca particles before and after dissolution

Element	Before the test		After the test	
	Atomic %	Weight %	Atomic %	Weight %
O	40.66	60.01	81.46	67.05
Mg	-	-	2.36	2.95
P	22.49	17.14	10.1	16.09
Cl	6.55	4.36	0.31	0.57
Ca	25.43	14.98	5.76	11.88
Na	2.58	2.65	-	-
Cu	2.29	0.85	-	-
5* (Ca/P)	*5.65*	-	*2.85*	-
5* (Ca+Mg)/ P	-		*4.56*	

EDX data indicates that the stoichiometry of the DETPMP solid complexes slightly decreases during the dissolution tests. Comparing the EDX data shown in Table 4.5 for the <100µm fraction before and after the dissolution test (Figure 4.13), it can be seen that the molar ratio of 5·Ca to P (as DETPMP is a penta-phosphonate, i.e. contains *five* phosphorus atoms) is *decreasing* from *5.65* to *2.85*, whereas 5·(Ca+Mg) to P ratio is *4.56* by the end of the dissolution tests.

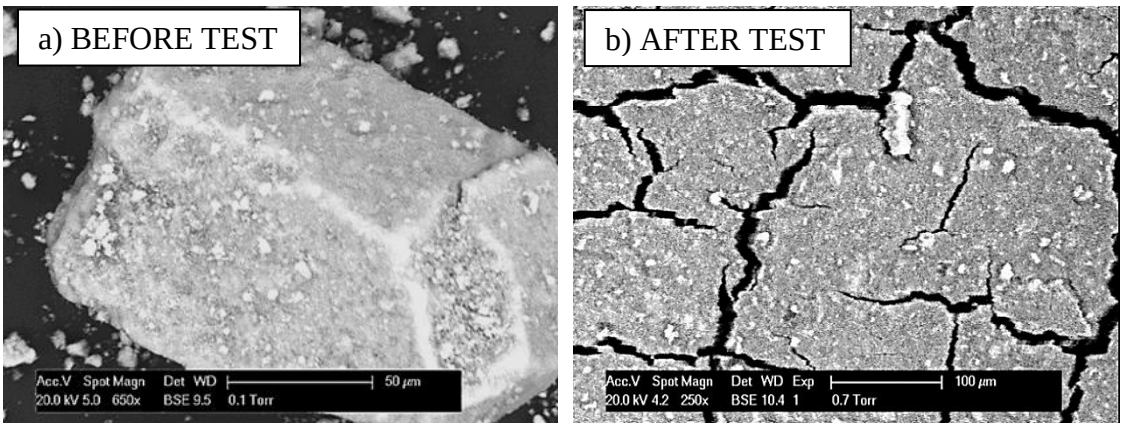

Figure 4.14 ESEM image of 100-250µm DETPMP_Ca precipitate particles before (a) and after (b) the dissolution experiments

Table 4.6 EDX signals on the 100-250µm DETPMP_Ca particles before/after dissolution

Element	Before the test		After the test	
	Atomic %	Weight %	Atomic %	Weight %
O	71.19	66.48	75.85	65.48
C	25.97	32.3	18.67	21.47
P	1.03	0.49	16.2	7.22
Ca	0.98	0.37	11.89	4.1
Mg	-	-	2.9	1.65
Cl	0.25	0.11	0.2	0.08
Cu	0.25	0.06	-	-
Na	0.23	0.15	-	-
S	0.09	0.04	-	-
5* (Ca/P)	*4.76*	-	*3.67*	-
5* (Ca+Mg)/ P	-		*4.56*	

The EDX data for the *100-250µm* and *>250µm* fractions are presented in Table 4.6 and Table 4.7, respectively. According to the data, the molar ratio of 5·Ca to P decreased by the end of the dissolution test from 4.76 to 3.67, and from 4.71 to 3.57 for the *100-250µm* and *>250µm* fractions, respectively. For the same fractions respectively, the 5· (Ca+Mg) to P ratio is equal to 4.56 and 4.51. This is in agreement with the ΔCa to ΔDETPMP ratio variation during the dissolution tests found via the numerical studies in section 4.3.2. The presence of Mg in the precipitate indicates that some Mg is incorporated into the precipitate phase during the dissolution Test 4, as suspected.

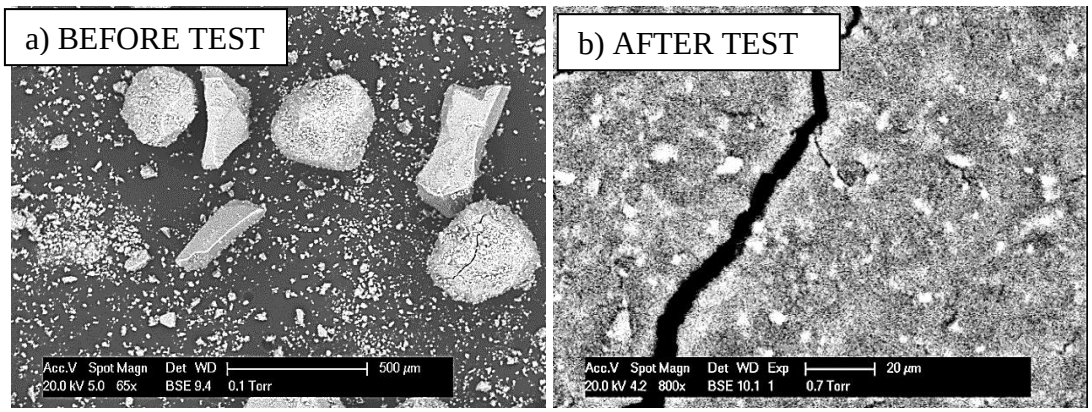

Figure 4.15 ESEM image of >250µm DETPMP_Ca precipitate particles before (a) and after (b) the dissolution experiments

Table 4.7 EDX signals on the >250µm DETPMP_Ca particles before/after dissolution test

Element	Before the test		After the test	
	Atomic %	Weight %	Atomic %	Weight %
O	70.49	66.42	15.62	20.91
C	25.27	31.72	66.58	66.91
P	1.73	0.84	12.93	6.71
Ca	1.63	0.61	9.23	3.7
Mg	-	-	2.42	1.6
Cl	0.34	0.14	0.37	0.17
Cu	0.19	0.04	-	-
Na	0.25	0.16	-	-
5* (Ca/P)	4.71		*3.57*	
5* (Ca+Mg)/ P			*4.51*	

4.3.4. *XRD for DETPMP/Ca Precipitates*

The EDX/ESEM images showed some morphology change in the DETPMP/Ca precipitate occurred during the bulk dissolution test (Series 6). To further check if a phase transition has occurred in the DETPMP/Ca precipitates, the precipitates were analysed on the X-Ray Diffractometer (XRD) to determine the exact structure of the material prior to and after the dissolution Tests 1-4.

The data is presented below in Figure 4.16, Figure 4.17, Figure 4.18 and for the different size fractions <100µm, 100-250µm, and >250µm, respectively. It can be seen from these graphs, no clear crystalline structures were detected within the precipitate samples collected after the dissolution test. This indicates, that all the solubility variations observed in the Test 1-4 studies were not due to the development of a new phase of distinguishable solubility. The re-speciation according to the apparent pH and the

complex stoichiometry variation should be the key process that defines the dissolution phenomena observed in the study.

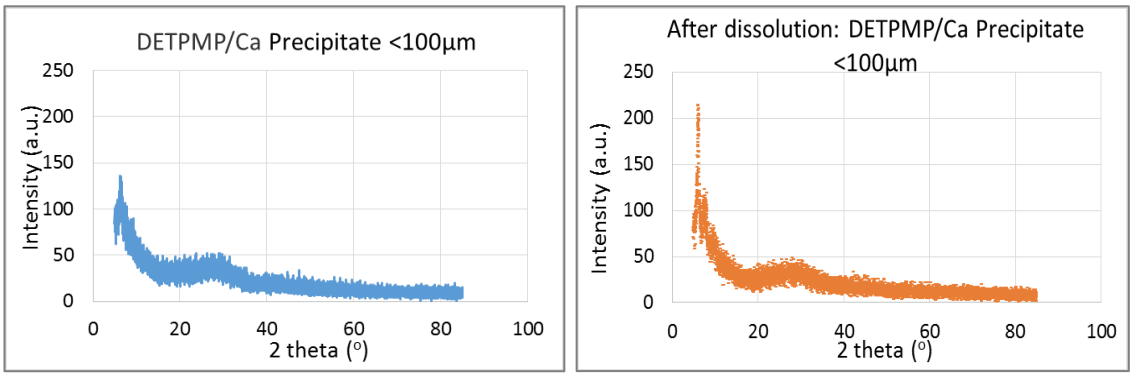

(a) before test **(b) after test**

Figure 4.16 X-Rays Diffraction Pattern of DETPMP Precipitate <100µm obtained before (a) and after (b) the dissolution test

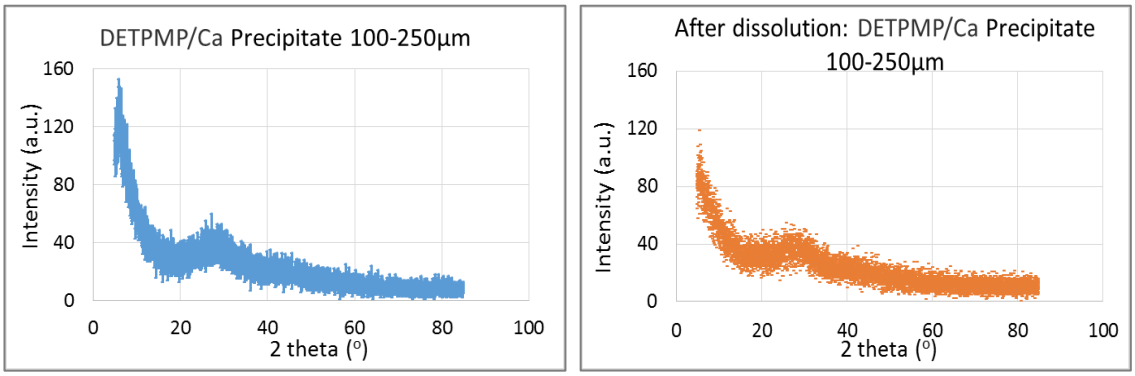

(a) before test **(b) after test**

Figure 4.17 X-Rays Diffraction Pattern of DETPMP Precipitate 100-250µm obtained before (a) and after (b) the dissolution test

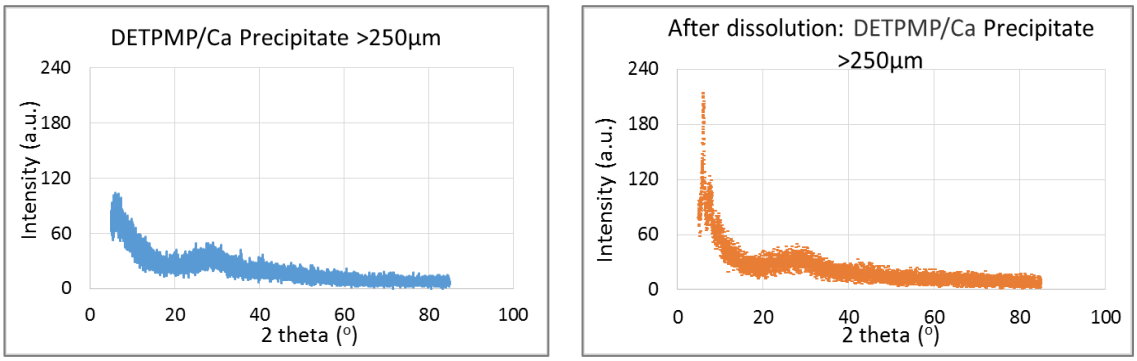

(a) before test **(b) after test**

Figure 4.18 X-Rays Diffraction Pattern of DETPMP Precipitate >250µm obtained before (a) and after (b) the dissolution test

4.4. Summary and Conclusions

In this section, the results of a non-equilibrium DETPMP_Ca precipitate dissolution study conducted in bulk solutions were reported. In this study, the stoichiometry of the precipitate continuously decreased after each of the 3 brine replacements from n = 5.5 to n = 3.5, which is also accompanied by pH change in the brine, leading to the phosphonate SI re-speciation, accordingly. Therefore, the numerical studies show that apparent pH, precipitate's stoichiometry and apparent solubility parameters are coupled.

It is proposed, that the solubility in the tested solutions varies not due to the transition from an amorphous to a crystalline phase. It was shown by ESEM/EDX, that there are some indications, like facets and edges appearing on the amorphous precipitate surface after the dissolution tests, which may indicate the onset of crystalline phase development. However, according to the XRD patterns, the crystalline structure has not been confirmed, the precipitate is still characterised as an amorphous material after the series of dissolution experiments.

The qualitative estimation of the phosphonate precipitate dissolution kinetics can be applied when designing the non-equilibrium experiments in porous media. Probably, to be able to observe the non-equilibrium dissolution effects, flooding at a wider range of flow rates should be performed, since dissolution does not occur rapidly.

The numerical studies explaining the reasons behind the solubility variation versus brine replacement show, that the precipitates with different stoichiometry will have different solubilities at a specific pH. Therefore, if using the Noyes-Whitney equation which requires the input of equilibrium solubility *Cs* (4.1), it would require a vast number of experiments, where the solubility is measured at a wide range of pH values. However, instead of using this approach, it is suggested to define a coupled system of pH/phosphonate speciation/stoichiometry, and once solved numerically, it can be used to determine the dissolution parameters of the phosphonate SI/Ca precipitates.

CHAPTER 5. NON-EQUILIBRIUM DISSOLUTION OF THE PHOSPHONATE_CALCIUM PRECIPITATES IN POROUS MEDIA

The non-equilibrium dissolution behaviour of the SI/Ca/Mg precipitate can be studied directly by dissolution experiments in the bulk and by dynamic sand pack flooding tests in porous media. The former test was discussed earlier in Chapter 4. Here, non-equilibrium kinetic dissolution experiments studying the DETPMP_Ca precipitate in a sand pack flood are presented. Monitoring the SI effluent concentration over time at various flow rates allowed us to observe non-equilibrium flow effects on the dissolution of phosphonate SI/Ca precipitates.

5.1. Introduction

The SI precipitate dissolution process, taking place in oilfields, is affected by the produced fluid flow rates, therefore, potentially, does not occur at full equilibrium. Therefore, the non-equilibrium dissolution behaviour of the phosphonate SI precipitates needs to be monitored in a porous media in order to develop a full precipitation/ dissolution model.

Stirring cannot be introduced in oilfield systems, however, flow rates may have a significant impact on the phosphonate inhibitor/divalents complexes dissolution. Therefore, in this Chapter a study on the phosphonate SI/divalent cation precipitate dissolution process under non-equilibrium flow conditions in *porous medium* is conducted.

The parameter that describes the effect of flow rates on dissolution is a *dissolution rate,* and this needs to be considered when modelling the precipitation/dissolution behaviour of the phosphonate SIs from their precipitated complexes. Dissolution rates can be defined only experimentally via the following equation:

$$\frac{dC}{dt} = r \cdot (Cs - C) \tag{5.1}$$

Where: dC/dt –dissolution rate (mg·L^{-1} s^{-1}), r – dissolution rate constant, s^{-1}; *Cs* – saturation concentration, i.e. solubility (mg/L); *C* – concentration in the bulk solvent/solution (mg/L).

To obtain the data for defining the dissolution rates, three flooding sand pack tests were performed in this study. Unlike all the previous flooding tests performed within the group, in the current experiments we did *not* induce precipitation *in situ*. The DETPMP/Ca precipitate was produced prior to the tests from bulk solution. This was then crushed and sieved to obtain narrow grain size fractions. Subsequently, the precipitate was mixed with quartz (silica sand) as a "support" mineral and the mixture was packed into a glass chromatography column. Flooding was then performed using Ca 2000ppm brine, at pH 6, at room temperature (T = 20^{o}C). Thus, the data obtained can be used to model the *coupled* desorption/dissolution processes occurring during the test. In the final flooding experiment, the column was packed only with the DETPMP/Ca precipitate. This was done to limit the release mechanism occurring in the system down to dissolution only, avoiding coupled adsorption/desorption process taking place on the quartz grains. A higher amount of the precipitate was introduced into all the sand packs on purpose, in order to observe the effect of multiple flow rates on the SI dissolution over relatively large cumulative volumes of injected brine. The return profiles of SI, Ca and pH were recorded.

Finally, to check if any phase transition occurred for the DETPMP/Ca precipitate during the flooding tests, the precipitate was analysed by X-Ray Diffractometer (XRD) and Environmental Scanning Electron Microscopy - Energy Dispersive X-Ray (ESEM-EDX). The XRD patterns of the precipitates were also measured prior to and after conducting the column flooding tests.

Thus, in this thesis we present our study of non-equilibrium dissolution of the DETPMP/Ca precipitate in flooding experiments:

I. Dissolution experiments performed at various flow rates in porous media, that contained sand mineral mixed with a *dry* powder of the DETPMP_Ca precipitate. Two experiments with different ratio of the precipitate, introduced into the column, were conducted (~14% and 9% by weight).
II. Flooding test with only the precipitate packed into the column.
III. XRD and ESEM/EDX patterns for the DETPMP/Ca precipitate obtained before and after flooding tests.

The aim of the work was to check if the solubility behaviour observed in our bulk tests as a function of brine replacement will also be observed in flooding tests conducted in porous media. The data obtained in the study will extend the understanding of

phosphonate SI precipitate dissolution in porous media and this can be directly used to model the dissolution behaviour of phosphonate/Ca precipitated complexes and calculate the dissolution rates under different flow rates.

5.2. Experimental Details

Some of the experimental details have already been given in previous Chapters, the references are given within the text. The Environmental Scanning Electron Microscopy - Energy Dispersive X-Ray (ESEM-EDX) and X-Ray Diffractometer (XRD) methods applied in the current study have already been described in Chapter 4 in sections 4.2.3 and **Error! Reference source not found.**, respectively.

5.2.1. *Materials*

Instead of using sandstone formation rock, sand was chosen as the mineral adsorbent to replicate a simple model of a sandstone formation and thus allowing to obtain repeatable results. Commercially available BDH GPR, 150-300 µm grain size sand was used in these experiments.

The structure of the phosphonate inhibitor studied, DETPMP, was shown earlier in Chapter 3, Table 3.1. The DETPMP/Ca precipitate was used in the current flooding tests, the precipitate preparation and characterisation were described in detail in sections 4.2.2 and 4.3.1 of Chapter 4. The middle 100-250µm fraction of the DETPMP/Ca precipitate was used in the sandpack tests, as this size fraction was closest to silica sand grain size (150-300µm).

A 2000 ppm Ca^{2+} brine was made up using $CaCl_2 \cdot 6H_2O$ (from Sigma Aldrich, used as received). The brine solution was filtered through a 0.45µm filter paper, degassed overnight and pH adjusted to pH 6.0 prior to use. Lithium (Li) and Iodide (I) tracer additives were used alternatively in the system to monitor and distinguish different injection stages of the flow experiment.

5.2.2. *Experimental Apparatus*

To carry out sand pack flooding experiments, it was necessary to use a glass column as a support to hold the sand in place. The schematic diagram of the sand pack flooding

apparatus is shown in Figure 5.1. This apparatus was designed primarily to carry out low pressure flood experiments. The column, fittings and tubing were supplied by Anachem. The glass column is 15cm long and has an internal diameter of 1.50cm.

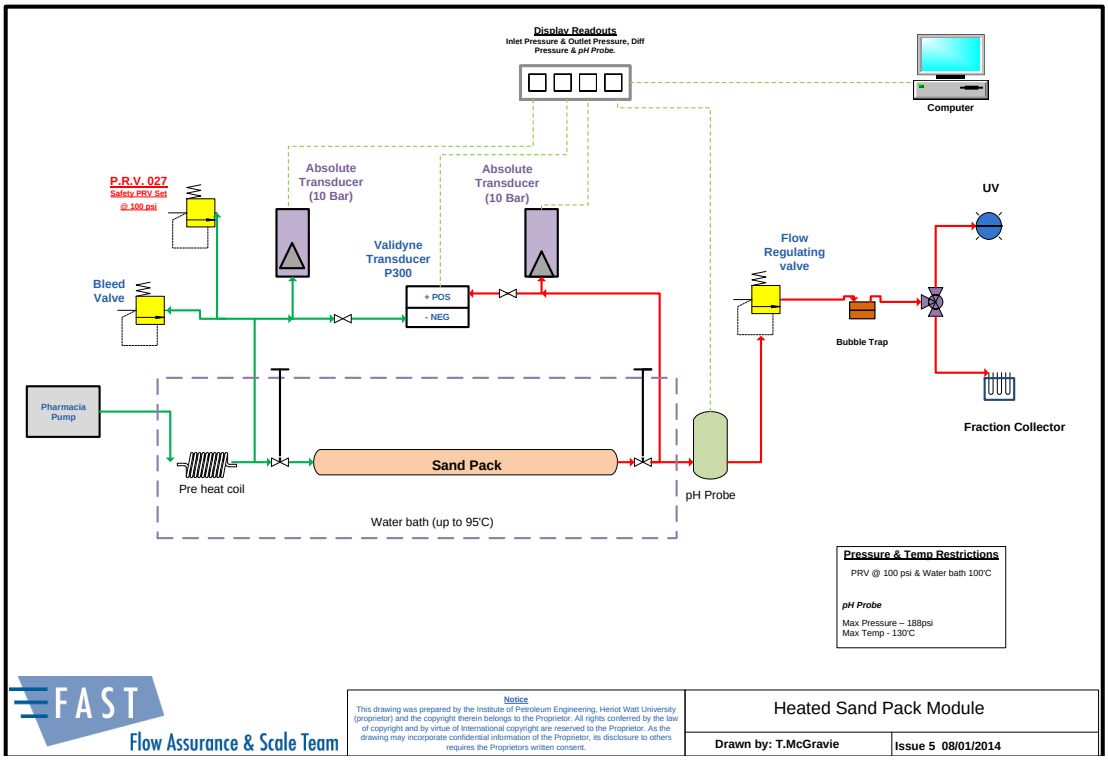

Figure 5.1 Schematic diagram of the sand pack rig

A dry slurry method was used for packing the sand and precipitate mixture to prevent (i) extensive dissolution of the precipitate while packing the column, and (ii) to obtain a homogenous porous medium. Also, since the DETPMP/Ca precipitate particles are lighter than the sand grains, it was found that during the wet packing, the sand/precipitate layers are forming, and the pack is not homogenous.

Thus, in this work dry precipitate powder was mixed with dry sand and the mixture was packed into the column. A detailed step by step list of instructions describing how exactly the various stages of the experiment were performed is presented below.

5.2.3. *General Sand Pack Flooding Procedure*

Dead Volume Measurement

This is the initial step in the experiment and it involves a tracer in/out test in order to calculate the system's dead volume – the volume of all tubulars within the system.

Potassium Iodide was used to prepare a tracer solution - 10ppm I^- in Ca^{2+} 2000ppm brine.

1. Two adjustable end pieces were connected using a short (15cm) glass column. Butt platens, with frits in place and one further frit to fill in any gap between them, were fitted. The volume occupied by the frits is considered as the pore space in the system.
2. Firstly, the system was purged with a Ca 2000ppm brine without any tracer to flush out any previous brine and to get the UV/Vis baseline level. A flow rate (Q) of 150ml/hr was used in all pre-conditioning tests.
3. After that, the iodide tracer solution is pumped to solvent change within the pump.
4. Injection of the iodide tracer solution is started. The UV/Vis Spectrophotometer is switched on as soon as the first drop occurs in the outline.
5. Once the UV-Vis readings reach a plateau, the pump and UV-Vis are stopped. The collected data is saved as a "tracer-in" file.
6. The solvent is changed to non-tracer Ca brine. Subsequently, steps 4-5 are repeated and the "trace out" measurements are collected.
7. By plotting the data obtained from these tracer in/out measurements, the system's dead volume is calculated.

Column Packing and System Connection

1. A fixed mass of both sand and precipitate (in sand packs 1 and 2a/2b), or precipitate only (pack 3) was prepared.
2. After the fixed end piece was fitted to the column, the sand/precipitate mixture or pure precipitate was introduced into the column, filling about 1/5 of the column length. Once it was compactly packed, the column was loaded further with sand/precipitate mixture.
3. The variable end piece was fitted once the substrate was fully loaded, a "finger" fitting was tightened.
4. The pump was attached to the column in a vertical orientation, so that injection occurs from the bottom to the top of the column. The column was flooded with Ca 2000ppm brine at 150ml/hr for one hour to allow any sand to settle and hence, removing any voids in the sand bed.
5. Once flooding had finished, the variable end piece was re-tightened, and the length of sand bed was measured.

6. Subsequently, the column was connected to the pump and the UV-Vis Spectrophotometer.
7. Flooding continued until the column shows no sign of further settling and a good, homogeneous sand bed is achieved with stable UV-Vis readings.

Pore Volume and Permeability Measurement

1. Trace in/out flooding was performed as described in "Dead Volume Measurement" section through the column packed with the substrate. A 10ppm iodide in Ca 2000ppm brine tracer solution was flooded at 150 ml/hr. An estimation of how long the pore volume would take at a specified flow rate was made by assuming 40% porosity in the column.
2. For the permeability measurement, flooding at five evenly spaced flow rates (30, 60, 90, 120, 150 ml/hr) for at least 5 minutes each was performed using 2000ppm Ca brine. The differential pressure, Δp, across the pack was recorded whilst flooding. The obtained Δp values were used to calculate the permeability of the pack via Darcy's law:

$$k = \frac{Q \cdot \mu \cdot L}{A \cdot \Delta p} \tag{5.2}$$

Where: k – permeability, mD; Q - flow rate, ml/min, μ – porosity, %; L – pack length, cm; A – cross area of the pack, cm^2; Δp – differential pressure, psi.

Post Flush (PF)

1. After the pore volume was measured at the test temperature, the apparatus was left to sit for 10-24 hours to make sure the system reached equilibrium.
2. The Ca brine with tracer (Li or I) was pumped at the desired flow rate. The differential pressure across the pack was monitored at 1 minute intervals. Samples were collected continuously for [SI] and [Ca] data.
3. The flow was stopped after a specific number of pore volumes. The sand pack column was shut in for another 10-24 hours.
4. Another flush at a different flow rate was performed, following steps 2-3.
5. Sample Collection:
   a. Initially, 2-2.5 ml samples were collected for the first ~5 pore volumes. This was increased to 5ml and 7.5ml during later stages.

b. The samples were analysed for major elements of interest: Ca and P. For this case, the samples were diluted in acidified distilled water (pH is 3 - 4) to avoid re-precipitation of any SI and Ca in the collected sample.

5.2.4. *Pack Characterization Data*

The parameters presented in Table 5.1 were measured for all the packs: sand packs 1-3. The experiments were performed using 2 different rigs. Thus, dead volumes varied significantly between sand pack 1 and sand pack 2/pack 3 experiments.

Table 5.1 Physical characteristics of sand pack 1, sand pack 2 and pack 3

Parameter	Sand Pack 1	Sand Pack 2	Pack 3 (only precipitate)
Length of the column, cm	15	15	15
Length of packed column, cm	8.43	7.41	4.16
Dead volume, ml	5.87	10.41	11
Pore volume, ml	10.14	7.91	8.11
Permeability, mD	797.5	627.3	107.3
Total volume, ml	14.86	13.06	7.35
Diameter, cm	1.5	1.5	1.5
Porosity, %	68	60	Close to 98% - precipitate swells with brine, which affects the porosity values obtained
Mass of sand, g	17.0	16.3	-
Mass of precipitate, g	2.8	1.7	3.65g
Precipitate percentage, %	14.1	9.4	100%

5.2.5. *Flooding Regimes*

To be able to observe the non-equilibrium dissolution effects, flooding at higher flooding rates is required, since dissolution is not expected to occur rapidly, according to the conclusions of Chapter 4. Equilibrium will probably be observed at the lowest flow rates, ~1-5 ml/h. Therefore, the suggested flow rates are from ~ 90ml/h to 1 ml/h. These flow rates are significantly lower than the ones observed in the field. However, if the flow rate effect is observed at the lower flow rates, this effect is going to be even more significant at the field production conditions. The data obtained in this experiment can be used to model the dissolution behaviour at the higher flow rates and therefore, predict the behaviour in the field conditions.

The details for the flooding regimes during sand packs 1-3 can be found in Table 5.2 (sand pack 1), in Table 5.3 and Table 5.4 (sand pack 2a and 2b), and in Table 5.5 (pack 3).

Table 5.2 Details on each stage of sand pack 1 (SP 1) experiment

Stage	Flow Rate, Q	Brine	Sample Dilution	Pore Volume (PV)	Fluid Residence Time, PV/Q
Ist Post Flush (PF)	30ml/hr	2000ppm Ca + 10ppm I	5* DW* acidified	~17	0.34h
IInd PF	12ml/hr	2000ppm Ca + 50ppm Li	10* DW acidified	~ +15	0.85h
IIIrd PF	3ml/hr	2000ppm Ca + 10ppm I	10* DW acidified	~ +15	3.4h

*DW – distilled water

Table 5.3 Details on each stage of sand pack 2a (SP 2a) experiment

Stage	Flow Rate	Brine	Sample Dilution	Pore Volume (PV)	Fluid Residence Time, PV/Q
Ist PF	90ml/hr	2000ppm Ca + 50ppm Li	10* DW acidified	~25	0.09
IInd PF	60ml/hr	2000ppm Ca + 10ppm I	10* DW acidified	~ +25	0.13
IIIrd PF	30ml/hr	2000ppm Ca + 50ppm Li	10* DW acidified	~ +30	0.26
IVth PF	2 ml/h	2000ppm Ca + 50ppm I	10* DW acidified	~ +40	3.96
Vth PF	1 ml/h	2000ppm Ca + 10ppm Li	10* DW acidified	~ +30	7.91

Table 5.4 Details on each stage of sand pack 2b experiment (SP 2b, back flooding of SP 2a)

Stage	Flow Rate, Q	Brine	Sample Dilution	Pore Volume (PV)	Residence Time, h PV/Q
Ist PF	1ml/hr	2000ppm Ca + 50ppm Li	10* DW acidified	~35	7.91
IInd PF	2ml/hr	2000ppm Ca + 10ppm I	10* DW acidified	~ +35	3.96
IIIrd PF	30ml/hr	2000ppm Ca + 50ppm Li	10* DW acidified	~ +20	0.26
IVth PF	60ml/hr	2000ppm Ca + 50ppm Li	10* DW acidified	~ +20	0.13
Vth PF	90ml/hr	2000ppm Ca + 10ppm I	10* DW acidified	~ +20	0.09
VIth PF	90ml/hr	2000ppm Ca + 50ppm I	10*DW acidified	~ +5	0.09

Table 5.5 Details on each stage of pack 3 experiment, that contains only precipitate

Stage	Flow Rate, Q	Brine	Sample Dilution	Pore Volume (PV)	Fluid Residence Time, h PV/Q
Ist PF	90ml/hr	2000ppm Ca + 10ppm I	10* DW acidified	~30	0.09
IInd PF	60ml/hr	2000ppm Ca + 50ppm Li	10* DW acidified	~ +25	0.13
IIIrd PF	30ml/hr	2000ppm Ca + 50ppm Li	10* DW acidified	~ +25	0.26
IVth PF	3ml/hr	2000ppm Ca + 10ppm I	10* DW acidified	~ +25	2.64
Vth PF	2ml/hr	2000ppm Ca + 50ppm Li	10* DW acidified	~ +25	3.96

5.3. Results and Discussion

If the dissolution shows non-equilibrium behaviour, then we expect that the inhibitor effluent concentration changes according to flow rate. At a sufficiently low flow rate, then the system would be at solubility equilibrium and the effluent should be constant at Cs, the equilibrium solubility of the SI/Ca complex. As the flow rate increases, the then the steady state effluent SI concentration will be lower than Cs; the faster the flow rate, the lower the effluent SI concentration will be. To characterise this behaviour, three dynamic flooding experiments have been conducted. All the characterisation parameters are shown in Table 5.1 in the previous section. The results of each pack flooding test will be discussed in turn.

5.3.1. *Non-Equilibrium Flooding Experiments: Sand Pack 1*

The first flooding experiment, sand pack 1 (SP 1), was carried out over the range of flow rates: 30ml/h, 12ml/h and 3 ml/h, using Ca 2000ppm brine at pH ~ 6.0 injected at temperature of 20^{o}C. This sand pack contained 14.1% of the DETPMP_Ca precipitate mixed with silica sand, with a measured porosity of 68%.

The higher porosity and lower permeability values are probably due to the dissolution of precipitate occurring during the pack characterisation, and due to properties of the precipitate to absorb liquid and swell. This phenomenon was noted on pack 3, which contained only the precipitate, where on removing the column from the rig the substrate was firmly held within the column, although had a high porosity, of close to 100%.

However, once the precipitate is dried, its volume decreases significantly, as can be seen in Figure 5.2(a). This the picture was taken after removing the column from the rig; note that the pack does not collapse and stays stable within the column; Figure 5.2b – the dry DETPMP/Ca precipitate significantly decreased in volume after 14 days drying in air at room temperature. Also, there were no visual signs of SP1 having collapsed during the test (Figure 5.3).

(a) **(b)**

Figure 5.2 Images of Pack 3 with DETPMP/Ca precipitate after completing the flooding tests (a) and the same Pack 3 precipitate after drying (b)

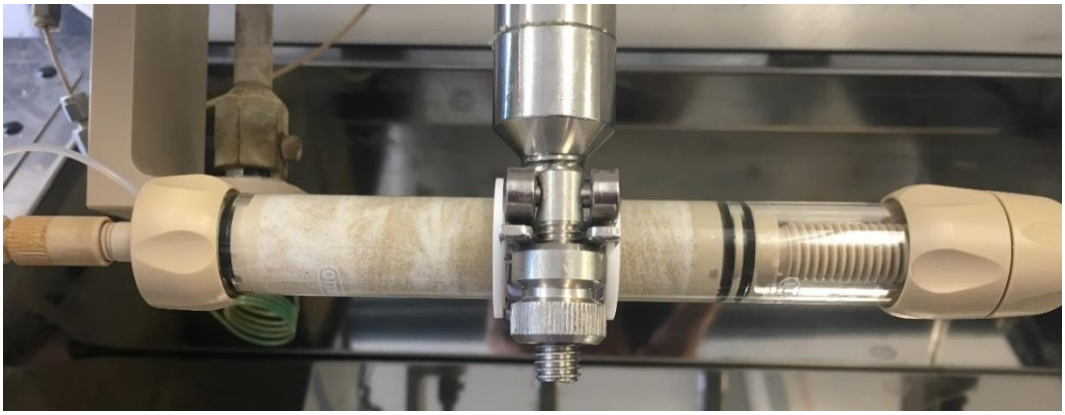

Figure 5.3 Sand pack 1 column packed with the mixture of sand and DETPMP_Ca precipitate

Before starting the flooding test at the assigned flow rates, the pack was pre-flushed with Ca 2000ppm brine to remove smaller dust-like particles that precipitate fraction may contain from the column. The overall volume of Ca^{2+} brine used for the preflush stage in SP 1 was ~ 250ml, or ~25 pore volumes (PV). Once the pack characterisation was

completed, the system was shut-in for 15 hours. Generally, the column was shut-in after each flooding regime to let the system reach equilibrium before flooding was started at a lower flow rate. All the solutions collected during the test were analysed by ICP-OES for SI, Ca and tracer (Li) content. Iodide was analysed online by a UV-Vis spectrometer.

The return profile of DETPMP in SP 1 is presented in Figure 5.4. The total flooding volume was ~ 47 PV. The dotted lines represent the shut-in periods. Flow rates and shut-in duration are shown to have a significant impact on the SI release. During the first postflush (PF) 1, the concentration of the inhibitor sharply increases, reaching 355ppm within the first ~2PV. This increase is due to the shut-in, where during this period the system had sufficient time to reach or get close to the DETPMP/Ca_n equilibrium solubility at that pH. After those 2PV, the DETPMP concentration starts declining due to flow rate effects, since dissolution cannot keep up with the flow rate, this non-equilibrium behaviour is as expected. By the end of the PF1 stage, the SI concentration reaches ~150ppm.

Subsequently, the PF 2 stage was performed at a lower rate of 12 ml/h, after an 8h shut-in period. The last PF3 stage for this sand pack was performed after a 23h shut-in period, at a lower rate of 3ml/h. As shown in Figure 5.4, during PF2 and PF3, the return slope is not as sharp as in PF1, due to the lower flow rates. At these flow rates the concentration of DETPMP in the effluent is much closer to the equilibrium solubility level, since the dissolution rate is closer to the flow rates applied.

The DETPMP concentration measured in the sand pack 1 corresponds to the apparent solubilities of the DETPMP/Ca precipitate measured during the bulk dissolution test (versus brine replacement). In that test, in the initial brine, the DETPMP apparent solubility for the 100-250 µm fraction was 353ppm, which is indeed what is seen in initial PF 1. The lowest DETPMP concentration was measured at 120-150ppm during the later flooding stages at lower flow rates. These numbers correspond reasonably well with the DETPMP apparent solubility measured in the second brine during the bulk dissolution tests, i.e. ~122ppm. This also indicates that the samples collected in the sand pack tests did not contain any contamination of fine particles, since the SI return concentrations are within the expected range.

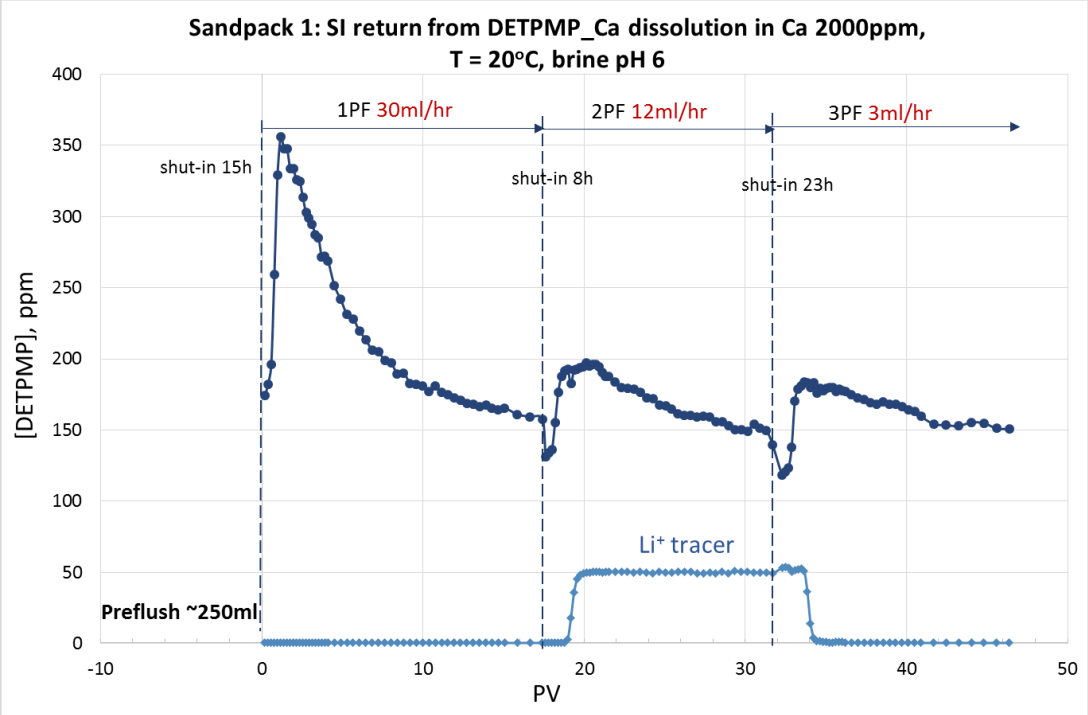

Figure 5.4 DETPMP concentration in the effluent during the sand pack 1 flooding test; T=20°C, flushing brine 2000ppm Ca^{2+}, pH 6.0

The equilibrium solubility values decrease versus volume of flooded brine. The highest SI concentration at ~350ppm was only reached during the first 15-hours shut-in. This higher concentration was *not* reached again even after a longer shut-in period of 23-hours. This is probably due to the fact, that by that stage the system has already been flushed with a much high~~er~~ volume of brine. Some precipitate has been already dissolved, and the pack is somehow deficient n precipitate. On the other hand, according to the bulk tests, the estimated equilibrium DETPMP concentration is expected to be lower at the later flooding stages, which is indeed what is observed.

Figure 5.5 shows that the Ca concentration does vary significantly over the entire experiment, which is similar to the bulk dissolution tests. Generally, the Ca concentration increases sharply within 1-2PV once flooding is started, and gradually decreases towards the end of each flush. During the first flush at 30ml/h, the concentration slightly decreases from ~2200ppm to 2150ppm, i.e. ΔCa~50ppm. By the end of the following PF 2, the Ca concentration reaches ~2100ppm, decreasing from the initial level by ~70ppm. For the last post-flush, the Ca level increases by ~200pm, which is due to an equilibrium dissolution effect.

Therefore, ΔCa and SI concentrations in the effluent depend on the flow rates: the highest Ca and DETPMP release is shown at the lower flow rates when dissolution occurs either at or fairly close to equilibrium. This is in agreement with the theory of non-equilibrium dissolution behaviour, that implies effluent concentration changes are affected by flow rate variation, until the flow rate and dissolution rates are in balance; and when in equilibrium, the apparent concentration stays constant.

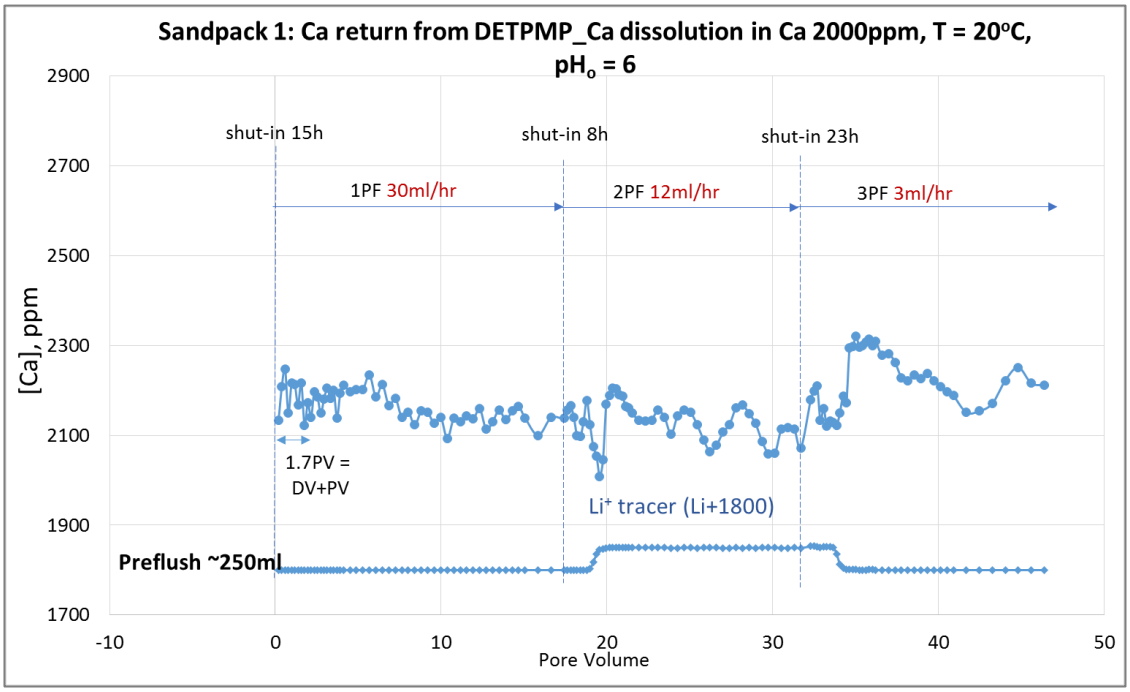

Figure 5.5 Calcium concentration in the effluent during sand pack 1 flooding tests, T=20°C, flushing brine 2000ppm Ca^{2+}, pH 6.0

The mass balances were calculated for the SP 1 experiment and are presented in Table 5.6. Overall, in this test the column has been flushed with ~72 PV of Ca 2000ppm brine, i.e. 25PV (pre-flush) + 47PV (the main part of the treatment). This table indicates, that 15.8% of total SI originally packed into the column has been collected during the experiment. Most of it, ~10%, is the SI that has been washed out during the pre-flush and pack characterisation that made up 25PV. Therefore, the higher SI return is shown to be at the initial stages of the sand pack flooding. This is in agreement with field data for squeeze treatments, where a significant amount of inhibitor is produced within the first ~5% of a squeeze lifetime. There is still a significant amount of the SI left in the pack ~84%, which is the amount of the SI that is retained either as (i) undissolved precipitate (mostly), (ii) dissolved SI species in the fluid, or (iii) species adsorbed on the silica grains.

Thus, the data obtained during the sand pack 1 study can be used to define the DETPMP/Ca complex dissolution rate according to the equation (5.1), however, the calculation also considers adsorption/desorption kinetics. Therefore, the data can be implemented into the coupled adsorption/precipitation treatments model and used to predict the SI return when both processes occur simultaneously.

Table 5.6 Sand pack 1 Mass Balance for DETPMP

In	Mass, mg	Percentage	Out	Mass, mg	Percentage
SI in ppt	1400	100%	SI out	85.43	6.10%
			Waste/preflush	135.19	9.70%
			Total	220.62	15.80%

SI left in pack	Mass, mg	Percentage
SI left	1179.38	84.20%
Including:		
SI retained on rock*	8.5	0.60%
*Retention mg/g rock	0.5	
*Rock mass	17000	

5.3.2. *Sand Pack 2*

To be able to further monitor the concentration variation versus volume of brine passing through the column, the sand pack 2 (SP 2) test was performed. The preflush in the SP 2 test was ~650ml versus ~250ml in the previous SP 1 test, i.e. 77PV versus 25PV. The overall flooding in SP 2 reached ~ 383PV, compared to ~72PV in SP 1. There were two series of flooding tests performed in sand pack 2 (Figure 5.6); these are denoted as sand pack 2a and sand pack 2b (SP 2a and SP 2b). All the details on the pack characterization and flooding regimes were presented above in Table 5.1, Table 5.3 and Table 5.4.

In the sand pack 2a experiment, five post-flush stages were conducted at flow rates of 90ml/h, 60ml/h, 30ml/h, 2 ml/h, and 1 ml/h using Ca 2000ppm brine at room temperature 20^{o}C, pH 6. These conditions are identical to those used in the sand pack 1 test. SP 2b was flooded at the same flow rates as SP 2a, but in the reverse order, i.e. with increasing flow rate. Each flooding stage was followed by a shut-in period between 9 and 69 hours,

which was varied during the experiment in order to estimate how quickly the system reached equilibrium during each of the shut-in periods.

Figure 5.6 Sand pack 2 column packed with the mixture of sand and DETPMP_Ca precipitate

Figure 5.7 presents the return profiles for DETPMP during the SP 2 experiment. According to the return profiles, the equilibrium solubility seems to decrease with the increasing volume of fluid that passes through the column. During the static shut-in periods, the system reached 130ppm, 100ppm, and 90ppm DETPMP concentration. These depended on the duration of shut-in period, as well as the volume of brine that had already been flooded. The highest SI concentration was recorded after the longest shut-in period, 69h, ~130ppm, where the system had enough time to reach equilibrium, but also only for the initial flooding stages. Considerably lower DETPMP concentrations were recorded after quite long shut-ins during the later stages of the experiment, i.e. after ~90 PV injected, ~90-100ppm.

At the beginning of the flood, the local fluid velocity increases immediately, thus the SI concentration goes up within the first ~2PV. This is the apparent SI solubility that has been reached within the column during the shut-in period. Once the SI dissolved during

the shut-in period has been flushed out the column during the first ~2 PV, further dissolution is affected by the flow rate that starts overcoming the dissolution rate and, as a result, the SI concentration gradually decreases. Therefore, the SI concentration drops significantly by the end of the highest flow rate regimes, performed at 90ml/h, 60ml/h, and 30ml/h. If the flood had continued, the concentration would reach the point when both rates are balanced. At the lower flow rates, the dissolution rate can "keep up with" the fluid velocity, which explains less significant SI concentration drop at the slowest flow rates, i.e. at 2ml/h and 1 ml/h.

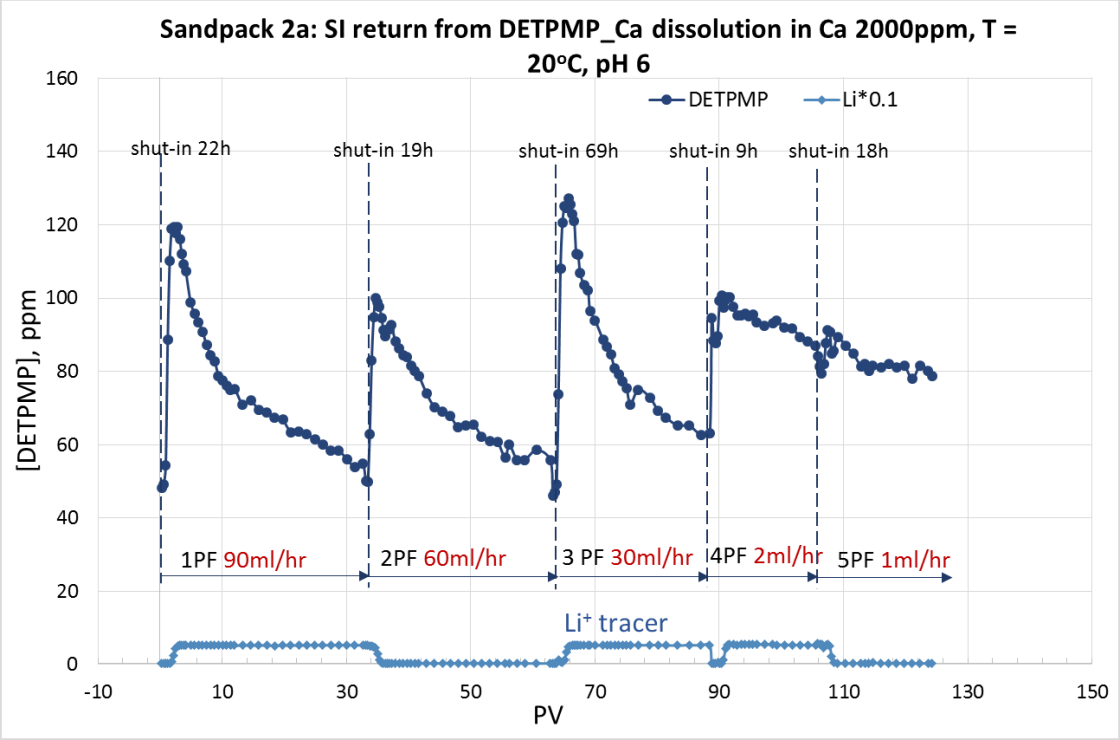

Figure 5.7 DETPMP concentration in the effluent during sand pack 2a: T=20°C, flushing brine 2000ppm Ca^{2+}, pH 6.0

The DETPMP return in the test is within the range of 50-130ppm. After ~163PV of brine passed through the column, at the lowest flow rates the SI concentration is within the range of 80-100ppm, which corresponds closely with the solubilities measured in the static dissolution tests after 2 brine replacements (~90ppm in that case).

The Ca return profile during this SP 2 experiment is presented in Figure 5.8. The effluent Ca values vary quite widely and much noise is detected, similarly to the Ca data obtained during the bulk dissolution tests, which causes difficulties with defining the correct data trend. However, the Ca return profile trends are all in agreement with the SI profile trends

during each flooding regime. The higher Ca and SI concentrations were detected at the lower flow rates. Generally, the Ca concentration decreases slightly by the end of each flushing stage, except in the later slowest flush rate at Q = 1ml/h, where the Ca return trend is increasing or stays stable over the entire flooding regime, which is probably because the system is close to equilibrium.

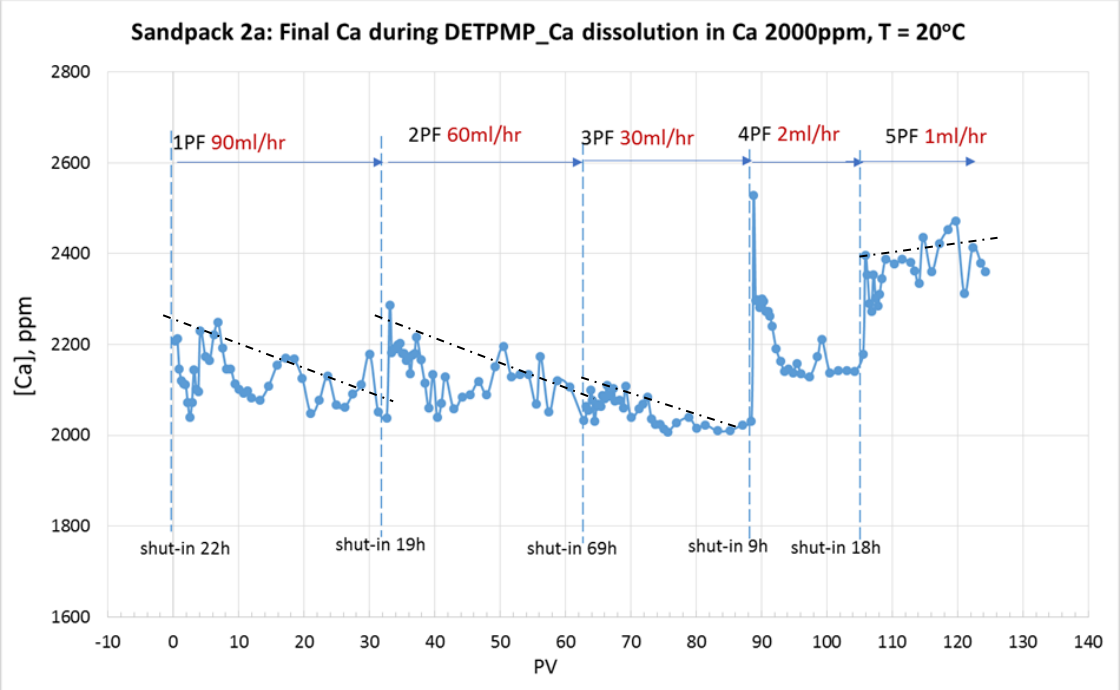

Figure 5.8 Ca concentration in the effluent during sand pack 2a flooding tests, T=20°C, flushing brine 2000ppm Ca^{2+}, pH 6.0

The pH profile for SP 2a is presented in Figure 5.9 and this is similar to the Ca return profile trend. The pH profiles were not measured inline or immediately after sample collection, hence any significant differences in readings between the sample sets may be due to solution evaporation. Therefore, the focus is mainly on the return pH trends as opposed to actual values.

Generally, pH increases when SI concentration increases and vice versa. Initial pH of the Ca 2000ppm brine is close to pH 6. Once the brine passes through the column, pH is shown to increase to ~ pH 6.8 – 7.2, as the pH is governed by the DETPMP_Ca precipitate dissolution. During each flooding stage, pH generally goes down, but at the slowest flow rates of 2 ml/h and 1ml/h, pH increases, probably because the dissolution occurs close to equilibrium.

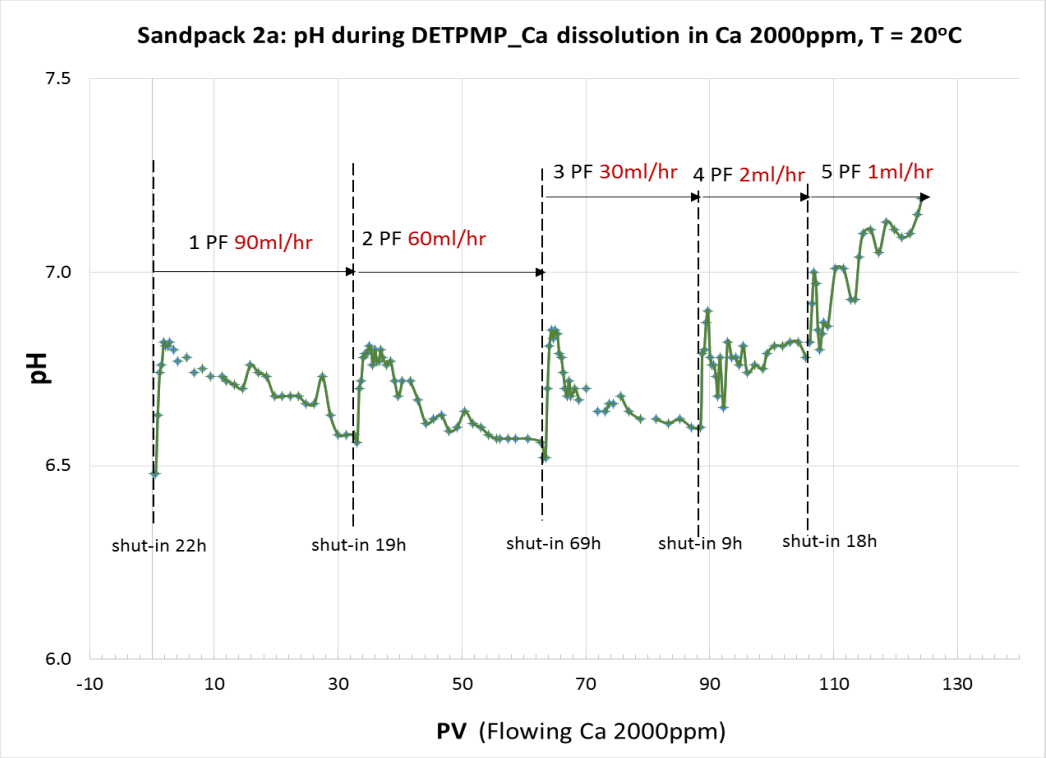

Figure 5.9 Effluent pH during sand pack 2a: T=20°C, flushing brine 2000ppm Ca^{2+}, initial pH ~ 6

By comparing SI return profiles in SP 1 and SP 2a, it can be noted that:

- the DETPMP concentration, releasing due to the DETPMP/Ca precipitate dissolution, continuously decreases with increasing flooding brine volume;
- the equilibrium solubility also apparently decreases with brine volume;
- the SI concentrations reached during the initial shut-in cannot be reproduced during the later flooding stages with similar duration shut-in periods.

Particularly, in SP 1 DETPMP is produced at a higher concentration of 355ppm and decreases to ~130ppm by the end of the test, i.e. after 72PV. In SP 2a, the overall flooding volume was ~ 205PV with the SI concentration in the effluent varying between 130ppm and 50 ppm.

The mass balance calculated for SP 2a is presented in Table 5.7. It indicates, that 27.4% of all the SI packed into the column has been collected during the experiment, most of which, ~19%, includes the amount of SI washed out during the pack characterisation as pre-flush (~650ml).

A significant amount of DETPMP (72.6%) remains in the pack. This must be the original precipitated SI (mostly) along with any SI dissolved in the fluid and some SI adsorbed on the sand. Percentage wise, this is a significantly lower number compared to sand pack 1, ~84%. This also explains the lower effluent concentrations of SI recorded at the end of SP 2, compared to SP 1.

The data is in agreement with the field data, where the return SI amount (governed by coupled desorption/dissolution mechanism) gradually decreases with the produced brine volume. The return behaviour shown in the sand pack studies also explains the disagreement raised earlier in the literature between the lower SI return concentrations in the field and the higher initially recorded SI solubilitites (Sorbie, Jiang et al. 1993). We show that the phosphonate SI releases at higher concentrations close to the initially measured equilibrium solubility only during the initial flooding stages. With increasing flooding volume, the equilibrium solubility of the precipitate decreases. This is due to re-speciation within the SI/Ca_n complex and the precipitate stoichiometry n changing with the volume of fluid that passes through the precipitate. This is also followed by pH variation in the system, that consequently affects the stoichiometry of the precipitate and the SI's apparent solubility in the bulk solution.

Table 5.7 Sand pack 2 Mass Balance

In	Mass,mg	Percentage	Out	Mass, mg	Percentage per initial SI
SI in ppt	850	100%	SI out	75.79	8.9%
			Waste/preflush	157.5	18.5%
			Total	233.3	27.4%

SI left in pack	Mass, mg	Percentage per initial SI
SI left	616.7	72.6%
Including:	8.2	1.0%
SI retained on rock*		
*Retention mg/g rock	0.5	
*Rock mass	16300	

5.3.3. *Sand Pack 2b*

For sand pack 2b, flooding was continued with the same brine at the same flow rates, but in the reverse order, from the lowest flow rate to the highest. If in sand pack 2b (SP 2b)

the SI concentration continues to decrease, the results are in agreement with the theory proposed above. Therefore, a comparison of the SP 2a and SP 2b return data would allow the qualitative model for the phosphonate SI return in precipitation squeeze treatments to be defined.

Before commencing the sample collection of flood SP 2b, the pack characterisation was carried out. Thus, ~100ml, or 12PV, was pre-flushed through the column. In sand pack 2b, there were also five post-flush flow stages conducted but in reverse order to sand pack 2a: starting at Q = 1ml/h, 2ml/h, 30ml/h, 60ml/h, and 90ml/h, using the same brine Ca 2000ppm at pH ~6.0, 20^{o}C.

In sand pack 2a, the highest SI concentration was reached during the 69 hour shut-in, therefore the first flooding regime in SP **2b** at 1 ml/h was started after a 67-hour shut-in period. However, as shown in Figure 5.10, even after 67 hours the DETPMP concentration increased up to only ~60ppm during the first shut-in period of SP 2b, which is well below the equilibrium solubility reached after a 69 hours shut-in in the previous SP 2a, i.e.~128ppm.

During the entire SP 2b flood (~160 PV), the scale inhibitor concentration gradually decreased from 60ppm to 20ppm (Figure 5.10). Even during an extended shut-in period, for example ~114 hours, the apparent SI solubility did not exceed 40ppm. After all the flooding regimes were conducted, there was an extended shut-in, ~ 13 days or 308 hours. However, even after that long period the peak concentration of DETPMP in the effluent was only at 45ppm. Therefore, the data obtained during SP 2a and SP 2b does not match. The SI concentration continued to decrease with the increasing volume of fluid that passed through the precipitate, which is in agreement with the data obtained for the bulk dissolution tests.

The lower concentrations of SI recorded in the tests are not due to an insufficient amount of the precipitated material remaining. According to the mass balance calculations, there was still a significant amount of the SI (~69% of the initially introduced precipitate amount, or 6.7% of the entire mixture that the column contains) remaining in the pack at the end of sand pack 2b.

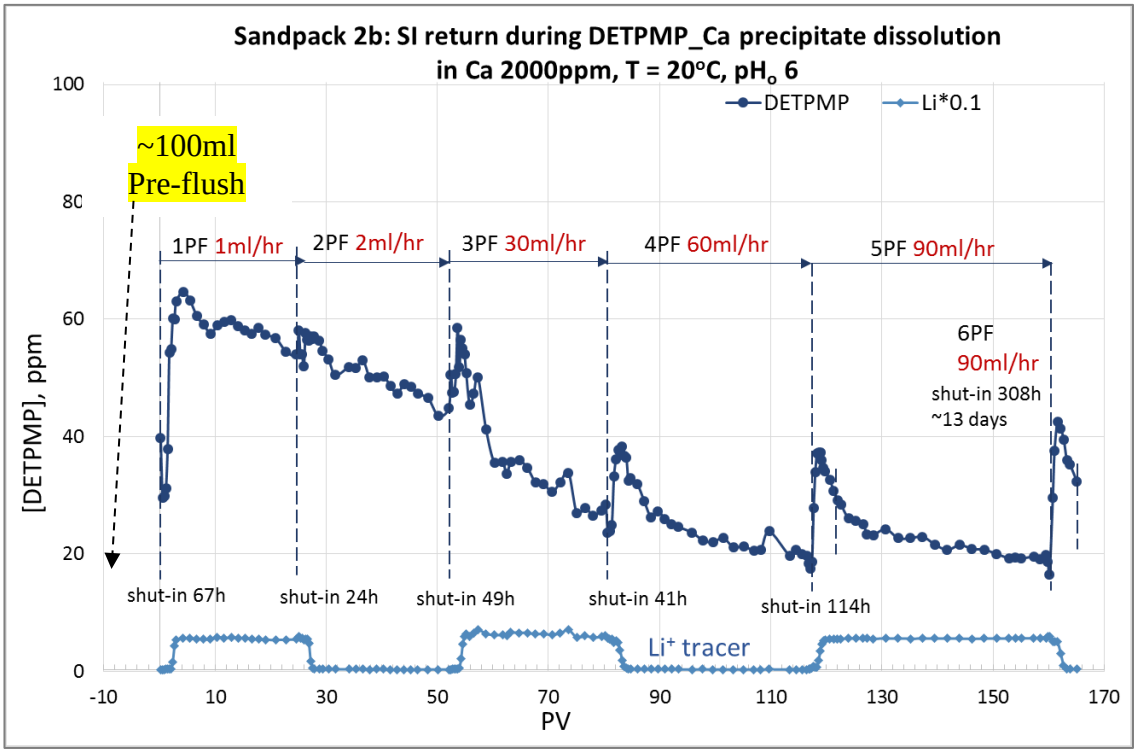

Figure 5.10 DETPMP concentration in the effluent during sand pack 2b, T=20°C, brine 2000ppm Ca^{2+}, pH 6.0

The Ca return profile is presented below in Figure 5.11. Again, similar to floods SP 1 and SP 2a, the Ca data is quite "noisy", which may be due to ICP analytical error ~10%. However, a smoother Ca return is recorded for the last flooding stage, where the concentration is constant. This corresponds with data obtained during the very last dissolution test versus brine replacement presented in Figure 4.9, where in series 4, the return profiles for both SI and Ca were smoother and the trends were clearer, compared to the earlier stages of the study. In SP 2b, when moving from the lower 2ml/h flow rate to the higher one at 30ml/h, there was a significant increase in the Ca concentration which is due to the higher flow rate effect.

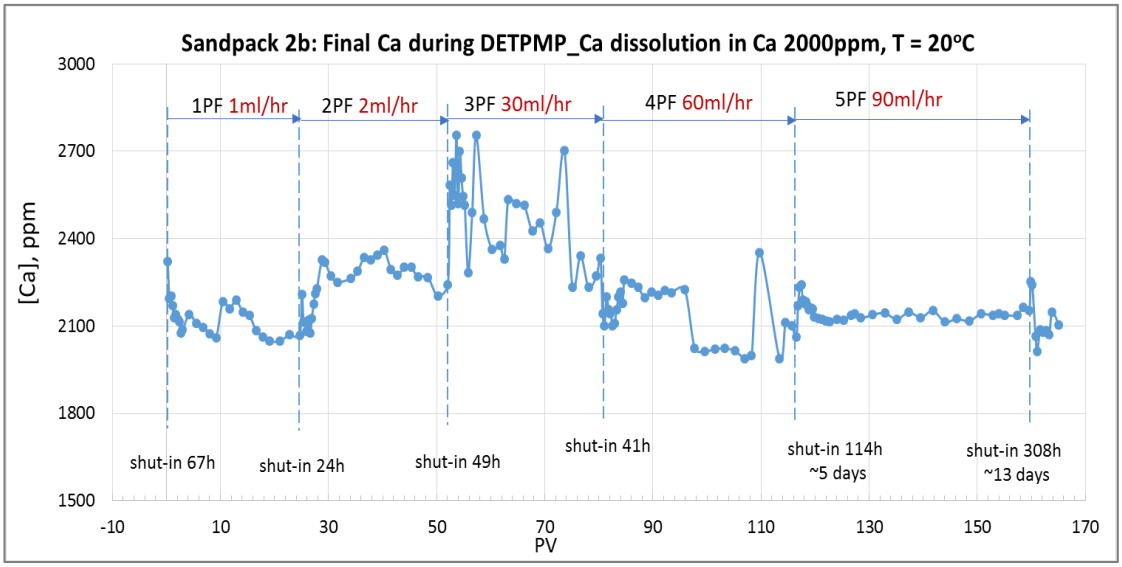

Figure 5.11 Ca concentration in the effluent during sand pack 2b, T=20°C, flushing brine 2000ppm Ca^{2+}, pH 6.0

The pH trend for flood SP 2b presented in Figure 5.12 corresponds well with the SI return profiles. When the Ca 2000ppm brine with an initial pH of 6 starts passing through the column, the pH initially increases, as governed by DETPMP_Ca precipitate dissolution. When the SI concentration starts decreasing due to the flow rate effect, pH also decreases. Generally, pH decreases over the whole of the SP 2b flood. These observed pH and SI return trends are as we would expect and in agreement with the results obtained from the static dissolution tests, described in Chapter 4 (sections 4.2.2 and 4.2.3).

To sum up, the return profiles of floods SP 2a and SP 2b do not match even if they have been obtained at the same flow rates. During SP 2a and 2b, it was observed that the SI concentration, that comes from the DETPMP/Ca precipitate dissolving in the return brine, decreased gradually with increasing volume of brine pumped into the column. Also, the equilibrium SI concentration reached during shut-in periods continued to decrease quite significantly. Even after a longer shut-in period of ~308 hours (13 days), the SI concentration in the effluent did not exceed 40ppm, compared to 130ppm recorded at the initial shut-in of ~69 hours in SP 2a.

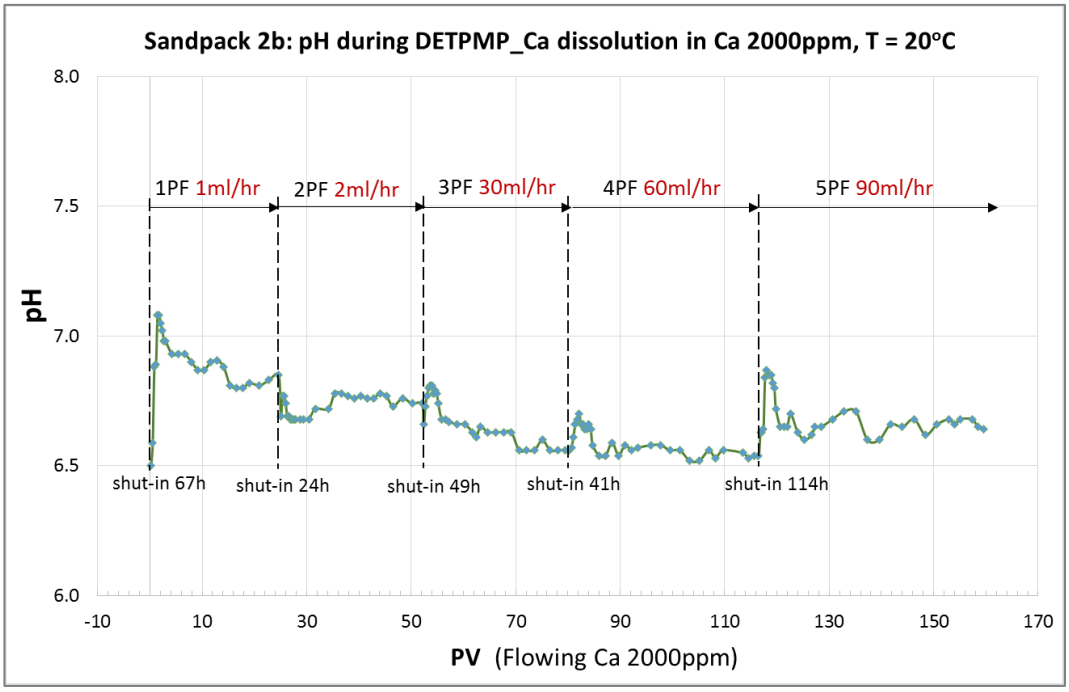

Figure 5.12 Effluent pH in sand pack 2b, T=20°C, flushing brine 2000ppm Ca^{2+}, pH 6

It has been shown, that dissolution behaviour of the DETPMP/Ca precipitate in a sand pack and bulk dissolution tests does not correlate with the "classical" dissolution model, that is currently used for the phosphonate SI precipitation/dissolution model.

According to the classical model, since the DETPMP/Ca precipitate contains only one type of phosphonate molecule and this is not a mixture of different species, it would be characterised by a specific equilibrium saturation concentration, or a specific solubility. For example, when some amount of material is dissolved, the chemistry of the precipitate should not change and not influence the equilibrium solubility characteristics, since the *same* SI molecules are releasing during an entire squeeze lifetime. Indeed, NMR data obtained for the DETPMP stock product used in the study clearly showed, that most of the phosphorus (P) containing substance was a "clear" penta-phosphonate. Moreover, the precipitation reaction itself allows the removal of all the P-containing impurities of the stock product, thus the DETPMP/Ca precipitate obtained in this work was a pure DETPMP/Ca precipitate without any crystalline impurities, which was proved by the XRD patterns. Therefore, the solubility decline throughout the sand pack tests was not due to the precipitate containing a mixture of different SI molecules with different solubility, that are releasing in turn, as was shown previously for polymer SI - PPCA/Ca precipitates (Farooqui and Sorbie 2016).

The solubility decline in the *phosphonate* SI/Ca precipitation treatments indicates the precipitate continuously re-speciates over the sand pack flooding stages, probably also leading to precipitate stoichiometry variation. The brine apparent pH also varied during the precipitate dissolution, which affected the speciation of the precipitate and the released SI ions. Thus, solution pH, phosphonate SI speciation in solution, and SI/Ca_n precipitate system must all be coupled within the precipitation model and solved numerically.

5.3.4. *Precipitate Pack 3*

In *precipitate pack 3*, the column contained only the DETPMP/Ca_5 precipitate, without any sand. The purpose of this specific design was to obtain data that characterizes the "pure" dissolution process, avoiding any dissolution/desorption processes that took place in floods SP 1 and SP 2 a, b. The precipitate fraction 100-250µm was used, which was the same as that used in the previous sand pack experiments. The precipitate pack 3 characteristics and flooding regimes were presented earlier in Table 5.1 and Table 5.5. There were five post-flush flow stages conducted: at Q = 90ml/h, 60ml/h, 30ml/h, 3 ml/h, and 2 ml/h. Each flooding stage was followed by a shut-in period of 18 - 192 hours.

Figure 5.13 shows the return profile of DETPMP for the precipitate pack 3 experiments. The column was pre-flushed with ~680ml brine prior to starting the flooding at 90ml/h in order to avoid any smaller precipitate particles coming out the pack during the experiment. The first flooding stage at 90ml/h was started after a 28h shut-in period. During the successive shut-ins, the observations were as follows:

- **First** shut in after 28h, the SI concentration reached 220ppm; followed by ~28PV of brine injection at flow rate, 90 ml/h;
- **Second** shut in after 114h, the SI concentration reached ~190ppm; followed by ~20PV of injection at flow rate, 60 ml/h;
- **Third** shut in after 192h, the SI concentration reached ~170ppm; followed by ~20PV of injection at flow rate, 30 ml/h;
- **Fourth** shut in after 18h, the SI concentration reached ~125ppm; followed by ~20PV of injection at flow rate, 3 ml/h;
- **Fifth** shut in after 114h, the SI concentration reached ~150 - 160ppm; followed by ~20PV of injection at flow rate, 2 ml/h;

Following this last (5th) shut-in when ~ 214PV of total volume had been injected into the pack, the concentration stayed quite high at 130ppm. The concentrations measured in the precipitate pack 3 test were considerably higher that the concentrations recorded after the same pore volumes injected in the previous sand packs 1 and 2. The reason behind this may be related to the adsorption/desorption processes kinetics that take place in those systems that affect the return concentration of the inhibitor after the precipitation squeeze treatments. However, overall, we find that all the SI return features highlighted in the previous sand pack studies describing non-equilibrium behaviour are also broadly confirmed by the precipitate pack 3 experimental data.

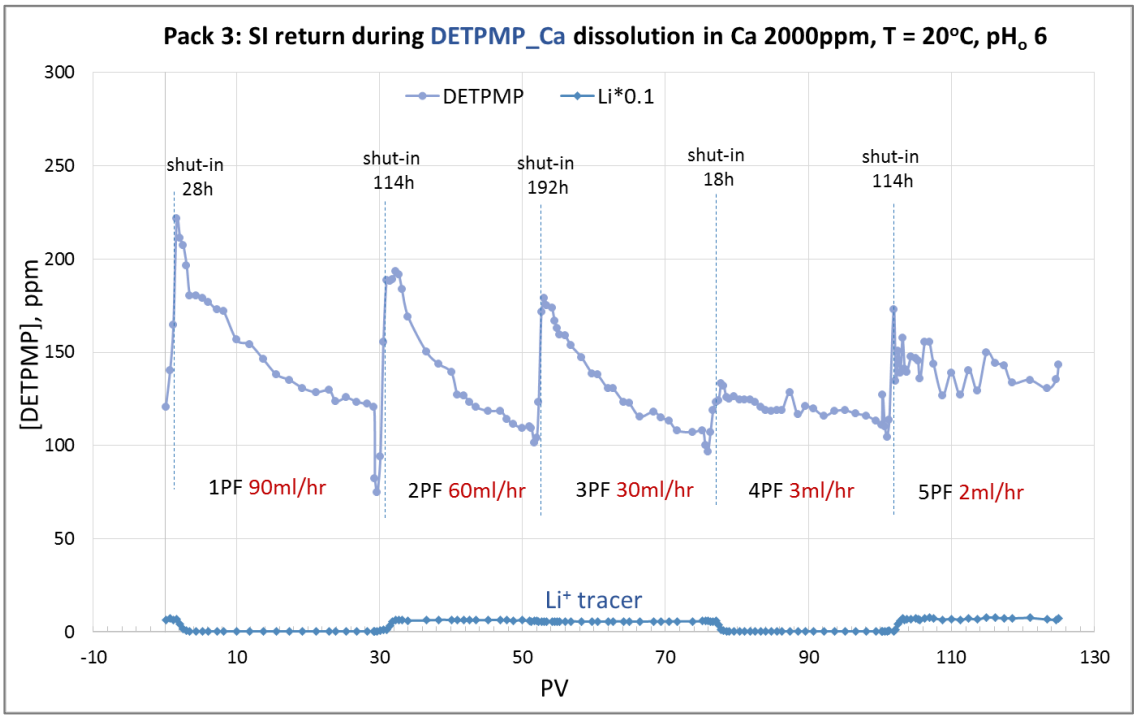

Figure 5.13 DETPMP concentration in the effluent during precipitate pack 3, T=20°C, flushing brine 2000ppm Ca^{2+}, pH 6.0

The Ca return profile obtained during the pack 3 experiments is presented in Figure 5.14. The quality of the Ca data is again rather noisy and causes difficulties in identifying the correct data trends, as in the previous sand pack tests and bulk dissolution tests. This is probably due to the ICP-OES 10% instrumental error, which at the recording concentrations range can allow variation up to 200ppm within the experimental error.

According to the available data, the Ca concentration was greatest during the highest 90ml/h and lowest 2ml/h flow rate regimes. At the lowest flow rates, this is expected to

be due to dissolution occurring close to equilibrium, whereas at higher flow rates, this may be caused by the higher local fluid velocity effects.

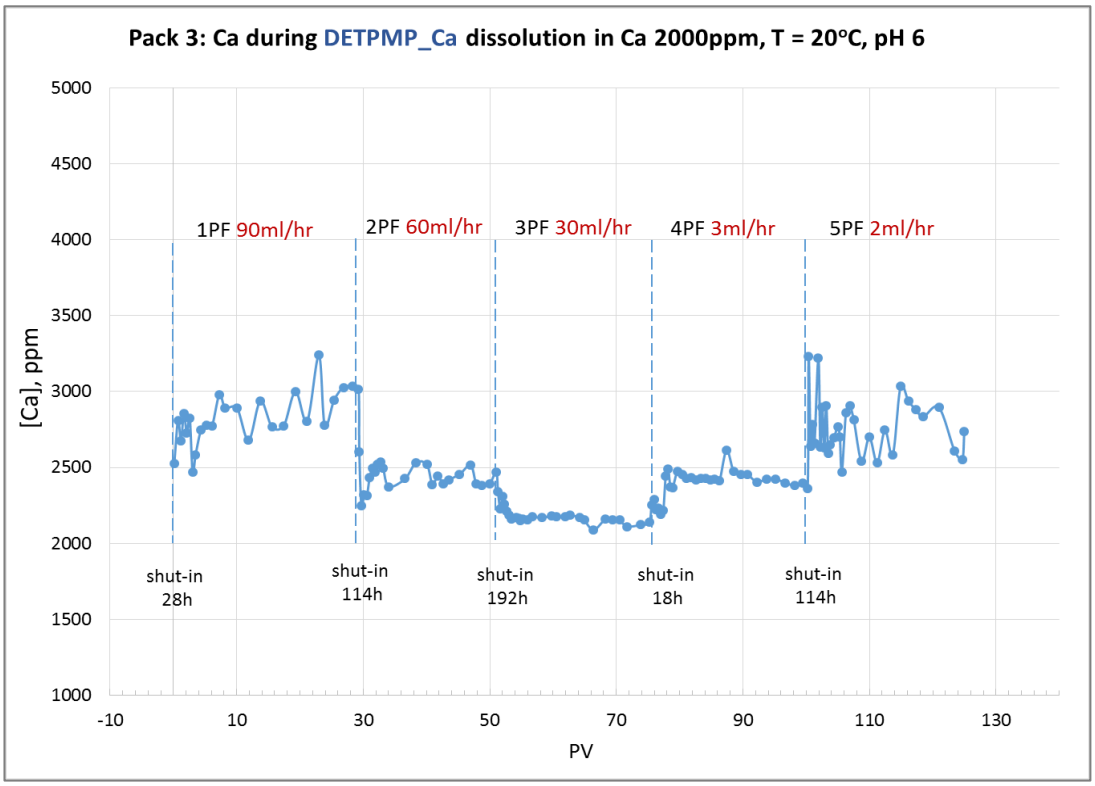

Figure 5.14 Ca concentration in the effluent during precipitate pack 3, T=20°C, flushing brine 2000ppm Ca^{2+}, pH 6.0

The pH effluent profile recorded for the pack 3 floods is shown in Figure 5.15 and it is "smoother" than those pH profiles obtained for sand packs SP 1 and SP 2. Generally, pH varies from 6.5 to 7.0 for all the flooding regimes conducted in this study, which agrees with the previous sand pack data. However, for future studies the use of inline pH-meter is suggested, so that values are continuously monitored during flooding stages allowing a more accurate pH profile to be obtained.

To sum up, the pack 3 flood used a column packed only with the DETPMP/Ca precipitate, without any sand, which allowed the pure non-equilibrium dissolution process to be monitored but avoided the adsorption/desorption reactions of the dissolved SI on the sand grains. The overall trends of SI, Ca and pH look similar to the ones obtained in sand packs SP 1 and SP 2a, b. The data obtained during the pack 3 flood can be used to model the dissolution process of the phosphonate/Ca precipitates, whereas the sand pack 1, and sand pack 2a, 2b data should be used as input to model the coupled desorption/dissolution process.

All of the pack flooding experimental data presented in this chapter is in agreement with the bulk dissolution test data presented in Chapter 4, and this all concludes that the equilibrium solubility of the DETPMP/Ca precipitate is subject to variation and this changes over the flood. Therefore, the approach adopted for modelling the dissolution of phosphonate SIs needs to be reconsidered. Equation (5.1) cannot provide accurate prediction of the SI concentration in the return brine, since it is not only the *dissolution rate* and the *specific solubility* that governs the phosphonate SI release in precipitation treatments. It has been shown, that the SI concentration in a return brine is a function of apparent pH, apparent stoichiometry of the SI/Ca_n precipitate, SI speciation at the apparent pH and dissolution rate. All these controlling parameters need to be coupled and solved numerically within the precipitation model to fully predict the phosphonates return in precipitation treatments. Carrying out these calculations is beyond the scope of this this thesis, but the results here can be used for the purposes of model validations.

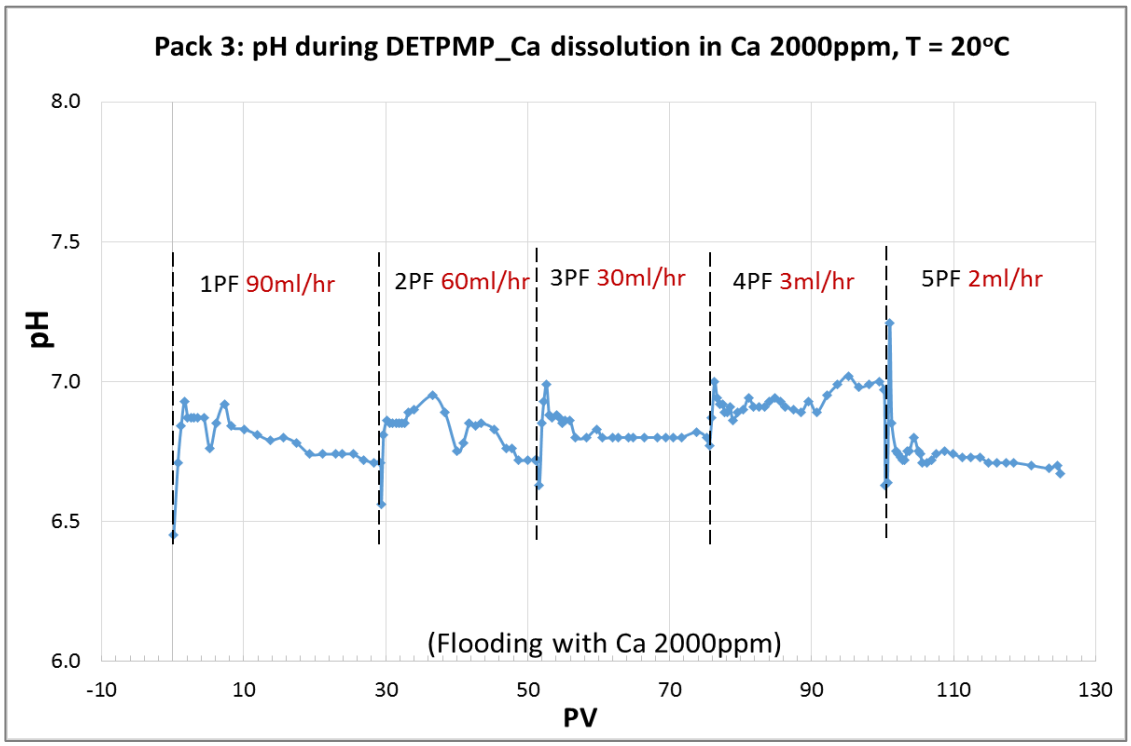

Figure 5.15 Effluent pH during precipitate pack 3 flooding tests, T=20°C, flushing brine 2000ppm Ca^{2+}, pH_o~ 6

5.3.5. *XRD data for Silica Sand and DETPMP/Ca Precipitate*

To check if a phase transition has occurred for the DETPMP/Ca precipitate, the precipitate/sand mixture obtained from sand pack 1 was analysed on the X-Ray

Diffractometer. The individual XRD patterns of the DETPMP/Ca precipitate (Figure 5.16) and the silica sand (Figure 5.17a) were recorded prior to sand pack 1. The XRD pattern for the sand/precipitate mixture left in the pack after the test is presented in Figure 5.17b.

The initial DETPMP/Ca precipitate has a typical pattern of an amorphous substance, whereas silica sand (quartz) has many well-determined peaks which is typical for a crystalline material. By comparing the silica sand (quartz) and precipitate/sand mixture patterns, conclusions on whether a new crystalline phase has appeared could be derived, if appropriate. However, no new peaks appeared in the mixed sand/precipitate pattern, shown in Figure 5.17b. Therefore, there is no other crystalline structure in the sand/DETPMP_Ca mixture after the sand pack 1, except the silica sand, which confirms the solubility variation observed in sand pack 1 test was *not* due to a new crystalline phase developing in the DETPMP/Ca precipitate.

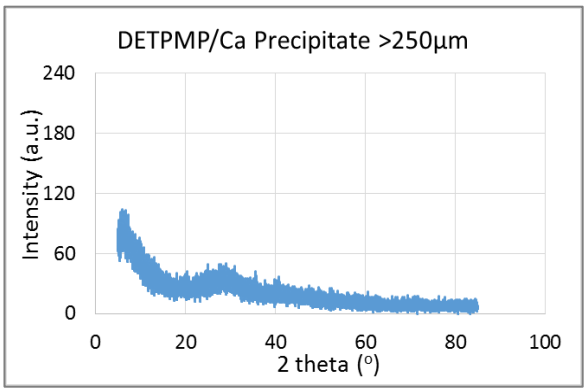

Figure 5.16 XRD pattern of DETPMP/Ca precipitate, obtained before sand pack 1 test

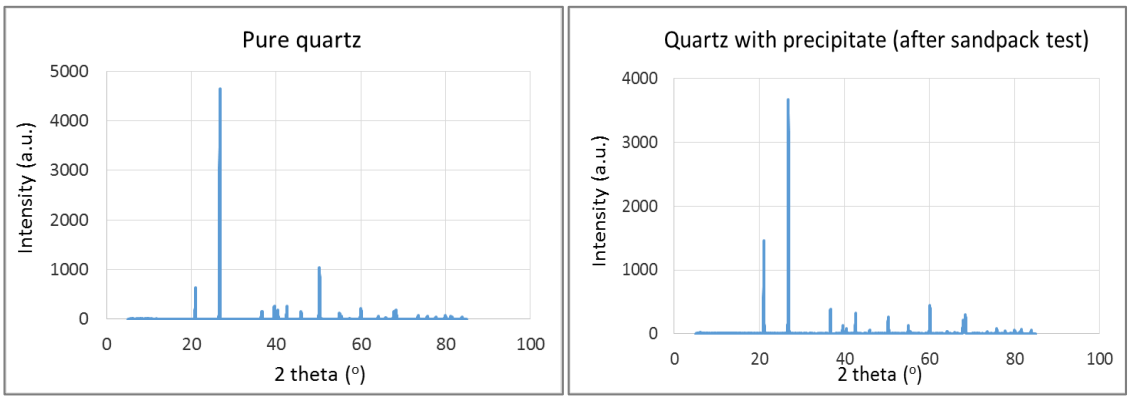

a) before test **b) after test**

Figure 5.17 XRD pattern of (a) silica sand and (b) sand/precipitate mix after sand sack 1

5.3.6. *Morphology of Silica Sand and DETPMP/Ca Precipitate Substrate by ESEM/EDX*

In addition to the studies conducted on the morphology and structure of the DETPMP/Ca precipitates during the bulk dissolution tests, the ESEM-EDX and XRD analyses were applied to examine the structural and morphological properties of the silica sand and DETPMP/Ca precipitate substrate prior to and after sand pack 1. The ESEM images for the silica sand and DETPMP/Ca precipitates recorded prior the test, and the mixed substrate obtained after flooding are shown in Figure 5.18 (a, b, c). EDX elemental analysis is summarised in Table 5.8 (a, b, c).

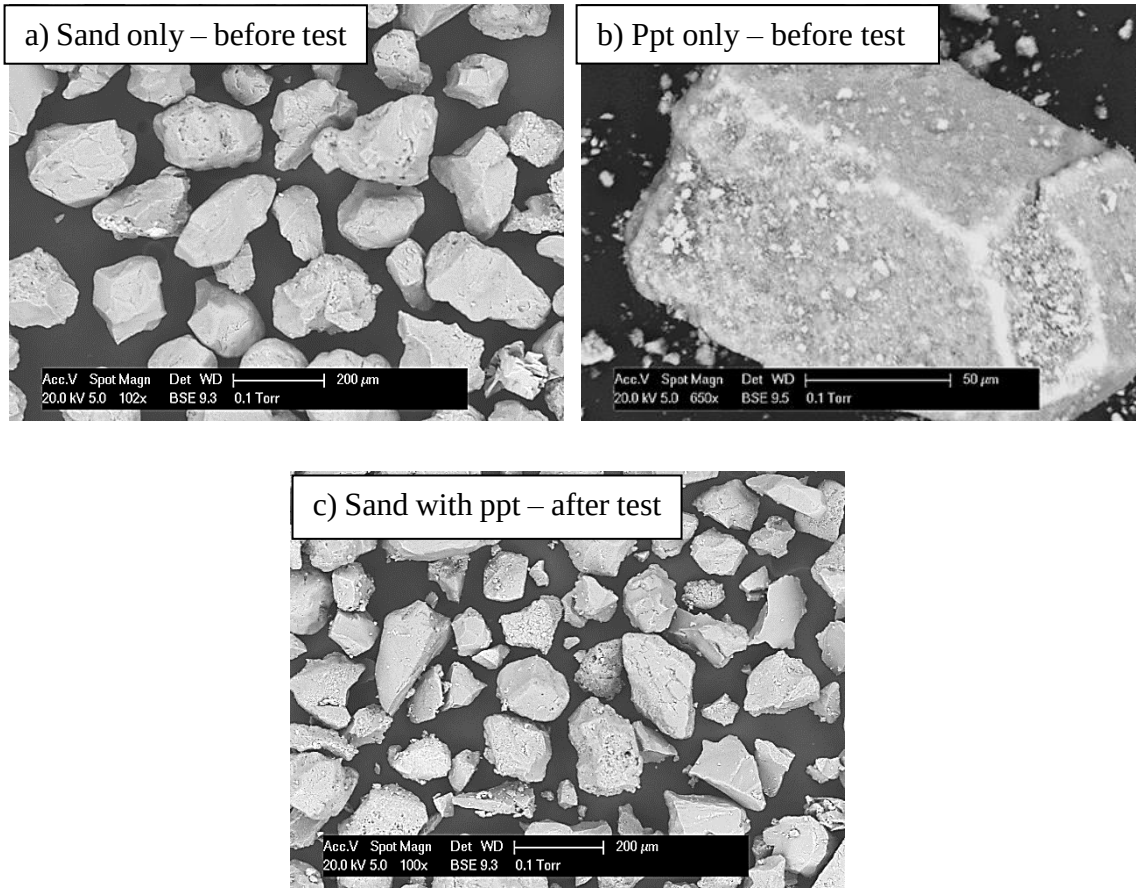

Figure 5.18 a) Sand particles 100-300µm before sand pack 1; b) DETPMP/Ca precipitate before sand pack 1; c) mixture of DETPMP/Ca sand/precipitate after sand pack 1

There are traces of precipitate particles shown in Figure 5.18c and the EDX data indicates the presence of phosphorus, chlorine and calcium left in the substrate after sand pack 1. According to the EDX data, the Ca/DETPMP molar ratio is *4.76* for the initial precipitate, which decreased slightly to *4.55* by the end of the sand pack test. These values are within the expected stoichiometry values and similar to those obtained for the bulk dissolution tests with brine replacement, shown in section 4.3.2.

It can be seen in Figure 5.19 that the shape of the DETPMP/Ca particles after flooding is slightly different compared to the flat and smooth surface of the grains before starting the experiment (Figure 5.18b). The higher levels of phosphorus and calcium detected in the absence of silicon atoms, proved that the characterised particle is a SI precipitate grain and not a silica sand particle (Table 5.9; Figure 5.18a). There are many irregular edges formed due to dissolution with smaller particles breaking off from the larger grains and being mobilised. The presence of these fine particles may also explain the higher SI return during the initial flooding stages.

Table 5.8 EDX signals on the silica sand (a), DETPMP/Ca precipitate (b), and their mixture after sand pack 1 (c)

a) 100-300 µm silica sand particles before the treatment

Element	Weight, %	Atomic, %
C	14.97	20.8
Si	21.1	12.53
O	63.93	66.67

b) DETPMP/Ca precipitate 100-250 µm before the treatment

Element	Weight %	Atomic %
O	66.48	71.19
C	32.3	25.97
P	0.49	1.03
Ca	0.37	0.98
Cl	0.11	0.25

c) mixture of sand/DETPMP_Ca precipitate after sand pack 1

Element	Weight, %	Atomic, %
C	14.11	19.86
Si	21.35	12.85
P	0.6	0.33
Ca	0.7	0.3
Cl	0.28	0.13
O	62.96	66.53

Table 5.9 EDX signals on the DETPMP/Ca precipitate after sand pack 1

Element	Weight, %	Atomic, %
P	18.86	15.09
Cl	16.21	11.33
Ca	29.01	17.94
O	35.93	55.65

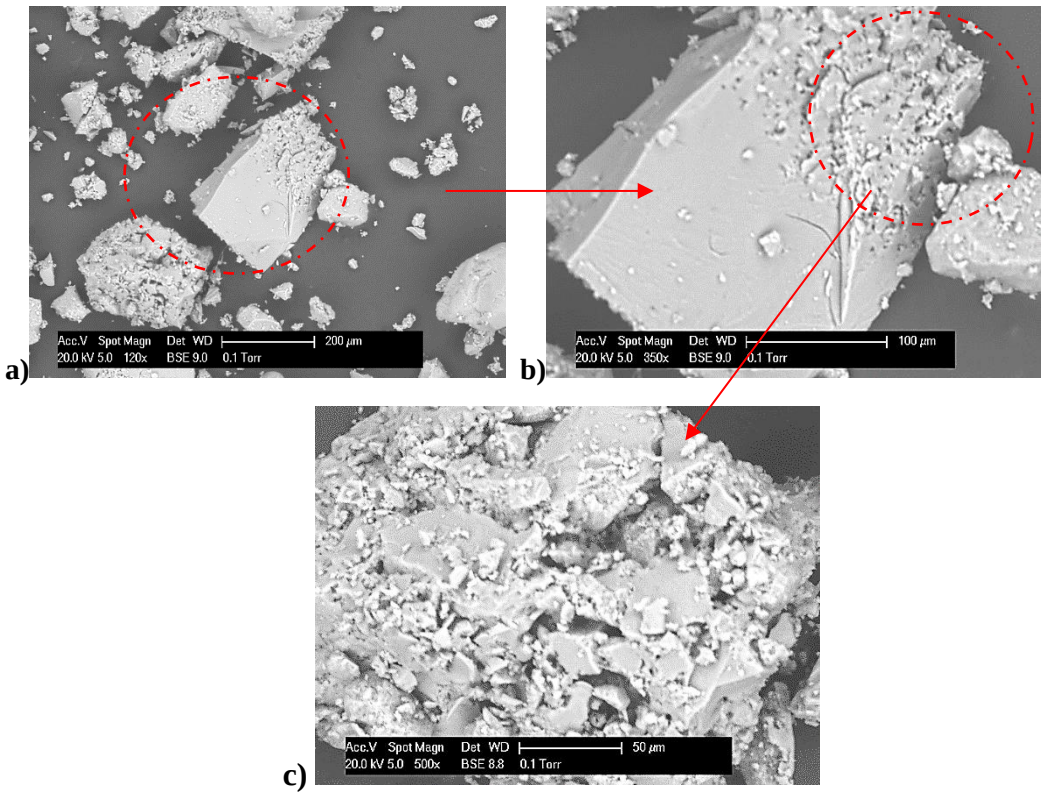

Figure 5.19 ESEM images of DETPMP/Ca precipitate particles after the flooding test in a mixture with sand, zoomed from the scale 120x (a) to 350x (b) and to 500x (c).

5.4. Summary and Conclusions

In this Chapter, DETPMP/Ca precipitate dissolution was monitored in non-equilibrium sand pack flooding tests. The main findings and conclusions obtained during this study are as follows:

1. The phosphonate SI return concentration in the precipitation pack floods depends on the flow rates used. Results from 3 flooding tests performed in the study demonstrate that the ~~effluent~~ SI concentration in effluent alters as the flow rate changes. SI return concentrations are higher and closer to some constant value at the lower flow rates, 1-3 ml/h, since dissolution, in this case, occurs close to equilibrium. At the higher flow rates, dissolution rates cannot "keep up" with the flow rates, therefore the SI concentration in the effluent decreases, until both rates are in equilibrium.

2. The equilibrium solubility Cs for the phosphonate/Ca precipitates is *not* a constant value. The equilibrium SI concentration decreased throughout the flooding test quite significantly. Even when a longer shut-in period of ~308 hours (13 days) after ~370

pore volumes was performed, the SI concentration in the effluent did not exceed 40ppm, compared to 130ppm recorded at the initial shorter shut-in of ~69 hours.

3. The DETPMP concentration in the return brine decreased gradually with increasing volume of brine passed through the column. This was observed during the longer sand pack 2a and 2b experiments, where the total flooding volume was ~370 pore volumes. However, even after such an extended flooding, the SI was produced at 20ppm at the highest flow rates, which is promising for the implementation of precipitation squeezes in the oilfield to return at low [SI] for a longer period of time giving extended scale protection if the field SI MIC is below 20ppm.

   This return behaviour also explains the disagreement raised earlier in the literature between the lower SI return concentrations in the field and higher initially recorded SI solubilities (Sorbie, Jiang et al. 1993). We have shown, that the phosphonate SI releases at higher concentrations, close to the initially measured equilibrium solubility, only during the initial flooding stages. With increasing flooding volume, the equilibrium solubility of the precipitates, as well as the SI concentration in the bulk, decrease.

4. Calcium concentration and the effluent pH were also monitored to investigate their involvement in the dissolution process. We have shown, that Ca return concentrations do not vary significantly, compared to SI concentrations, over the entire flooding test. pH in the system is shown to be governed by DETPMP/Ca precipitate dissolution. Generally, the higher the apparent pH value is, the higher the SI inhibitor concentration released into the effluent. This is in agreement with the earlier dissolution tests performed in the bulk solutions, where the apparent solubility was found to be a function of apparent pH.

5. The dissolution behaviour of the DETPMP/Ca precipitate observed in the sand pack tests does not correlate with the "classical" simple dissolution model that is currently used in SI precipitation models for phosphonates. According to the classic model, since the DETPMP/Ca precipitate contains only one type of phosphonate molecule, and not a mixture of different species, then the phosphonate precipitate should be characterised by a specific saturation concentration, or a specific equilibrium solubility, Cs. However, we have shown that the equilibrium solubility of the phosphonate SI precipitate is *not* a constant value and varies over the flood.

Therefore, a different approach is proposed to define the phosphonate concentration in the return brine of a precipitation treatment. This is based on the following findings:

- The phosphonate SI return is governed by the phosphonate/Ca precipitate's continuous re-speciation over the flood leading to the leftover precipitate showing a reduction in its stoichiometry with Ca.

- Brine pH varies during the precipitate dissolution and the apparent pH in turn affects the speciation of the precipitate.

The apparent pH, and phosphonates speciation, and bulk solubility should be coupled together and solved numerically in an appropriate precipitation model. The data obtained from the flow experiments in sand pack 1 and 2 can be used to model the SI return after a coupled precipitation/adsorption treatment, whereas the precipitate pack 3 return profile describes the "pure" dissolution of the SI without involving any adsorption/desorption mechanism. All the data obtained in the current study over the dynamic flooding tests can be used as input to solve the precipitation/dissolution model for phosphonate scale inhibitor and define its release behaviour in precipitation squeeze treatments.

CHAPTER 6. PRECIPITATION BEHAVIOUR OF PHOSPHATE ESTER SCALE INHIBITORS

6.1. Introduction

The main generic classes of scale inhibitor (SI) which have been extensively applied in precipitation squeeze treatments are organic phosphonates and polymeric scale inhibitors. To date, scale inhibition mechanisms of these SIs (Sorbie and Laing 2004, Shaw, Sorbie et al. 2012, Shaw, Sorbie et al. 2012), as well as their retention mechanism, i.e. adsorption and precipitation behaviour in squeeze treatments, have been well established (Shaw and Sorbie 2014, Shaw and Sorbie 2015, Farooqui and Sorbie 2016, Farooqui, Sorbie et al. 2016). In the current Chapter, another class of SIs – phosphate ester chemistry will be presented. The performance mechanism and precipitation behaviour of the phosphate ester SIs are not fully understood, therefore required some detailed investigation.

Generally, phosphate esters are more familiar to petroleum engineers as corrosion inhibitors (McGregor 2004, Brown, Saleh et al. 2015, Yepez, Obeyesekere et al. 2015), as well as being used as gelling (Burnham, Harris et al. 1980, Samuel, Nasr-El-Din et al. 2005) and lubricant additives (Johnson and Hils 2013). Chemical packages made up of phosphate esters and aluminium ions have been extensively used as a gelling agent in fracturing fluids and for sand control for the last 40 years. The application is based on the interactions between the aluminium and phosphate-group which cross-link in the system (see Figure 6.1), and this in turn results in viscosity increasing very significantly. This provides desired net pressure to control proppant placement and fluid losses.

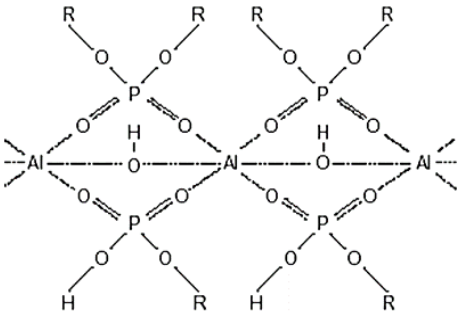

Figure 6.1 Gelation mechanism of conventional phosphate ester-based gelled oils (Burnham, Harris et al. 1980)

Other phosphate ester applications are based on their ability to form films on a wide range of different surfaces – from crystals nuclei (scale inhibition) to steel pipes (corrosion inhibition and lubrication). However, very little information is available on the phosphate ester chemistry in the context of scale inhibition. Previous published data is limited to a few corefloods and some field case studies (Jordan 2000, Jordan, Johnston et al. 2016, Sutherland and Jordan 2016). Examples have been presented where phosphate esters show higher retention and improved scale inhibition at much lower concentrations than the standard phosphonates and polymers (Jordan, Johnston et al. 2016).

It has been reported, that phosphate esters show improved performance over the phosphonates and polymers at lower temperatures, below 70^{o}C. Currently, polymeric SIs are applied to protect the well from scale formation at lower temperatures due to their higher performance at temperatures < 80^{o}C. However, most of those polymers do not contain phosphorus in the structure, therefore, *cannot* be detected by conventional fast and routine analytical techniques, such as ICP (Inductively Coupled Plasma Spectroscopy). The advantage of the ICP method is the ability to detect low SI concentrations, down to 0.5ppm active, which is an especially important criterion for field SI analysis. Alternative methods that can be used to detect and assay polymeric SIs, such as wet chemical techniques, may not always give this level of accuracy. Phosphate ester chemistry due to the phosphorus atoms in the structure can be analysed by ICP, therefore it is a promising alternative to polymeric SIs for lower temperature applications.

Phosphate esters are also recognised as being environmentally acceptable chemicals. This environmental friendliness of phosphate esters is a great advantage in their application as corrosion and scale inhibitors in sensitive environments such as the North Sea (Braga, Martin et al. 2002). This shows another advantage of phosphate ester SIs over some polymeric species that fail to meet the environmental requirements particularly in terms of their biodegradation behaviour.

Phosphate esters are chemicals derived from phosphoric acid and various classes of alcohols, for example poly glycols, long carbon chain alkyl alcohols etc. When it comes to chemistry, one of the most typical reactions for phosphate esters is a hydrolysis reaction. Phosphate esters can suffer hydrolysis through both acid and base catalysis as well as by reacting with water molecules themselves. The reaction yields phosphoric acid and an alcohol:

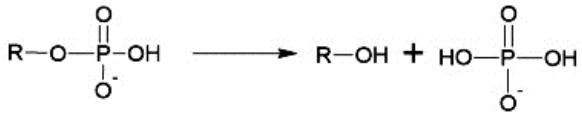

(6.1)

The reaction kinetics depends on temperature, solution pH and on the presence of some ions, for example halides, which can induce hydrolysis. The reaction rate increases significantly with increasing temperature (Kirby and Varvoglis 1967) and also in the presence of some divalent and trivalent cations (Morrow, Buttrey et al. 1992, Connolly, Banaszczyk et al. 1994). Corrosion products can catalyse the hydrolysis of phosphate esters, if the concentration of the chemical is below the critical micelle concentration (Alink, Outlaw et al. 1999).

Therefore, some of the fundamentals of phosphate esters chemistry have already been established. However, when it comes to their application in scale inhibition, there is still insufficient information to understand the behaviour of phosphate esters under field/reservoir conditions. Since the current dissertation is focused on precipitation squeeze applications, the aim of this Chapter is to examine the precipitation behaviour of phosphate ester inhibitors and how the conditions at which the precipitation process occurs affect the inhibition efficiency of precipitated and re-dissolved phosphate ester SIs in a context of precipitation treatments. This aspect of phosphate ester SIs has not been studied previously.

The research was conducted for two phosphate ester chemicals of different chemical structure PE_1 and PAPE obtained from different chemical suppliers. The study includes:

I. Precipitation tests using different batches of both SIs with calcium cations (Ca^{2+}) under various pH and temperature conditions. As a result, the factors affecting the phosphate ester/Ca_n precipitates stoichiometry (i.e. “n”) are defined.

II. Measuring inhibition efficiencies (IE) of stock, supernatant solution and precipitated and then re-dissolved phosphate ester SIs obtained at different pH and temperature values. When SI is delivered into the reservoir as a precipitate, the inhibition efficiency of the precipitated and then re-dissolved SI species may differ from the efficiency of the stock product, for various reasons. This may have an impact on the minimum inhibition concentration (MIC) and overall squeeze lifetime. Therefore, when designing precipitation squeeze treatments, the effect of

the precipitation process on the performance of the precipitated and re-dissolved SI species must be investigated.

The results obtained in this work are of practical significance for the effective design of phosphate ester precipitation squeeze treatments, since this chemistry represents (i) a more environmentally acceptable alternative to phosphonates, and (ii) a chemical that is significantly easier to detect within produced brine than many polymers used by the industry, many of which are phosphorus free polymers.

6.2. Experimental Details

6.2.1. *Materials*

The structures of the active phosphate ester compounds are shown in Table 6.1 (as obtained from the suppliers). Two commercially available phosphate ester scale inhibitors PE_1 and PAPE were used to conduct (i) precipitation tests in brines made with $CaCl_2 \cdot 6H_2O$ and (ii) inhibition efficiency tests in synthetic North Sea Sea Water (NSSW) and Nelson Forties Formation Water (NFFW) made up from the salts listed in Table 6.2 and Table 3.3, all from Sigma Aldrich and used as received. All scale inhibitor concentrations quoted are *active* concentrations. For some of the precipitation tests, there were two batches (named as Batch-1 and Batch-2) of the PE_1 and PAPE stocks used in order to highlight the repeatability of the test results. These different batches (of the *same* chemical) were purchased with an ~ 2 year interval between receiving each of the batches.

Table 6.1 Chemical structures of the tested phosphate esters

Scale Inhibitor	Chemical Structure
PE_1 Phosphate Ester 1 (di-ester and tri-ester mixture)	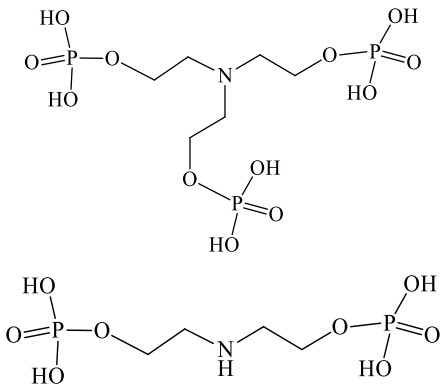

PAPE Polyalcohol Phosphate Ester	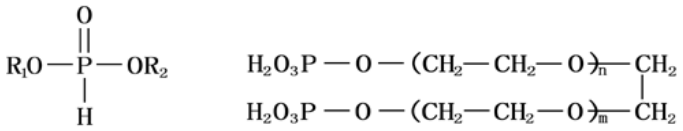

As the exact molecular weights of the phosphate esters are unknown, the stoichiometry of the phosphate ester complexes, denoted as SI_Ca_n was found as the ratio of moles of Ca to P (instead of Ca to SI). Precipitation tests were conducted at a fixed pH 5.5 and 9.5 and at temperatures 20°C, 60°C and 95°C (for PE_1) and at 60°C and 95°C (for PAPE). Some of the precipitation experiments were conducted in duplicate using different batches of PE_1 and PAPE stocks.

Solutions containing SI in the concentration range 1000-3000 ppm active with 2000 ppm Ca were pH adjusted to either pH 5.5 or pH 9.5 using dilute HCl (aq) and/or NaOH (aq). After the initial adjustment, the pH value was re-checked continually and re-adjusted if required, until a stable pH at the target value was achieved. This step was very important since, upon initial pH adjustment, the precipitation of a SI_Ca^{2+} complex occurs and causes a variation in solution pH. Subsequently, the solutions were left at the test temperature (20°C, 60°C or 95°C). After 24 hours, to facilitate phase separation, the test bottles were placed in a centrifuge for 10 minutes. Finally, the precipitates and supernatant solutions were collected using vacuum filtration through a 0.45 µm filter. All the precipitates were re-dissolved by adding a few drops of 35% wt. HCl which led to SI association back into its acid form and dissolution of the SI/Ca complexes (Shaw and Sorbie 2014).

By assaying the re-dissolved SI/Ca precipitate solutions by ICP, it was possible to directly find the [SI] and [Ca^{2+}] in the precipitates. In earlier section 3.3.1, it was found that the direct precipitate analysis gives "smoother" profiles of the stoichiometry versus the Ca^{2+}/SI molar ratio than "supernatant" analysis. However, the "supernatant" analysis has been also performed and the comparison of both methods is presented in the Section 6.3.

6.2.2. *Precipitation and Re-Dissolution Experiments*

The main reason for conducting IE experiments in this work was to compare the inhibition performance of precipitated SI with its supernatant solution and the commercial stock product. Therefore, prior to the inhibition efficiency tests, a series of precipitation and re-

dissolution experiments were carried out to obtain the SI precipitates.

SI was added to the solution containing 2000 ppm Ca. Solutions were then pH adjusted to pH 5.5 or 9.5, depending on the particular test conditions. As described above, precipitation of the SI_Ca complexes led to pH variation, therefore pH had to be re-checked continually until a stable pH of 5.5 was achieved. Subsequently, solutions were placed into a waterbath at the required test temperature and left there for 24 hours. After that time, the precipitate was collected using vacuum filtration with 0.45µm filters and was dissolved by adding a few drops of 35% HCl to the DW solution. 1ml of sample was removed from the collected supernatant and added to 9ml DW before being analysed by ICP for its SI concentration – the data was used for further calculations and to prepare SI solutions for the IE experiment.

6.2.3. *Static Barium Sulphate Inhibition Efficiency Test*

The main reason for conducting IE experiments in this work is to compare inhibition performance of precipitated SI with its supernatant solution and the commercial stock product. These were obtained by following the precipitation test procedure described above, at the required temperatures and pH values. The procedure for the static barium sulphate IE tests of the precipitated and then re-dissolved phosphate esters was described earlier in section 3.2.4. The identical procedure was used for the current studies as well. The approach and test methodology applied in this study are schematically shown in Figure 6.2.

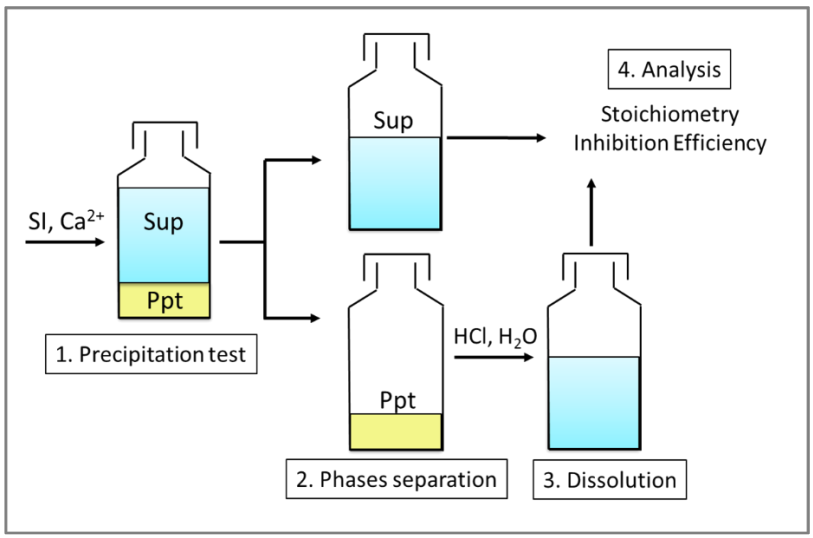

Figure 6.2 Precipitation test methodology

To be able to compare the inhibition efficiencies of phosphate ester species at different temperatures, the saturation ratio (SR) was kept constant. For the lower temperature IE tests at 20°C, 40°C, 60°C and 80°C the NSSW composition was changed slightly, in order to keep the saturation ratio in all the systems at the same level as the 95°C test (~322.6). The saturation ratio for NSSW/NFFW versus temperature is shown in Figure 6.3. These NSSW compositions used for the calculations in the MultiScale software are presented below in Table 6.2.

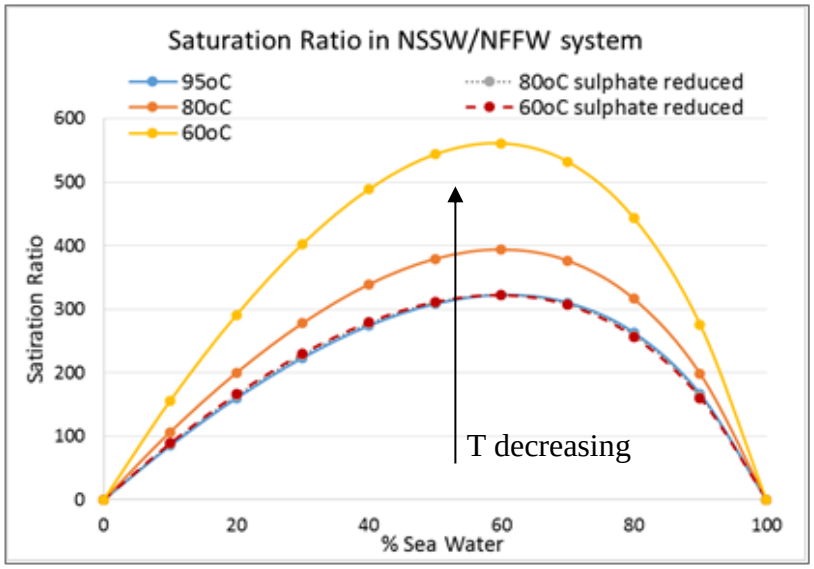

Figure 6.3 Saturation ratio profile for NSSW/NFFW mixing brines

Table 6.2 NSSW composition for inhibition efficiency tests at lower temperatures

Ion	Concentration in NSSW, ppm				
	20°C test	**40°C test**	**60°C test**	**80°C test**	**95°C test**
Na^+	10890	10890	10890	10890	10890
Ca^{2+}	428	428	428	428	428
Mg^{2+}	1368	1368	1368	1368	1368
K^+	460	460	460	460	460
Ba^{2+}	0	0	0	0	0
Sr^{2+}	0	0	0	0	0
Adjusted SO_4^{2-}	546	1038	1690	2420	2960
Cl^-	19773	19773	19773	19773	19773

6.3. Results and Discussion

6.3.1. *PE_1_Ca Precipitation Behaviour: Stoichiometry*

Precipitation tests for the PE_1 product were performed in Ca^{2+} 2000ppm brine whilst varying pH and temperature, to define the effect of these factors on the precipitation

behaviour of phosphate ester chemistry. For the phosphonate SIs (Shaw and Sorbie 2014, Shaw and Sorbie 2015) and polymeric SIs (Farooqui, Sorbie et al. 2016), these were found to be key factors determining the stoichiometry and chemical properties of the precipitates that form, and, in turn, the release behaviour of the phosphate ester species from its precipitate into the bulk.

Since the molecular weight of the PE_1 product was unknown, the stoichiometry of PE_1_Ca complexes was found as a ratio of moles of calcium to moles of phosphorus, i.e. the Ca:P ratio, instead of Ca to PE_1 molar ratio. PE_1_Ca precipitates were obtained at the following pH and temperatures:

- T = 20°C* at pH 5.5
- T = 95°C* at pH 9.5
- T = 60°C at both pH 5.5 and 9.5

The tests marked with * were performed with 2 different batches of the PE_1 stock: Batch-1 and Batch-2, obtained from the same supplier, to see if the results were consistent between different batches. Since the phosphate ester product is not made up by a single molecular formula, but rather by a mix of different species, some variations may take place. However, the chemical content of both batches is expected to be identical.

It was observed during the tests, that the phosphate esters ~~inhibitors~~, similar to phosphonate and polymeric SI species, can form complexes with divalent cations, particularly with Ca. Precipitates with lower solubility were extracted from the PE_1/Ca bulk system. Initially "cloudy" and insoluble PE_1_Ca complex at 20°C transits into a transparent gel whilst heating it up to T = 95°C (see Figure 6.4). The process onset occurs at a temperature ~ 80°C. After cooling the bottles back to 20°C, it is observed that solutions are clear. Therefore, an exposure to the higher temperature may alter the chemical and physical properties of the phosphate ester solutions. The temperature impact on the phosphate ester solutions will be discussed further in CHAPTER 7.

It can be noted in Figure 6.5, that the viscosity of the PE_1/Ca bulk system at 95°C alters with an increase in PE_1 concentration from 1000ppm to 3000ppm, where 1000ppm is quite water-like, whereas the 3000ppm aqueous solution becomes thicker and more gel like. The viscosity increase may occur due to interactions between the calcium and the phosphate-group, when heat is applied, leading to some cross-linking in the system and

hence a viscosity increase. Once the bottles are cooled down to room temperature, the viscosity drops. There are several papers describing a similar effect, but for the phosphate ester-aluminium systems (Burnham, Harris et al. 1980, Samuel, Nasr-El-Din et al. 2005). Figure 6.1, presented earlier in the current Chapter, schematically shows this cross-linking mechanism that may cause the viscosity increase. This viscosity increase was observed only in the PE_1/Ca solutions, and not for the PAPE/Ca system. The difference in the chemical structure of the PAPE and PE_1 products could be the reason for the different types of precipitation behaviour observed here.

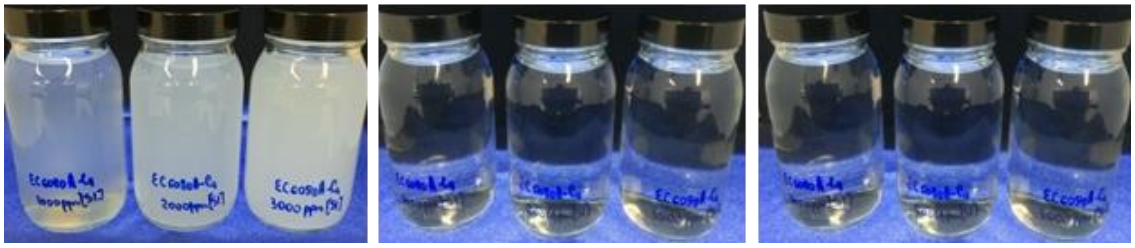

20°C after heating to 95°C cooling back to 20°C

Figure 6.4 PE_1/Ca system behaviour at different temperatures

1000 ppm SI + 2000 ppm Ca **3000 ppm** SI + 2000 ppm Ca

Figure 6.5 Gel formation in PE_1/Ca bulk at 95°C, pH 5.5

The stoichiometry could not be established at pH 5.5 and 95 °C due to higher solubility of the precipitate at these conditions. Therefore, the pH was increased to be able to precipitate higher amount of SI. After filtering the prepared solutions, the PE_1/Ca precipitates were collected. It was noticed, that the PE_1 precipitates were gel-like sediments (Figure 6.6), which was quite different to the phosphonate precipitates which were used in the previous work.

Figure 6.6 PE_1_Ca precipitate, collected after filtering PE_1/Ca solution at T=95°C, pH 9.5

PE_1_Ca Stoichiometry for Different Batches

The stoichiometry data from both the supernatant and precipitate analysis of the PE_1_Ca_n complexes precipitated from *Batch-1* and *Batch-2*, at pH 5.5 and T = 20°C, are presented in Figure 6.7 and Figure 6.8, respectively. These graphs present ΔCa versus ΔP for the supernatant method, or Ca against P for the precipitate method. Therefore, the slope gives the ΔCa /ΔP ratio in the precipitated PE_1_Ca_n complex, or the stoichiometric coefficient n.

The Ca/P ratio in these PE_1_Ca complexes for Batch-1 and Batch-2 are found to be ~ *3.4 and 2.9* (supernatant method), or ~ *4.2 and 3.0* (precipitate method), respectively. Generally, the stoichiometry values for Batch-2 are slightly lower than those ones measured for Batch-1, however, all numbers are within the range of n ~ *2.9- 4.2*.

Batch-1 PE_1_Ca: 20°C, pH 5.5

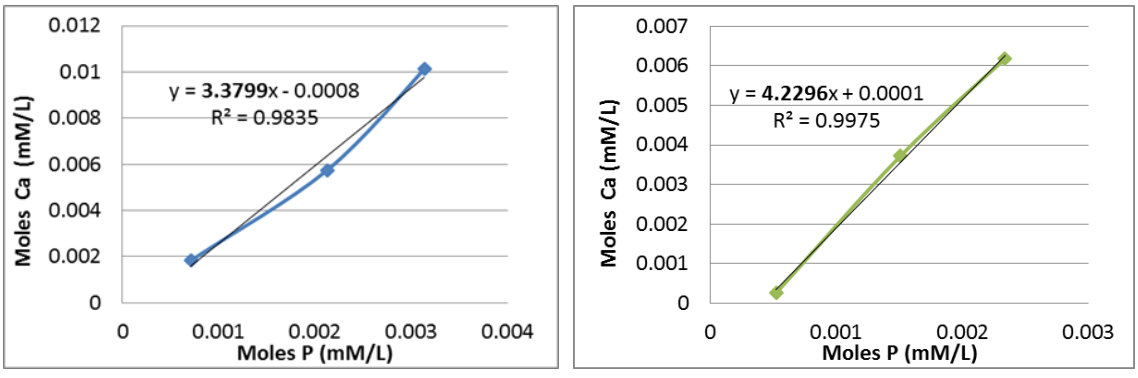

Supernatant Precipitate

Figure 6.7 ΔCa (mM/L) versus ΔP (mM/L) in PE_1/Ca complexes in supernatant and precipitate at pH 5.5, 20°C, [Ca^{2+}] = 2000ppm, [SI] = 1000, 2000, and 3000ppm (Batch-1)

The stoichiometry values obtained by the precipitate and supernatant methods are slightly different, which probably occurs due to the specifics of the experimental procedure applied in this study. According to the methodology used for the supernatant analysis, a sample was taken from the top solution after centrifuging the test bottles. However, since the phosphate ester stock product is made up by different chemical structures – di-ester and tri-ester (shown in Table 6.1), centrifuging may cause weight distribution of different SI/Ca complexes from the top to lower layers of the solution in a bottle. Therefore, the stoichiometry values found by the supernatant method are expected to be slightly lower than ones, obtained by the precipitate analysis, or at least the values may vary slightly. To get an average concentration of the SI in the supernatant and minimize the variations in the supernatant and precipitate data, it is suggested to take a sample of supernatant after the filtration step.

Batch-2 PE_1_Ca: 20°C, pH 5.5

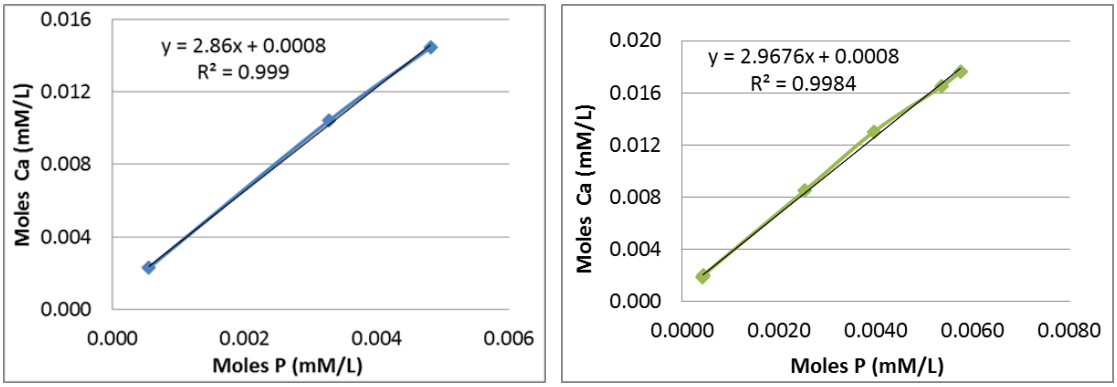

Supernatant Precipitate

Figure 6.8 ΔCa (mM/L) versus ΔP (mM/L) in PE_1/Ca complexes in supernatant and precipitate at pH 5.5, 20°C, [Ca^{2+}] = 2000ppm, [SI] = 1000 - 3000ppm

The stoichiometry also varies slightly for Batch-1 and Batch-2 stock products. This probably occurs due to the stock product containing different SI species that can bind with Ca, forming complexes of different stoichiometry. Theoretically, n_{max} is equal to 2 and 3 for di- and tri-esters, respectively, however, the stock may also contain other Ca binding components that are not labelled, therefore some variations from these stoichiometry values still may occur. The stoichiometry that is reported here is the average value for all the precipitated components of the PE_1 stock product, therefore, if there is a slight variation in the composition of the different batches, then stoichiometry values may also be subject to variation.

In the next step, the precipitation tests were performed for the same SI product – PE_1, but at higher pH and temperature, i.e. pH 9.5 and 95ºC. The stoichiometries (n values) of the PE_1_Ca complexes at these conditions are ~ *4.3* (Batch-1) and ~*3.6* (Batch-2). Again, similarly to the data obtained at the lower pH, the Batch 2 stoichiometry values are somehow lower than those for Batch-1.The stoichiometry data for the PE_1_Ca complex obtained at these conditions through the precipitate method are shown in Figure 6.9 for Batch-1 (a) and Batch-2 (b).

PE_1_Ca: 95ºC, pH 9.5

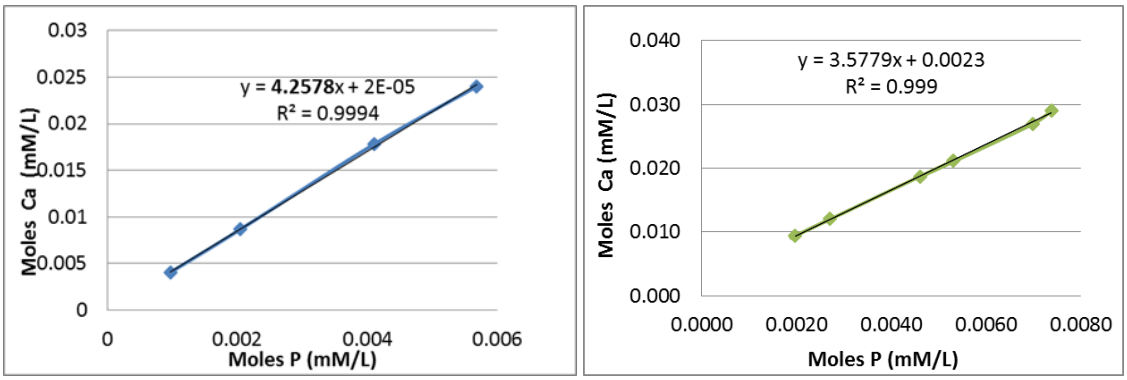

a) Batch-1 (precipitate) **b) Batch-2 (precipitate)**

Figure 6.9 ΔCa (mM/L) versus ΔP (mM/L) in PE_1/Ca precipitate at pH9.5, 95ºC, [Ca^{2+}] = 2000ppm, [SI] = 1000- 3000ppm obtained from Batch-1(a) and Batch-2(b)

Table 6.3 combines all the stoichiometry data obtained from the precipitation tests for the two different PE_1 batches. Values marked with * represent data from the Batch-2 stock product. The stoichiometry values of all the PE_1_Ca complexes obtained for the *Batch-2* of PE_1 stock are slightly lower than the corresponding data of Batch-1 PE_1. This may be caused by experimental error or a slight difference in the composition of the stock SI. Since the PE_1 stock product composition is made up of a mixture of di- and tri-phosphate esters which also contains some P-containing components, the precipitates that form do not have a single molecular structure. Thus, a slight variation in a proportion of the active compounds could cause a variation in the average stoichiometry values. Generally, the Ca/P ratio for the PE_1_Ca precipitates is found to stay in the range ~2.7 to ~3.6 (Batch-2) and ~2.9 to ~4.3 (Batch-1). Although these figures are approximate, they are sufficient for us to make comparisons with the (more accurate) phosphonate/Ca stoichiometry values.

Table 6.3 Comparison of stoichiometry data obtained for PE_1_Ca complexes precipitated from PE_1 Batch-1 and Batch-2*

Comlplex	Test pH	Test temperature, °C	Ca/P, or stoichiometry	
			precipitate method	supernatant method
PE_1_Ca	5.5	20	4.2/3.0*	3.4/2.9*
	9.5	95	4.3/3.6*	-

PE_1_Ca Stoichiometry: pH and Temperature Effects

In order to highlight the effect of temperature and pH variation on the stoichiometry of the PE1/Ca complexes, in addition to the experiments reported above, a series of tests was conducted at a temperature of 60°C. This data would define the stoichiometry of the PE_1_Ca precipitate at the conditions close to the field squeeze treatment application conditions, since the inhibition efficiency performance of phosphate esters was found to be better in the temperature range of 60-80°C (see next section). The stoichiometry of the PE_1_Ca complexes at 60°C was measured only for *Batch-2* at pH 5.5 (Figure 6.10) and pH 9.5 (Figure 6.11).

Batch-2 PE_1_Ca: 60°C, pH5.5

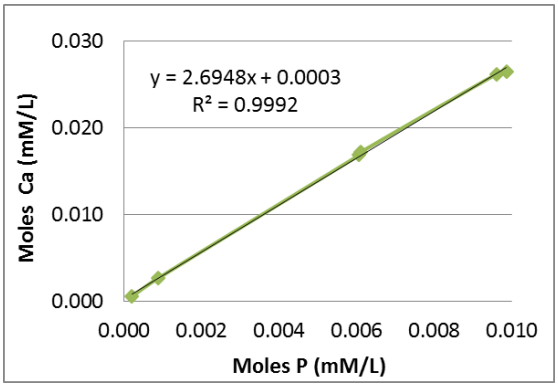

precipitate

Figure 6.10 ΔCa (mM/L) versus ΔP(mM/L) in PE1/Ca precipitate at pH 5.5, 60°C, [Ca^{2+}] = 2000ppm, [SI] = 1000- 3000ppm (Batch-2)

Batch-2 PE_1_Ca: 60°C, pH9.5

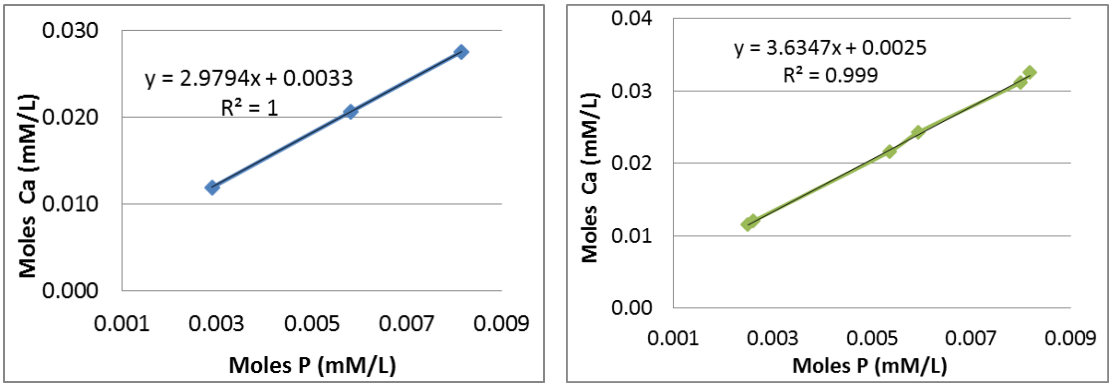

supernatant precipitate

Figure 6.11 ΔCa (mM/L) versus ΔP (mM/L) in PE_1/Ca complexes by supernatant and precipitate analysis at pH 9.5, 60°C, [Ca^{2+}] = 2000ppm, [SI] = 1000- 3000ppm (Batch-2)

The stoichiometry of the complexes formed at 60°C and pH 5.5 is found to be ~ *2.7* (precipitate method) and slightly higher at pH 9.5, i.e. ~*3.0* and ~*3.6* (supernatant and precipitate methods, respectively). Hence, no significant temperature effect is observed for the PE_1 precipitated complexes, as the stoichiometry values measured at 60°C correspond quite closely with the values obtained for the PE_1_Ca complexes at 20°C and 95°C.

Thereby, the stoichiometry of the PE_1_Ca precipitates was measured in the temperature range of 20-95°C; at pH 5.5 and 9.5; all the data is summarized in Table 6.4. The main conclusions reached from this study for the PE_1 phosphate ester are:

- Generally, temperature does not have a significant impact on the stoichiometry of the PE_1_Ca complexes obtained at the same pH. For example, the stoichiometry values obtained at pH 9.5 and at 60°C and 95°C are identical, i.e. ~3.6 (precipitate methods) and ~3.0 (supernatant method).
- A slight decrease in stoichiometry at pH 5.5 is shown when the test temperature increases from 20°C to 60°C. It was also found that the amount of the PE_1_Ca precipitate, that is produced, also decreases when moving from 20 to 60°C. Therefore, the lower amount of precipitate produced for the 60°C tests may affect the accuracy of the stoichiometry measured at those conditions.
- Stoichiometry of the PE_1_Ca complexes slightly increases with increasing solution pH.

- The Ca/P ratio for the PE_1_Ca precipitates is found to stay in the range ~2.7 to ~3.6 for Batch-2 and ~2.9 to ~4.3 for Batch-1, at these test conditions (temperature range of 20-95°C; pH 5.5 and 9.5.

Table 6.4 Combination of all the stoichiometry data obtained for PE_1_Ca complexes precipitated from PE_1 Batch-1* and Batch-2

Complex	Test pH	Test temperature, °C	Ca/P precipitate method	Ca/P supernatant method
PE_1_Ca	5.5	20	4.2*/3.0	3.4*/2.9
	5.5	60	2.7	-
	9.5	60	4.3*/3.6	3.0
	9.5	95	3.6	3.0

6.3.2. *PAPE_Ca Complex Stoichiometry at different pH and T*

This section presents the stoichiometry data for another series of phosphate ester complexes for the PAPE_Ca_n precipitates. The experiments were conducted at two pH values, pH 5.5 and pH 9.5, and two temperatures, T = 60°C and 95°C. Some of the tests were repeated in duplicate with two different PAPE stock batches obtained from the same supplier (Batch-1 and Batch-2), although it was expected that both the batches had identical chemical content.

PAPE_Ca Stoichiometry at Higher Temperature 95°C

The stoichiometry data of the PAPE_Ca complexes, obtained from Batch-1 and Batch-2 stock products, at T = 95°C and different pH values is discussed below. At this temperature, the stoichiometry of PAPE_Ca precipitate does not change significantly when increasing pH from pH 5.5 to pH 9.5. The stoichiometry of the PAPE_Ca complexes found for *Batch-1* at 95°C at pH 5.5 are ~ *3.7/4.1*, and at pH 9.5 ~ *3.5/3.8*, by supernatant/precipitate analyses. The data for the different pH values is shown in Figure 6.12 and Figure 6.13, respectively. The precipitate method shows slightly higher values of n than the supernatant method, which was also observed for the PE_1 product reported above.

The stoichiometry data for the *Batch-2* PAPE_Ca complexes obtained at the same conditions, i.e. at 95°C, pH 5.5 and pH 9.5 is shown in Figure 6.14a for pH 5.5 test, and in Figure 6.14b - for pH 9.5. The PAPE_Ca complex stoichiometries are shown to be ~

3.0 and ~ *3.2* at pH 5.5 and 9.5, respectively. Again, as in case with PE_1_Ca complexes, the stoichiometry values obtained at different pH values are quite close to each other.

Batch-1 PAPE_Ca: pH 5.5, 95ºC

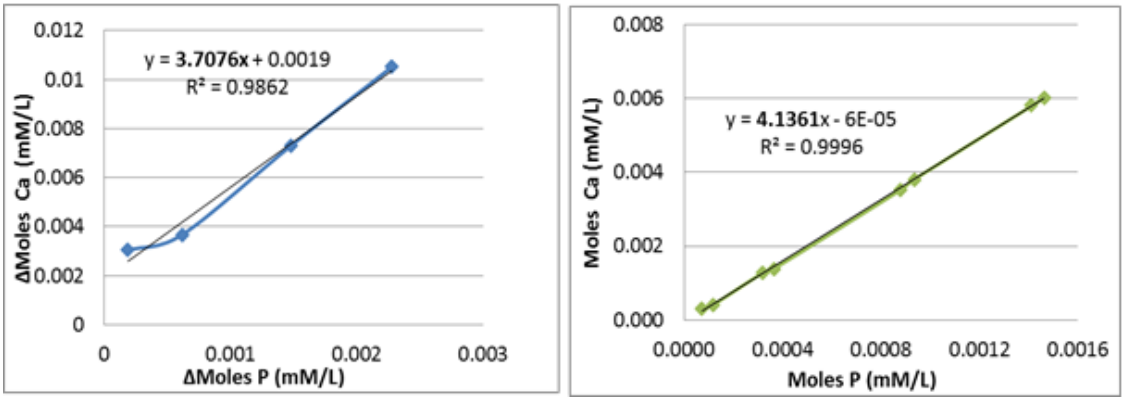

Supernatant Precipitate

Figure 6.12 ΔCa (mM/L) versus ΔP in PAPE (mM/L) in supernatant and precipitate at pH 5.5, 95ºC, [Ca^{2+}] = 2000ppm, [SI] = 1000, 2000, and 3000ppm (Batch-1)

Batch-1 PAPE_Ca:pH 9.5, 95ºC

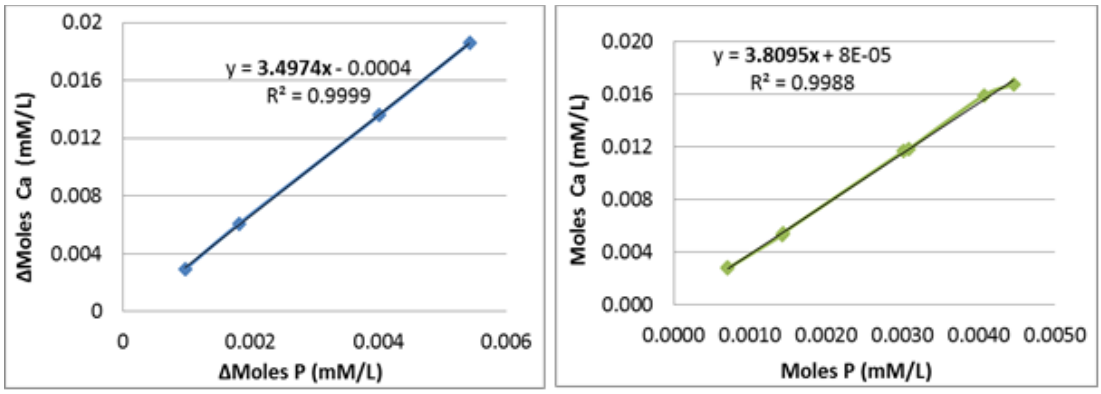

Supernatant Precipitate

Figure 6.13 ΔCa (mM/L) versus ΔP in PAPE (mM/L) in supernatant and precipitate at pH 9.5, T=95ºC, [Ca^{2+}] = 2000ppm, [SI] = 1000-3000ppm (Batch-1)

Stoichiometry values of all the PAPE_Ca complexes obtained for *Batch-2* of the PAPE stock product are slightly lower than the corresponding data for *Batch-1*. This trend was also noticed for the PE_1_Ca complexes, described in the previous sub-section. We suggest this to be either due to experimental error or slight difference in the composition of the stock SI. Since the stock PAPE product is a composition made up by mono- and di-phosphate esters with different molecular weights, a slight variation in the proportion of

the compounds in the stock solution could lead to a variation in the average stoichiometry values of the precipitates that form. Also, pH is shown to not significantly impact the stoichiometry of the phosphate ester PAPE/Ca complexes.

Batch-2 PAPE_Ca: 95ºC, pH 5.5 and 9.5

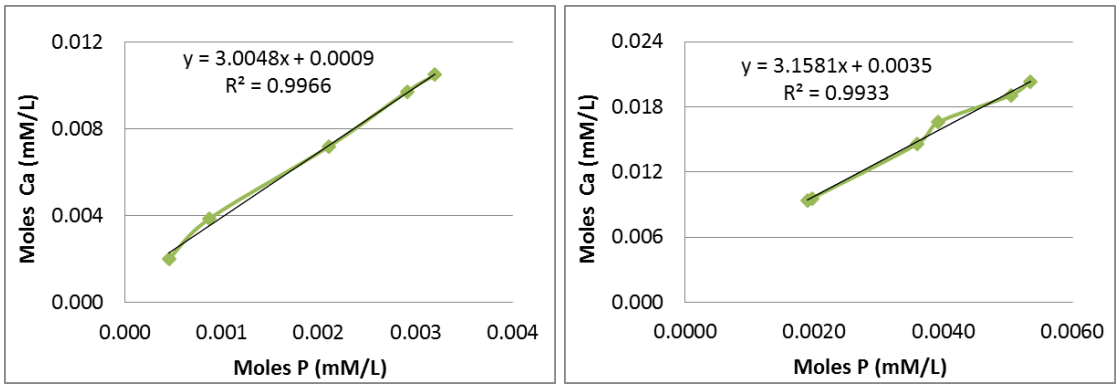

pH 5.5 precipitate pH 9.5 precipitate

Figure 6.14 ΔCa (mM/L) versus ΔP in PAPE (mM/L) in precipitate at pH 5.5(a) and Ph 9.5 (b), 95ºC, [Ca^{2+}] = 2000ppm, [SI] = 1000-3000ppm (Batch-2)

The stoichiometry data for the PAPE_Ca complex was also obtained at the lower temperature of *60ºC*, which is closer to the conditions where phosphate ester SIs are applied (lower reservoir temperatures up to 80°C). The data from the precipitation experiments for *Batch-2* PAPE product, conducted at pH 5.5 and pH 9.5, shown in Figure 6.15 and Figure 6.16. Stoichiometry of the PAPE_Ca precipitated complexes at pH 5.5 are ~ *2.9/2.8* and at pH 9.5 are ~*4.1/3.9*, by supernatant/precipitate methods, respectively. At 60ºC, the stoichiometry of the PAPE_Ca complexes increases quite significantly with increasing solution pH from pH 5.5 to 9.5.

Batch-2 PAPE_Ca: 60°C, pH 5.5

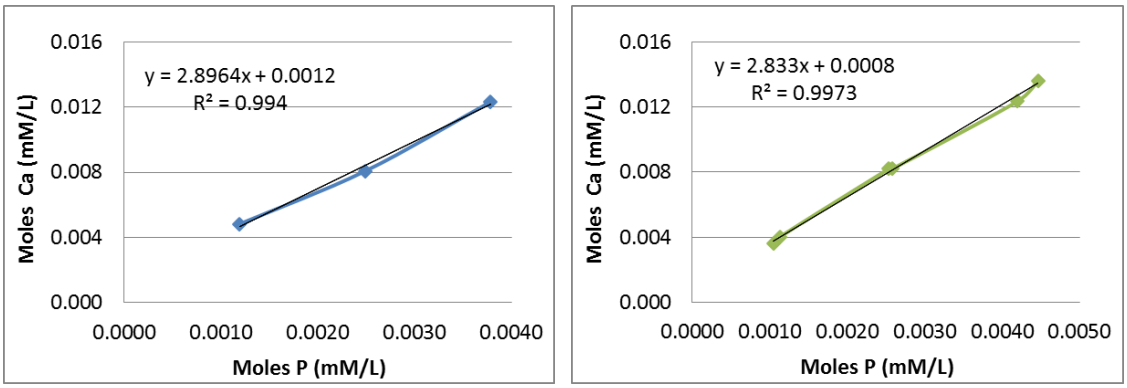

Supernatant Precipitate

Figure 6.15 ΔCa (mM/L) versus ΔP in PAPE (mM/L) in supernatant and precipitate at pH 5.5, 60°C, [Ca^{2+}] = 2000ppm, [SI] = 1000- 3000ppm (Batch-2)

Batch-2 PAPE_Ca: 60°C, pH 9.5

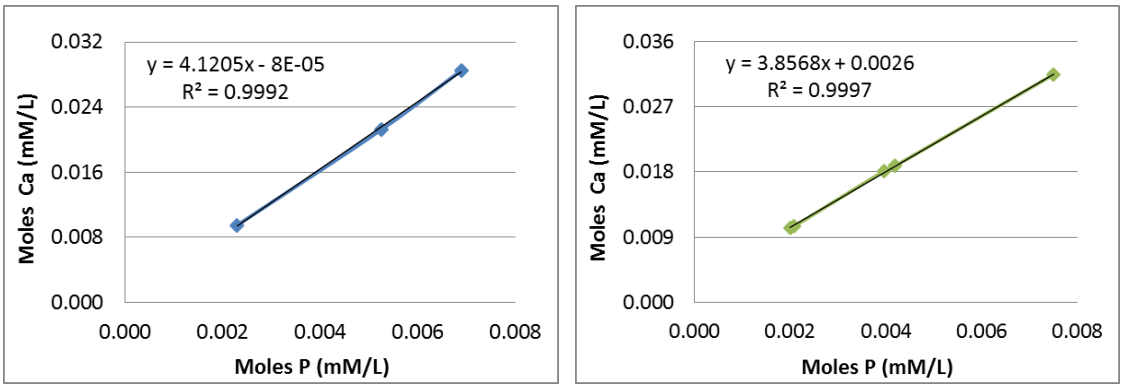

Supernatant Precipitate

Figure 6.16 ΔCa (mM/L) versus ΔP in PAPE (mM/L) in supernatant and precipitate at pH 9.5, 60°C, [Ca^{2+}] = 2000ppm, [SI] = 1000-3000ppm (Batch-2)

Overall, the stoichiometries of the PAPE_Ca complexes, obtained at pH 5.5 and 9.5 and temperatures of 60°C and 95°C, are measured to be within the range from ~2.8 to ~4.1 for both batches of the PAPE product.

Table 6.5 summarises all the stoichiometry data for the PE_1_Ca and PAPE_Ca complexes obtained at different pH values and temperatures. Since the data between the different batches was varying slightly, to make more accurate conclusions, only the data for Batch-2 was included in the table. For both phosphate ester products, Batch-2 was tested over a wider temperature range. Generally, all the stoichiometry values are within the range of *2.7-3.6* for PE_1, and *2.8-4.1* for the PAPE phosphate ester products. As the stoichiometry

of the precipitates formed at different pH and temperature values are very close to each other, this means that the molar ratio Ca/P in phosphate ester complexes does not significantly depend on solution pH, as with phosphonate and polymer SIs cases (Shaw and Sorbie 2015). It can be noted that the stoichiometry data obtained for both PE_1 and PAPE are close to each other (~3-4). This shows quite a high chelating capacity for phosphate esters, especially when compared to the stoichiometries of the phosphonate/Ca complexes, where the maximum theoretically possible Ca/P ratio is equal to 1, at high pH when all the phosphonate groups are fully dissociated (Shaw and Sorbie 2015).

Table 6.5 Comparison of stoichiometry data obtained for $PE_1\_Ca_n$ and $PAPE\_Ca_n$ complexes precipitated from Batches-2

Comlplex	Test pH	Test temperature, °C	Ca/P precipitate method	Ca/P supernatant method
PE_1_Ca	5.5	20	3.0	2.9
	5.5	60	2.7	-
	9.5	60	3.6	3.0
	9.5	95	3.6	3.0
PAPE_Ca	5.5	60	2.8	2.9
	5.5	95	3.0	-
	9.5	60	3.9	4.1
	9.5	95	3.2	-

From the application point of view, this means that the phosphate ester chemistry would require a higher concentration of calcium ions to be available in the brine to (i) enhance SI retention via a precipitation mechanism and also (ii) to provide adequate inhibition efficiency, as it is the Ca and SI complex, rather than "free" SI ions, that are involved in the scale inhibition mechanisms (Boak, Graham et al. 1999).

6.3.3. *Precipitation pH Effect on Inhibition Efficiency of the Phosphate Ester_Ca Complexes*

The PE_1_Ca precipitates and supernatant solutions described/generated in section 6.3.1 have been further analysed for their inhibition efficiency (IE) performance against barium sulphate. It has been established for polymeric PPCA SIs (Farooqui and Sorbie 2016), that precipitated SI has a much higher IE for barite scales than the stock SI. For polymeric SIs, this has been shown to be due to the fact that the precipitate is richer in higher molecular weight components of the polymer and these tend to give higher inhibition

efficiency performance. In the current work, in Chapter 3.4, it was shown that precipitation does not significantly affect the final IE of the precipitated phosphonate SIs, i.e. the IE of precipitated phosphonates are shown to be the same as the stock SI solutions. In order to check the precipitation effect on the phosphate ester SI performance against barium sulphate, the inhibition efficiency of the precipitated phosphate ester SIs was evaluated and compared to their associated supernatant and stock solutions inhibition efficiency performance.

PE_1_Ca complexes

The key point here is to establish the pH effect during the precipitation reaction on the performance of the formed precipitate and supernatant solution and compare them to those of the stock phosphate ester products. The PE_1 precipitate and supernatant solution were obtained after mixing the SI solution with Ca^{2+} brine. The formed PE_1/Ca precipitate was separated from the supernatant solution and re-dissolved in distilled water by adding a few of drops of HCl. These supernatant and re-dissolved precipitate solutions were tested for their inhibition efficiency performance.

Figure 6.17 presents IE test results for precipitated and re-dissolved SI complexes of PE_1_Ca at pH 5.5 and T=95^{o}C. These results are compared to the IE data for the corresponding supernatant and PE_1 stock solutions. The precipitate and supernatant solutions were obtained at *pH 5.5* and *T=20^{o}C*. Data shows the precipitate performance is poor at these test conditions, whereas the supernatant performance is close to/slightly lower than that of the stock solution.

Probably, the supernatant solution is mostly saturated by more active components, whereas the precipitate is formed from the less active components of the PE_1 stock product. According to the information obtained from the supplier, the stock PE_1 is actually a mixture of di- and tri-phosphate esters and also contains some residual orthophosphate. At a pH value close to neutral, di-esters are the least, whereas tri-esters are the most reactive phosphate esters towards hydrolysis (Kirby and Varvoglis 1967). The hydrolysis products are less efficient towards barium scale inhibition. Based on this information and the IE data shown in Figure 6.17, it may be assumed that the precipitate is probably rich in tri-ester species which are more reactive towards hydrolysis (i.e. have higher thermal degradation rates) and hence shows lower IE in the 95^{o}C test. Therefore, the supernatant

solution mainly contains phosphate di-ester species, which are less sensitive to hydrolysis reaction at current test conditions and show a higher performance more similar to the stock.

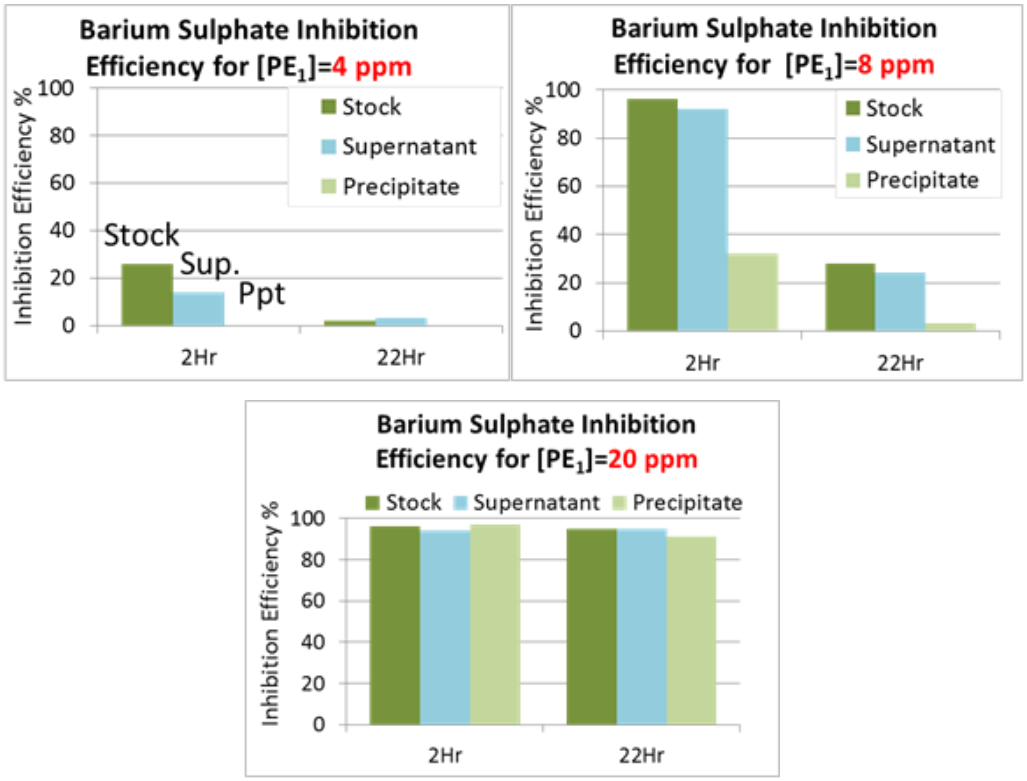

Figure 6.17 Barite inhibition efficiencies of PE_1_Ca precipitate, supernatant and stock at pH5.5, 95°C

We particularly focus on the inhibition efficiency of precipitated SI products, since the current thesis is in a context of precipitation squeeze treatments. Therefore, the performance of two PE_1 precipitates obtained at two pH values, viz. pH 5.5 and 9.5, were compared at the IE test conducted at pH 5.5 and 95°C. The data obtained from this experiment is shown in Figure 6.18. The stock shows the highest IE, followed by the precipitate generated at pH 9.5, then by the precipitate from pH 5.5. The pH 9.5 precipitate performance is very close to that of the stock solution. Under the higher pH 9.5 conditions, it is thought that the greatest precipitation of the active SI components occurs, which stabilizes the complexes and slows down the hydrolysis reaction. Hence, by controlling the precipitation pH we can 'design' the performance of the precipitated phosphate esters to be used in further processes, such as a precipitation squeeze applications.

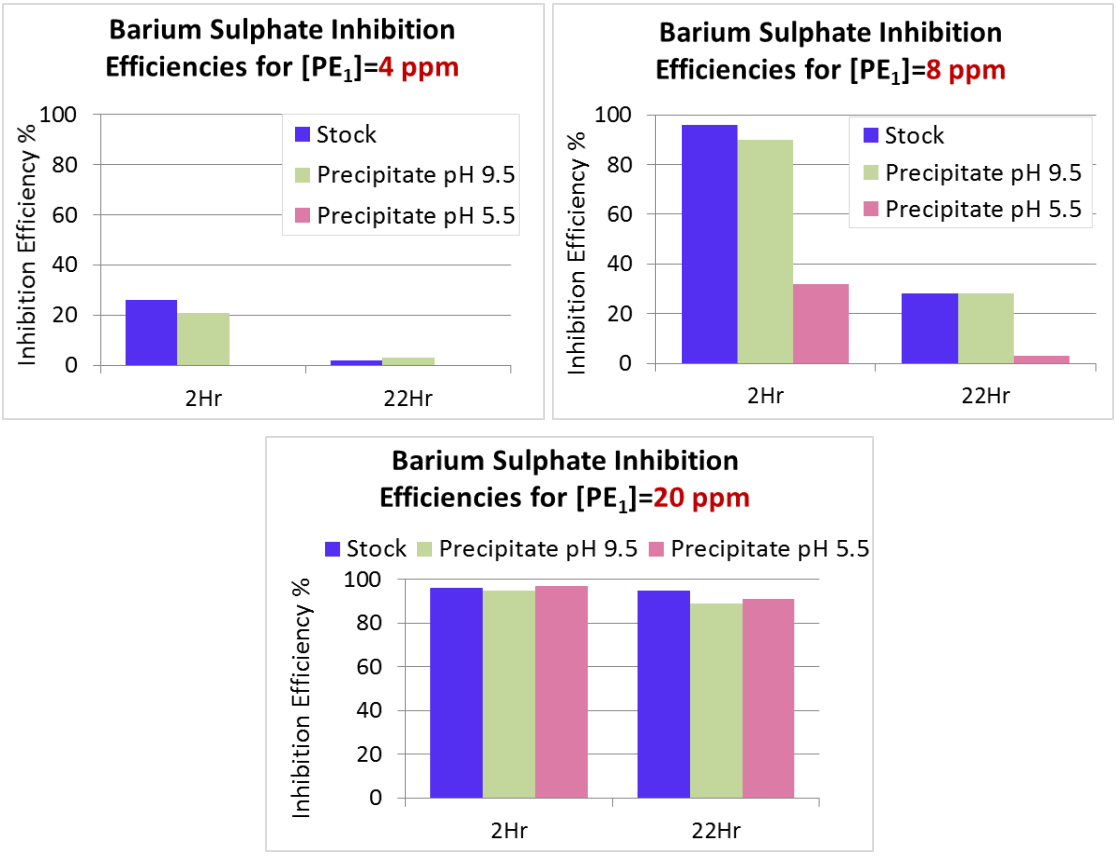

Figure 6.18 Barium sulphate inhibition efficiencies of PE_1_Ca precipitates obtained at pH9.5 and 5.5 and stock solution at pH5.5, 95ºC

PAPE_Ca Complexes

It has been found, that the PAPE_Ca complex has lower solubility across the entire range of test temperatures, i.e. 20 - 95ºC. Therefore, the PAPE precipitates and supernatant solutions were obtained after mixing the SI solution with the Ca^{2+} brines at pH 5.5 and pH 9.5 followed by hot filtration at 95ºC.

Figure 6.19 presents IE data for the PAPE_Ca re-dissolved precipitate and its supernatant solution obtained at pH5.5 and 95ºC and is compared to the PAPE stock product efficiency at the same conditions as the precipitation test, i.e. T = 95ºC and pH 5.5. Very poor performances for the PAPE_Ca complexes are observed under the current pH and T conditions. The precipitate and supernatant show up to 5% efficiency over the entire concentration range up to 30ppm, which is quite low for this class of SI. This "lost" efficiency is in question, as both components of the stock solution, precipitate and supernatant, show very low efficiency, whereas the stock solution presents quite high IE. There may be some material degradation occurring in these solutions due to the high rate

of the hydrolysis reaction at the higher temperatures. This assumption was further investigated, and the results proved that the PAPE stock product suffers severe thermal degradation due to hydrolysis at temperatures above ~80°C (section 7.3.2).

Precipitation conditions: pH5.5, 95°C

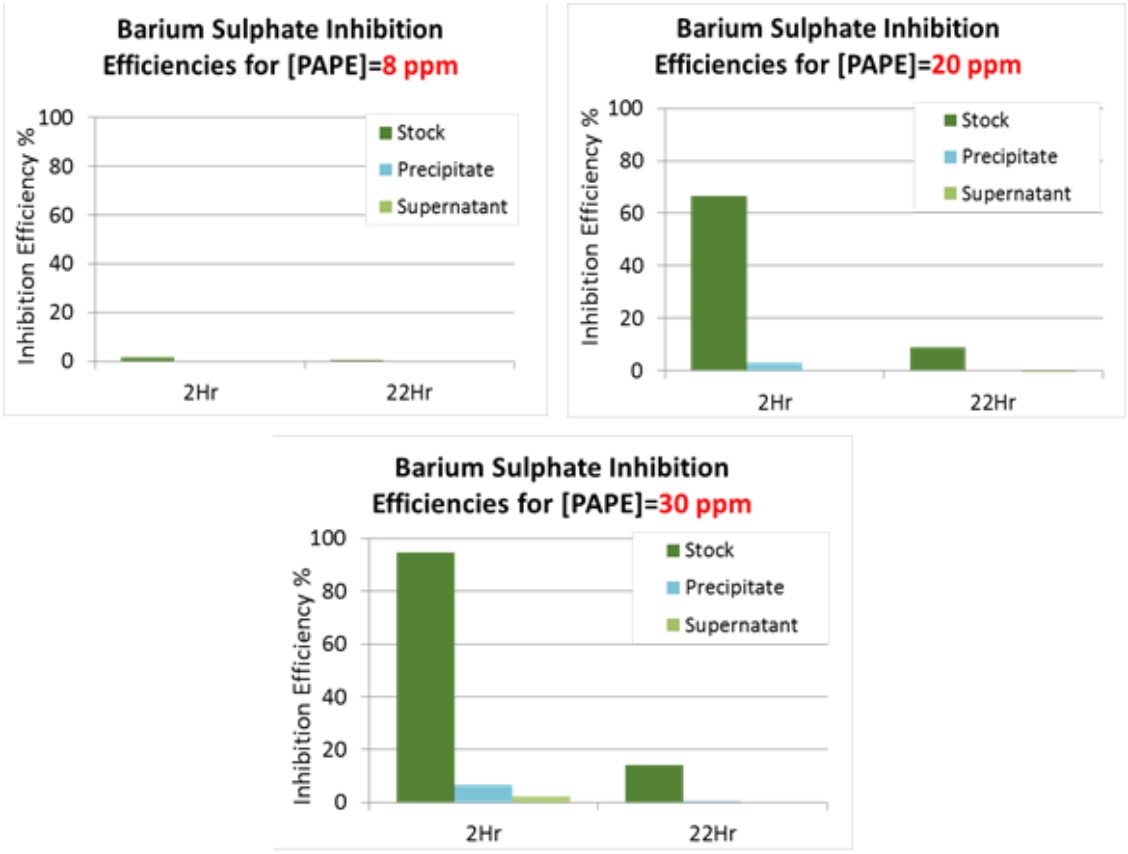

Figure 6.19 Barium sulphate inhibition efficiencies at pH5.5, 95°C of PAPE stock, PAPE_Ca precipitate and supernatant obtained at pH 5.5, 95°C

The IE data for the PAPE_Ca precipitate and supernatant solutions generated at the higher pH 9.5 and T = 95°C but tested for their IE at 95°C and pH 5.5 (closer to the field conditions), are presented in Figure 6.20. The precipitate obtained under these conditions shows high IE performance which is quite close to that of the stock solution which contradicts the results obtained for the previous tests at the lower pH5.5.

In Figure 6.21, we compare the inhibition performances of the PAPE *precipitates* obtained at different pH values, pH 5.5 and pH 9.5. The PAPE_Ca precipitate generated at pH 9.5 shows a performance significantly higher than that of the corresponding pH 5.5 precipitate. The same trend was observed for the PE_1 product, supporting the conjecture that SI *precipitation at the higher pH* leads to the active SI components precipitating out.

If so, this would leave the less active components of the phosphate ester in the supernatant; e.g. these components could be P-containing impurities.

Precipitation conditions: pH9.5, 95°C

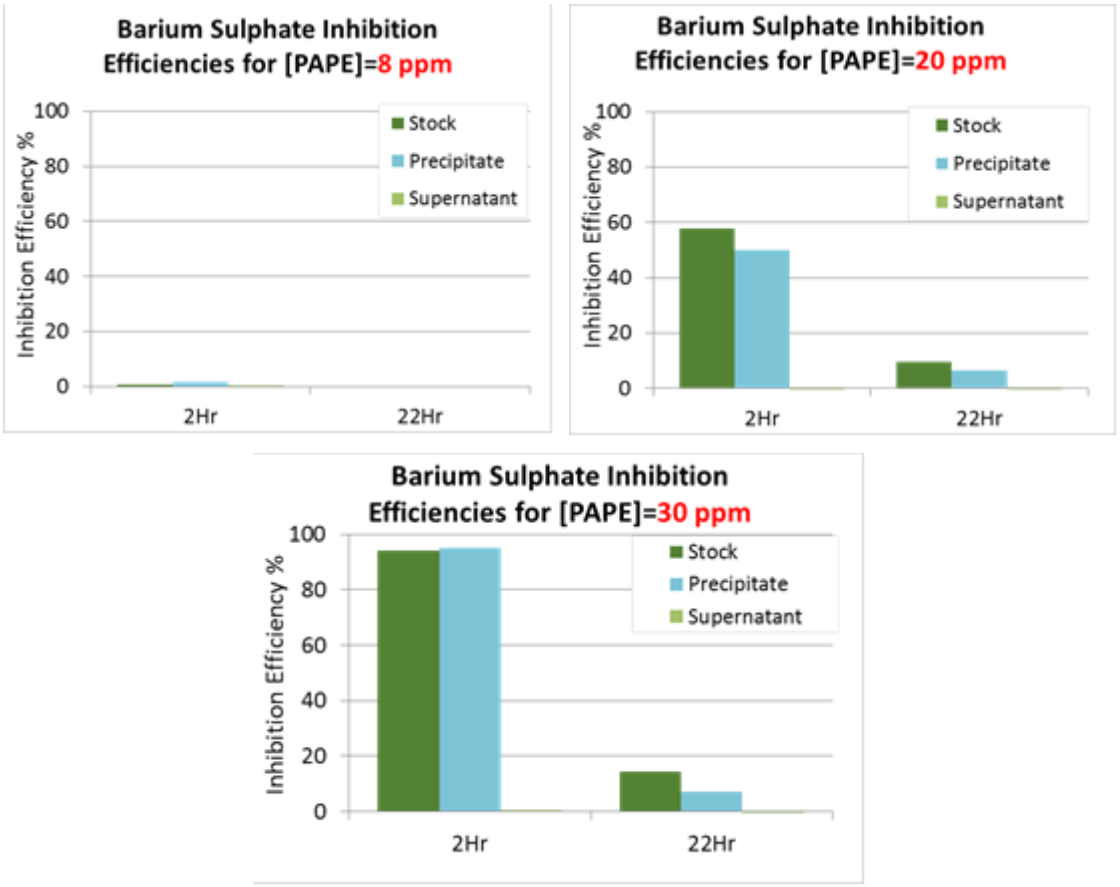

Figure 6.20 Barium sulphate inhibition efficiencies at pH5.5, 95°C of PAPE stock, PAPE_Ca precipitate and supernatant obtained at pH 9.5, 95°C

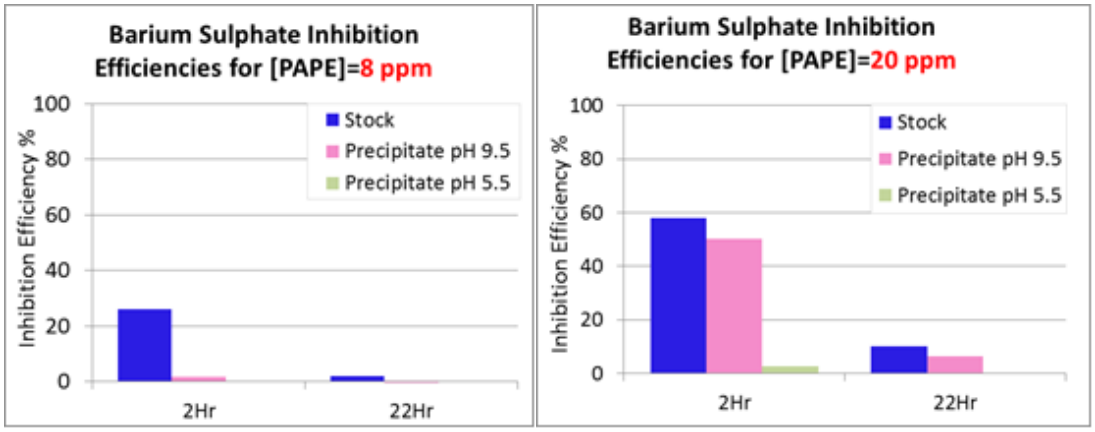

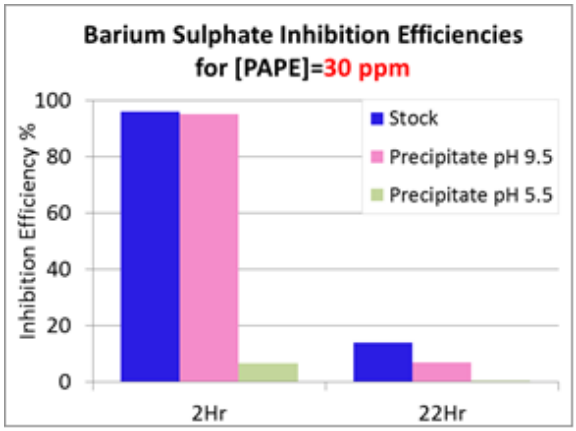

Figure 6.21 Barium sulphate inhibition efficiencies of different PAPE_Ca precipitates, pH5.5, 95°C

6.3.4. *Temperature Effect on the Inhibition Efficiency of Phosphate Ester_Ca Precipitates*

There are recommendations in the literature to apply phosphate esters to tackle scale problems in lower temperature reservoirs. For instance, in previous work, a phosphate ester SIs showed better performance and some potential for extended squeeze lifetime at temperatures between 40°C and 70°C (Jordan, Johnston et al. 2016).

By comparing the IE test results for different precipitates in the previous sub-section, we have shown that at the higher temperature of 95°C the phosphate ester products (particularly re-dissolved precipitate and supernatant) show poorer performance, especially in the long-term tests (22 hour). To understand the relationship between the temperature and the performance of the phosphate ester SIs, IE tests were conducted for PE_1_Ca and PAPE_Ca precipitates, supernatant solutions and SIs stock product at different temperatures from 20°C to 95°C. Both precipitation and IE test temperatures were varied-in order to determine the impact of the conditions of each process on the IE data obtained. Overall, there were 5 series of precipitation/inhibition efficiency tests performed. This was to establish if there were any temperature effects, originating during the precipitation and precipitate's dissolution stages, that affected the inhibition efficiency performance of the phosphate ester SI species:

1. Precipitate/supernatant obtained at 20°C and tested for their IE at 95°C
2. Precipitate/supernatant obtained at 20°C and tested for their IE at 60°C
3. Precipitate/supernatant obtained at 60°C and tested for their IE at 60°C

4. Precipitate/supernatant obtained at 40°C and tested for their IE at 40°C
5. Precipitate/supernatant obtained at 20°C and tested for their IE at 20°C

When temperature is varied in the system, the saturation ratio (SR) - a thermodynamic factor determining scaling tendency in the current brine, is going to vary accordingly. For barium sulphate, a decrease in temperature increases the scaling tendency, i.e. the SR. Therefore, to be able to compare the inhibition efficiency performance of the phosphate ester species at different temperatures, the SR must be kept constant. To keep it at a value of SR ~ 322 for all the IE tests, which was the SR of the system tested earlier, NSSW/NFFW mixing ratio=60:40, T = 95°C, pH5.5, NSSW compositions were adjusted by reducing the concentration of sulphate anions (see Table 6.2) for the lower temperature IE experiments. These scaling calculations were run on the MultiScale software.

Figure 6.22 and Figure 6.23 present the performance data for *PE_1_Ca precipitates and supernatants* which were obtained at the same temperature of *20°C* but were tested for their IE at *95°C and 60°C*, respectively. It can be seen, the supernatant, precipitate and stock performances are much higher in the lower temperature IE tests. The precipitate performance dropped significantly from ~100% to ~0 in the 4ppm test when temperature was increased from 60°C to 95°C. The stock and supernatant show much poorer IE at the higher temperature, however, the drop is not as significant, compared to the precipitate case.

Precipitation at 20°C, IE test at 95°C

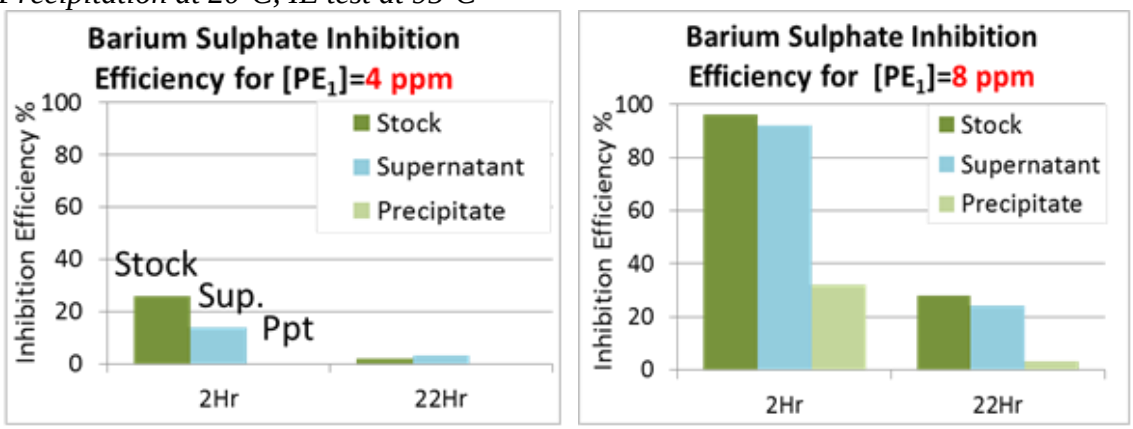

Figure 6.22 Barite inhibition efficiencies of PE_1_Ca precipitate/supernatant/ obtained at pH5.5, 20°C and stock PE_1 at pH5.5, 95°C

Precipitation at 20°C, IE test at 60°C

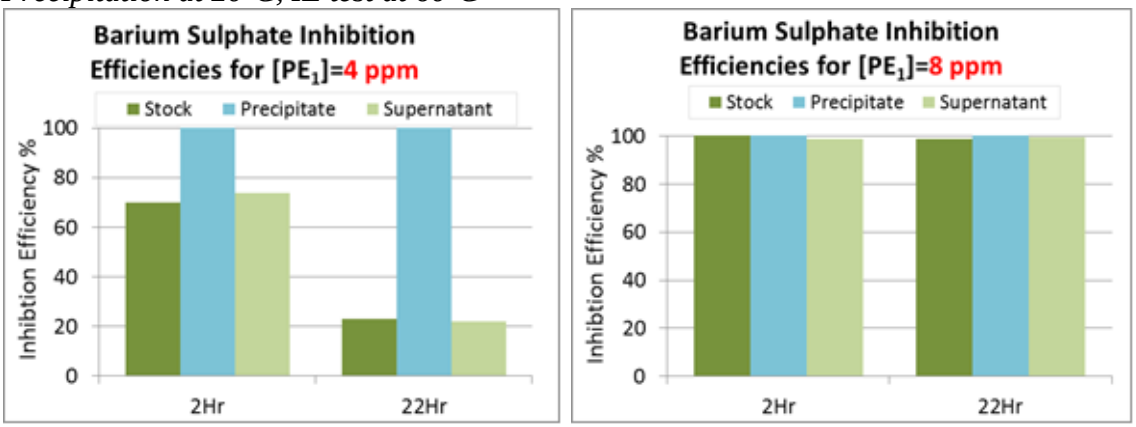

Figure 6.23 Barite inhibition efficiencies of PE_1_Ca precipitate/supernatant/ obtained at pH5.5, 20°C and stock PE_1 at pH5.5, 60°C

Both precipitation and IE tests at 60°C

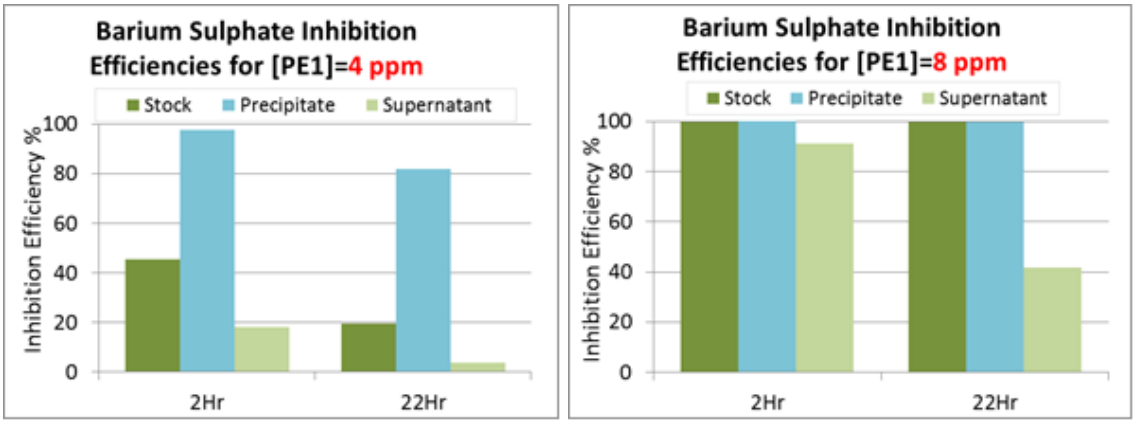

Figure 6.24 Barite inhibition efficiencies of PE_1_Ca precipitate/supernatant/ obtained at pH5.5, 60°C and stock PE_1; at pH5.5, 60°C

Figure 6.24 presents the performance data for the PE_1_Ca precipitate and supernatant generated *at T = 60°C* and tested for IE at the *same* temperature. Compared to the precipitate/supernatant solutions used for the previous test (Figure 6.23), the current test solutions were exposed to two 60°C heatings, where the overall exposure period was 24 hours (precipitation test) and 22 hours (IE test), which is 24 hours at 60°C longer than in the previous test. The data shows the supernatant and precipitate performances at pH 5.5 are much higher in the case where the precipitates were generated at 20°C not 60°C (Figure 6.23). Hence, exposure to the initial higher temperature of the precipitation process negatively affects the following inhibition performance of the PE_1. However, the decrease in inhibition efficiency performance at 60°C is less significant than for the 95°C IE test (Figure 6.22), when both have had the initial precipitate generated at 20°C.

Figure 6.26 and Figure 6.25 present the performance data for PE_1_Ca precipitates and supernatants which were obtained and tested for their IE at the same temperatures, i.e. at 20°C and 40°C, respectively. It can be seen, that precipitated and re-dissolved SI shows a significantly higher inhibition efficiency than the stock and supernatant at either temperature. In addition, the supernatant, precipitate and stock performances are much higher at the lower temperature IE test, i.e. at 20°C over 40°C. At 20°C, 2ppm of the precipitated and then re-dissolved PE_1 already provides the minimum inhibition concentration (MIC) at both 2 and 22-hour tests, whereas for the 40°C and 60°C (Figure 6.24) experiments, the MIC is slightly higher, at 4ppm.

Both precipitation and IE tests at 20°C

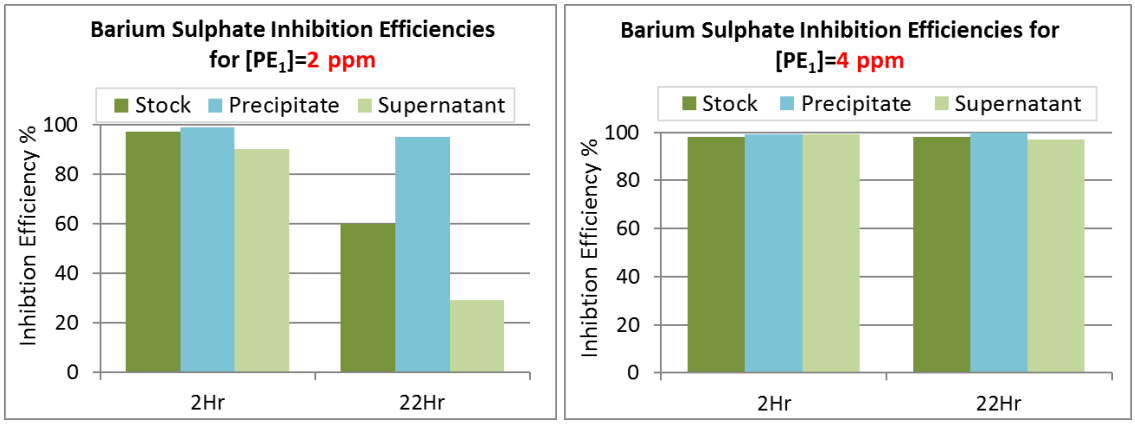

Figure 6.25 Barium sulphate inhibition efficiencies of PE_1_Ca precipitate/supernatant/ obtained and tested at pH5.5, 20°C

Both precipitation and IE tests at 40°C

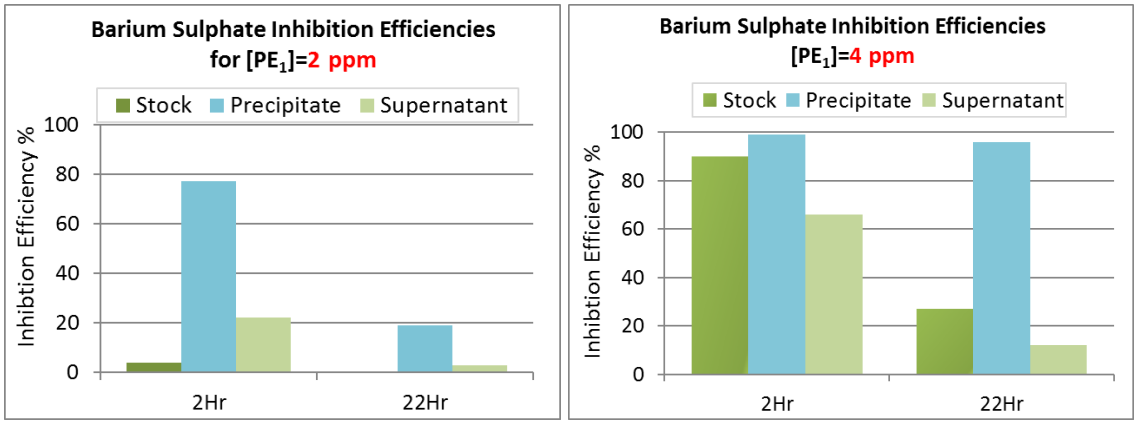

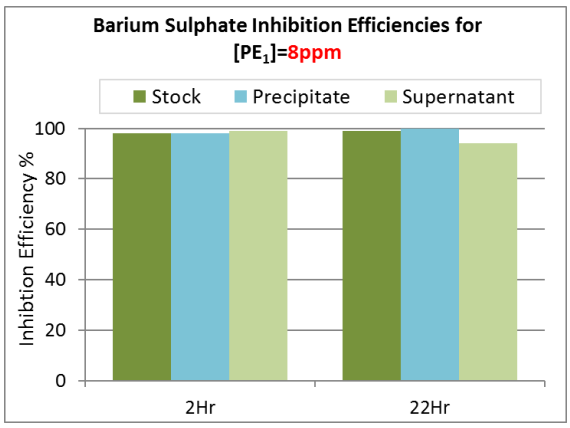

Figure 6.26 Barium sulphate inhibition efficiencies of PE_1_Ca precipitate/supernatant/ obtained and tested at pH5.5, 40°C

PAPE_Ca complexes: Temperature Effect

To obtain the precipitate and supernatant from the PAPE/Ca systems for further testing in IE experiments, precipitation tests were performed at the same conditions, as the IE tests for the listed PAPE/Ca components: at T = 60°C, 80°C, and 95°C, and pH5.5. These conditions represent a field case, where the SI precipitate is formed at the reservoir temperature and has to perform under the same conditions during the squeeze lifetime. The NSSW composition for the lower temperature IE experiments was adjusted by reducing the concentration of sulphate anions, thus the saturation ratio was kept constant at SR~ 322.

Figure 6.27 and Figure 6.28 show the performance data for the PAPE_Ca *precipitate* and *supernatant* tested at T = 60°C, 80°C, 95°C and at pH 5.5. The inhibition efficiency performance of both components was found to *decrease* when test temperature was *increased*. Very poor performance was observed at 95°C, especially in the long-term tests (22 hour). At the lower temperatures, it is the precipitates that show the highest IE, followed by the stock and supernatant solutions.

The inhibition efficiency performance of PAPE *stock* solutions at different temperatures 60°C, 80°C, 95°C and pH 5.5 are presented in Figure 6.29. The data clearly shows the IE performance of PAPE declines with increasing temperature and the most significant drop occurs at 95°C.

PAPE_Ca Precipitate

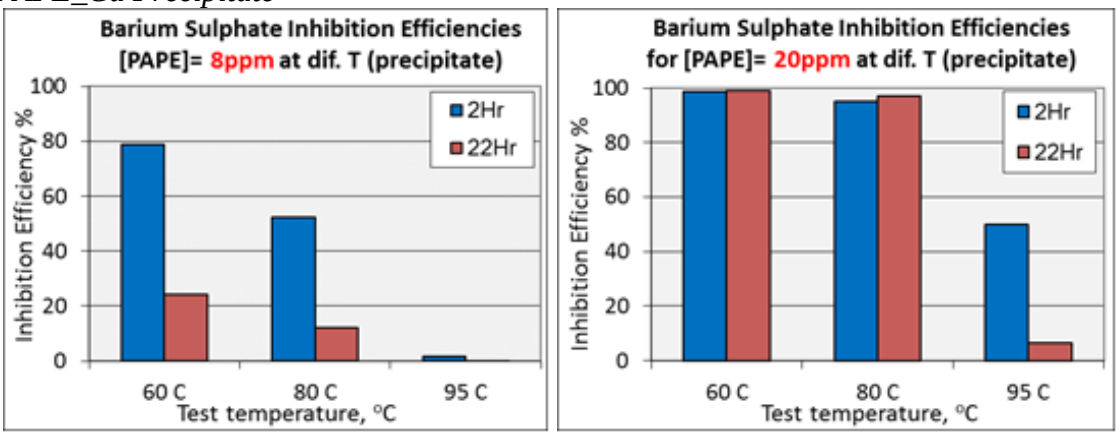

Figure 6.27 Barium sulphate inhibition efficiencies of PAPE_Ca precipitates at pH5.5 and T= 60°C, 80°C, 95°C

PAPE_Ca Supernatant

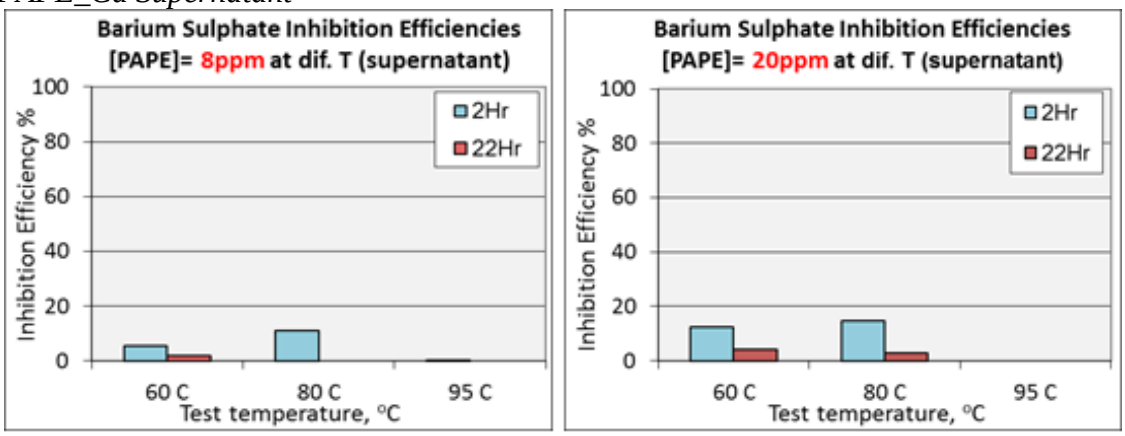

Figure 6.28 Barium sulphate inhibition efficiencies of PAPE_Ca supernatant at T= 60°C, 80°C, 95°C; pH5.5

PAPE Stock

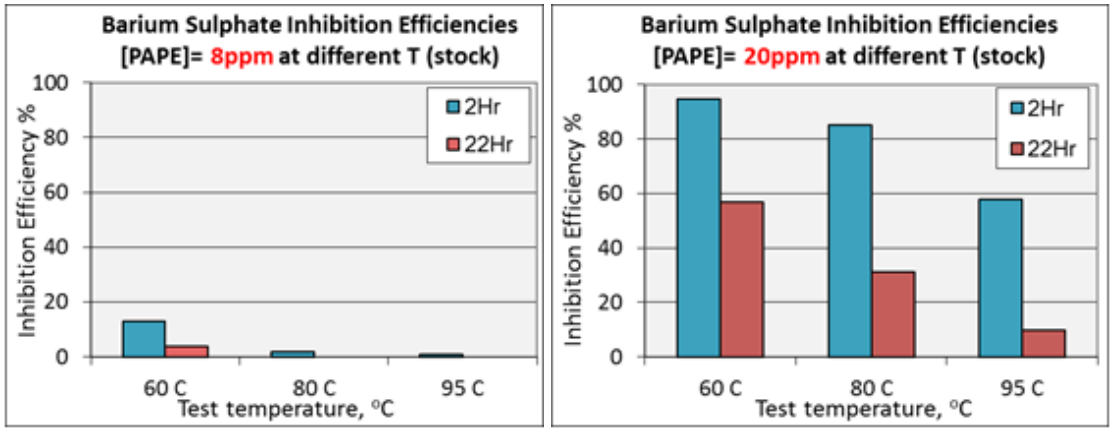

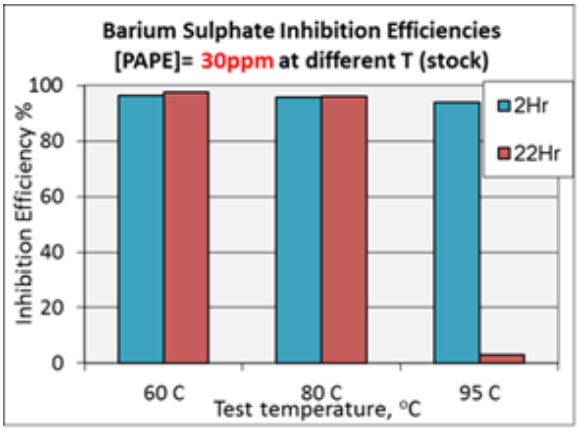

Figure 6.29 Barium sulphate inhibition efficiencies of PAPE_Ca stock at different temperatures: 60°C, 80°C, 95°C and pH5.5

Figure 6.30 and Figure 6.31 present the performance data for the PAPE_Ca precipitates and supernatants which were generated and tested for inhibition efficiency performance at lower temperatures of 40°C and 20°C, respectively. The data shows that the precipitated and re-dissolved SI shows significantly higher efficiency performance than the stock and supernatant at both test temperatures. Thus, it is the precipitates formed at the lower temperatures, that shows the highest IE, followed by the stock and supernatant solutions. In addition, the supernatant, precipitate and stock performances are much higher at the lower temperature IE test, i.e. at 20°C. At this temperature, 4ppm of the precipitated and then re-dissolved PAPE already provides the minimum inhibition concentration (MIC), which is the concentration of the scale inhibitor that can inhibit 85-90% of potentially forming scale, at both 2 and 22-hour tests, whereas for the 40°C experiments, MIC has not been reached even for 8ppm of the precipitated PAPE.

Precipitation and IE test at 40°C

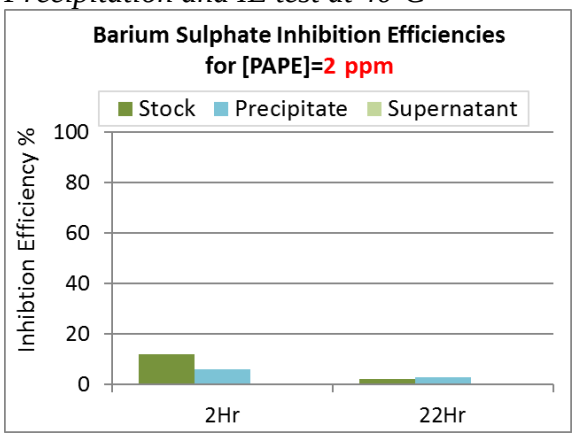

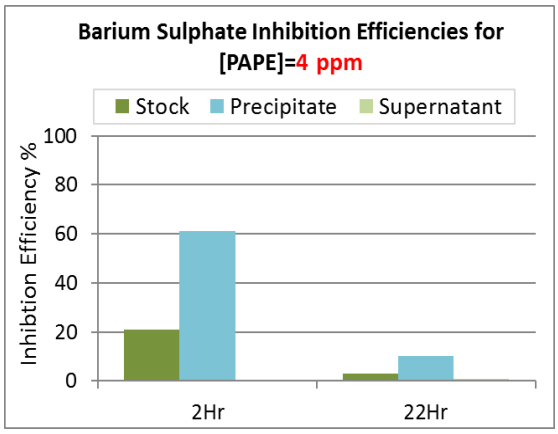

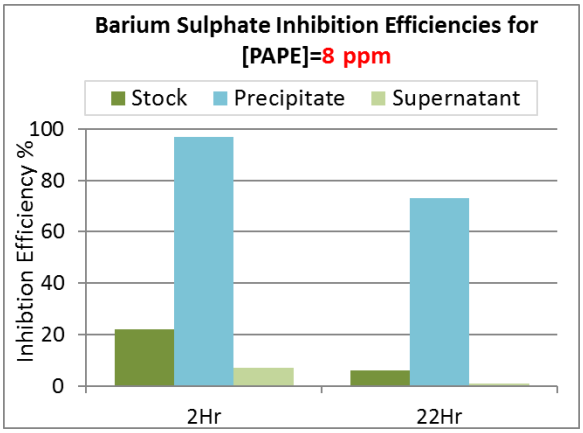

Figure 6.30 Barite inhibition efficiencies of PAPE_Ca precipitate/supernatant/stock obtained and tested at pH5.5, 40ºC

Hence, it is shown that a temperature increase has a negative effect on the inhibition efficiency performance of the PAPE and PE_1 phosphate ester products. However, at temperatures between 20ºC and 80ºC, the inhibition efficiency performance decreases less significantly than that observed for the 95ºC test.

Precipitation and IE test at 20ºC

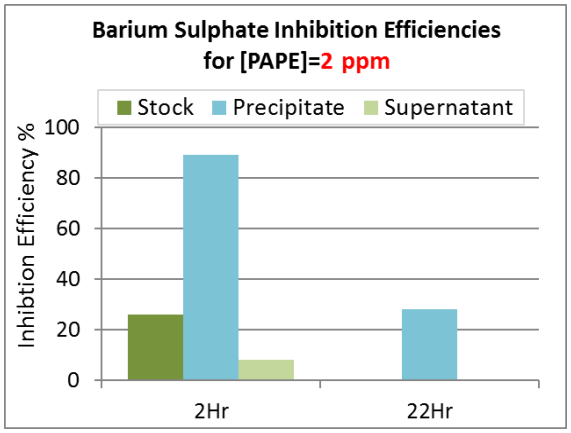

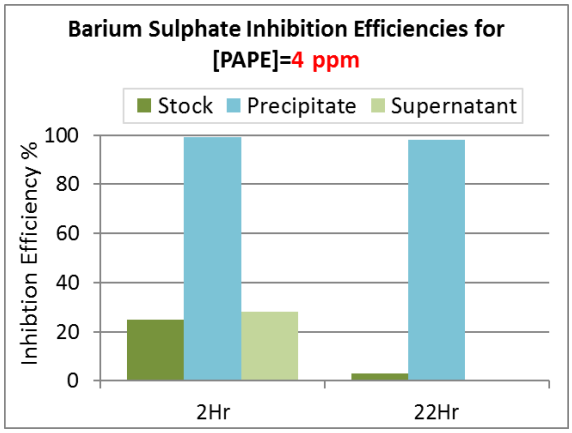

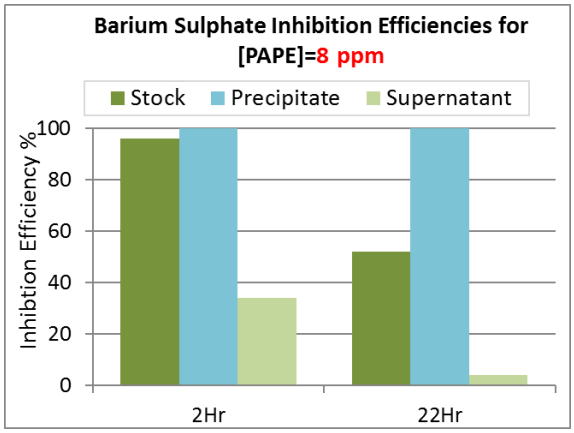

Figure 6.31 Barite inhibition efficiencies of PAPE_Ca precipitate/supernatant/stock obtained and tested at pH5.5, 20ºC

6.4. Summary and Conclusions

The current research was conducted for two phosphate ester scale inhibitor chemicals, PE_1 and PAPE. The study included SI precipitation tests with Ca^{2+} cations, yielding $PE_1\_Ca_n$ and $PAPE\_Ca_n$ complex precipitation, where the stoichiometry *n* was established as a molar ratio of calcium to phosphorus under various pH and temperature conditions. Subsequently, the inhibition efficiency performance of the precipitated phosphate ester complexes was measured and compared to those of the stock product and supernatant solution. The effect of the precipitation reaction conditions, such as pH and temperature, on the inhibition efficiency performance of the precipitated and re-dissolved phosphate ester species was also investigated. The main conclusions derived from the study are listed below.

The precipitation behaviour of the phosphate esters is shown to be quite *different* to that of the phosphonate and polymeric scale inhibitors*:*

- Generally, all the stoichiometry values are within the range of *2.7-3.6* for PE_1_Ca, and *2.8-4.1* for PAPE_Ca phosphate ester complexes. This is a high chelating capacity being shown for the phosphate ester inhibitors, particularly when compared to the stoichiometry's of the phosphonate/Ca complexes, where the maximum theoretically possible Ca/P ratio is equal to 1, and this only occurs at higher pH values (pH>10) when all the phosphonate groups are fully dissociated (Shaw and Sorbie 2015).

- The molar ratio of Ca/P in the phosphate ester complexes does not significantly depend on solution pH and precipitation temperature, this behaviour again is in contrast to that of the phosphonate and polymer SIs.

Precipitation pH Effect on Inhibition Efficiency Performance: Precipitation pH is shown to be a key factor defining inhibition efficiency of the PE_1_Ca and PAPE_Ca precipitates. The inhibition efficiency performance of the precipitated and then re-dissolved phosphate ester complexes is highest, when the precipitation occurs at higher pH. This is due to a high proportion of the active SI components precipitating at higher pH, which leaves the supernatant product without any active SI components. Taking this into an account, it can be concluded that by controlling the precipitation pH, there is the potential to 'design' the inhibition efficiency performance of the precipitated scale inhibitor.

Temperature Effect on Inhibition Efficiency Performance*:* The inhibition efficiency performance of the precipitated and then re-dissolved phosphate esters, supernatant solutions and stock products generally decreases with increasing temperature in the range of 20-95^{o}C. This probably occurs due to the increasing rate of the hydrolysis reaction at temperatures above 80^{o}C, which leads to the thermal degradation of the active SI components. At lower temperatures, up to 80^{o}C, it is the precipitates that show the highest IE, followed by the stock and then the supernatant solutions.

Field Significance: From the application point of view, phosphate esters require a greater concentration of calcium ions to be available in the brine to (i) enhance SI retention via the precipitation mechanism and (ii) provide adequate inhibition efficiency, as it is the Ca and SI complexes, rather than "free" SI ions, that are believed to be involved in the scale inhibition mechanisms (Boak, Graham et al. 1999).

In coupled adsorption/precipitation treatments, it is the precipitated SI that is expected to stay longer within the formation, thus its performance will potentially determine the minimum inhibition concentration (MIC), i.e. the time when the next treatment must be repeated. Since the precipitated phosphate ester product has a higher performance than the stock product, then the MIC must be determined for the precipitated species rather than for the stock product. On the other hand, this means that the higher performance of the precipitated species potentially leads to extended squeeze lifetimes, when phosphate esters are allowed to be retained within the formation through precipitation.

CHAPTER 7. INHIBITION EFFICIENCY OF PHOSPHATE ESTER SCALE INHIBITORS

7.1. Introduction

This work is a continuation of the study started in CHAPTER 6 on the phosphate ester fundamentals, with a focus on their application for scale inhibition. Chapter 6 defined the precipitation behaviour and stoichiometry of the precipitated phosphate ester/calcium complexes, as well as indicating how the precipitation reaction conditions affect the final inhibition efficiency of the precipitated phosphate ester products, under various pH and temperature conditions.

In this Chapter, the focus is not on the precipitation process, but on the general performance of the *stock* phosphate ester solutions at different temperatures. Phosphate ester inhibition efficiency profiles are compared to those obtained for the "classic standard" SIs used by the industry: poly-vinyl sulphonated co-polymer, VS-Co and penta-phosphonate DETPMP products, at different temperatures.

The motivation to obtain these "performance versus temperature" profiles for the different SI classes is to define a temperature range where phosphate esters perform better than the classic chemistries. This is also supported by the confirmation from the literature, that states phosphate ester SIs can potentially be applied for barium sulphate inhibition at lower temperatures, up to 70^{o}C (Jordan, Johnston et al. 2016).

Indeed, there are a number of onshore and offshore reservoirs of lower temperature, where sulphate scale inhibition is a great challenge, since the performance of commonly used phosphonate SIs is limited. Phosphonate SIs do not usually perform well at lower temperatures, therefore polymeric SIs are often applied in these circumstances. However, to detect polymers within the produced brines, more complicated and time consuming wet chemical analytical techniques are required. In addition, some polymeric species fail to meet the environmental requirements particularly in term of their biodegradation behaviour. Thus, scale inhibitors which would (i) provide effective scale protection at the lower temperatures, (ii) meet all the specified environmental standards for use in the offshore environment and (iii) require convenient and low-cost (ICP) analysis are of great interest.

Phosphate esters meet all the specified standards for use in the offshore environment and can be detected by the routine and low-cost ICP analytical method. Therefore, this class of SI *may* be a good alternative to the polymers for these specific conditions, if they perform either as good as, or even better than the polymeric SIs at lower temperatures. This will be explored in more detail in this chapter.

The aims of the study is to:

I. Establish the temperature range and conditions at which phosphate ester inhibitors perform best and when it may outperform the classical chemistries currently used in the industry. This includes inhibition efficiency performance studies over a wide temperature range between 20^{o}C and 80^{o}C:
    a. at a lower saturation ratio, to observe the effect of temperature variation on inhibition efficiency performance;
    b. at "natural" saturation ratios by letting it vary with temperature without any adjustment, in order to represent real field conditions.
II. Define the inhibition *mechanism* of the phosphate esters, based on the "temperature versus performance" profiles, when compared with those of the conventional SIs.
III. Explain the inhibition efficiency performance data trends using both Nuclear Magnetic Resonance (NMR) and Fourier Transform Infrared Spectroscopy (FTIR) analysis, to show the structural changes in the phosphate ester species over the temperature range 20-95^{o}C.

Thus, in this study we will be able to (i) define the scale inhibition mechanism that the phosphate ester predominantly works through, and (ii) determine the temperature ranges most optimal for phosphate ester application. Should the phosphate ester show optimal performance at test conditions, recommendations on its application in oilfields will be proposed.

7.2. Experimental Details

7.2.1. *Materials*

The exact compositions of the phosphate ester products used in the study are not available, however the structures of the active compounds obtained from the suppliers are shown in

Table 6.1. These two commercially available phosphate ester scale inhibitors supplied by Nalco Champion (PE_1) and Shandong Taihe (PAPE) were used to conduct the inhibition efficiency performance tests in synthetic North Sea Sea Water (NSSW) and Nelson Forties Formation Water (NFFW) made up by NaCl, $CaCl_2{\cdot}6H_2O$, $MgCl_2{\cdot}6H_2O$, KCl, $BaCl_2{\cdot}2H_2O$, $SrCl_2{\cdot}6H_2O$ and Na_2SO_4 from Sigma Aldrich - all were used as received. The phosphonate SI DETPMP (structure shown in Table 3.1) supplied by Italmatch and polymeric SI VS-Co (structure shown in Figure 2.3) from Nalco Champion were used for these comparison studies. All concentrations quoted in this section are *active* concentrations.

7.2.2. *Static Barium Sulphate Inhibition Efficiency Test*

Static barium sulphate inhibition efficiency (IE) tests of the phosphate esters products were carried out over a wide range of temperatures from 20°C to 80°C at 2 hours (short-term) and 22 hours (longer-term) tests. There were 2 cases of IE tests examined in this study:

- *Case 1:* tests conducted at "natural" saturation ratios letting its vary with temperature without any adjustment, to represent real field conditions;
- *Case 2:* tests conducted at constant saturation ratio, ~322 (saturation ratio at 95°C system), to observe the effect of temperature variation on inhibition efficiency performance

Sampling was performed after mixing North Sea Sea Water (NSSW) with Nelson Forties Formation Water (NFFW) at ratio 60:40, respectively. This mixing ratio of NSSW and NFFW represents the most severe saturation ratio (SR) conditions for scale inhibition, refer to the maximum on the profile in Figure 6.3. Prior to mixing the brines, SI was dissolved in the NSSW to give appropriate concentrations so that when mixed with the NFFW, they gave the intended final SI concentrations. Subsequently, samples of NSSW containing SI and NFFW were placed in an oven and water bath at test temperature for an hour. Sodium acetate/acetic acid buffer was used to buffer all samples at pH 5.5. All the details for the IE performance tests and associated analysis are described in section 3.2.4.

The NFFW and NSSW compositions used for *Case 1* are shown in Table 7.1, whereas the adjusted NSSW compositions for the *Case 2* tests were given earlier in Table 6.2.

These NSSW compositions were calculated using MultiScale software. The saturation ratio of each was adjusted to a value of ~322, which is the normal saturation ratio at 95°C, for a NSSW/NFFW = 60:40 mixing system. When the SR was kept constant, the potential barium sulphate scale mass also stayed constant, at 0.798 mmol/kg solvent, over the entire temperature range 20-80°C (calculated using Multiscale software).

Table 7.1 NSSW and NFFW compositions

North Sea Sea Water (NSSW)			Nelson Forties Formation Water (NFFW)		
Ion	C, ppm	Composition	Ion	C, ppm	Composition
Na^+	10890	NaCl	Na^+	31275	NaCl
Ca^{2+}	428	$CaCl_2.6H_2O$	Ca^{2+}	2000	$CaCl_2.6H_2O$
Mg^{2+}	1368	$MgCl_2.6H_2O$	Mg^{2+}	739	$MgCl_2.6H_2O$
K^+	460	KCl	K^+	654	KCl
Ba^{2+}	0	$BaCl_2.2H_2O$	Ba^{2+}	269	$BaCl_2.2H_2O$
Sr^{2+}	0	$SrCl_2.6H_2O$	Sr^{2+}	771	$SrCl_2.6H_2O$
SO_4^{2-}	2960	Na_2SO_4	SO_4^{2-}	0	Na_2SO_4
Cl^-	19773	-	Cl^-	55279	-

7.2.3. *FTIR Spectroscopy*

Fourier Transform Infrared (FTIR) Spectroscopy was run on a Thermo Scientific Nicolet iS5 instrument for only the PAPE_Ca precipitates, obtained at the different temperatures. Since the method requires powder samples, the PE_1_Ca gel-like precipitates could not be characterised by this particular instrument. In order to obtain the precipitates, SI at a concentration of 2000ppm was added to brine containing 2000ppm Ca^{2+}. The solutions were then pH adjusted to pH 5.5 which had to be re-checked continually until a stable pH of 5.5 was achieved. Subsequently, one of the solutions was left at room temperature (T= 20°C), whilst another two were placed into a waterbath and oven at their required test temperatures of 60°C and 95°C and were left there for 24 hours. Subsequently, the precipitates were collected using vacuum filtration with 0.45µm filter papers, then they were left to dry in the open air for 48 hours before running them on the FTIR spectrometer.

7.2.4. *NMR Spectroscopy*

To study the structure of the molecules that the PAPE and PE_1 stock solutions contain, as well as to identify if there was any thermal degradation occurring in the solutions, the nuclear magnetic resonance (NMR) analytical technique was applied. Initially, ^{31}P and ^{13}C chemical shifts were recorded on a Bruker AVIII-300 instrument at 121.5MHz and 75.5MHz, respectively. ^{13}C spectra were supplemented by the 1H Distortion-less

Enhancement by Polarisation Transfer (DEPT) method – this allows the primary -CH_3, secondary -CH_2-, tertiary CH and quaternary C atoms to be distinguished. The top DEPT spectrum shows CH and CH_3 signals, whereas CH_2 signals face down, quaternary C are not shown on the 1H DEPT, and thus the structure was easily recognisable (Figure 7.1).

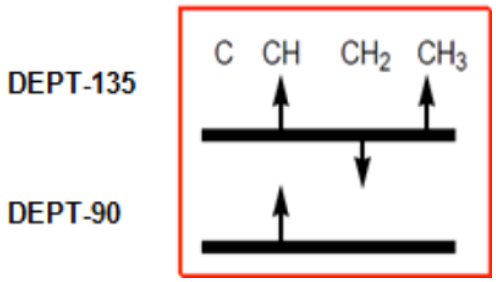

Figure 7.1 NMR 1H DEPT: detection of different C atoms

However, those initially recorded NMR profiles were qualitative and could not prove quantitatively the structural changes in the molecules of the phosphate esters. Subsequently, quantitative ^{13}C NMR profiles were obtained from a Bruker AVI-400MHz spectrometer, operating at 100.6MHz for ^{13}C.

The samples were 0.3-0.4M solutions of each SI prepared in 15 ml of DW. The solutions were divided into 3 test bottles, each was placed in an oven set at a different test temperature: 20, 80 and 95^{o}C. After 48 hours, the solutions were removed and cooled to the room temperature. Subsequently, 0.63 ml of each SI sample was added to 0.07 ml of deuterium oxide D_2O, directly into a glass NMR tube. To ensure the samples are homogeneous, the tubes were placed for 10 min in the ultrasonic bath prior to running the NMR.

7.3. Results and Discussion

7.3.1. *Phosphate Ester Inhibition Efficiency versus Temperature: Comparison with Phosphonate and Polymer*

Case 1: Inhibition Efficiency at "Natural" Saturation Ratio

For a barium sulphate scaling system, the saturation ratio which determines the severity of scaling in the system, is related to temperature. The saturation ratio of all the sulphate scales increases with decreasing temperature, making the lower temperature conditions

more challenging for scale inhibition. In the Case 1 tests, the saturation ratio was not fixed, therefore it was varying "naturally", i.e. increasing with decreasing temperature (see Figure 7.2). Inhibition efficiency performance tests against barium sulphate were run for phosphate ester SIs PE_1 and PAPE alongside the conventional chemistries – penta-phosphonate DETPMP and co-polymer VS-Co. These chemistries represent the "classic" SIs currently used in the industry for barium sulphate scale inhibition. The experiments were conducted over a wide temperature range, from 20 to 80^{o}C and at pH5.5.

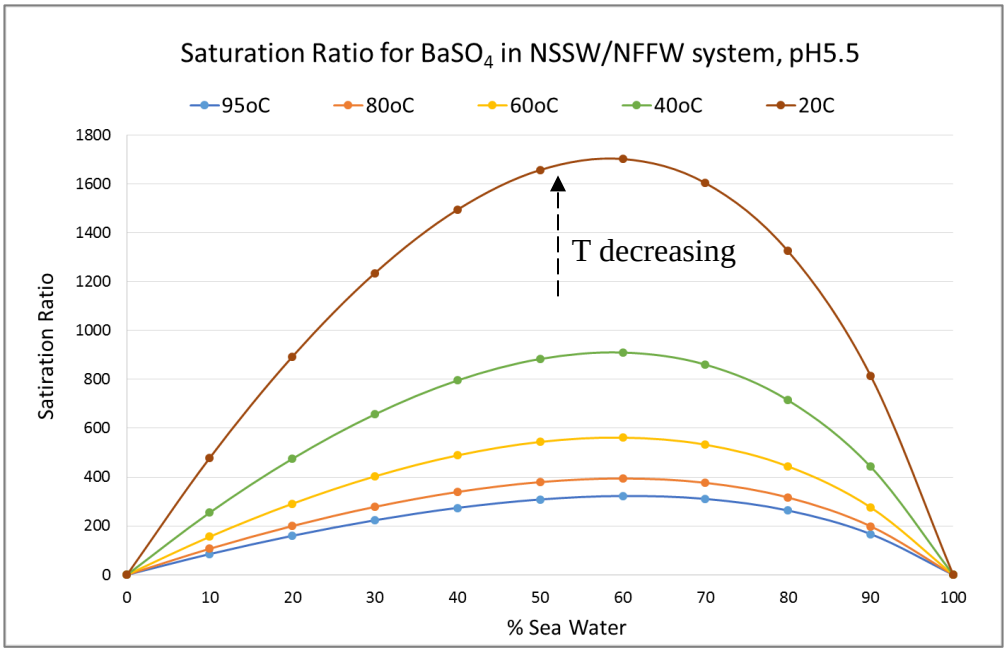

Figure 7.2 Barium sulphate saturation ratio at different temperatures, pH5.5

The performance profiles of all those SIs (PE_1, PAPE, DETPMP and VS-Co) were compared in order to:

1) Check, if the performance of the phosphate ester chemistry could compete with the "classic" SIs used in the oilfield, i.e. phosphonates and polymers;
2) Determine the temperature range at which the phosphate ester performs at its best in terms of scale inhibition against barium sulphate;
3) Propose the inhibition mechanism that phosphate ester chemistry predominantly performs through.

The inhibition efficiency performance data for the stock products of penta-phosphonate DETPMP, co-polymer VS-Co, and phosphate esters SIs PE_1 and PAPE tested at the lowest investigated temperature of *20^{o}C* and pH 5.5 are shown in Figure 7.3. The

saturation ratio for $BaSO_4$ is extremely high at this temperature condition, SR~1700, hence the performance of most of the SI chemistries (DETPMP, PAPE, PE_1) is poor, except co-polymer VS-Co, which shows quite high inhibition efficiency at 20^oC and such a high SR, even at very low concentrations. This trend has already been established in other work on polymeric SIs (Sorbie and Laing 2004), where the performance was shown to increase with decreasing temperatures due to the kinetics of the barium sulphate scaling regime dominating over the thermodynamics.

By examining the inhibition efficiency profile, the inhibition mechanism that predominantly occurs in the system may also be defined. As described in the literature review, in supersaturated solutions, scale generally forms through the following steps until equilibrium is achieved:

- Nucleation
- Crystal growth around the nucleus
- Growth of small crystals into larger ones, i.e. agglomeration.

Therefore, SIs work by means of nucleation inhibition and crystal growth retardation, but to different degrees (Boak, Graham et al. 1999, Sorbie and Laing 2004). For example, it has been found, that phosphonates predominantly operate through the crystal growth mechanism, whereas polymers tend to inhibit scale in the earlier stages, working through nucleation inhibition.

Temperature proves to have important effects on both scale formation and kinetics. At the lower temperatures, the crystal growth is limited, thus at these conditions the nucleation stage is predominant and scale inhibitors operating through nucleation inhibition as they are expected to have greater performance than those mainly working at the crystal growth stage. With increasing temperature, crystal growth rates increase, thus SIs working through crystal growth retardation are going to outperform. SIs that predominantly work through crystal growth retardation have to show greater efficiency at higher temperatures, whereas nucleation inhibitors – at cooler conditions. Hence, analysing the SI performance versus temperature profiles should allow insight into the predominant mechanism that the particular SI operates through.

It can be seen in Figure 7.3, that at 20^oC all the SIs perform better in the short-term test, which means at this temperature, all of them should work predominantly as crystal growth

inhibitors. Poorer long-term efficiency is normally due to irreversible consumption of the SI within the first 2 hours of the test. Once the SI species are adsorbed on the surface of the forming nuclei, this leaves considerably lower concentrations of the chemical left in the bulk to inhibit further growing crystals.

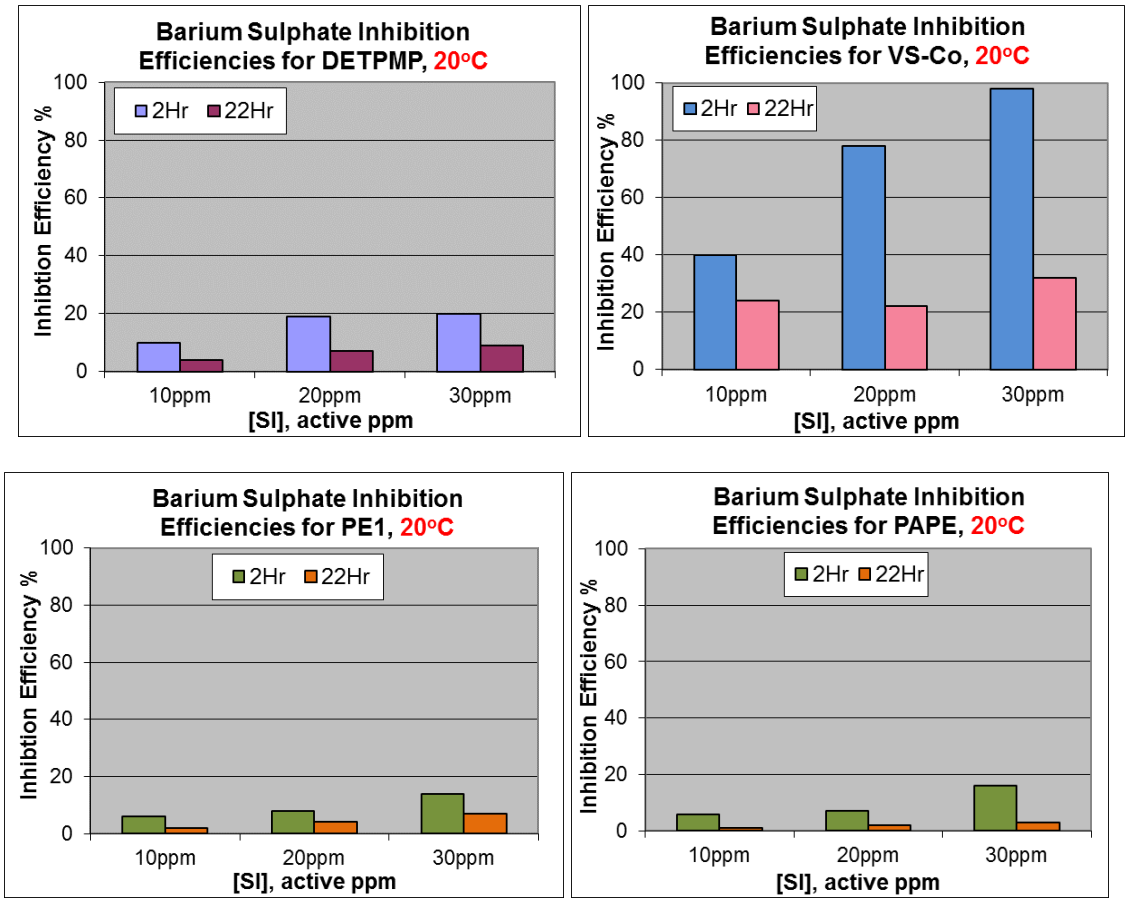

Figure 7.3 Barium sulphate inhibition efficiencies of DETPMP, VS-Co, PE_1 and PAPE at pH5.5, T=20°C, SR ~ 1700

The inhibition efficiency data for the same stock products of penta-phosphonate DETPMP, co-polymer VS-Co, and phosphate esters SIs PE_1 and PAPE tested at 40°C and pH 5.5 is shown in Figure 7.4. With an increase in temperature from 20 to 40°C, the saturation ratio decreases from ~1700 to ~910, which accounts for the observed improvement in scale inhibition performances of DETPMP, PE_1 and PAPE at 40°C. This effect is especially significant for the DETPMP and PE_1 performance profiles.

In addition, the performance trend for DETPMP at 20°C shows a typical nucleation inhibition mechanism where the performance at 2hr is greater than at 22hr however as the temperature is increased to 40°C these trends switch. The 22hr performance of the DETPMP becomes significantly better than the 2hr indicating that a crystal growth

blocking mechanism is perhaps now more dominant for the DETPMP at the longer residence time. This is also in line with the fact that the saturation ratio at 40°C has decreased dramatically by almost half which allows the DETPMP to work through its most predominant mechanism to inhibit barium sulphate scale formation at 40°C.

The phosphate esters performance profiles are very similar to that of the co-polymer VS-Co, hence, these are likely to operate as nucleation inhibitors under the current conditions.

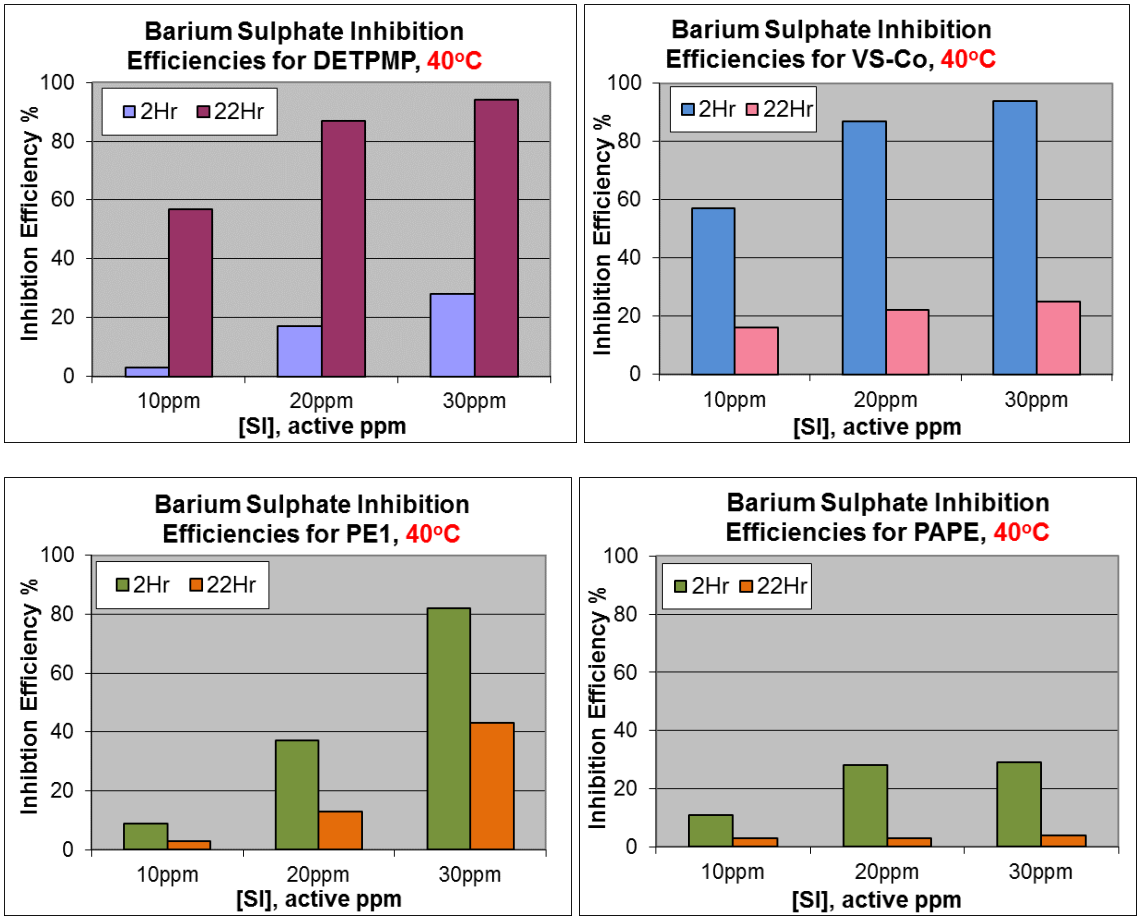

Figure 7.4 Barium sulphate inhibition efficiencies of DETPMP, VS-Co, PE_1 and PAPE at pH5.5, T=40°C, SR ~ 910

The inhibition efficiency data for the same inhibitors obtained at 60°C and pH 5.5 are shown in Figure 7.5. With an increase in temperature from 40°C to 60°C, the saturation ratio decreased from ~910 to ~560. For these conditions, the PE_1 chemistry shows the greatest performance for 20 and 30ppm SI among the tested inhibitors. The VS-Co and PAPE performances have slightly decreased or stayed the same, whereas the inhibition efficiencies of DETPMP and PE_1 have significantly increased, specifically the 2hr residence performance for DETPMP and for all [SI]s and residence times for PE_1. Thus,

it can be assumed that at 40-60°C, DETPMP inhibits barium sulphate scale predominantly through the crystal growth mechanism, whereas VS-Co and both phosphate ester products PE_1 and PAPE are performing mainly through nucleation inhibition.

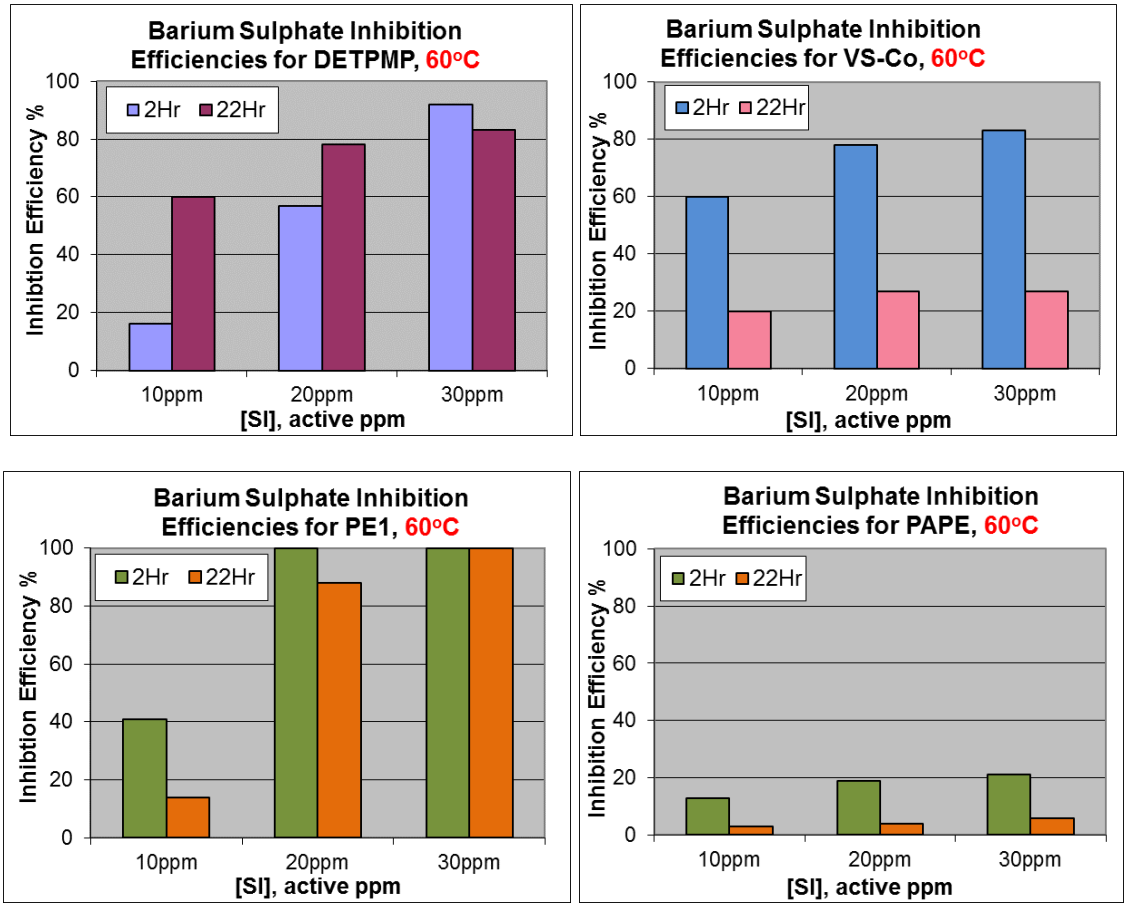

Figure 7.5 Barium sulphate inhibition efficiencies of DETPMP, VS-Co, PE_1 and PAPE at pH5.5, T=20°C, SR ~ 560

The inhibition efficiency data for the same SIs, except PAPE, tested at 80°C and pH 5.5 are shown in Figure 7.6. With a further increase in temperature to 80°C, the saturation ratio decreases from ~560 to ~400. This drop in SR allowed all the SIs to perform better in the short-term tests, whilst there was a slight decline in the longer-term 22hr tests which is linked to the consumption of the SIs with an increase in residence time (Shaw and Sorbie 2013).

Both phosphate ester products PE_1 and PAPE are likely to perform through the nucleation inhibition mechanism at lower temperatures, similarly to the co-polymer VS-Co, however, depending on the test conditions, they also work as a crystal growth retardants.

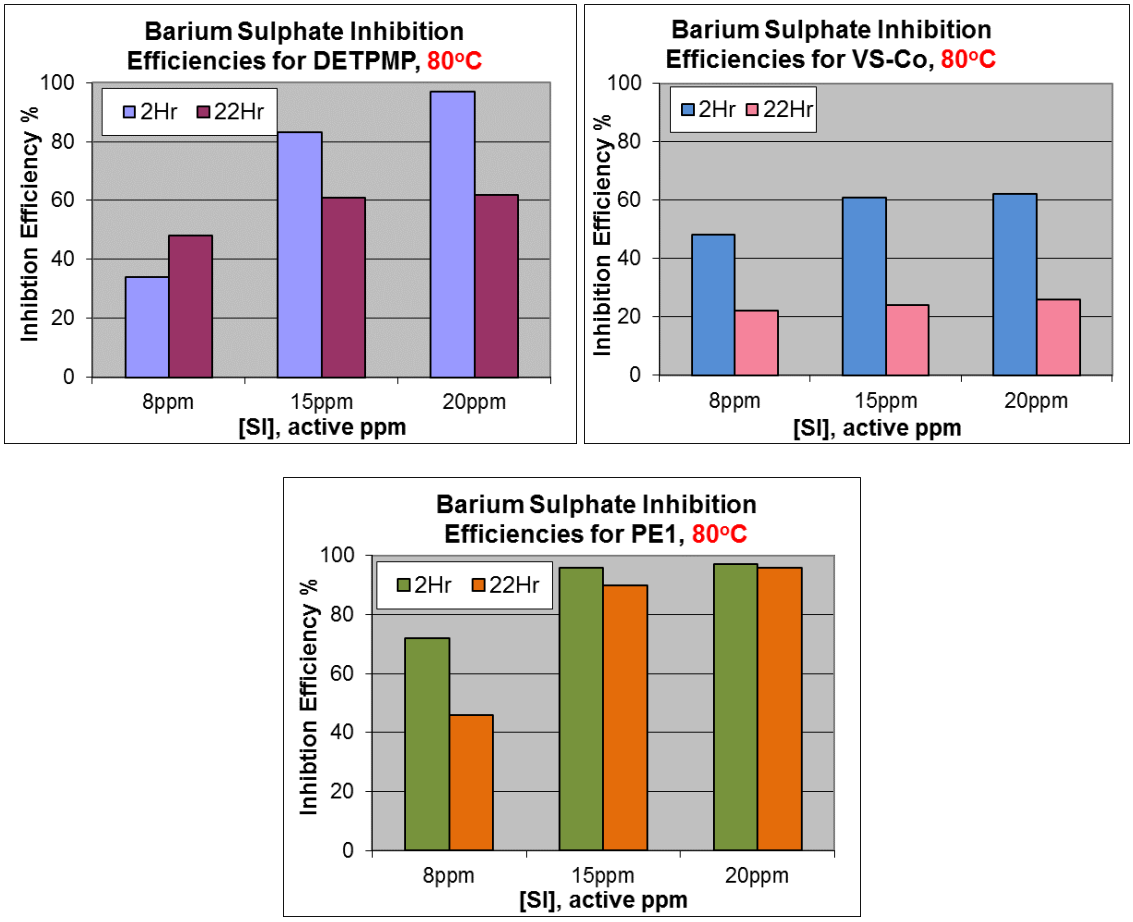

Figure 7.6 Barium sulphate inhibition efficiencies of DETPMP, VS-Co, and PE_1 at pH5.5, T=20°C, SR ~ 400

The results from this study show:

- The phosphate ester PE_1 product shows quite high inhibition efficiency against barium sulphate, similarly to conventional SIs, whereas the performance of the PAPE product is quite poor at the tested conditions;
- The optimum temperature range at which PE_1 inhibitor performs at its best is T = 60-80°C, where its efficiency is slightly higher than the performance of the "classic" chemistries that were used for comparison in this work: penta-phosphonate DETPMP and co-polymer VS-Co;
- The phosphate ester SI mainly shows higher inhibition efficiency performance at the short term (2 hour) tests. Comparing the performance versus temperature profiles of PE_1 with those of penta-phosphonate DETPMP and co-polymer VS-Co, the similarity between polymer and phosphate ester performance trends was observed, suggesting that phosphate ester chemistry performs through both nucleation inhibition and crystal growth retardation mechanisms.

Case 2: Constant Saturation Ratio

In this test, the saturation ratio was kept constant at ~ 322 in all the inhibition efficiency performance tests. This SR represents the SR in a NSSW/NFFW=60:40 mix, 95°C, pH5.5 system. These IE tests were performed for the phosphate ester products PE_1 and PAPE at 20°C and 40°C. The obtained data was then compared to the performance data of the "classic" SIs DETPMP and VS-Co for the same conditions. To achieve a constant SR, the NSSW composition for the lower temperature IE experiments had to be adjusted by reducing sulphate anions concentration. This constant SR avoided higher SR effects affecting the SIs performance and allowed only the temperature effect on the SIs performance to be examined. A better understanding of the phosphate ester scale inhibition mechanism at the lower temperatures was hence gained.

Figure 7.7 and Figure 7.8 show the inhibition efficiency performance data for DETPMP, VS-Co and the phosphate esters PE_1 and PAPE, tested at pH 5.5 and T = 20°C and 40°C, respectively. The IE of all the inhibitors is significantly higher than previously observed for the case 1 "natural" SR performances shown earlier, due to the impact of a lower SR here in case 2. Therefore, the lower saturation ratio requires lower SI concentrations to obtain the same degree of inhibition efficiency performance for all the chemistries.

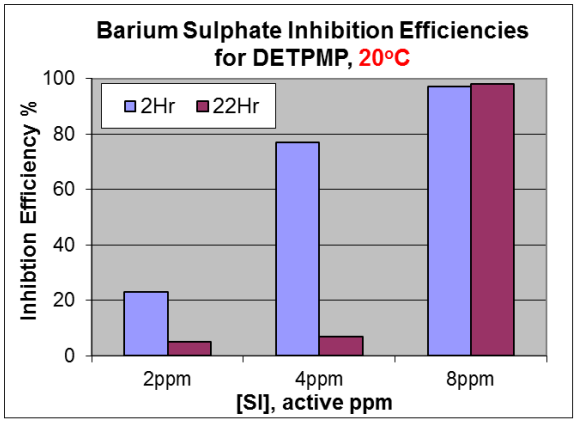

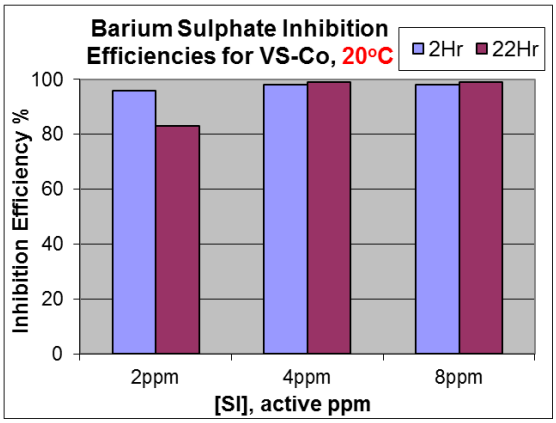

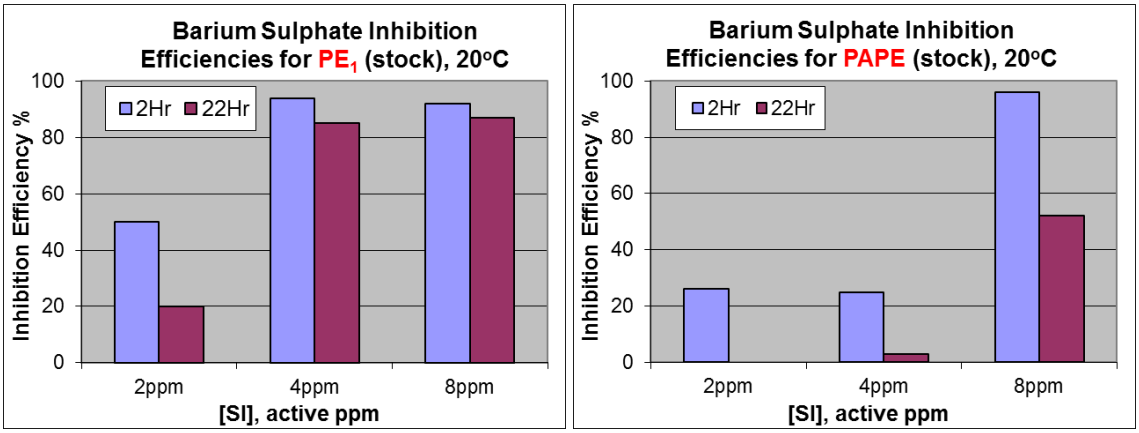

Figure 7.7 Barium sulphate inhibition efficiencies of DETPMP, VS-Co, PE_1 and PAPE at pH5.5 and T=20°C, SR = 322 (adjusted)

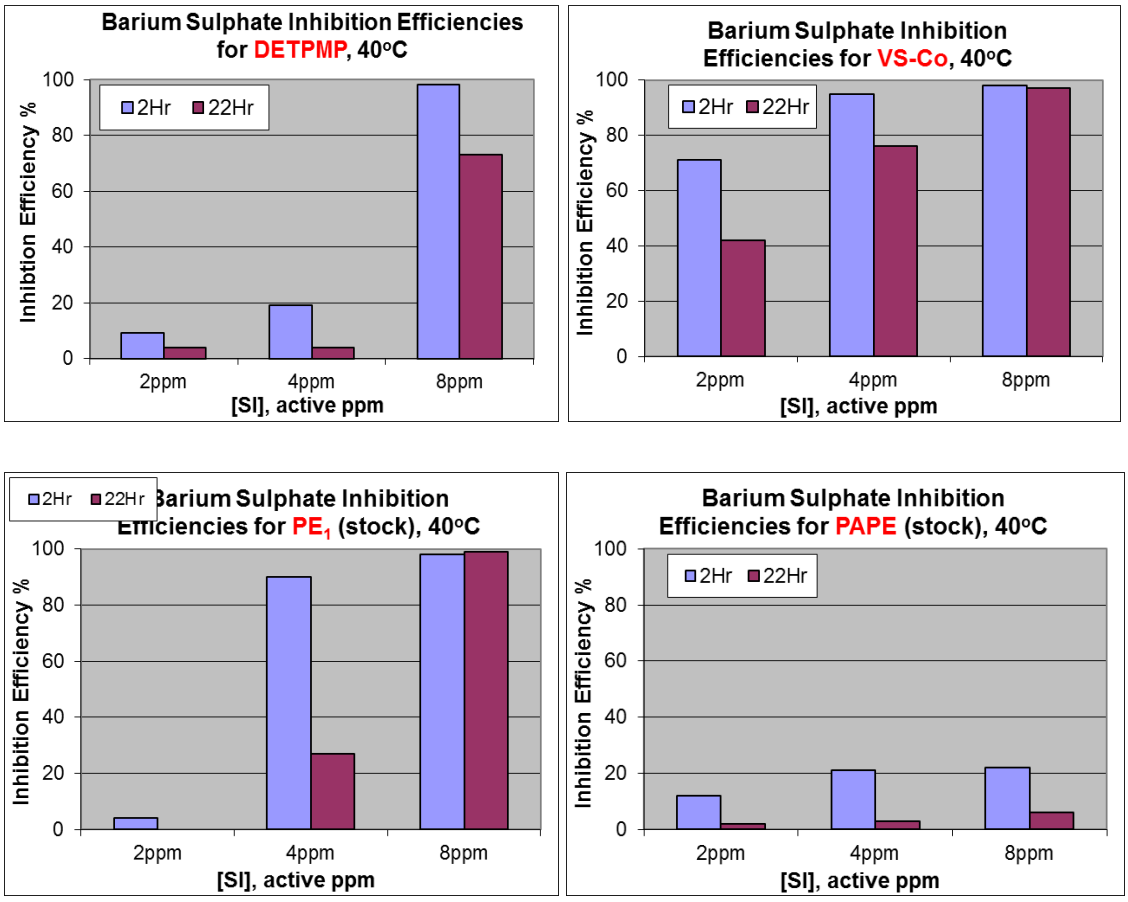

Figure 7.8 Barium sulphate inhibition efficiencies of DETPMP, VS-Co, PE1 and PAPE at pH5.5 and T=40°C, SR = 322 (adjusted)

At these lower temperatures and lower SR, the phosphate ester PE_1, along with the co-polymer VS-Co, show the highest performance against barium sulphate among all the chemistries tested. The performance trends of all the chemistries tested are similar with performance more effective for the short-term tests rather than long-term. At the lower

temperatures, scale crystal growth is limited, hence, at this stage all SIs would be expected to work through the nucleation inhibition mechanism.

7.3.2. *NMR analysis*

The phosphate ester PE_1 and PAPE stock solutions were analysed by NMR – Nuclear Magnetic Resonance. The objective of this study was to monitor the structure of the phosphate ester stock solutions versus temperature increase, to check if thermal degradation was occurring during the test. If any structural change has occurred, after aging the phosphate ester solutions at higher temperatures, the individual carbon atomic ratio should have changed, and this can be detected in the NMR spectrum.

In this work, ^{31}P NMR and 2 series of ^{13}C NMR tests were performed. These different NMR methods can define any structural changes occurring with either phosphorus or carbon atoms or their surroundings within the molecule. In *Series 1*, PE_1 and PAPE stock solutions were analysed, after being heated for 24 hours at 20°C, 60°C, 80°C and 95°C. The data obtained in this study provided only *qualitative* information on the structure of the compounds in the SI stock solutions, hence this was supplemented by the 1H Distortionless Enhancement by Polarisation Transfer (DEPT) method that can distinguish primary $-CH_3$, secondary $-CH_2-$, tertiary CH and quaternary C carbon atoms (refer to Figure 7.1).

Figure 7.9 and Figure 7.10 present the ^{13}C NMR chemical shifts of the PAPE and PE_1 stock solutions along with the 1H DEPT data. According to the 1H DEPT chemical shifts, all C contained in both the phosphate ester SIs are secondary carbon atoms. This is consistent with the available structures obtained from the supplier. All peaks lay in the range of 53-68 ppm for PE_1 and 53-73 ppm for PAPE, which are typical areas for $RO\mathbf{C}H_2R$ (50 – 75 ppm) and $R\mathbf{C}H_2NH_2$ (35 – 65ppm). There were no new peaks appearing/disappearing on the spectra, although some changes in the peak areas were detected. However, these plots cannot provide any quantitative data, since the peak areas here do not correlate with the concentration of the particular carbon atoms in the molecule, and mainly depend on the number of H atoms bound to each carbon (as well as on several other factors).

As hydrolysis is a reversible reaction, the detection of reaction products might be impeded as the solutions spectra were obtained after cooling back to 20ºC. However, a colour change was visibly noticeable in the PE_1 solutions during the heating process; the solution colour changed from dark to light amber.

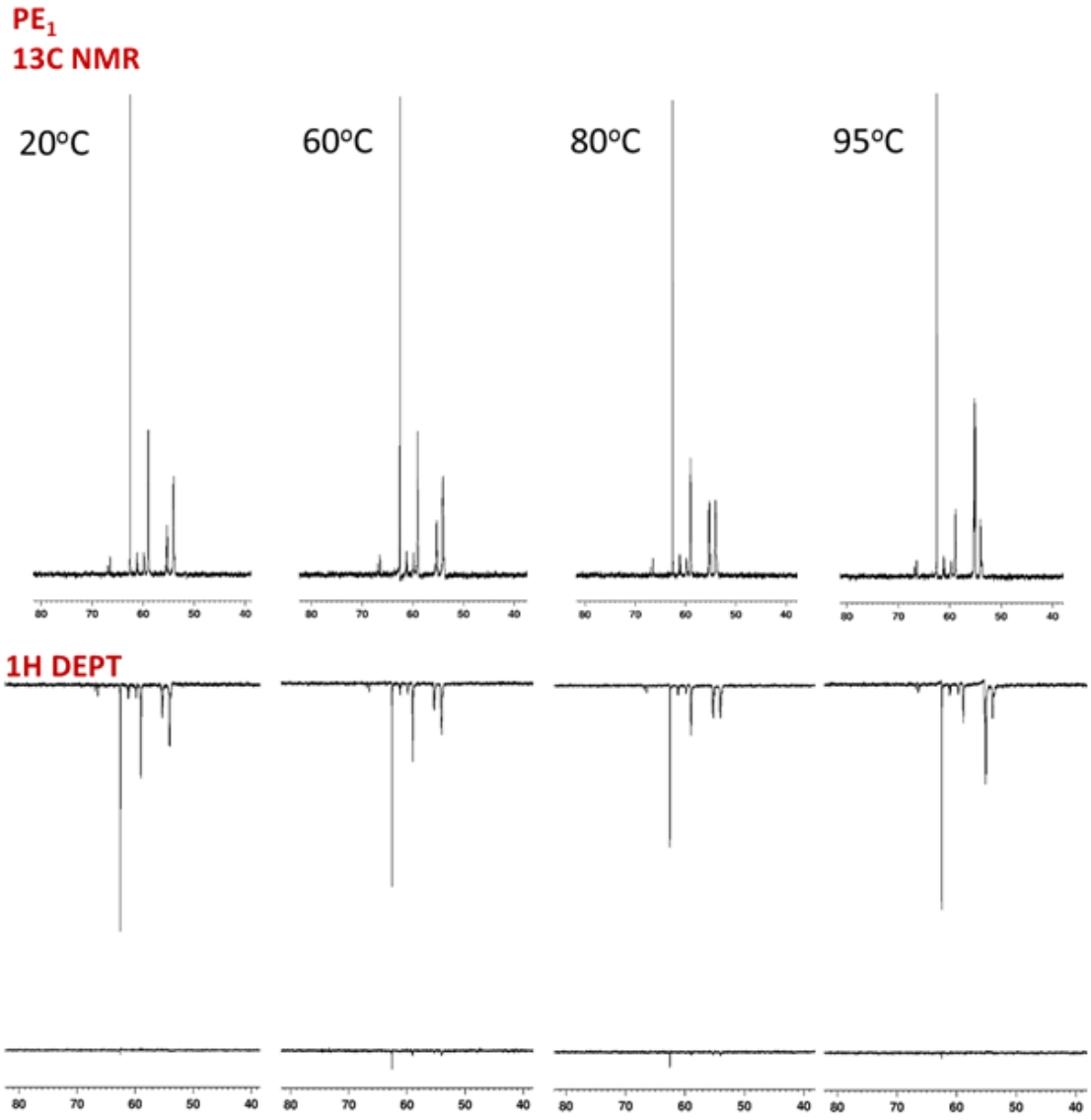

Figure 7.9 ^{13}C NMR and 1H DEPT chemical shifts of PE_1 stock solutions obtained after heating at temperatures of 20, 60, 80 and 95ºC and cooling back to 20ºC

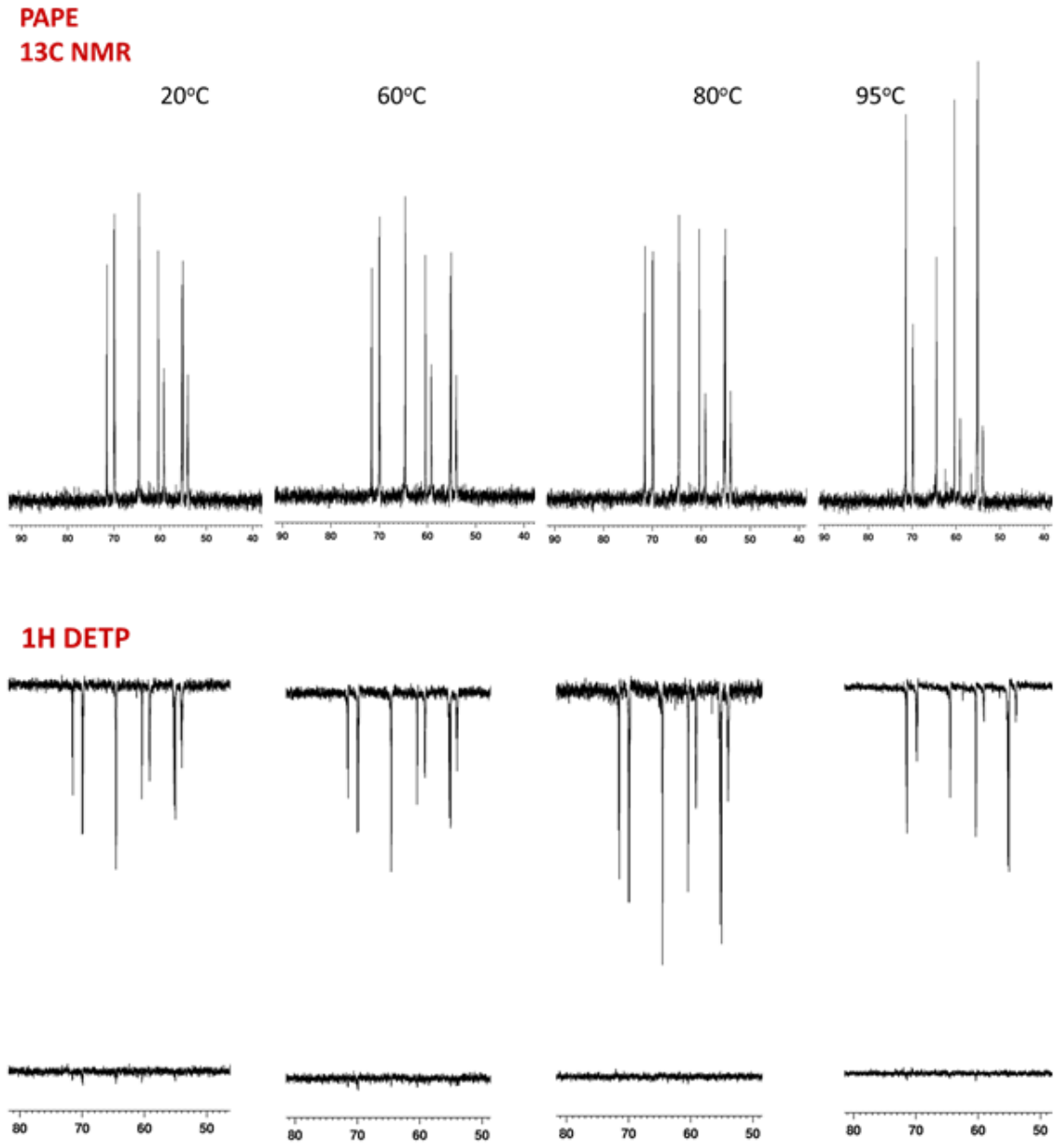

Figure 7.10 ^{13}C NMR chemical shifts of PAPE stock solutions obtained after heating at temperatures of 20, 60, 80 and 95°C and cooling back to 20°C

Figure 7.11 and Figure 7.12 present the ^{31}P NMR chemical shifts for the PE_1 and PAPE samples, respectively. Both ^{31}P NMR spectra show that all phosphorus presented is as P of the phosphonate group. There is no significant difference between the 20°C and 95°C spectra for both phosphate ester products, therefore if thermal degradation has occurred, phosphorus appears to remain in the structure of the phosphonate group.

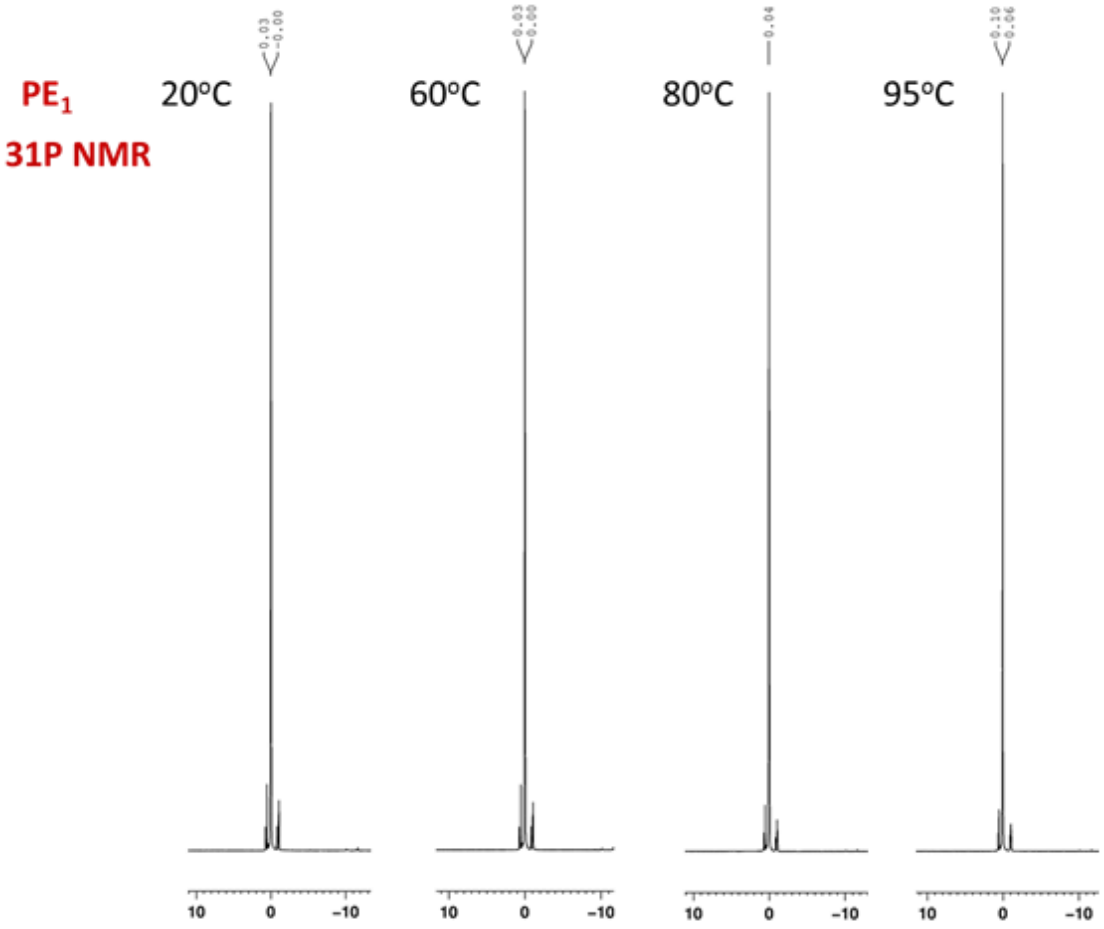

Figure 7.11 ^{31}P NMR chemical shifts of PE_1 stock solutions obtained after heating at temperatures of 20, 60, 80 and 95°C and cooling back to 20°C

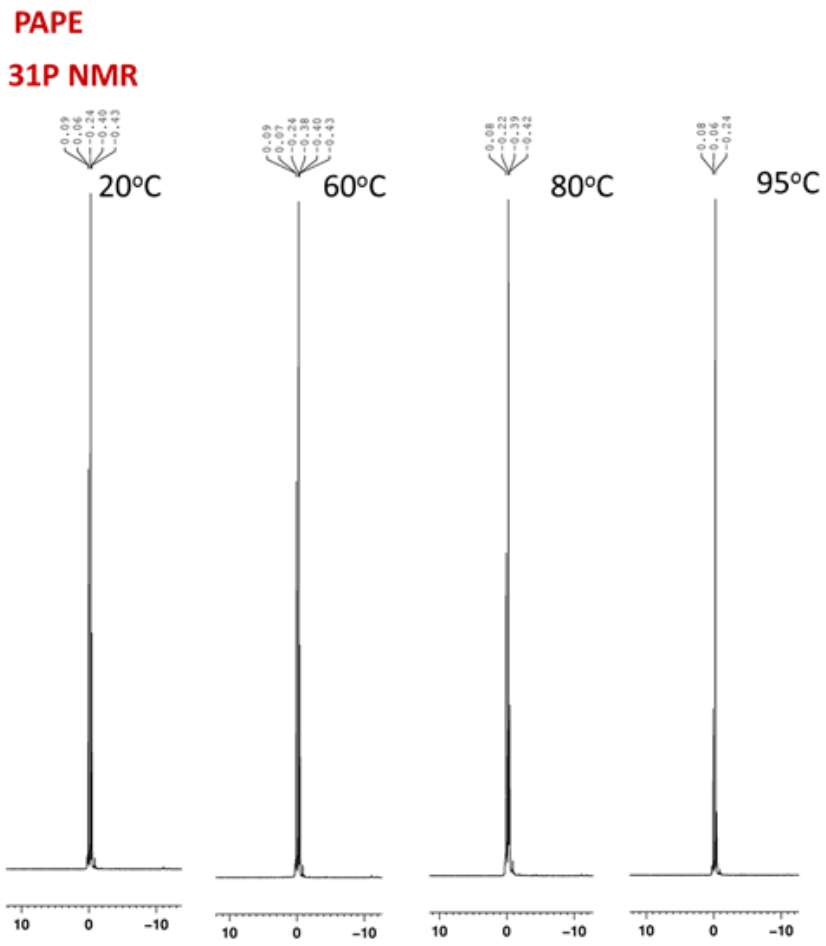

Figure 7.12 ^{31}P NMR chemical shifts of PAPE stock SI solutions obtained after heating at temperatures of 20°C, 60°C, 80°C and 95°C and cooling back to 20°C

In *Series 2*, ^{13}C NMR chemical shift profiles of the PAPE and PE_1 stocks were obtained after heating the solution samples to 20°C, 80°C and 95°C for 48 hours and allowing them to cool back to room temperature. This study was run on a different NMR machine that allowed *quantitative* data to be obtained, therefore the atomic proportion of each carbon atom could be calculated by integrating the areas under each ^{13}C peak shown on the profile.

The NMR chemical shift profiles for PE_1 and PAPE are shown in Figure 7.13 and Figure 7.14. For the PE_1 product, in the range 20-80°C, no significant changes occurred within the inhibitor species. At 95°C however, some significant changes in the peak areas were detected. A peak recorded at 55.1 ppm increased whilst peaks at 54.1 and 59.0 ppm decreased. These changes in peak areas indicate that decomposition occurred in the solutions at T = 95°C.

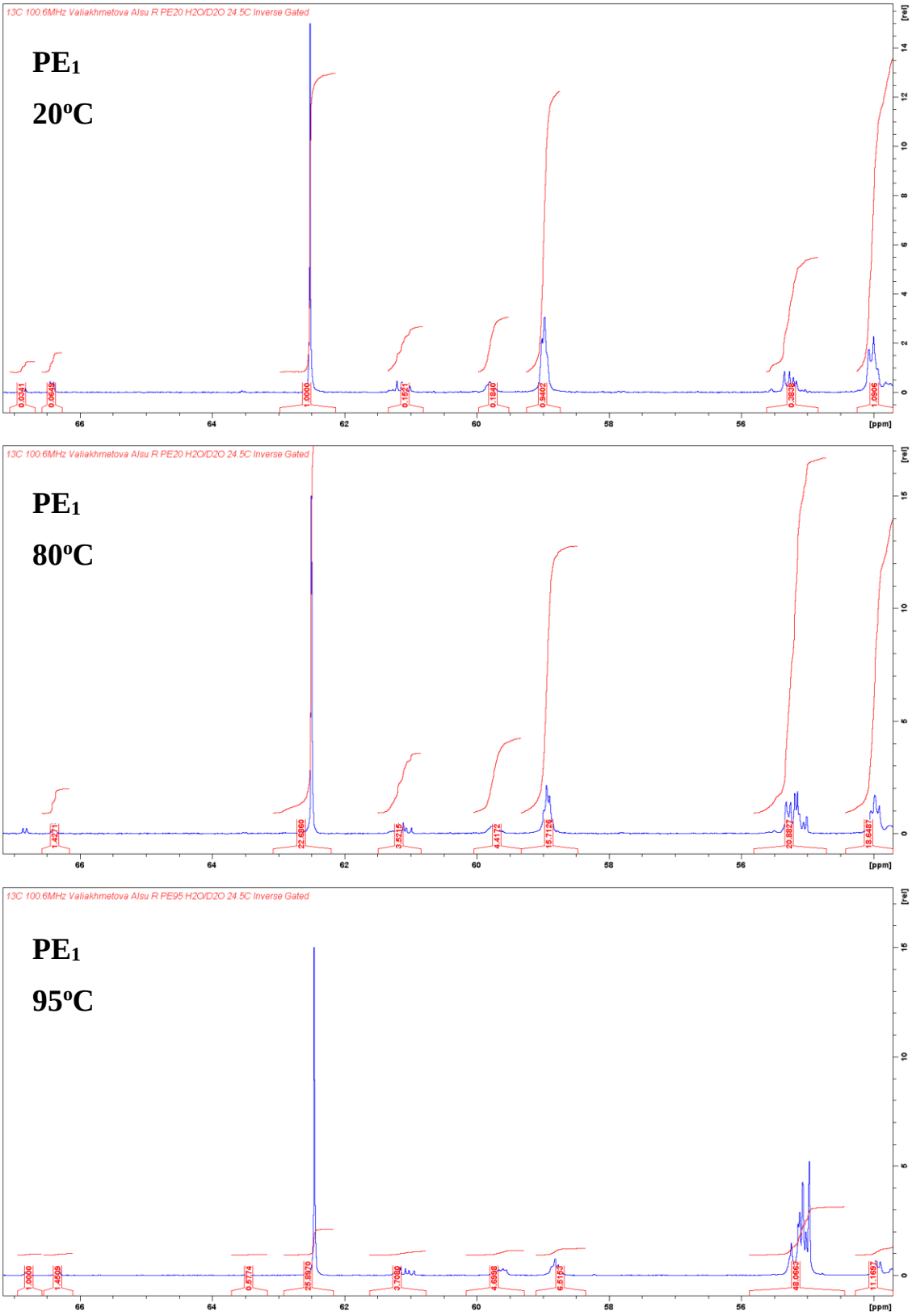

Figure 7.13 Quantitative ^{13}C NMR chemical shifts of PE1 stock solutions obtained after heating at 20ºC, 80ºC and 95ºC and cooling back to 20ºC

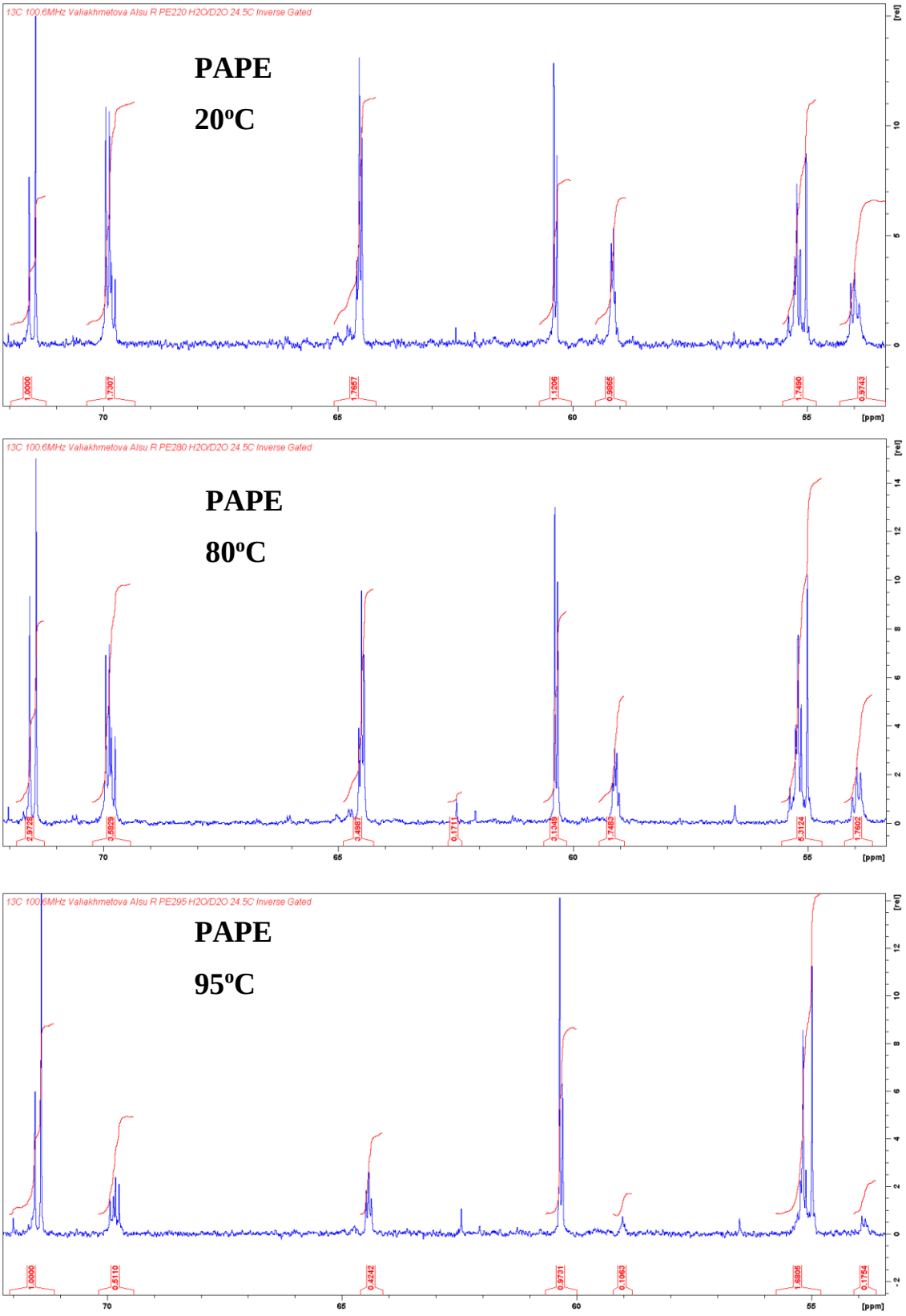

Figure 7.14 Quantitative 13C NMR chemical shifts of PAPE stock SI solutions obtained after heating at temperatures of 20ºC, 80ºC and 95ºC and cooling back to 20ºC

For PAPE, when the temperature increased up to 95ºC, the intensity of peaks at 54.9 ppm, 60.4 ppm, and 71.6 ppm increased whereas the intensity of the nearby peaks at 54.0 ppm, 59.1 ppm and 64.5 ppm and 69.9 ppm decreased, as shown in Figure 7.14. Again, this change in peak intensity (area) indicates decomposition has occurred in the solutions at the T = 95ºC. These results explain the inhibition efficiency performance data decline observed at the higher temperatures, as this performance decline relates to the thermal degradation of the stock phosphate ester product.

7.3.3. *FTIR Analysis*

In the current work, the IE test results show that increasing the temperature, negatively affects the performance of both phosphate esters, PE_1 and PAPE. This negative effect of temperature gets more significant at 95ºC and in the longer term tests (where obviously the heating exposure time is the longest). The reasons for this behaviour might not only be the SI consumption occurring over time in the scaling systems (Shaw and Sorbie 2013), but it may be due to SI degradation or deactivation at the higher temperatures, that phosphate esters are sensitive to, due to hydrolysis reactions.

To check this assumption, FTIR spectra were recorded only for the PAPE_Ca precipitates obtained at different temperatures: T = 20, 60, 95ºC. The possible structure of the PAPE obtained from the supplier has been already shown earlier in Table 6.1. According to this available PAPE structure, then the expected characterictic peaks responsible for stretching/bending vibrations on the IR spectrum should be the following bonds: P=O, P-O-H, P-H, P-O-C, C-C, C-H, C-O-C.

The FTIR spectrum of PAPE_Ca formed at 20ºC is shown in Figure 7.15 and the following bands can be observed:

3158 cm^{-1} – adsorbed water molecules and OH stretching (usually at 3100-3600 cm^{-1})
2949 cm^{-1} – C-H stretching of sp2 carbon atom
2359 cm^{-1} – P-H stretching
1648 cm^{-1} – O-H stretching in O=P-OH group
1460 cm^{-1} – C-H bending
1128 cm^{-1} – P-O rocking in P-O-C
1081, 1008 cm^{-1} – O-C rocking in P-O-C

967 cm^{-1} – P-H bend wag 990-885 cm^{-1}, strong in molecules with C-O-P, interacts with C-O-P stretch

765 cm^{-1} – P-O stretch in P-O-C

532-400 cm^{-1} – stretches/bends of variable C-O bounds

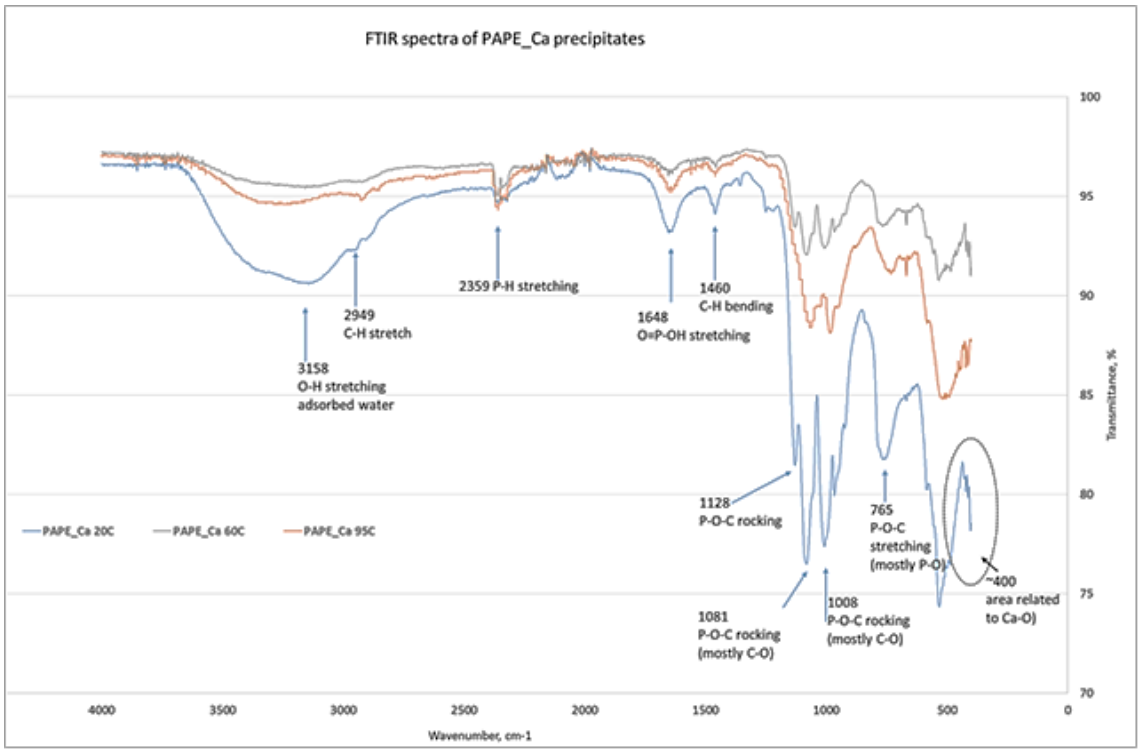

Figure 7.15 FTIR spectra of PAPE_Ca precipitates obtained at 20, 60, 95ºC and pH5.5

With temperature increasing, the intensity of the peaks representing P-O rocking in P-O-C (1128 cm^{-1}) and O-C rocking in P-O-C (1081, 1008 cm^{-1}) decreases and the 1128 cm^{-1} peak disappears at 95ºC. This may confirm the hydrolysis reaction occurs at higher temperatures which involves the cleavage of the P-O bonds in the P-O-C fragment of phosphate ester molecule, as follows:

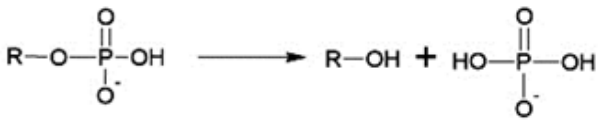

Therefore, this data explains the decrease in inhibition efficiency performance of the precipitated and then re-dissolved SI species at higher temperatures, tested in the previous Chapter.

7.4. Summary and Conclusions

1. The PE_1 product can be recommended for application at lower temperature conditions below 80°C. This is due to the phosphate ester PE_1 showing quite high inhibition efficiency performance against barium sulphate within the range of 60-80°C, where the efficiency of PE_1 is even slightly higher than the performance of the "classic" chemistries used for a comparison in this work, i.e. penta-phosphonate DETPMP and co-polymer SI VS-Co. The PAPE inhibitor shows quite poor inhibition efficiency at the conditions that the current tests were performed.
2. The phosphate ester SIs showed higher efficiency at lower saturation ratios. At these conditions, lower SI concentrations are required to obtain the same degree of inhibition efficiency.
3. It is suggested, that the phosphate ester chemistry performs through the nucleation inhibition mechanism at 20-40°C, similarly to polymeric SIs, whereas at 60-80°C, predominantly crystal growth retardation mechanism is taking place.
4. The inhibition efficiency of the *stock* phosphate ester SIs is shown to decline with increasing temperature. This decline was due to decomposition occurring in the PE_1 and PAPE solutions at T = 95°C, observed by NMR techniques.
5. The FTIR technique was also applied to the phosphate ester *precipitates* after obtaining those from the precipitation experiments at various temperatures. The obtained data indicates thermal degradation occurred in the PAPE precipitates at the higher temperature of 95°C.

Thus, in this study the PE_1 product was shown to be a promising alternative to polymer SIs and could be recommended for squeeze treatment applications in the reservoirs with lower temperatures, or for continuous injection at the top side production facilities, where processes occur at lower temperatures.

CHAPTER 8. CONCLUSIONS AND RECOMMENDATIONS

The original aim of this PhD thesis was to develop a qualitative dissolution model for the phosphonate scale inhibitor/metal precipitate in the context of precipitation squeeze treatments. In addition, establishing the effect of the precipitation reaction on the performance of the released inhibitor species was also an aim of the study. As a result, a qualitative model was obtained, which in theory, should supplement the currently used quantitative dissolution model and provide all the necessary experimental data, such as the equilibrium solubility Cs and kinetic dissolution rate.

It was highlighted from this doctoral work that the model currently being used, does not consider all the factors and cannot ~~not~~ accurately determine the phosphonate SI release from the precipitate. Hence, the additional factors that define the dissolution process were both examined and validated, via the experimental studies. From the results presented in this thesis, we were able to supplement the current dissolution model with experimental data, identify the missing points in this model and defining the parameters that need to be considered to develop a full quantitative dissolution model that describes phosphonate SI release in precipitation squeeze treatments.

Once the data and the qualitative model are appropriately implemented into the SQUEEZE code, that is used in the industry to design squeeze treatments, this should allow more accurate predictions of the inhibitor returns in produced brine and the inhibitor's fate in SI precipitation squeeze treatments.

The main conclusions from the various chapters in this thesis are given as follows:

Chapter 3. Equilibrium Solubility and Inhibition Efficiency of Phosphonate_Calcium Magnesium Precipitates

1. It is shown that the initial solubility of the precipitated phosphonate SI complexes, which form during squeeze treatments, are determined mainly by the brine injected during the treatment. The phosphonate/metal complexes become much more soluble as the proportion of Mg in the "squeeze" brine increases. Temperature also affects the solubility of the precipitates, making them less soluble with increasing temperature and vice versa. Therefore, when higher

retention via the precipitation mechanism is required (i.e. lowest solubility), it is advantageous to keep the Mg/Ca ratio at a low level during squeeze treatments (ideally, remove all Mg from the squeezed brine).

2. The solubility of the precipitate changes when the "squeeze" brine is replaced by the produced brine, once the well is brought back on to production after the squeeze treatment. This flowback brine will determine the subsequent solubility of the precipitated complex. Observations show, that any change of Mg/Ca molar ratio in a brine during SI re-dissolution causes a re-distribution of Ca, Mg and SI concentrations (and pH) between the precipitate and bulk solution, leading to the solubility variation. The stoichiometries n_1 and n_2 of the SI_Ca_{n1}_Mg_{n2} precipitated complexes also vary because of re-speciation.

3. All SI_Ca_Mg precipitates were tested and show high solubility over a wide range of Mg/Ca molar ratios, from all Mg to all Ca and over a temperature range, 20 - 95^{o}C. Therefore, the solubility stays within a concentration range that it is usually well above typical minimum inhibition concentrations (MIC) levels, thus ensuring that a sufficient amount of dissolved SI is available for scale prevention.

4. The precipitation process itself does not affect the final inhibition efficiency of the phosphonate SIs. Generally, the inhibition performance of the precipitated and then re-dissolved phosphonate complexes are approximately the same as the stock SI solution for all three phosphonate species (DETPMP, HEDP, OMTHP) studied in this work.

Chapter 4. Dissolution of Phosphonate Calcium_Magnesium Complex in Bulk

1. Both the experimental and numerical studies show that the SI/Ca_n precipitate re-speciates while dissolving in the brine, changing the *stoichiometry* n, SI apparent *solubility,* and bulk *pH*. Since the SI apparent solubility determines SI concentration in return brine during squeeze treatments, it is of interest to be able to predict the solubility variation. To achieve this, it is shown that the coupled system of three parameters, listed above, needs to be solved numerically. Therefore, the data is needed to supplement the current dissolution model (based only on the Noyes-Whitney equation) with the coupled system of three

parameters: bulk pH, phosphonate speciation or solubility in bulk, precipitate stoichiometry *n* in the SI/Ca_n complexes.

2. It is shown that the solubility variation is not related to any phase transition of the precipitate from an amorphous to a crystalline form. According to the XRD patterns obtained after the series of dissolution experiments, a crystalline structure was not identified. The characteristics of the precipitate remain the same, i.e. as an amorphous material.
3. The solubility variation, observed in this study, explains the decrease in the return SI concentration observed in the oilfields during squeeze lifetimes. For instance, the concerns raised earlier in the literature regarding discrepancy between the experimental higher SI solubilities, measured in the laboratory, and the lower return concentrations observed in the oilfields at the end of the squeeze lifetime. The conclusions of the current study clearly indicate the reasons determining such behaviour.

Chapter 5. Non-Equilibrium Dissolution of the Phosphonate Calcium Precipitates in Porous Media

1. It is shown, that the phosphonate SI return concentration in precipitation squeeze treatments depends on the flow rates. Dissolution at the higher concentrations occurs at the lowest flow rates, when the system is close to equilibrium. In contrast, at the higher flow rates, non-equilibrium dissolution occurs. It cannot "keep up" with the flow rates, therefore the SI concentration in the effluent decreases, until both dissolution and flow rates are equilibrated.

2. The equilibrium solubility for the phosphonate/Ca precipitates is *not* constant over the entire flood tests. It decreases quite significantly, which corresponds with the conclusions obtained from the bulk tests, reported in the Chapter 4 (and summarised above), confirming and explaining the SI return concentration decrease observed during squeeze lifetimes in oilfields. From an application point of view, although the solubility decreases over the squeeze lifetime, the concentration of the SI produced clearly exceeded typical minimum inhibitor concentration (MIC) levels for phosphonate SIs.

3. The dissolution of the DETPMP/Ca precipitate is governed by solution pH and vice versa, therefore these parameters are interconnected. The higher the apparent pH value is, the higher the SI inhibitor concentration released into the effluent, and vice versa. This is in agreement with the conclusion obtained from the bulk tests, presented in Chapter 4.

4. The dissolution behaviour of the DETPMP/Ca precipitate observed in the flooding tests does not correlate with the "classic" phosphonate SI dissolution model that is currently applied. According to the classic model, since the DETPMP/Ca precipitate contains only one type of phosphonate molecule, not a mixture of the different species, the phosphonate precipitate should be characterised by a specific saturation concentration, or a specific equilibrium solubility, that should not vary over the flood. However, in this work, it is shown that the equilibrium solubility of the phosphonate SI precipitates is *not* a constant value and varies over the flooding tests.

   Therefore, we propose a different approach, to define the phosphonate concentration in the return brine, for precipitation treatments. This should be based on the following findings:

   - SI return is governed by the phosphonate/Ca precipitate's continuous re-speciation over the flooding stage that leads to the precipitate's stoichiometry variation.
   - The pH values also vary over the dissolution process, controlling re-speciation of the precipitate, and therefore, the apparent solubility.
   - Phosphonate/metal precipitates with a different stoichiometry will have a different solubility.

5. To obtain the full precipitation model, apparent pH, stoichiometry of the phosphonate/metal precipitate, and apparent solubility should be coupled and solved numerically. The data obtained from sand pack 1 and 2 can be used to model the SI return after the coupled precipitation/adsorption treatments, whereas the precipitate pack 3 return profile can be used to describe the kinetics of the "pure" dissolution process, avoiding adsorption/desorption mechanisms.

Therefore, all the data obtained in the current study is input data to solve the precipitation/dissolution model for the phosphonate scale inhibitor and define its release concentrations in precipitation squeeze treatments.

Chapter 6. Precipitation Behaviour of Phosphate Ester Scale Inhibitors

In addition to establishing a qualitative precipitation and dissolution model for phosphonate SIs, described in Chapters 3-5, the precipitation behaviour of another class of scale inhibitors, viz. phosphate esters, was studied. The study included SI precipitation tests of two phosphate ester chemicals, PE_1 and PAPE, with Ca^{2+} cations, yielding $PE_1\_Ca_n$ and $PAPE\_Ca_n$ precipitates. The stoichiometry *n* was established as a molar ratio of calcium to phosphorus under various pH and temperature conditions.

The precipitation behaviour of the phosphate esters was found to be *different* to that known for the phosphonate and polymeric scale inhibitors*:*

- Generally, all the stoichiometry values for the phosphate ester complexes are within the range of *2.7-3.6* for PE_1_Ca, and *2.8-4.1* for PAPE_Ca. The phosphate ester inhibitors show a high chelating capacity, particularly when compared to the stoichiometry's of the phosphonate/Ca complexes, where the maximum theoretically possible Ca/P ratio is equal to 1, and this only occurs at higher pH values (pH>10) when all the phosphonate groups are fully dissociated ((Shaw and Sorbie, 2015a)).
- The molar ratio of Ca/P in the phosphate ester complexes does not significantly depend on solution pH and precipitation temperature, in contrast to that of the phosphonate and polymer SIs.

Subsequently, the inhibition efficiency performance of the precipitated phosphate ester complexes was measured and compared with the stock product and supernatant solution;

- The precipitation pH is shown to be a key factor in defining the inhibition efficiency of the PE_1_Ca and PAPE_Ca precipitates. The inhibition efficiency performance of the precipitated and then re-dissolved phosphate ester complexes is highest, when precipitation occurs at higher pH. This is due to the highest percentage of the more active SI components precipitating out at higher pH, leaving the supernatant product with less active SI components. Complexation

may also be a factor that slows down the hydrolysis reaction of the phosphate ester species and therefore positively affects the stability of the phosphate ester species.

- By controlling the pH of the brine during precipitation, there is the potential to 'design' the inhibition efficiency performance of the precipitated scale inhibitor.
- The trend of the inhibition efficiency performance of the precipitated and then re-dissolved phosphate esters, supernatant solutions and stock products generally *decreases* with increasing temperature, in the range of 20-95^{o}C. This probably occurs due to an increasing rate of hydrolysis reaction at temperatures above 80^{o}C, which leads to the thermal degradation of the active SI components.
- At the lower temperatures, up to 80^{o}C, it is the precipitates that show the highest IE, followed by the stock and then the supernatant solutions.
- From an application point of view, phosphate esters would require a higher amount of calcium ions available in the brine to (i) enhance SI retention via precipitation mechanism and (ii) provide adequate inhibition efficiency, as it is the Ca and SI complexes, rather than "free" SI ions, that are believed to be involved in the scale inhibition mechanisms ((Boak, Graham and Sorbie, 1999)).
- Hence, the higher performance of the precipitated species, compared to the stock product, could potentially lead to extended squeeze lifetimes, when phosphate esters are retained within the formation via precipitation.

Chapter 7. Inhibition Efficiency of Phosphate Esters in Precipitation Squeeze Processes

- The PE_1 product is recommended for application in lower temperature conditions below 80^{o}C. This is due to the phosphate ester PE_1 showing a good inhibition efficiency performance against barium sulphate within the range of 60-80^{o}C, where the efficiency of the PE_1 is even slightly higher than the performance of the "classic" chemistries used as a comparison in this work, i.e. phosphonate DETPMP and polymeric SI VS-Co.
- The PAPE inhibitor shows poor inhibition efficiency performance over the range 20-95^{o}C.
- The phosphate ester SIs show higher efficiency at lower saturation ratios and hence, lower SI concentrations are required to maintain the same degree of inhibition efficiency performance observed in the higher scaling system.

- It is suggested, that the phosphate ester chemistry performs through the nucleation inhibition mechanism at 20-40°C, similarly to polymeric SIs, whereas at 60-80°C, predominantly crystal growth retardation mechanism is taking place.
- The inhibition efficiency performance of both the *stock* and *precipitated* phosphate ester SIs is shown to decline with increasing temperature. This decline has been identified by NMR and FTIR techniques as decomposition occurring in the PE_1 and PAPE solutions at T = 95°C.
- According to the results obtained for one of the products (PE_1), the phosphate ester is a promising alternative to polymer SIs and has the potential for recommendation for use in squeeze treatment applications in reservoirs with lower temperatures, or for continuous injection at the top side production facilities, where processes occur at lower temperatures.

Recommendations for Future Work

The main aim of this work was to define a qualitative model that describes phosphonate scale inhibitor dissolution processes, as well as the effect of the precipitation reaction on the activity of the released inhibitor species, during precipitation squeeze treatments. This qualitative coupled model was presented in the current thesis. The next phase of the study should involve incorporating this model view to simulate precipitation SI treatments for phosphonates. The development of a full (equilibrium) coupled model of the scale inhibitor dissociation, the binding of the Ca/Mg and the resulting precipitation should be coupled with the brine/carbonate substrate chemistry. Indeed, exactly such a development programme is currently in progress in the FAST group at Heriot-Watt University, and they will be modelling the results produced in this thesis.

In addition, some other topics that might be studied in the context of the current are listed below:

- The kinetics of the coupled model view suggested in this work should also be solved numerically. Dissolution rate should be calculated from the data obtained during sandpack studies to supplement Noyes-Whitney equation in the current precipitation/dissolution model. The data obtained from sand pack 1 and 2 can be used to model the SI return after the coupled precipitation/adsorption treatments, whereas the precipitate pack 3 return profile can be used to describe the kinetics

of the "pure" dissolution process, avoiding adsorption/desorption mechanisms. As a result, the mathematical model and the generated solubility data and dissolution rates may be implemented into the SQUEEZE software.

- It is suggested that the effects of Mg^{2+} ions and Mg/Ca variation should be studied in the flooding brine in sand-pack studies. In the static tests, it was shown that varying Mg/Ca ratio in the brine affects the solubility of the precipitated SI/divalent cation complexes. Therefore, it is worth examining the precipitate dissolution kinetics when the brine composition (i.e. Mg/Ca ratio) is varying over the flooding period. This would model one of the various field scenarios, for example, when injection water breaks through causing the produced brine composition to change or when the squeeze brine is replaced by the produced brine with different Mg/Ca ratio.
- From the static tests it was found, the impact of the Mg/Ca ratio variation in brine on the solubility of the phosphonate/Mg/Ca precipitates becomes less significant with increasing temperature. Therefore, it is suggested to examine the precipitate dissolution process at elevated temperatures, that are closer to the field reservoir conditions, by performing the sandpack flooding tests at 90-95ºC.
- It is suggested to perform in-line pH measurement during these sandpack studies, proposed above, to obtain more accurate pH results and validate the proposed coupled model.

Another focus of the thesis was precipitation behaviour of the phosphate ester scale inhibitors. The following topics might be studied to continue this study:

- Phosphate esters scale inhibition mechanisms should be studied in detail via dynamic inhibition efficiency tests (i.e. using tube blocking rig to define scale formation delay) and via ESEM/EDX analyses of scale deposits formed in the presence of phosphate ester scale inhibitors, to monitor crystallographic characteristic changes in the presence of phosphate esters, similar to what has been done for phosphonates and polymeric SIs. This will add clarity on our conjecture in this work that phosphate ester scale inhibitors perform predominantly through a nucleation inhibition mechanism.

- Phosphate ester precipitation and binding constants should be modelled and solved numerically using the data obtained in precipitation tests of the current research.
- Inhibition efficiency tests can be carried out for another type of phosphate ester scale inhibitor, in order to define the correlation between the chemical structure and thermal stability or inhibition performance of phosphate ester products.
- Dissolution behaviour of the phosphate ester/Ca precipitates might be studied via dynamic sand pack tests using the experimental procedure adopted in this study for the phosphonate SI precipitates.

REFERENCES

AL-ROOMI, Y. M. & HUSSAIN, K. F. 2016. Potential Kinetic Model for Scaling and Scale Inhibition Mechanism. *Desalination,* 393, 186-195.

AL SALAMI, A. R. & A. KADER, A. A. M. 2010. Downhole and Topside Scale Challenge B!B. *SPE Abu Dhabi International Petroleum Exhibition and Conference, ,* Abu Dhabi, UAE: Society of Petroleum Engineers.

ALINK, B. A., OUTLAW, B., JOVANCICEVIC, V., RAMACHANDRAN, S. & CAMPBELL, S. 1999. Mechanism of Co2 Corrosion Inhibition by Phosphate Esters. *CORROSION 99,* 1999/1/1/, San Antonio, Texas: NACE International, 19.

ALMUBARAK, T., NG, J. H. & NASR-EL-DIN, H. 2017. Oilfield Scale Removal by Chelating Agents: An Aminopolycarboxylic Acids Review. *SPE Western Regional Meeting,* 2017/4/23/, Bakersfield, California: Society of Petroleum Engineers.

BADER, M. S. H. 2006a. Nanofiltration for Oil-Fields Water Injection Operations: Analysis of Concentration Polarization. *Desalination,* 201, 106-113.

BADER, M. S. H. 2006b. Sulfate Scale Problems in Oil Fields Water Injection Operations. *Desalination,* 201, 100-105.

BARAKA-LOKMANE, S., LESAGE, N., FAYED, A., JUNGAS, M., HENG, S., JACOB, M. & PEDENAUD, P. 2018. Sea Water Desulphation – Optimisation of Scale Treatment and Reduction of Opex & Capex. *SPE International Oilfield Scale Conference and Exhibition,* Aberdeen, Scotland, UK: Society of Petroleum Engineers.

BENTON, W. J., COLLINS, I. R., GRIMSEY, I. M., PARKINSON, G. M. & RODGER, S. A. 1993. Nucleation, Growth and Inhibition of Barium Sulfate-Controlled Modification with Organic and Inorganic Additives. *Faraday Discussions,* 95, 281-297.

BOAK, L. S., GRAHAM, G. M. & SORBIE, K. S. 1999. The Influence of Divalent Cations on the Performance of Baso Scale Inhibitor Species. *SPE International*

Symposium on Oilfield Chemistry, Houston, Texas: Society of Petroleum Engineers.

BONNETT, N., FIELER, E. R. & HEN, J. 1991. Application of a Novel Squeeze Scale Inhibitor in the Beryl Field. *Offshore Europe*, 1991/1/1/, Aberdeen, United Kingdom: Society of Petroleum Engineers.

BRAGA, T. G., MARTIN, R. L., MCMAHON, J. A., ALINK, B. A. O. & OUTLAW, B. T. 2002. Combinations of Imidazolines and Wetting Agents as Environmentally Acceptable Corrosion Inhibitors. Patent WO2000049204A1.

BROWN, B., SALEH, A. & MOLONEY, J. 2015. Comparison of Mono- to Diphosphate Ester Ratio in Inhibitor Formulations for Mitigation of under Deposit Corrosion. *CORROSION*, 71, 1500-1510.

BREEN, P. J., DIEL, B. N. & DOWNS, H. H. 1990. Correlation of Scale Inhibitor Structure with Adsorption Thermodynamics and Performance in Inhibition of Barium Sulfate in Low-pH Environments. *SPE Annual Technical Conference and Exhibition*, New Orleans, Louisiana: Society of Petroleum Engineers.

BROWNING, F. H. & FOGLER, H. S. 1995a. Effect of Synthesis Parameters on the Properties of Calcium Phosphonate Precipitates. *Langmuir*, 11, 4143-4152.

BROWNING, F. H. & FOGLER, H. S. 1995b. Precipitation and Dissolution of Calcium-Phosphonates for the Enhancement of Squeeze Lifetimes. *SPE Production & Facilities*, 10, 03, SPE-25164-PA.

BROWNING, F. H. & FOGLER, H. S. 1996a. Effect of Precipitating Conditions on the Formation of Calcium−Hedp Precipitates. *Langmuir*, 12, 5231-5238.

BROWNING, F. H. & FOGLER, H. S. 1996b. Fundamental-Study of the Dissolution of Calcium Phosphonates from Porous-Media. *AIChE Journal*, 42, 2883-2896.

BROWNING, F. H. & FOGLER, H. S. 1996c. Fundamental Study of the Dissolution of Calcium Phosphonates from Porous Media. *AIChE journal*, 42, 2883-2896.

BROWNING, F. H. & FOGLER, H. S. 1996a. Effect of Precipitating Conditions on the Formation of Calcium−Hedp Precipitates. *Langmuir*, 12, 5231-5238.

BURNHAM, J. W., HARRIS, L. E. & MCDANIEL, B. W. 1980. Developments in Hydrocarbon Fluids for High-Temperature Fracturing. *Journal of Petroleum Technology,* 32, 217-220.

CONNOLLY, J. A., BANASZCZYK, M., HYNES, R. C. & CHIN, J. 1994. Reactivity of a Chelated Phosphate Ester. *Inorganic Chemistry,* 33, 665-669.

CRABTREE, M., ESLINGER, D., FLETCHER, P., MILLER, M., JOHNSON, A. & KING, G. 1999. Fighting Scale—Removal and Prevention. *Oilfield Review,* 11, 30-45.

DYER, S. J. & GRAHAM, G. M. 2002. The Effect of Temperature and Pressure on Oilfield Scale Formation. *Journal of Petroleum Science and Engineering,* 35, 95-107.

FAN, J. C. J., BAIN, D., BRUGMAN, H. H., ENOCH, K. & GRACE, L.D. 2002. Laboratory and Field Development of a Novel Environmentally Acceptable Scale and Corrosion Inhibitor. *CORROSION 2002*, Denver, Colorado: NACE International.

FAROOQUI, N. M. & SORBIE, K. S. 2016. The Use of PPCA in Scale-Inhibitor Precipitation Squeezes: Solubility, Inhibition Efficiency, and Molecular-Weight Effects. *SPE Production & Operations*, 31, 03, SPE-169792-PA.

FAROOQUI, N. M., SORBIE, K. S. & BOAK, L. S. 2016. The Solubility and Dissolution of PPCA_Ca Complex in Precipitation Squeeze Processes. *SPE International Oilfield Scale Conference and Exhibition*, Aberdeen, Scotland, UK: Society of Petroleum Engineers.

FRIEDFELD, S. J., HE, S. & TOMSON, M. B. 1998. The Temperature and Ionic Strength Dependence of the Solubility Product Constant of Ferrous Phosphonate. *Langmuir,* 14, 3698-3703.

GDANSKI, R. D. 2008. Formation Mineralogy Impacts Scale Inhibitor Squeeze Designs. *Europec/EAGE Conference and Exhibition*, Rome, Italy: Society of Petroleum Engineers.

GDANSKI, R. D. & FUNKHOUSER, G. P. 2005 Published. Mineralogy Driven Scale Inhibitor Squeeze Designs. *SPE European Formation Damage Conference*, 2005/1/1/, Sheveningen, The Netherlands: Society of Petroleum Engineers.

GRAHAM, G. M., BOAK, L. S. & SORBIE, K. S. 2003. The Influence of Formation Calcium and Magnesium on the Effectiveness of Generically Different Barium Sulphate Oilfield Scale Inhibitors, SPE 81825, J. SPE Production Facilities, V. 18(1), p.28, 2003.

GRAHAM, G. M., DYER, S. J., SORBIE, K. S., SABLEROLLE, W. R., SHONE, P. & FRIGO, D. 1998. Scale Inhibitor Selection for Continuous and Downhole Squeeze Application in HP/HT Conditions. *SPE Annual Technical Conference and Exhibition*, New Orleans, Louisiana: Society of Petroleum Engineers.

HENNESSY, A. J. B. & GRAHAM, G. M. 2002. The Effect of Additives on the Co-Crystallisation of Calcium with Barium Sulphate. *Journal of Crystal Growth,* 237-239, 2153-2159.

HERNANDES, R., MELO, V. L., SANTOS, J. A. M., ROSARIO, F. F., BEZERRA, M. C. M. & DA ROSA, K. R. S. A. 2008. Scale Management in Espadarte Field. *SPE International Oilfield Scale Conference,* Aberdeen, UK: Society of Petroleum Engineers.

JARRAHIAN, K., SORBIE, K. S., SINGLETON, M. A., BOAK, L. S. & GRAHAM, A. J. 2018. The Effect of pH and Mineralogy on the Retention of Polymeric Scale Inhibitors on Carbonate Rocks for Precipitation Squeeze Treatments. *SPE International Conference and Exhibition on Formation Damage Control*, Lafayette, Louisiana, USA: Society of Petroleum Engineers.

JOHNSON, A., ESLINGER, D. & LARSEN, H. 1998. An Abrasive Jetting Scale Removal System. *SPE/ICoTA Coiled Tubing Roundtable*, Houston, Texas: Society of Petroleum Engineers.

JOHNSON, D. & HILS, J. 2013. Phosphate Esters, Thiophosphate Esters and Metal Thiophosphates as Lubricant Additives. *Lubricants,* 1, 132.

JORDAN, M. & MACKAY, E. 2016. A Retrospective Review of 10 Years of Scale Management in a Deepwater Field: From Capex to Plateau Production. *SPE*

International Oilfield Scale Conference and Exhibition, Aberdeen, Scotland, UK: Society of Petroleum Engineers.

JORDAN, M. M., JOHNSTON, C. J. & SUTHERLAND, L. 2016. Impact of Reservoir Temperature on Scale Inhibitor Retention - the Challenge of Ultra-Low Temperature Sandstone Reservoirs. *SPE International Oilfield Scale Conference and Exhibition*, Aberdeen, Scotland, UK: Society of Petroleum Engineers, 13.

JORDAN, M. M., SELAND, G., FEASEY, N., GRAFF, C.J. . 2000. Latest Advances in Bio-Degradation of Scale Inhibitors. Laboratory and Field Evaluation of a "Green" Carbonate and Sulphate Scale Inhibitor with Deployment Histories in the North Sea and Alaska. *11th International Oil Field Chemical Symposium*, Fagernes, Norway.

JORDAN, M. M., SJURAETHER, K., COLLINS, I. R., FEASEY, N. D. & EMMONS, D. 2001. Life Cycle Management of Scale Control within Subsea Fields and Its Impact on Flow Assurance, Gulf of Mexico and the North Sea Basin. *SPE Annual Technical Conference and Exhibition*, New Orleans, Louisiana: Society of Petroleum Engineers.

JORDAN, M. M., SORBIE, K. S., CHEN, P., ARMITAGE, P., HAMMOND, P. & TAYLOR, K. 1997. The Design of Polymer and Phosphonate Scale Inhibitor Precipitation Treatments and the Importance of Precipitate Solubility in Extending Squeeze Lifetime. *International Symposium on Oilfield Chemistry*, Houston, Texas: Society of Petroleum Engineers.

KAN, A. & TOMSON, M. 2010. *Scale Prediction for Oil and Gas Production. SPE-132237-MS. SPE International Oil and Gas Conference and Exhibition in China*, Beijing, China.

KAN, A., YAN, L., BEDIENT, P., ODDO, J. & TOMSON, M. 1991. Sorption and Fate of Phosphonate Scale Inhibitors in the Sandstone Reservoir: Studied by Laboratory Apparatus with Core Material. *SPE Production Operations Symposium*: Society of Petroleum Engineers.

KAN, A. T., FU, G., AL-SAIARI, H. A., TOMSON, M. B. & SHEN, D. 2009. Enhanced Scale-Inhibitor Treatments with the Addition of Zinc. SPE-114060-PA. SPE Journa, 14, 04.

KAN, A. T., FU, G. & TOMSON, M. B. 2005. Adsorption and Precipitation of an Aminoalkylphosphonate onto Calcite. *Journal of Colloid and Interface Science,* 281, 275-284.

KAN, A. T., FU, G., TOMSON, M. B., AL-THUBAITI, M. & XIAO, A. J. 2004. Factors Affecting Scale Inhibitor Retention in Carbonate-Rich Formation During Squeeze Treatment. SPE Journal, 9, 280-289.

KELLAND, M. 2014. *Production Chemicals for the Oil and Gas Industry*, Boca Raton: CRC Press.

KIRBY, A. J. & VARVOGLIS, A. G. 1967. The Reactivity of Phosphate Esters. Monoester Hydrolysis. *Journal of the American Chemical Society,* 89, 415-423.

LAWLESS, T. A., BOURNE, H. M. & BOLTON, J. R. 1993. Examining the Potential for Corrosion Inhibitor and Scale Inhibitor Compatibility in a Multifunctional Squeeze Strategy. *SPE International Symposium on Oilfield Chemistry*, New Orleans, Louisiana: Society of Petroleum Engineers.

MACKAY, E. J., JORDAN, M. M. & TORABI, F. 2003. Predicting Brine Mixing Deep within the Reservoir and Its Impact on Scale Control in Marginal and Deepwater Developments. *SPE Production and Facilities*, 18, 210-220.

MCGREGOR, W. M. 2004. Novel Synergistic Water Soluble Corrosion Inhibitors. *SPE International Symposium on Oilfield Corrosion*, Aberdeen, United Kingdom: Society of Petroleum Engineers.

MORROW, J. R., BUTTREY, L. A. & BERBACK, K. A. 1992. Transesterification of a Phosphate Diester by Divalent and Trivalent Metal Ions. *Inorganic Chemistry*, 31, 16-20.

OLAJIRE, A. A. 2015. A Review of Oilfield Scale Management Technology for Oil and Gas Production. *Journal of Petroleum Science and Engineering,* 135, 723-737.

OTANI, S. 1960. Crystal Habit Modification of Strontium Sulfate. I. Habit-Modifying Action of Foreign Substances. *Bulletin of the Chemical Society of Japan,* 33, 1543-1548.

PAIRAT, R., SUMEATH, C., BROWNING, F. H. & FOGLER, H. S. 1997a. Precipitation and Dissolution of Calcium− ATMP Precipitates for the Inhibition of Scale Formation in Porous Media. *Langmuir,* 13, 1791-1798.

POETKER, R. H. & STONE, J. D. 1956. Corrosion Control of Gas-Lift Wells. *Drilling and Production Practice,* New York: American Petroleum Institute.

POYNTON, N., KELLY, C., FERGUSSON, A., RAY, J., WEBB, P. & STRONG, A. 2004. Selection and Deployment of a Scale Inhibitor Squeeze Chemical for the BP Miller Field. *SPE International Symposium on Oilfield Scale,* Aberdeen, United Kingdom: Society of Petroleum Engineers.

PUTNIS, A., PUTNIS, C. V. & PAUL, J. M. 1995 Published. The Efficiency of a Dtpa-Based Solvent in the Dissolution of Barium Sulfate Scale Deposits. *SPE International Symposium on Oilfield Chemistry,* San Antonio, Texas: Society of Petroleum Engineers.

RAISTRICK, B. 1949. The Influence of Foreign Ions on Crystal Growth from Solution. 1. The Stabilization of the Supersaturation of Calcium Carbonate Solutions by Anions Possessing O-P-O-P-O Chains. *Discussions of the Faraday Society,* 5, 234-237.

RAMSTAD, K., TYDAL, T., ASKVIK, K. M. & FOTLAND, P. 2005. Predicting Carbonate Scale in Oil Producers from High Temperature Reservoirs. SPE Journal, V.10 (4).

SAMUEL, M. M., NASR-EL-DIN, H. A. & JEMMALI, M. 2005. Field Application of a Novel Viscoelastic Gelled Oil System for Sand Fill Cleanout Operations. *SPE International Improved Oil Recovery Conference in Asia Pacific,* Kuala Lumpur, Malaysia: Society of Petroleum Engineers.

SARIG, S. & RAPHAEL, M. 1972. The Inhibiting Effect of Polyphosphates on the Crystallization of Strontium Sulphate. *Journal of Crystal Growth,* 16, 203-208.

SAWADA, K., MIYAGAWA, T., SAKAGUCHI, T. & DOI, K. 1993. Structure and Thermodynamic Properties of Aminopoly-Phosphonate Complexes of the Alkaline-Earth Metal Lons. *Journal of the Chemical Society, Dalton Transactions,* 3777-3784.

SHAW, S., WELTON, T. D. & SORBIE, K. S. 2012. The Relation between Barite Inhibition by Phosphonate Scale Inhibitors and the Structures of Phosphonate-Metal Complexes. *SPE International Conference on Oilfield Scale*, Aberdeen, UK: Society of Petroleum Engineers.

SHAW, S. S. & SORBIE, K. 2015a. Structure, Stoichiometry, and Modeling of Mixed Calcium Magnesium Phosphonate Precipitation Squeeze-Inhibitor Complexes. *SPE Production & Operations*, 30(01), 06-15.

SHAW, S. S. & SORBIE, K. 2015b. Synergistic Properties of Phosphonate and Polymeric Scale-Inhibitor Blends for Barium Sulfate Scale Inhibition. SPE Production & Operations 30(01), 16-25.

SHAW, S. S., SORBIE, K. & BOAK, L. S. 2012a. The Effects of Barium Sulfate Saturation Ratio, Calcium, and Magnesium on the Inhibition Efficiency--Part I: Phosphonate Scale Inhibitors. SPE International Conference on Oilfield Scale, Aberdeen, UK: Society of Petroleum Engineers.

SHAW, S. S., SORBIE, K. & BOAK, L. S. 2012b. The Effects of Barium Sulfate Saturation Ratio, Calcium, and Magnesium on the Inhibition Efficiency: Part II Polymeric Scale Inhibitors. SPE International Conference on Oilfield Scale, Aberdeen, UK: Society of Petroleum Engineers.

SHAW, S. S. & SORBIE, K. S. 2013. Scale-Inhibitor Consumption in Long-Term Static Barium Sulfate Inhibition Efficiency Tests. *SPE Production & Operations*, 28, 376-386.

SHAW, S. S. & SORBIE, K. S. 2014. Structure, Stoichiometry, and Modeling of Calcium Phosphonate Scale-Inhibitor Complexes for Application in Precipitation-Squeeze Processes. SPE Production & Operations, 29(02), 139-151.

SHEN, D., ZHANG, P., KAN, A. T., FU, G., ALSAIARI, H. A. & TOMSON, M. B. Control Placement of Scale Inhibitors in the Formation with Stable Ca-Dtpmp Nanoparticle Suspension and Its Transport in Porous Medium. *SPE International Oilfield Scale Conference*: Society of Petroleum Engineers.

SHEN, J. & CROSBY, C. C. 1983. Insight into Strontium and Calcium Sulfate Scaling Mechanisms in a Wet Producer. *Journal of Petroleum Technology*, 35(7),1249-1255.

SORBIE, K. S. 2010. A General Coupled Kinetic Adsorption/Precipitation Transport Model for Scale Inhibitor Retention in Porous Media: I. Model Formulation. *SPE International Conference on Oilfield Scale*, Aberdeen, UK: Society of Petroleum Engineers.

SORBIE, K. S. 2012. A Simple Model of Precipitation Squeeze Treatments. *SPE International Conference on Oilfield Scale*, Aberdeen, UK: Society of Petroleum Engineers.

SORBIE, K. S. & GDANSKI, R. D. 2005. A Complete Theory of Scale Inhibitor Transport, Adsorption/Desorption and Precipitation in Squeeze Treatments. *SPE International Symposium on Oilfield Scale*, Aberdeen, United Kingdom: Society of Petroleum Engineers.

SORBIE, K. S., JIANG, P., YUAN, M. D., CHEN, P., JORDAN, M. M. & TODD, A. C. 1993. The Effect of Ph, Calcium, and Temperature on the Adsorption of Phosphonate Inhibitor onto Consolidated and Crushed Sandstone. *SPE Annual Technical Conference and Exhibition*, Houston, Texas: Society of Petroleum Engineers.

SORBIE, K. S. & LAING, N. 2004a Published. How Scale Inhibitors Work: Mechanisms of Selected Barium Sulphate Scale Inhibitors across a Wide Temperature Range. *SPE International Symposium on Oilfield Scale*, Aberdeen, United Kingdom: Society of Petroleum Engineers.

SORBIE, K. S. & LAING, N. 2004b Published. How Scale Inhibitors Work: Mechanisms of Selected Barium Sulphate Scale Inhibitors across a Wide Temperature Range. *SPE International Symposium on Oilfield Scale*, 2004/1/1/, Aberdeen, United Kingdom: Society of Petroleum Engineers, 10.

SORBIE, K. S. & MACKAY, E. J. 2000. Mixing of Injected, Connate and Aquifer Brines in Waterflooding and Its Relevance to Oilfield Scaling. *Journal of Petroleum Science and Engineering*, 27, 85-106.

SORBIE, K. S., WAT, R. M. S. & TODD, A. C. 1992. Interpretation and Theoretical Modeling of Scale-Inhibitor/Tracer Corefloods.

SORBIE, K. S., YUAN, M. D., TODD, A. C. & WAT, R. M. S. 1991 Published. The Modelling and Design of Scale Inhibitor Squeeze Treatments in Complex Reservoirs. *SPE International Symposium on Oilfield Chemistry*, 1991/1/1/, Anaheim, California: Society of Petroleum Engineers.

SUTHERLAND, L. & JORDAN, M. 2016 Published. Enhancing Scale Inhibitor Squeeze Retention with Additives. *SPE International Oilfield Scale Conference and Exhibition*, 2016/5/11/, Aberdeen, Scotland, UK: Society of Petroleum Engineers, 17.

TANTAYAKOM, V., FOGLER, H. S., CHAROENSIRITHAVORN, P. & CHAVADEJ, S. 2005. Kinetic Study of Scale Inhibitor Precipitation in Squeeze Treatment. *Crystal Growth & Design,* 5, 329-335.

TANTAYAKOM, V., FOGLER, H. S. & CHAVADEJ, S. 2005 Published. Study of Scale Inhibitor Reactions in Precipitation Squeeze Treatments. *SPE International Symposium on Oilfield Chemistry*, 2005/1/1/, The Woodlands, Texas: Society of Petroleum Engineers.

TANTAYAKOM, V., FOGLER, H. S., DE MORAES, F. F., BUALUANG, M., CHAVADEJ, S. & MALAKUL, P. 2004. Study of Ca−ATMP Precipitation in the Presence of Magnesium Ion. *Langmuir,* 20, 2220-2226.

TODD, A. C., YUAN, M. D. & MCCRACKEN, I. R. 1994. Part 3: Sulphate and Carbonate Scale Prediction in North Sea Oil and Gas Fields. *Geological Society, London, Memoirs,* 15, 105-118.

TODD, M. J., SAVIN, A. J. & SORBIE, K. S. 2012. Dual Chelant Mechanism for the Deployment of Scale Inhibitors in Controlled Solubility/Precipitation Treatments. *SPE International Conference on Oilfield Scale*, Aberdeen, UK: Society of Petroleum Engineers.

TOMSON, M. B., KAN, A. T. & FU, G. 2004 Published. Control of Inhibitor Squeeze Via Mechanistic Understanding of Inhibitor Chemistry. *SPE International*

Symposium on Oilfield Scale, 2004/1/1/, Aberdeen, United Kingdom: Society of Petroleum Engineers.

TOMSON, M. B., KAN, A. T., FU, G., SHEN, D., NASR-EL-DIN, H. A., SAIARI, H. A. & AL THUBAITI, M. M. 2008. Mechanistic Understanding of Rock/Phosphonate Interactions and Effect of Metal Ions on Inhibitor Retention. SPE Journal, 13(3), 325-336.

VALIAKHMETOVA, A., SORBIE, K.S., BOAK, L.S., SHAW, S.S. 2016. Solubility and Inhibition Efficiency of Phosphonate Scale Inhibitor_Calcium_Magnesium Complexes for Application in Precipitation Squeeze Treatment. SPE International Conference and Exhibition on Formation Damage Control, Lafayette, Louisiana, USA: Society of Petroleum Engineers.

VAZQUEZ, O., SORBIE, K. S. & MACKAY, E. J. 2010. A General Coupled Kinetic Adsorption/Precipitation Transport Model for Scale Inhibitor Retention in Porous Media: Ii. Sensitivity Calculations and Field Predictions. *SPE International Conference on Oilfield Scale*, Aberdeen, UK: Society of Petroleum Engineers.

VETTER, O. J. 1976. Oilfield Scale-Can We Handle It? *Journal of Petroleum Technology*, 28, 1402-1408.

VETTER, O. J. & FARONE, W. A. 1987. Calcium Carbonate Scale in Oilfield Operations. *SPE Annual Technical Conference and Exhibition*, Dallas, Texas: Society of Petroleum Engineers.

WYLDE, J. J., TURNER, N., AUSTILL, M., OKOCHA, C. & OBEYESEKERE, N. 2017. Development, Testing and Field Application of a Novel Combination Foamer-Iron Sulfide Scale Inhibitor-Corrosion Inhibitor in East Texas. *SPE International Conference on Oilfield Chemistry*, Montgomery, Texas, USA: Society of Petroleum Engineers.

XIAO, J., KAN, A. T. & TOMSON, M. B. 2001. Acid−Base and Metal Complexation Chemistry of Phosphino-Polycarboxylic Acid under High Ionic Strength and High Temperature. *Langmuir*, 17, 4661-4667.

YEPEZ, O., OBEYESEKERE, N. & WYLDE, J. 2015. Development of Novel Phosphate Based Inhibitors Effective for Oxygen Corrosion. Part II: Electrochemical Characterization. *CORROSION 2015,* Dallas, Texas: NACE International, 14.

YUAN, M. D. & TODD, A. C. 1989. Prediction of Sulfate Scaling Tendency in Oilfield Operations. *SPE International Symposium on Oilfield Chemistry*, 1989/1/1/, Houston, Texas: Society of Petroleum Engineers.

ZHANG, H., MACKAY, E. J., CHEN, P. & SORBIE, K. S. 2000. Non-Equilibrium Adsorption and Precipitation of Scale Inhibitors: Corefloods and Mathematical Modelling. *International Oil and Gas Conference and Exhibition in China*, 2000/1/1/, Beijing, China: Society of Petroleum Engineers.

ZHANG, P., SHEN, D., RUAN, G., KAN, A. T. & TOMSON, M. B. 2016a. Mechanistic Understanding of Calcium-Phosphonate Solid Dissolution and Scale Inhibitor Return Behavior in Oilfield Reservoir: Formation of Middle Phase. *Physical Chemistry Chemical Physics,* 18, 21458-21468.

ZHANG, Y., SHAW, H., FARQUHAR, R. & DAWE, R. 2001. The Kinetics of Carbonate Scaling—Application for the Prediction of Downhole Carbonate Scaling. *Journal of Petroleum Science and Engineering,* 29, 85-95.